Towards deeper understanding of structure, properties and applications of selected phytochemicals *via* theoretical routes

Thesis submitted to the
University of Calicut
in partial fulfillment of the requirements
for the award of the degree of
Doctor of Philosophy
in
Chemistry

by

VINDUJA P.

DEPARTMENT OF CHEMISTRY
UNIVERSITY OF CALICUT
KERALA-673635
FEBRUARY 2023

CERTIFICATE

This is to certify that the thesis entitled "**Towards deeper understanding of structure, properties and applications of selected phytochemicals via theoretical routes**", submitted to the University of Calicut, in partial fulfilment of the requirements for the award of **Degree of Doctor of Philosophy in Chemistry** is a bonafied record of research work done by **Ms. Vinduja. P**, during the period 2019-2023 in the Department of Chemistry at University of Calicut, under my supervision and guidance and the thesis has not formed the basis for the award of any Degree/Diploma/Associateship/Fellowship or other similar title to any candidate of any University. The contents of this thesis have been checked for plagiarism using the software 'Ouriginal" and the similarity index falls under permissible limit. The corrections recommended by the adjudicators have been incorporated in the thesis and the contents in the thesis and the soft copy are the same.

University of Calicut

Dr. K. Muraleedharan
Professor
Department of Chemistry
University of Calicut
Kerala

DECLARATION

I hereby declare that the thesis entitled **"Towards deeper understanding of structure, properties and applications of selected phytochemicals via theoretical routes"** is the bonafide report of the original work carried out by me under the supervision of Dr. K. Muraleedharan, Professor, Department of Chemistry, University of Calicut, for the award of the degree of Doctor of Philosophy in Chemistry Under the Faculty of Sciences, University of Calicut, Kerala. The content of this thesis has not been submitted to any other institute or University for the award of any degree or diploma.

Calicut University   **Vinduja. P**

ACKNOWLEDGEMENTS

By the grace of Almighty God, I must say it is the moment when my ship comes in and I am going to submit my thesis. This was similar like going back over each experience I had during the course of these four years of research. In pursuing this academic endeavour, I feel extremely appreciative for the inspiration, support, and encouragement that came my way in spades, and it is an honour for me to express the same in words.

At the outset, I am highly indebted to my supervisor, Dr. K. Muraleedharan, Department of Chemistry, University of Calicut, Malappuram, Kerala, India, for his timely guidance and constant supervision as well as for providing necessary information regarding my studies & also for his support in completing this research.

I express my sincere gratitude to Dr. Rajeev S Menon, HOD of Department of Chemistry, University of Calicut, who has always been very affectionately concerned and creatively helpful for providing all the facilities for completing my research. I would like to thank former HODs of the department, Dr. P. Raveendran and Dr. A. I. Yahya, for providing basic facilities for my research program. Besides, my I would like to acknowledge, the present faculty members of our department, Dr. Abraham Joseph., Dr. N. K. Renuka., Dr. M. T. Ramessan., Dr. P. Pradeepan., Dr. N. N. Binitha., Dr. Susmita De., Dr. T. D. Suja., Dr. Derry Holaday., Dr. Fazalurahman Kuttasery., and Dr. Roymon Joseph. I offer my genuine thanks to every one of my

I have a strong belief in the spiritual power of God and me continually thankful to him for the blessing that he had showered on me.

Though many have not been mentioned, none is forgotten.

Vinduja P

Dedicated to My Parents

Preface

Natural products' relevance in medicine, agriculture, and industry has prompted extensive investigations into their production, biosynthesis, and biological activity. Despite this, we still know very little about their true functions in nature. Clearly, scientific interest in the components and mechanisms involved in the beneficial properties of fruits and vegetables has fuelled this research. Phytochemicals are a diverse, bioactive, and widespread group of plant secondary metabolites that are an important element of the human diet and have a wide range of biological activities.

The eight chapters that make up the thesis entitled "Towards deeper understanding of structure, properties, and applications of selected phytochemicals *via* theoretical routes". Chapter 1 provides a brief introduction to polyphenols, their classification, and applications in both medicinal and industrial fields. Besides this, it presents major computational works in the field of anti-oxidant, molecular docking, and molecular dynamic simulation studies on polyphenols. Chapter 1 also deals with the detailing and former studies on the molecules under study. Chapter 2 discusses the materials and computational approach employed for this investigation. Chapter 3 gives detailed information on structure and reactivity of coumestrol and its derivatives. It also discusses a comparative evaluation on the anti-oxidant and anti-cancer activity of coumestrol derivatives with coumestrol molecule.

In chapter 4, the effects of solvents on metal chelation are discussed in detail along with the structure, stability, and electronic

characteristics of the Zn^{2+} chelates of the herbacetin molecule. The chapter also concentrates on the impact of Zn^{2+} ion on herbacetin's anti-oxidant action in polar and non-polar solvents. The final section of this chapter uses in silico molecular docking studies against AChE2 and BChE targets to explore the anti-AD potential of the herbacetin molecule. Chapter 5 concentrates on the structural and electronic exploration of the gossypetin molecule. The UV-filtering capacity and antioxidant potential of gossypetin against reactive oxygen species like •OH, •OOH, and reactive nitrogen species like •NO_2 is also described in this chapter.

Chapter 6 focuses on the identification of bioactive components found in the herbs C. *hirsutus* and R. *rosea* and their antiviral activity towards COVID 19 major protease 6LU7 with the use of molecular docking and molecular dynamic modeling studies. By using density functional theory (DFT) at the B3LYP/6-31++G(d,p) level of theory, we eventually determine the ideal structures of the molecules from each plant that have the highest binding affinity to the designated target.

In chapter 7, a comparative evaluation of anti-corrosive properties of the molecules herbacetin and gossypetin with the well-researched green corrosion inhibitor quercetin is conducted by he help of an important computational tool, Monte Carlo (MC) simulation, and the results are well supported by the DFT parameters. Chapter 8 provides a summary of the studies' key conclusions as well as some recommendations for additional research.

Contents

Chapter 2   **135-194**

Computational Methodology

List of Figures

List of Tables

Chapter 1
Introduction and Review of Literature

1.1 Introduction

Hippocrates said almost 2000 years ago, "Let food be thy medicine, and medicine be thy food," and natural food products have been studied for their health advantages since then. Plant foods, such as vegetables and fruits, provide the human body with calories and other needed nutrients and play an important role in human health. Over the last 16 years, research on plant secondary metabolites has increased, and these substances have been carefully evaluated for their potential to benefit human health. These phytochemicals (PC) are recognised to play a vital part in plant adaptation to their environment, as well as being a valuable source of active medicines. The benefits of PCs include their accessibility, specificity of reaction, and low toxicity. Phytochemicals appear to have established a niche in the pharmaceutical business in recent decades and are now being utilised in the design and development of new pharmacological medications. Furthermore, these chemicals are frequently employed in pharmaceutical research to improve the bio-efficacy and bioavailability of traditional medications. More than half of these molecules have antibacterial, antifungal, anti-inflammatory, and anticancer actions, demonstrating the wide range of benefits of PCs for human societies [1].

Other than pharmaceutical applications, the phytochemicals have been widely used as one of the most intriguing nature-based molecules in a variety of sectors including textiles, food, cosmetics, dye-sensitized solar cells, energy storage, organic electronics and photovoltaics, biocompatible organic phototransistors, pH indicators,

and point-of-care diagnostics because of their numerous intrinsic and distinctive features as the bioactive compound. Furthermore, a large range of phytochemicals have a variety of intriguing optical and electrochemical properties, paving the door for their use as optical and electrochemical (bio)sensors in clinical/health diagnostics, environmental monitoring, food quality control, and bioimaging. Despite the profound and obvious impact of using non-natural chemicals in everyday life, there is still a growing demand and motivation to replace them with natural-based substances such as phytochemicals, due to the negative consequences of non-natural chemical use on human and environmental health [2].

Because of their diversity in structures, phytochemicals have yet to be assigned a precise classification. Depending on their involvement in plant metabolism, phytochemicals have traditionally been classed as main or secondary metabolites. Sugars, amino acids, proteins, nucleic acid purines and pyrimidines, and chlorophylls, come under primary metabolites. Secondary metabolites are low-molecular-weight compounds that have a wide range of chemical structures and biological functions. In contrast to primary metabolites, secondary metabolites are not required for organism growth and reproduction. These secondary metabolites from plants are promising options for human nutrition. Chemicals such as alkaloids, terpenes, flavonoids, lignans, plant steroids, curcumins, saponins, phenolics, and glucosides are examples of secondary metabolites [3].

1.2 Phenolic compounds

Phenolic compounds are one of the major categories of secondary plant components with health benefits and are produced by

fruits, vegetables, tea, cocoa, and other plants. Phenolics are chemical compounds that have a hydroxyl group (OH) that is directly linked to an aromatic hydrocarbon group. The simplest type of natural chemical in this group is phenol (C_6H_5OH), which is standard for other antimicrobial agents. Phenolics are significant defensive chemicals since they are a secondary metabolite. The antioxidant capabilities of phenolics are critical in establishing their significance as protective agents against free radical-mediated disease processes. Anti-inflammatory, anti-carcinogenic, bactericidal, antiseptic, anthlemintic properties and other biological qualities describe their health advantages. Other antibacterial drugs use phenol as a standard. They're found in practically every plant and have been the subject of numerous chemicals, biological, agricultural, and medical research. They have a variety of structures, but they all have hydroxylated aromatic rings in common (e.g., flavan-3-ols). Polymerization of phenolic compounds into bigger molecules such as phenolic acids (proanthocyanidins; condensed tannins) and lignans is common. In addition, phenolic acids can be found in food plants as esters or glycosides conjugated with other natural substances such as flavonoids, alcohols, hydroxy fatty acids, sterols, and glucosides [4].

1.2.1 Flavonoids

Flavonoids are the most abundant and well-studied group of plant phenols. They are water soluble pigments found in the vacuoles of plant cells as aglycones, glucosides, and methylated derivatives. Floral colouring, UV filtration, and symbiotic nitrogen fixation are just a few of the functions that flavonoids play. Chemical messengers,

physiological regulators, and cell cycle inhibitors are all possible roles for them. Because of their multiple biological properties like antioxidant, anti-allergic, anti-microbial, cytotoxic anti-cancer, antioxidant, anti-inflammatory, and anti-viral, they have become widely popular. The ability to act as potent antioxidants that can protect the human body from hazardous free radicals and reactive oxygen species is the most well-known attribute of practically every group of flavonoids [5].

Flavonoids have become an essential component in a wide range of nutraceutical, pharmacological, therapeutic, and cosmetic applications. The carbon of the C ring on which the B ring is bonded, as well as the degree of unsaturation and oxidation of the C ring, can be used to split flavonoids into various subgroups. Isoflavones are flavonoids in which the B ring is connected in position 3 of the C ring. Neoflavonoids are those in which the B ring is joined in position 4; those in which the B ring is linked in position 2 can be further split into numerous subgroups based on the structural properties of the C ring including flavones, flavonols, flavanones, flavanonols, flavanols or catechins, anthocyanins [6].

The flavan nucleus, which is made up of 15 carbon atoms organised in three rings (C6-C3-C6) and denoted A, B, and C, is the most basic flavonoid structure. The level of oxidation and substitution pattern of the C ring differ between flavonoid classes, while the substitution pattern of the A and B rings differs between individual compounds within a class. In the light phase of photosynthesis, flavonoids act as catalysts and/or regulators of iron channels involved

in phosphorylation. Flavonoid intake can range from 50 to 800 mg per day, depending on the intake of fruits, vegetables and beverages such as red wine, tea, and unfiltered beer [7].
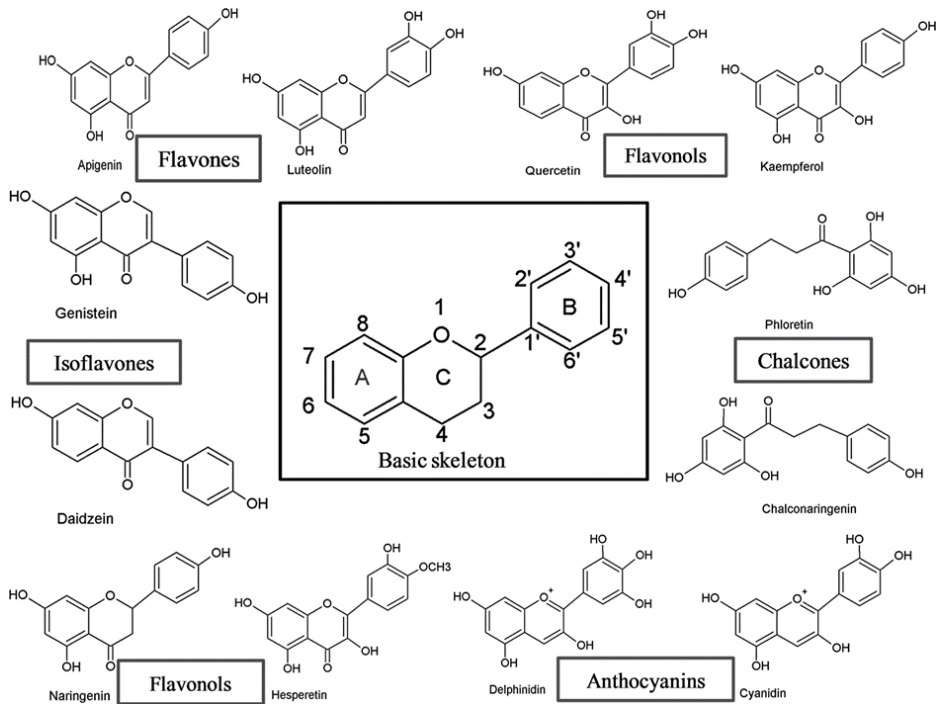
Fig. 1.1. Classification of phytochemicals

1.2.2 Phytoestrogen

Phytoestrogens are estrogenic chemicals found throughout the plant kingdom. Phytoestrogens, also called "dietary estrogens," are polyphenolic nonsteroidal phytochemicals structurally like female hormone estradiol. According to a large body of knowledge consumption of phytoestrogens may be an additional effective tool for preventing and treating a variety of dysfunctions and diseases related to ageing, mental processes, metabolism, malignant transformation,

cardiovascular diseases, and reproduction - breast and prostate cancers, menopausal symptoms, osteoporosis, atherosclerosis and stroke, and neurodegeneration [8, 9]. Phytoestrogens are classified (**Fig. 1.1**) as chalcones, flavonoids (flavones, flavonols, flavanones, isoflavonoids), lignans, stilbenoids, and miscellaneous based on their chemical structure and production patterns. Isoflavonoids, a subset of flavonoids that contains chemical groups such as isoflavones, isoflavanones, pterocarpanes, and coumestans, should be given special attention [10, 11]. Phytoestrogens are found in a variety of foods, including fruits, vegetables, and whole grains. They're found in a variety of edible and medicinal plants, especially from the Leguminosae family [10, 11]. Soy, red clover, kudzu, hops, licorice, rhubarb, yam, and chasteberry are examples of plant extracts with estrogenic properties [12]. Daidzein, genistein, formononetin, biochanin A, and coumestan coumestrol are the most well-known phytoestrogens [13].

A growing body of evidence suggests that phytoestrogens may potentially offer health benefits related to cardiovascular diseases, cancer, osteoporosis, and menopausal symptoms. This evidence comes from molecular and cellular biology experiments, animal studies, and, to a limited extent, human clinical trials. These possible health advantages are in line with epidemiological data showing a lower incidence of heart disease, different malignancies, osteoporotic fractures, and menopausal symptoms among communities who eat a plant-based diet, particularly in societies where soy consumption has been traditionally high [14].

1.3 Applications of Polyphenols

1.3.1 Medicine

Plants and their preparations have been used as medicines since antiquity. Folk medicine practitioners utilise a variety of herbal mixtures to treat various illnesses. Natural compounds generated from plants are harmless to normal cells and are also better tolerated, therefore they are gaining interest in current medicine development. According to estimates, the plant kingdom contains at least 250,000 species, of which 10% have been studied for pharmaceutical purposes. In human systems, phytochemicals and their metabolites like alkaloids, flavonoids, phenolics, tannins, glycosides, gums, resins, and oils found in root, leaf, flower, stem, and bark serve a variety of pharmacological roles [15].

1.3.1.1 Antioxidant effectiveness of plant polyphenols

Oxidative stress is characterised by an imbalance between the generation of reactive metabolites and free radicals, also known as reactive oxygen species (ROS), and their removal by defence mechanisms, such as antioxidants. Oxidative stress can harm lipids, proteins, carbohydrates, and DNA in cells and tissues, resulting in membrane damage, fragmentation, or random cross-linking of molecules including DNA, enzymes, and structural proteins. It can even cause cell death brought on by DNA fragmentation and lipid peroxidation. The molecular underpinnings of cardiovascular illnesses, cancer, neurodegenerative disorders, diabetes, and autoimmune disorders are built upon these oxidative stress-related side effects. The

normal cellular metabolism generates ROS, which is crucial in stimulating signalling pathways in cells in response to alterations in intra- and extracellular environmental circumstances. The mitochondrial respiratory chain produces the majority of ROS within cells. Aerobic cells generate ROS like superoxide anion ($O_2^{\cdot-}$), hydroxyl radical ($OH\cdot$), hydrogen peroxide (H_2O_2), and organic peroxides as typical by-products of the biological reduction of molecular oxygen during endogenous metabolic activities. The respiratory chain is the level at which an electron is transferred to a molecule of oxygen, and the mitochondria's membranes contain the electron transport chains. Nitric oxide (NO), which can form reactive nitrogen species, is also produced by the mitochondrial respiratory chain under hypoxic environments (RNS). By excessively stimulating lipid peroxidation, ROS/RNS can also produce additional reactive species. Different antioxidant strategies have involved either increasing endogenous antioxidant enzyme defences (such as superoxide dismutase, glutathione peroxidase, glutathione reductase, and catalase) or enhancing non-enzymatic defences (such as glutathione, vitamins) through dietary or pharmacological means in order to counteract and neutralise the harmful effects of ROS/RNS [16]. By scavenging free radicals and reducing oxidative stress, antioxidants can postpone, decrease, or prevent the oxidation of an oxidizable substrate. The oxidant load rises and the defence against ROS is compromised under disease circumstances. In these situations, an external supply of antioxidants is necessary to counteract the harmful effects of oxidative stress [17].

The most prevalent antioxidants in the diet are polyphenols. It comprises up to 1g of total daily intake, which is substantially more than all other groups of phytochemicals and known dietary antioxidants. To put this into perspective, this is 100 times higher than the intake of carotenoids and vitamin E, and about 10 times higher than the intake of vitamin C. Nutritionists have only recently become aware of the health benefits of dietary polyphenols, despite the fact that they are widely distributed in plants. The antioxidant vitamins, carotenoids, and minerals were the antioxidants that had received the most research up to the mid-1990s. After 1995, studies on flavonoids and other polyphenols' antioxidant capacities and impacts on disease prevention got going [18]. The most significant mechanisms of their antioxidant activity are said to be free radical scavenging, in which the polyphenols can stop a chain reaction from occurring from free radicals, as well as suppression of free radical formation by controlling enzyme activity or chelating metal ions involved in free radical production. Another potential antioxidant pathway for these chemicals involves interactions between polyphenolic molecules and other physiological antioxidants [19].

ROS, such as O_2, H_2O_2, or $HClO$, can be immediately captured by flavonoids like quercetin and catechin [20, 21]. The flavonoids with the highest free radical neutralising activity are quercetin and myricetin, followed by kaempferol. This class of phenols can exert direct action by absorbing unpaired ROS electrons, which results in the production of less reactive species. In essence, flavonoids function as buffers, scavenging free radicals to produce the flavin radical, which is

far less reactive due to its more dislocated unpaired electrons [22]. By chelating and removing transition metal ions like iron or copper, flavonols like quercetin can also prevent the generation of ROS brought on by the Fenton reaction [23]. Polyphenols may also block ROS-producing enzymes including xanthine oxidase and nicotinamide adenine dinucleotide phosphate (NADP) oxidase as well as cell detoxification mechanisms like superoxide dismutase, catalase, or glutathione peroxidase [24]. Tea's polyphenols have noticeable antioxidant capabilities in vitro and are up to five times more powerful than vitamins C or E. Epigallocatechin gallate, a flavonoid present in tea, has recently been identified to modulate the activity of glutathione and the enzyme cytochrome P450, potentially regulating ROS generation [25]. Another excellent source of antioxidant polyphenols is wine, which also contains phenolic acids, resveratrol, flavonols, flavanols, procyanidins, and anthocyanins [26, 27]. Resveratrol has been found to induce SOD enzymes in cardiac myoblasts and endothelial cells [28]. Additionally, aortic segments and vascular smooth muscle cells with catalase or glutathione peroxidase are upregulated by resveratrol [29]. Due to its high flavonoid content, particularly epicatechin and catechin, cocoa stands out among foods high in polyphenols [30]. Scientists have taken a keen interest in studies of cocoa and its derivatives because of the products' composition, which makes them excellent candidates for use as functional foods in the prevention and/or treatment of cardiovascular disease and diseases associated with oxidative stress [31].

Plant polyphenols have been researched in an effort to find compounds that protect against a variety of diseases such as cardiovascular and neurodegenerative diseases, cancer, diabetes, autoimmune disorders, and some inflammatory diseases that are linked to oxidative stress and free radical-induced damage.

1.3.1.2 Phytochemicals in neurogenerative diseases

Diseases that cause the loss of neurons are typically recognised as neurodegenerative diseases which include copious disorders like Alzheimer's (AD), Parkinson's (PD), Huntington's (HD), amyotrophic lateral sclerosis (ALS), and other less recurring diseases Alzheimer's disease (AD), Parkinson's disease (PD), Huntington's disease (HD), amyotrophic lateral sclerosis (ALS), and other less common diseases. The majority of neurodegenerative events are mostly caused by ageing [32]. Ageing is the prime culprit for most neurodegenerative events. There are several substances being investigated to treat neurodegenerative diseases (NDs), but most only have minor symptomatic benefits and a host of negative side effects. The researchers are forced to look into additional therapeutic techniques that finally target the causal components of the neurodegeneration due to the rapid progression of the neurodegenerative illnesses that increase the burden and the concomitant lack of viable treatment strategies. Targeting many processes, including OS, neuroinflammation, aberrant protein aggregation, neurotrophic factor insufficiency, disruption in mitochondrial function, and apoptosis, phytochemicals have a significant potential to exert their neuroprotective effects [32]. The effectiveness of phytochemicals in treating neurodegenerative illnesses

including Alzheimer's disease (AD) and Parkinson's disease has been supported by a growing body of research [33]. By altering the receptor activity of particular inhibitory neurotransmitters, phytochemicals play a critical part in preserving the chemical equilibrium of the brain.

Numerous studies show that certain phytochemicals and phytonutrients play an exceptional neuroprotective impact in neurodegenerative illnesses due to their antioxidant and anti-inflammatory properties [34-37]. All of these substances contain nourishing elements including propolis, vitamin E, and polyunsaturated fatty acids in addition to polyphenols like ginseng, resveratrol, curcumin, and rosmarinic acid [38, 39]. The number of hydroxyl (-OH) groups present in the aromatic rings A and B, as well as the existence of a 4 carbonyl with a 2,3-unsaturation in ring C, determine the structure of catechol-containing flavonoids with antioxidant properties [40]. Flavonoids release another proton to scavenge superoxide, singlet oxygen, hydroxyl, and peroxyl radicals and donate a proton to generate a phenoxyl radical. In actuality, the diol group created a complex structure with copper, ferric iron, and other transition metal ions that is crucial in avoiding the production of ROS [41].

The polyphenols, catalase, glutathione peroxidase, glutathione reductase, glutathione S-transferases, and superoxide dismutase upregulate the ROS-scavenging enzymes [42]. The stimulation of cellular signalling pathways by polyphenols may raise the levels of these antioxidants [43]. Xanthine oxidase, which produces ROS, can be suppressed by flavonoids like luteolin, kaempferol, and apigenin

[44, 45], and inducible nitric oxide synthase can be inhibited by polyphenols from amentoflavone and blueberries (iNOS) [46]. In addition, it has been noted that flavonoids such myricetin, baicalein, and quercetin, as well as non-flavonoids like protocatechuic acids and gallic acid, were shown to chelate copper and iron ions as well as reduce the production of free radicals [40, 47]. Ginkgo biloba leaf-derived naringenin, quercetin, amentoflavone, resveratrol, hesperetin, and bilobalide as well as luteolin attach to the ATP-binding site on receptors and enzymes, activate PI3K/Akt and PKC signalling pathways, and help restore cognitive and memory deficits. In H2O2 treated PC12 cells, pretreatment of hesperetin and its structural counterparts, isosakuranetin and isorhamnetin, have been linked to increased cell viability and catalase activity, as well as decreased membrane deterioration, ROS production, cellular calcium influx, and caspase-3 activity [48]. Salvia miltiorrhiza is a traditional Chinese plant that contains resveratrol, salvianolic acid, and curcumin. Both in vivo and in vitro studies have shown that these compounds protect neurons by activating PI3K/Akt. Hesperetin increases Akt signalling while decreasing pro-apoptotic proteins like caspase-9 and caspase-3, Bad, and apoptosis signal-regulated kinase 1 in hippocampus neurons [49].

By stimulating the Keap-1-Nrf-antioxidant response element (ARE) signalling pathway, polyphenols regulate the expression of antioxidant enzymes. Through its association with nuclear factor erythroid 2-related factor 2, Keap-1 prevents the activation of the signal (Nrf2). Keap-1 can be dissociated from the Nrf2 complex by

astaxanthin, carnosol, baicalein, lycopene, carnosic acid, lutein, and hydroxytyrosol [50]. The most prevalent type of dementia is Alzheimer's disease (AD), which is characterised by the development of intracellular neurofibrillary tangles (NFTs) and extracellular senile plaques [51]. Numerous investigations have discovered that ferulic acid, polymethoxyflavones, tannic acid, genistein, and galangin decrease β -secretase and also enhance behavioural impairment in animal models of AD [52]. In addition, 7,8-dihydroxyflavine, quercetin, rutin, icariin, luteolin, epigallocatechin gallate, resveratrol, and others reduced the expression of β-secretase. The cleavage of APP into harmless N-terminal substances, including soluble APP and C-terminal α factor, was increased by genistein, oleuropein, epigallocatechin gallate, and curcumin in the presence of α-secretase [53].

1.3.1.3 Phytochemicals in cancer treatment

Numerous targets in the pathways and mechanisms involved in carcinogenesis, tumour cell growth and death, inflammation, metastatic spread, angiogenesis, and drug and radiation resistance are influenced by polyphenols. Carcinogenesis is a multi-step process that involves numerous signalling events. Polyphenols act on a variety of targets in pathways and systems related to carcinogenesis, tumour cell growth and death, inflammation, metastasis dissemination, angiogenesis, or drug and radiation resistance [54]. Because of their safety, minimal toxicity, and widespread availability, dietary polyphenols have long been utilised to treat cancer. Moreover, as compared to synthetic molecules, drug discovery and development using plant-based

chemicals are less expensive. According to population-based studies, a high intake of vegetables and fruits is linked to a lower risk of cancer [55]. The polyphenols not only inhibit cancer-causing signalling pathways, but they also work in tandem with chemotherapy and radiotherapy. They are preferred because they act differently on cancer cells only while leaving normal cells unaffected [15]. Thus, naturally polyphenols' cancer chemoprevention and therapeutic potential are of tremendous interest [55].

Many polyphenols have been found as active ingredients in plant species, which have been discovered to inhibit the progression and development of tumours in cancer patients. Antitumor actions are mediated by polyphenols in several ways. They target abnormally expressed molecular factors, alleviate oxidative stress, control cell growth factors, block malignant tissue angiogenesis, and cause apoptosis in rapidly proliferating cells. For example, some polyphenols (*e.g.*, resveratrol, gallocatechins), flavonoids (*e.g.*, methoxy licoflavanone, alpinumisoflavone), and brassinosteroids (*e.g.*, homocatasterone and epibrassinolide) induce apoptosis in cancer cells [56, 57], whereas curcumin, thymol, rosmarinic acid, -carotene, quercetin, rutin, allicin, gingerol, epigallocatechin gallate, and coumarin all have antioxidant properties that help them fight cancer [15].

Ellagic acid (EA) is a phenolic compound found in ellagitannins in grapes, nuts, strawberries, black currents, raspberries, green tea, pomegranates, and the stem and bark of Eucalyptus globulus, Eucalyptus maculata, and nuts [58]. It causes apoptosis in

prostate and breast cancer cells, as well as inhibiting different kind of cancer spread like colon cancer, breast cancer, prostate cancer, skin cancer, oesophageal cancer, and osteogenic sarcoma [59-61]. EA possesses in vitro and in vivo cancer chemopreventive qualities, and it is a novel and very successful method for minimising cancer carcinogenesis [62].

Apigenin is a flavonoid produced from edible plants that has been shown to be anticancer in various experimental and biological studies. By regulating numerous signalling pathways, it causes cell growth arrest and apoptosis in a variety of malignancies, including breast, lung, liver, skin, blood, colon, prostate, pancreatic, cervical, oral, and stomach tumours [63]. Curcumin, a natural component derived from the rhizome of Curcuma longa plants, has piqued the curiosity of numerous researchers working on solid malignancies during the last half-century. Curcumin, interestingly, is an excellent alternative to current medications due to its relatively low risk profile, even at high dosages. Curcumin has been shown to have high antifungal action against Candida, Cryptococcus, Aspergillus, Trichosporon, and Paracoccidioides bacteria, implying that curcumin anticancer medications may also have an antifungal effect, assisting cancer patients in avoiding invasive fungal infections [64]. Curcumin, a natural chemical, has been proven to suppress cancer cell proliferation and metastasis as well as induce cell cycle arrest and apoptosis in a number of studies [65].

Red berry cyanidin glycosides have antioxidant and anticancer properties in a variety of ways. They block mitogen-induced metabolic

pathways and reduce the expression of inducible nitric oxide synthase (iNOS) and cyclooxygenase-2 (COX-2) genes in colon cancer cells [66]. Fisetin (3,7,3,4-tetrahydroxyflavone), a flavonol found in apples, persimmons, grapes, kiwis, strawberries, onions, and cucumbers, has been proven to prevent or slow the growth of cancer cells in culture and implanted tumours in vivo. Fisetin modulates a diverse set of upstream kinases, transcription factors, and their rviaulators to target various components of intracellular signalling pathways, including cell survival and death regulators, and tumour angiogenic and metastatic switches [67, 68]. Hesperetin, 3',5,7-trihydroxy-4'-methoxy flavanone [69], cause cell cycle arrest in human acute promyelocytic leukaemia HL-60 cells by affecting various signalling networks, including MAPK, NFκB, JAK/STAT, PI3K/Akt, Wnt, and mTOR [70]. The anticancer effects of genistein, a soybean isoflavone, are mediated by suppression of the NFκB and Akt signalling pathways [71]. Gingerol, a component of ginger, affects a number of cancer-related cell signalling pathways, including Nuclear Factors (NFκB), Signal Transducer and Activator of Transcription 3 (STAT3), Activator Protein-1 (AP-1), -catenin, Growth Factor Receptors (EGFR, VEGFR), Mitogen-Activated Protein Kinases (MAPK), and pro-inflammatory mediators (TNF- α and COX-2). In vitro and in vivo research back up gingerol's cancer-fighting abilities [72]. In colon cancer cells, gingerol inhibits Erk1/2/JNK/AP-1 signalling and causes caspase-dependent death [73].

Kaempferol is a common flavonoid, found in many vegetables and fruits and has been reported to have wide anti-cancer properties including breast cancer, prostate cancer, bladder cancer, cervical

cancer, colon cancer, liver cancer, lung cancer, ovarian cancer, and leukaemia [74]. In human breast cancer MDA-MB-453 cells, kaempferol stops the cell cycle in the G2/M stage by inhibiting CDK1 [74]. Kaempferol also inhibits pancreatic cancer cell growth and migration *via* acting on the proto-oncogene tyrosine protein kinase (Src), Erk1/2, and Akt pathways [75]. Rosmarinic acid is a caffeic acid and 3,4-dihydroxyphenyllactic acid ester often found in plants belonging to the Boraginaceae and Nepetoideae [76]. In colon cancer cells, rosmarinic acid lowers COX-2 activity and Erk phosphorylation [76]. Rosmarinic acid inhibits the activity of DNA methyltransferase and interferes with the RANKL/RANK/OPG networks in breast cancer cells. In melanoma and leukaemia U938 cells, it also targets the PKA/CREB/MITF pathway and NFκB activation respectively [76].

Resveratrol is a natural polyphenolic stilbene extracted from a variety of plants, foods, and beverages that modulates a variety of biological and pharmacological targets and signalling pathways. Because of its potential application in chemoprevention and treatment of various cancers, it has gotten a lot of interest as a promising and multitarget anticancer drug [77]. Resveratrol inhibits carcinogenesis by upregulating p53 and BAX proteins and downregulating NFκB, AP-1, hypoxia induced factor 1 (HIF-1), MMPs, Bcl-2, cytokines, cyclins, cyclin dependent kinases (CDKs), and COX-2 proteins, among others [78]

1.3.1.4 Immunomodulatory and Anti-Inflammatory Role of Polyphenols

Inflammation is a necessary immunological response to exogenous stimuli like as microbial infection, cell/tissue injury, and irradiation with characteristic features, such as swelling, redness, heat, and pain [79, 80]. Persistent inflammation is well established to be a significant factor in a number of human conditions, including cancer, type II diabetes, obesity, rheumatoid arthritis, neurodegenerative diseases, and cardiovascular diseases [81]. Polyphenols have demonstrated both in vitro and in vivo anti-inflammatory activity, indicating their advantageous use as therapeutic agents in a variety of acute and chronic illnesses [82, 83]. As a result, the anti-inflammatory and immune-modulating properties of dietary polyphenols have been the subject of several epidemiological and experimental studies [84]. In addition to their anti-oxidant properties like ROS (reactive oxygen species) scavenging, these natural compounds' capacity to alter the expression of several pro-inflammatory genes like multiple cytokines, lipoxygenase, nitric oxide synthases, and cyclooxygenase, as well as their anti-oxidant properties, contribute to the regulation of inflammatory signalling [85]. Many therapy methods are in clinical testing as the incidence of inflammatory illnesses rises. The complexity and diversity of the human body's inflammatory system pose a significant difficulty in treating inflammatory illnesses [86]. As a result, a thorough understanding of inflammatory processes is essential for identifying new molecular targets and creating new medications to treat immune-related illnesses [87]. Furthermore, it is critical to

discover novel anti-inflammatory medications with sufficient specificity, minimum side effects, and high efficacy from a variety of sources [88].

Numerous studies have demonstrated that polyphenols have an immune-modulating effect. For example, certain polyphenols affect immune cell populations, regulate cytokine production, and alter the expression of genes that promote inflammation [89, 90]. For instance, resveratrol's anti-inflammatory characteristics were primarily responsible for its cardioprotective effects. According to in vivo and in vitro research resveratrol can inhibit COX, inactivate PPAR-gamma, and stimulate eNOS (endothelial nitric oxide synthase) in mouse and rat macrophages [91, 92]. The pro-inflammatory cytokines TNF-α (tumour necrosis factor alpha) and IL-6 (interleukin-6) are inhibited by the resveratrol analogue RVSA40 in RAW (Murine macrophages cell line) 264.7 macrophages [93]. The expression of TNF and IL-1, as well as the adhesion molecules like ICAM-1 and VCAM-1 in human umbilical vein endothelial cells and inflammatory mediators like prostaglandins and leukotriens, have all been shown to be suppressed by curcumin. Additionally, it blocks the activity of several inflammatory enzymes, including IKK (inhibitor of kappa kinase), MAPK (mitogen-activated protein kinase), and LOX (lipoxygenase) in human endothelial cells. And furthermore, curcumin inhibits the expression of TLR-2 and TLR-4, STAT3 (signal transducer and activator of transcription), and NFκB (nuclear factor kappa-light-chain-enhancer of activated B cells), while in vivo, it increases PPAR (peroxisome proliferator-activated receptor gamma) in male adult rats

[94-96]. Quercetin was also demonstrated to reduce leukotriens synthesis in human polymorphonuclear leukocytes. Caffeic acid phenethyl ester inhibits TLR4 activation and LPS-mediated NFκB in macrophages [97]. The polyphenols such as Gingerol and Quercetin can activate the production of adiponectin known for its anti-inflammatory effects [94, 98]. A number of in vitro studies have discovered that other polyphenols, such as oleanolic acid, curcumin, kaempferol-3-O-sophoroside, EGCG, and lycopene, inhibit high mobility group box1 protein, a crucial chromatin protein that interacts with nucleosomes, transcription factors, and histones to regulate transcription and play a crucial role in inflammation [99].

Utilization of polyphenols is directly linked to a change in the number and differentiation of particular immune cells. Oral treatment of polyphenols derived from the fruit date to male C3H/HeN mice results in an increase in T helper 1 (Th1), natural killer (NK), macrophages, and dendritic cells (DCs) in Peyer's patches and spleen [90]. Polyphenols can increase the number of regulatory T cells (Treg or suppressor T cells) in humans that have the (CD4 + CD25 + Foxp3+) phenotype and are implicated in immunological tolerance and autoimmune regulation [100-102]. The *in vivo* studies showed that the amount of functional Treg in the spleen, pancreatic lymph nodes, and mesentheric lymph nodes increase when the green tea compound epigallocatechin-3-gallate is administered to Laboratory inbred strain (BALB)/c mice. Foxp3 and IL10 expression is increased when Jurkat T cells are treated with EGCG or green tea *in vitro* [103]. A flavone known as baicalin, which is derived from the Huangqin herb, causes

HEK 293 T cells to produce Foxp3 and activates splenic CD4 + CD25+ T cells to function as functional Treg [104]. Flavonoids also exhibit an agonistic impact on the aryl hydrocarbon receptor (AhR) and bind to xenobiotic-responsive sites in the promoter regions of several genes, including Foxp3, increasing its expression [105]. Polyphenols have an impact on both Th1 and Th17 populations. In particular pathogen-free C57/BL6 female mice, EGCG inhibits Th1 differentiation and decreases the quantity of Th17 and Th9 cells [106], whereas Baicalin inhibits Th17 differentiation in vitro and reduces IL-17 production [107].

It is well recognised that macrophages play a significant role in the inflammatory response. They start inflammation by releasing cytokines and pro-inflammatory mediators like IL-6 and TNF-α [108]. By blocking cyclooxygenase-2 (COX-2) and inducible nitric oxide synthase (iNOS), polyphenols suppress macrophages and lower levels of TNF- α, IL-1-β, and IL-6 are produced [109]. As shown by in vitro research ferulic acid-rich Chinese propolis [110], coumaric acid made from an extract of Lonicera japonica [111] and kalanchoe gracilis [112] are excellent examples in this case utilising RAW 264.7 cells. Cytokines are significant mediator proteins that are crucial for the immune system's networked communication. Quercetin and catechins, two polyphenols that influence the synthesis of both pro- and anti-inflammatory cytokines, increase the release of IL-10 while inhibiting the production of TNFα and IL-1-β [113, 114].

Nuclear factor NFκB complex protein called kappa-light-chain-enhancer of activated B cells is essential for DNA transcription,

cytokine synthesis, and cell survival. It regulates a cell's reactions to various stimuli, including immunological, inflammatory, stressful, and proliferative responses [115]. The polyphenols also have the ability to alter the NFκB activation cascade at various points, such as by influencing IKK activation and controlling oxidant levels or by influencing NFκB binding to DNA, which results in a significant anti-inflammatory effect and may explain their potential value in treating chronic inflammatory conditions. For example, quercetin inhibits IKK and NFκB activation and decreases NFκB's capacity to bind DNA in mouse BV-2 microglia treated with LPS and IFN-ɼ [116]. Luteolin also inhibits IKKs in LPS-induced epithelial and dendritic cells and suppresses NFκB activation, pro-inflammatory gene expression, and cytokine production in murine macrophages RAW 264.7 and mouse alveolar macrophages [117].

1.3.1.5 Effects of polyphenols on cardiovascular diseases

Numerous studies conducted recently have shown the health advantages of polyphenols, with particular focus being placed on their protective effects against cardiovascular disease, which is currently the leading cause of mortality worldwide. Age, sex, and genetic predisposition are some of the main CVD risk factors that cannot be modified, however, food and lifestyle are modifiable risk factors [118]. As a result, recent research supports the idea that risk factors such as oxidative stress, vascular inflammation, and endothelial dysfunction along with elevated plasma cholesterol play a significant role in the development of CVD [119]. Numerous investigations on humans have shown that atherogenesis, hypertension, and the development of

various CVD are all influenced by altered oxygen use and/or increased production of reactive oxygen species (ROS).

The physiochemical characteristics of polyphenols that enable them to take part in various metabolic cellular oxidation-reduction reactions may be partially responsible for their capacity to modulate the activity of various enzymes and thereby interfere with signalling mechanisms in various cellular processes [31]. Animal and human studies have demonstrated that polyphenols lower cardiac levels of reactive oxygen species (ROS) and malondialdehyde (MDA), a metabolite produced when ROS and oxidised low-density lipoproteins (LDL) attack fatty acids in cell membranes.

Nitric oxide (NO) production and bioavailability must be sufficient for vascular homeostasis to occur. The control of vascular tone is fundamentally mediated by NO. Therefore, the positive effects of polyphenols at the vascular level may be influenced by the lowered quantities of NO-destroying oxygen radicals [28, 120]. The vasodilator effects of polyphenols can, however, be attributed to a variety of routes. Red wine's polyphenolic chemicals may cause endothelium-dependent relaxation, according to studies done on the aorta rings and mesenteric arteries of rats [121]. This action is primarily mediated *via* NO generation, and it has been demonstrated that polyphenols regulate NO production in endothelial cells *via* an external calcium-dependent mechanism [122]. By opening up K^+ channels or blocking Ca^{2+}-ATPase in the endoplasmic reticulum, resveratrol and quercetin cause a rise in the intracellular calcium concentration in endothelial cells. The anthocyanin delphinidin, which is present in red wine, can also

activate endothelial cells and cause them to produce more intracellular Ca^{2+} [31].

Numerous published research link inflammatory and immunological responses to the arterial damage brought on by atherosclerosis [123]. Oxidative stress results in a rise in enzymes like cyclooxygenase (COX) and lipooxygenase (LPO), which are implicated in the production of factors including interleukins and chemokines. It has been demonstrated that polyphenols, specifically quercetin, suppress COX and LPO [124]. Given its capacity to prevent the manufacture of prostaglandins, resveratrol is also regarded as a compound having anti-inflammatory effects. The main molecular target for the anti-inflammatory actions of polyphenols in the vasculature is probably nuclear factor kappa beta (NF-κB) [125]. The phosphorylation of its active subunit P65 is necessary for the effective activation of NFκB's transcription [126]. The P65 phosphorylation process may be blocked by the polyphenols, making NFκB transcriptionally inactive [127]. The actions of certain polyphenols, such as resveratrol, are mimicked by the overexpression of deacetylase sirtuin 1 (SIRT1), as well. Resveratrol has been demonstrated to support SIRT1's deacetylation of P65 [128].

Improved lipid profiles are one of the most often researched positive benefits of polyphenols [129]. This may result in the prevention of atherosclerosis, which is the gradual occlusion of the arteries caused by fat build-up in the arterial wall. These lipids penetrate the endothelium and undergo oxidation in macrophages as well as endothelial and vascular smooth muscle cells [130]. The

oxidation of LDL and high-density lipoprotein (HDL), which is followed by endothelial cell dysfunction and the recruitment of macrophage foam cells, may be accelerated by the formation of ROS and reactive nitrogen species. Another effect is the proliferation of smooth muscle cells in the neointima region as a result of the migration of smooth muscle cells from the tunica media to the intima. All of this results in the extracellular matrix being deposited excessively and the leucocytes, monocytes, and T lymphocytes adhering to the vascular endothelium. The build-up of macrophages in this region destroys the oxidised LDL molecules while also inducing an inflammatory response, which includes the necessary cell recruitment and proliferation as well as smooth muscle cell migration [131]. Atheroma plaque, which essentially stops the vessel, can form when extracellular matrix deposits grow surrounding the inflammatory location. The rupture of the atherosclerotic plaque and platelet activation that results in thrombosis are the latter stages of the atherogenic process [132]. Numerous studies mention the preventive role that monomeric and oligomeric flavanols play in preventing LDL oxidation [133-135]. Red wine polyphenols have an immediate impact on postprandial lipemia, and they also lower plasma lipid concentration in red wine and grape juice [136]. When red wine is consumed with meals, there is a considerably lesser increase in lipid hydroperoxides, which are extremely atherogenic and normally present after eating [137]. Additionally, giving polyphenols orally to hypercholesterolemic rabbits slows down the formation of neointima and the buildup of lipids in the iliac artery [138]. The lipoprotein profile is greatly benefited by cocoa flavanoids. It has been demonstrated that giving

cocoa procyanidins to rabbits fed a hypercholesterolemic diet over an extended period of time reduces plasma lipid hydroperoxide levels while concurrently raising plasma antioxidant capacity [31]. The oxidised LDL autoantibodies (OLAB), which play a protective function in atherosclerosis, were boosted in amount by olive oil polyphenols [139].

1.3.1.6 Polyphenols and type II diabetics

The rising incidence of type 2 diabetes (T2D) is directly related to nutritional excess and a sedentary lifestyle. However, a diet high in fruits and vegetables is inversely connected to the development of T2D; these advantageous effects are mostly ascribed to phenolic chemicals [140]. There is mounting evidence that different dietary polyphenols may fend off diabetes. In general, both non-specific mechanisms, which rely on a broad anti-oxidant activity, and specific mechanisms, which involve interactions with important signalling proteins, are responsible for the health advantages of polyphenols. Additionally, polyphenols have been demonstrated to influence metabolic enzymes, nuclear receptors, gene expression, and several signalling pathways, indicating that their impact goes far beyond only limiting oxidative processes [141]. Moreover, it has been proposed that polyphenols can reduce significant T2D effects (such as fasting and postprandial hyperglycemia) by preventing the activity of disaccharidases in the intestinal lumen. This may restrict the breakdown of dietary polysaccharides, hence lowering the absorption of simple sugars. The same is also true, albeit to a smaller amount, for adipose tissue's uptake of glucose. Skeletal muscle is a considerable

mass of tissue, and an increase in this tissue's uptake of glucose greatly contributes to keeping blood sugar levels low. It's interesting to note that polyphenols may also have significant anti-diabetic effects *via* increasing the absorption of glucose in muscle and adipocytes. The dyslipidemic and hyperglycemic abnormalities that define type 2 diabetes (T2D) often begin in the liver, with hepatic insulin resistance being significantly linked to both decreased glucose storage and increased glucose production. Additionally, polyphenols may have anti-diabetic effects by reducing hepatic glucose output and raising hepatic glucokinase activity, which boosts glucose utilisation to encourage the storage of energy in the form of glycogen (i.e. gluconeogenesis). It has been hypothesised that polyphenols operate on insulin-secreting cells to increase insulin production, protect pancreatic beta-cells from glucotoxicity, and reduce T2D [142].

It has also been suggested that polyphenols may prevent T2D through anti-inflammatory properties because obesity-related T2D is linked to a low-grade inflammatory state. Particularly, polyphenols including curcumin, capsaicin, gingerol, catechins, resveratrol, and quercetin have been demonstrated to have anti-inflammatory effects by directly suppressing NFκB activity, the release of inflammatory cytokines, and mitogen-activated protein kinase (MAPK) pathways [137, 143-147]. Thiazolidinediones (TZD), a common class of anti-diabetic medications, target the peroxisome proliferator-activated receptor (PPARγ). The isoflavones genistein and daidzein, which are primarily derived from soybeans, ψ-baptigenin, hesperidin, 2′-hydroxy chalcone are also well-known PPARγ ligands [148]. Anthocyanins

have been demonstrated to improve diseases associated with obesity in animal models and are well known for their anti-oxidative and anti-inflammatory activities [149-151]. In 2001, Brownlee put forth a unifying theory that linked the production of reactive oxygen species (ROS) in the mitochondria to the pathogenesis of T2D, including the activation of PKC and NF-B, the flux of the polyol and hexosamine pathways, and the formation of advanced glycosylation end products [152]. Capsaicin, genistein, and catechins, have all been demonstrated to induce uncoupling protein 2 (UCP2) expression in WAT, hence suggesting UCP2-dependent buffering of ROS occurs in mitochondria [153-155]. So the identification of bioactive polyphenol metabolites from various fruits and plants and could lead to the discovery of novel cultivars to produce more effective functional foods and nutraceuticals to prevent T2D and other inflammatory disorders in obese patients.

1.3.2 Polyphenols in industry

1.3.2.1 Cosmetics

The science of altering one's appearance, known as cosmetology, has been practised since the dawn of time. The concept of employing herbs for beauty in India can be traced back to traditional medicine texts such as Ayurveda. Furthermore, plant extracts, in whole or in part, have been utilised for different skin, hair, and overall aesthetic disorders for millennia. Because polyphenols are generated from naturally renewable elements and may command high prices with suitable branding, they are a particularly potential sector for building an environmentally and economically sustainable development path.

There is also the possibility of vertically integrating the sector from components to consumer end-products with very modest infrastructure investment, notably in the case of polyphenol-based cosmetics. As a result, a phytochemical company that begins by obtaining plants for extraction of the required components can quickly progress to manufacturing creams and lotions, with significantly less reliance on external investment than heavy manufacturing sectors. According to market data, the herbal trade is on the rise, with the herbal cosmetics business playing a key part in fuelling this global need for herbals [156].

Reactive oxygen species contribute much to the organism's degenerative processes [157]. Free radicals and the onset of early ageing are closely related, as demonstrated by epidemiological and experimental investigations [158, 159]. As a preventative step, some applied antioxidants can prevent the negative effects of free radicals, leading to normal development of skin structural proteins [160]. Numerous studies connected phenolic compounds' chemical structure to their antioxidant action. In addition to reducing and chelating ferric ions that promote lipid peroxidation, the presence of phenolic nuclei serves as an effective sensor of reactive species [161].

The most common cosmetics that contain phyto-extracts are skincare products, which are designed to protect the skin from oxidative damage and to prevent or slow the ageing process. Extrinsic factors, such as pollution, chemicals, and UV radiation, have a significant impact on skin ageing. Extrinsic factors can harm the epidermis, causing skin to age faster. Several natural antioxidants, such

as curcumin, resveratrol, epicatechin, ellagic acid, and the flavone, apigenin, are popular in cosmetic industries producing various anti-ageing products and are capable of reducing physiological symptoms of ageing by counteracting reactive oxygen species (ROS), protecting and stimulating matrix-associated proteins, absorbing UV radiations, and maintaining the water balance in the skin [162-164]. There are various by-products of plant origins that have found their way into cosmetic industries, such as rind and pith from Agave, pulp and seed core from Apple, outer bracts, receptacles, and stems from Artichoke, and so on [165].

Chestnuts, especially chestnut fruits and foliage, are rich in phenolic compounds such as rutin, hesperidin, quercetin, apigenin, morin, galangin, kaempferol, and isoquercitin [166, 167]. Basile *et al.,* investigated and confirmed the antibacterial activity of a C. sativa leaves aqueous extract against E. coli, Klebsiella pneumoniae, Enterobacter aerogenes, Staphylococcus aureus, Proteus vulgaris, Pseudomonas aeruginosa, and Enterobacter cloacae [166]. A surfactant-free topical formulation including an ethanolic *C. sativa* leaf extract was characterised by Almeida *et al.,* in a study. After a 6-month storage period at 20 °C, no changes in pH or DPPH-scavenging activity were observed, and an in vivo moisturising effect was exhibited that lasted at least 4 hours after product application. This formulation's topical safety and stability were confirmed. It could be useful in the prevention and treatment of diseases caused by oxidative stress, as well as photoaging [168].

Herbal extracts are commonly used in cosmetic products because of their anti-oxidant qualities. In addition to antioxidant activity, flavonoids have UV protection and metal chelating capabilities. Rosemarinic acid (rosemary), hypericin (Saint John's Wort), and oleirupein are some of the chemicals found in the polyphenolics class (olive leaf). Aside from that, herbal extracts have been employed for their anti-inflammatory qualities on the skin. These drugs inhibit the inflammatory changes that occur as a result of cutaneous ageing and hence may aid in the reversal of age-related symptoms [156].

Aphrodisiac, astringent, cooling, demulcent, and emollient characteristics of Trigonella foenum-graecum Linn. Hair care, hair loss, hair growth, hair colouring, skin cleansing, skin toning, and stimulation are some of its cosmetic applications, and it is also good for facial skin care. The bark, fruit, seed, flowers, leaves, gum, and sap of the Neem tree are all utilised for medical and cosmetic purposes. It's been used to treat boils, catarrhal affections, eczema, and a variety of other skin conditions. The chemical elements of neem are considered antimicrobial and natural preservatives in cosmetics. Neem's limonoids and tetranortriterpenoids are employed in a variety of cosmetic products such as toothpaste, soaps, and shampoos [169, 170]. Because of its healing, mending, and re-equilibrating qualities, Mimosa tenuiflora (Willd.) Poiret is indicated for products with cutaneous regeneration activity, and sun or after-sun protection products. It's found in cosmetics that help with capillary resistance and peripheral microcirculation, such as dermatological treatments, Astringent lotions

and acne gels [171]. Aloe vera Linn. is good for sunburn, small burns, wrinkles, bug bites, skin irritations, minor wounds, and scratches. According to studies, the clear gel has a dramatic potential to cure wounds, ulcers, and burns by coating the damaged areas with a protective coating that speeds up the healing process [172].

Aloe gel's capacity to improve skin circulation and eliminate dead skin cells is one of its most beneficial aesthetic features, giving the skin a brighter, younger appearance. It also lowers wrinkles, removes blemishes, and protects the skin from infections [173]. Aloe shampoo can assist with dry, brittle hair [174]. Salicylic acid, which possesses keratolytic and bacteriostatic effects, is also said to be included in the gel. Because of its antiphlogistic, bacteriostatic, and moisturising properties, it is also recommended as a preventive for dry skin that is prone to inflammation [175]. Turmeric powder paste has been used as an antibacterial and skin nutrition for millennia. Turmeric's primary ingredient, curcumin, is a polyphenol utilised in skin care products. It serves as an antioxidant as well as a protection against rancidity in moisturising lipids.

1.3.2.2 Textiles

The textile industry is the second largest producer of pollution after the oil industry [176]. There is growing evidence and awareness of the environmental harm caused by the textile industry's rising pollution, the wearer's exposure to carcinogenic synthetic textile dyes, the depletion of fossil fuels, the disruption of the ecological balance, and ecological imbalance itself. As a result, the textile industry's research and development efforts are focused on revitalising plant-

based dyes and additives for a more sustainable future [177]. Up until the development of the first synthetic dye in 1856, only natural dyes produced from plant leaves, roots, bark, insect secretions, and minerals were available to mankind for the colouring of textiles [178]. Due to their high biodegradability, low toxicity, green chemistry, and possible use in the textile dyeing and finishing business, herbal colourants are currently a more appealing option. Natural colourants derived from plant sources are regarded as innovative agents for giving textiles multifunctional qualities such as antibacterial, insect repellent, deodorising, and UV protection. Numerous herbs, including turmeric, tulasi, neem, rose, indigo, lemon grass, castor, and ber, can be used to give the fabric medicinal benefits and aroma [179].

In the textile industry, surface modification of textile materials using polymers is becoming more and more important. Functional polyphenols have undergone substantial research among numerous natural and artificial polymers. Polyphenols are the most popular natural bioactive compounds due to their distinct bioactivities, which were previously described. This is especially true in the manufacture of particular functional textiles for medical and skin care purposes. Some polyphenols, such anthocyanin flavonoids, are widely used as natural colourants [180]. By using enzyme catalysis with or without additional substrates, colourless polyphenols can also be converted into coloured compounds [181]. Numerous investigations on the natural phenolic sources used to colour textile products have been published. The most represented and promising source of natural pigments and dyes is plant polyphenols [182, 183].

Bio-active chemicals from plant-based materials such as boldo, chestnut, thyme, peppermint, and gambier were used in the Tintex colour process on natural fabrics such as cotton, wool, and lyocell. As a result, ethically coloured fabrics with antibacterial qualities are produced. The procedure is environmentally beneficial because it does not use salt in the manufacturing process. These extract treatments are mild and was fast in the right amounts. The colour's long-term stability and antibacterial properties are appropriate. As a result, textiles that are both sustainable and functional are produced. A novel plant-based fabric colouration obtained from natural sources such as fruits, spices, and plants attained great attention. Natural coloured eucalyptus cloth sheets were introduced by Buffy USA. A mixture of tea, eucalyptus, and pomegranate was used to create a grey tone. Turmeric, gardenia, and walnut were used to create a blush tone. Blue tones from indigo, safflower and rose would be promoted by the brand. Areetha nut and Shikakai are natural biosurfactants used for washing antique textiles and shampooing hair because they are organic and safe. Herbal residue that is left after washing is naturally medicinal, aromatic, skin-softening, and ecosmart. The tiny residue that eventually makes its way into water systems is eco-friendly and is securely digested by the earth, leaving no effluents, emissions, or carbon footprints behind [184].

1.3.2.3 Dye sensitized solar cells

Recent studies into the use of natural resources in the manufacture of solar cells are a result of the demand for a greener and more ecologically friendly energy generation [185]. The Dye-Sensitized Solar Cell is a photoelectrochemical device that uses

organic dyes to produce energy from light, in contrast to traditional, solid semiconductor solar cells (1st and 2nd generation). It functions on a similar concept to how green plants use photosynthesis. Photosynthesis is the process through which light is changed into chemical energy. When photons strike chlorophyll and other pigments, photo-induced charge separation causes electrons to be ejected [186].

Because they are affordable, plentiful, and sustainable, natural dyes as photosensitizers for DSSCs are particularly appealing. Fruit, leaves, flowers, and algae can all be utilised to extract vegetable dyes that can then be employed in DSSCs [187-192]. Anthocyanins, a type of water-soluble vegetable colours obtained from flowers like malvaceae and anthurium, and leaves like Norway maple, have also been used as DSSC sensitizers by the same group [193]. They obtained an efficiency of 0.56 percent by extracting anthocyanins from California blackberries. Another family of vegetable dyes that have been used in DSSCs to achieve an efficiency up to 2.7 percent are betalains [188, 194]. These colours can be seen in a variety of plant tissues, especially in caryophyllales [195], such as flower petals, fruits, leaves, stems, and roots. An anthocyanin with an o-hydroxychinon moiety is thought to be responsible for the effects of a black rice extract [196]. Among 20 plant extracts, a different study found that a mangosteen pericarp extract had the best effectiveness, at 1.17 percent. Rutin has been identified as the substance that is active [197]. A comprehensive comparison indicated a Rhoeo spathacea extract with an efficiency level of 1.49 percent as an appealing source among others

[198]. The anthocyanins, and anthocyanidins' glycosides, appear to be more effective than the anthocyanidins [199].

1.3.2.4 Sensors

Numerous phytochemicals have enticing optical and electrochemical properties that open the door to their development as optical and electrochemical (bio)sensors for clinical/health diagnostics, environmental monitoring, food quality control, and bioimaging [2]. The creation of sensitive and specific (bio)sensors that incorporate phytochemicals into their construction and design is crucial and would be viewed as a significant step toward developing green (bio)sensing systems. The use of phytochemicals in sensing applications dates back many centuries, and "Litmus paper," which is made by immobilising litmus dye (a combination of different dyes/pigments extracted from lichens) in filter paper, may serve as an interesting example of one of the earliest applications of phytochemicals in sensing. Since the early 14th century, when Spanish alchemist Arnaldus de Villa Nova first employed litmus paper to evaluate acidity/alkalinity, it has been one of the most extensively used pH indicators [200].

Some flavonoids function as chromic materials, changing colour in response to ions and pH levels. The creation of eco-friendly and recyclable smart packages, wearable fabric sensors, and gas and ion sensing all benefit from the appealing properties of these materials. Furthermore, natural pigments attached to fibrous materials can result in halochromic or pH-sensitive fabrics, which can change colour in reaction to pH changes. Anthocyanins have been used by several

research teams for pH sensing, smart packaging, and even wound healing procedures. As a reversible pH sensor in the range of 1–14 in a saliva specimen, electrospun cellulose nanofibers functionalized with anthocyanin, derived from red cabbage, were utilised [201]. It is capable of determining alcohol intake and the progress of wound healing. A fast-acting, repeatable, and stable pH sensor biofilm was created using anthocyanin that was isolated from *B. blakeana Dunn* and immobilised on chitosan. The created pH sensor film demonstrated excellent potential for application as a smart package for pork and fish freshness monitoring [202]. Due to their ability to change colour with an increase in pH brought on by volatile amines created by storing meat, the extracted natural colours (anthocyanins) from red cabbage and rose flowers were immobilised on filter paper and subsequently employed as intelligent packages [203]. In order to create an optical gas sensor for the detection of formaldehyde, Meng et al. immobilised rose anthocyanin within ormosil, an organically modified silicate/silica [204]. According to Da Silva et al., a colorimetric sensor for the detection of Al (III) in aqueous samples was created by immobilising anthocyanins in a polymer composition made of carboxymethylcellulose and starch. In this research, black rice's starch and anthocyanins were isolated [205]. Quercetin is a fluorescent sensor was used for Cu(II) determination in water samples [206]. It has been shown that quercetin phosphate may detect Pb(II) fluorescence in soil and water samples [207]. For Al(III) sensing in food packaging, quercetin-carboxymethyl chitosan film has also been used [208]. Density functional theory simulations and spectrophotometric evidence

both supported quercetin's potential as a chemoprobe for Fe(III) sensing [209].

Maclura tinctoria, Maclura pomifera, and Psidium guajava extracts are rich in yellowish flavonol pigment known as morin. Jiang et al. developed the Ce(IV)-bromhexine hydrochloride-morin system for the flow injection chemiluminescent measurement of bromhexine hydrochloride. For sensitive fluorescence determination of Al(III) in a "off/on" mode, sodium morin sulfonic acid was used as the morin derivative dye, and [MSA:Al(III)] complex for fluoride anions in a "off/off" mode [210]. It has been observed that rutin (Qur-3-O-rutinoside), also known as rutoside or sophorin, is a nonfluorescent or very weakly fluorescent flavonoid, yet it exhibits good electrochemical activity. Using fluorescent CDs and rutin, Kong et al. developed a fluorescence resonance energy transfer (FRET) device for sensing Al(III) [211]. Yang *et al.,* demonstrated that isorhamnetin, a flavonoid derived from Ginkgo Biloba leaves, could be successfully employed for fluorescence sensing of Cu(II) in samples of river and lake water as well as fruits and vegetables. The complex formation Cu(II)-isorhamnetin and resulting fluorescence quenching of isorhamnetin was considered as the postulated mechanism for fluorescence detection of Cu(II) [212]. Kaempferol-Al(III) [213] and Kaempferol-Eu(III) [214] complexes were used in combination with surface-enhanced fluorescence effect of silver nano particles as fluorescent probes for nucleic acid detection.

Catechin is a naturally occurring flavanol that is frequently found in tea and is typically used as a chelator to detect metal ions.

Using a catechin-dopamine fluorescence sensor, it was possible to detect Hg(II) and Cu(II) in water samples with extreme sensitivity [215]. Chalcones are a class of polyphenolic chemicals from the flavonoid family that have aromatic ketone and enone structures. A multi-signaling chemosensor that can detect copper(II) fluorimetrically, colorimetrically, and electrochemically was created using chalcone as the optical active unit and ferrocene as the electrochemical moiety attached to triazole-capped triethoxysilane [216]. The chalcone derivatives have also been used to detect cyanide anions (CN⁻) [217] and thiophenols in seawater samples [218] as well as for hydrazine sensing/bioimaging in living cells and zebrafish embryos [219].

1.3.2.5 Corrosion inhibitors

The metallic materials, particularly alloys, are widely used as building and construction materials, because of their many advantageous qualities, such as great mechanical power and cost effectiveness. However, the majority of metals and their alloys are extremely reactive in their pure form and easily degrade through corrosive reactions with the elements of the atmosphere. The corrosion issue is more severe when metallic ores are processed to produce pure metals. These procedures use acidic solutions that are highly concentrated and cause the breakdown of metallic components as well as surface contaminants like rust and scale. Therefore, many external chemicals known as corrosion inhibitors are added to the acidic solutions to reduce the loss of metallic components. These additives

adsorb and create a barrier that keeps the metals away from hostile environments [220].

A significant and well-researched industrial issue, corrosion of metals and alloys have found a promising research area in green chemistry. Due to their safety, biodegradability, ecological acceptability, and renewability, green inhibitors are generating a lot of interest in the corrosion sector [221]. The presence of aromatic hydroxyl groups is primarily responsible for polyphenols' corrosion-inhibiting effects. This is once more explained by the capacity of heteroatoms to donate electrons to coordinate bonds with open d orbitals of metal. Additionally, interactions with rings that contain conjugated bonds and electrons allow molecules to adsorb on metal surfaces [222]. El-Etre published a report on how olive leaf extracts can prevent corrosion in carbon steel. Dry olive leaves were cooked in water for three hours, and then the filtrate was evaporated, leaving behind a solid residue that was used to make the necessary inhibitor solutions. The adsorption of oxygen atoms' lone pairs of electrons, which create a covering layer and serve as a barrier between the steel surface and the hostile solution, was thought to be the cause of the phenomenon that prevents steel from corroding in acid. Additionally, the arrangement of oxygen atoms around the aromatic rings of phenols may suggest that phenolic molecules are compelled to be adsorbed horizontally onto the steel surface. Olive (Olea europaea L.) leaf extract in aqueous form contains polyphenolic substances with antioxidant potential. Oleuropein and hydroxytyrosol were found as the principal components. The additional polyphenols in the mixture

include gallic acid, tyrosol, and oleuropein aglycone. Oleuropein quickly breaks down into hydroxytyrosol and elenolic acid, hence hydroxytyrosol may be the primary factor inhibiting the process [223].

In a more recent study, a methanol extract from the *Cryptostegia grandiflora* plant which is rich in myricetin, quercetin, and rutin was used to evaluate the polyphenol composition and anticorrosion qualities of mild steel [224]. Abdallah and coworkers used a different strategy, choosing four distinct commercial phenols, and analysing each one's individual inhibitory effects on steel corrosion. The presence of amine, hydroxyl, aldehyde, or carboxyl groups in ortho-position with regard to the phenol served to identify the compounds. The following was the order of inhibitory effectiveness: It goes $NH_2 > OH > CHO > COOH$. The sequence led to the conclusion that compounds with electron donating groups work as inhibitors more effectively than those with electron withdrawing groups. The electron-donating groups boost adsorption, raise electron density, and make the system more nucleophilic, all of which increase the effectiveness of inhibition. Additionally, theoretical calculations for HOMO-LUMO orbitals were given [225]. According to Wei Tan et al., condensed tannin was the factor in the inhibitory properties of *Rhizophora apiculata*'s extracts [226]. Studies showed that high concentrations of gallic acid, tannic acid, and ellagic acid are responsible for the anticorrosive activity of *Punica granatum* plant extract [227]. The efficiency of Lavandula mairei (LM) for MS in inhibiting corrosion in a 1M HCl system was examined using experimental and theoretical methods and the authors reported

glucuronide of quercetin-3 as the major content responsible for its anticorrosion activity. The study also explained the donor-acceptor mechanism, in which a number of heteroatoms with polar functional groups served as adsorption sites, by DFT analyses of neutral and mono-protonated quercetin-3-glucuronide's interactions with MS surface [220].

Several extracts are evaluated as inhibitors against metallic corrosion due to their environmentally friendly behaviour and excellent inhibitory efficiency. Naturally, plant extracts have a variety of simple to complex phytochemicals that can efficiently adsorb across metal surfaces and form shields. Aqueous extracts are chosen because of their generally more sustainable qualities, while organic solvents can also be used to make extracts. Furthermore, the majority of organic solvents are relatively expensive, making their usage for extraction an inefficient use of resources. Furthermore, the majority of organic solvents are poisonous and unfriendly to the environment, which severely restricts their usage in extraction [220].

All the above mentioned studies outline the importance of polyphenols in both biological system as well in the industrial field. There are still a lot of opportunities to be explored in the filed of phytochemicals. For instance, computational studies offer tremendous potential in revealing properties and potential of phytochemicals. Aspects such as anti-oxidant nature, molecular docking, molecular dynamic simulation, and corrotion inhibition nature are discussed in the next sections.

1.4 Free radical-scavaging properties of phenols: quantum chemistry modelling

In the human body, free radicals are produced by metabolic reactions taking place in living cells. Free radical generation can also be aided by external elements like stress, pesticides, radiation, contaminated water, and different medical procedures. Free radicals can harm biomolecules including proteins, lipids, and DNA because of their high reactivity, which can start radical chain reactions. As a result, bodily tissues are damaged. Free radicals have also been suggested as a significant contributor to ageing and a number of chronic illnesses, such as cancer, diabetes, cardiovascular disease, and neurological problems. Therefore, it is crucial to find agents that can protect against free radicals. Extensive studies have been done on the antioxidant activity of phenols as well as the physico-chemical characteristics and structural aspects of phenolic compounds that govern their potential to act as antioxidants [228-230]. Particularly, with the advancement of computational approaches, theoretical calculations have recently developed into effective tools (requiring less money and time) for estimating the antioxidant activity of a molecule with an accuracy comparable to or better than those acquired by experiments. The early computational investigations either focused on a small set of compounds or used empirical structure descriptors and semiempirical quantum chemical calculations, or they were carried out on simple substituted monophenols. The scientific community now has easy access to computer resources thanks to recent technological

advancements, which have substantially aided theoretical studies on the anti-oxidant capabilities of phenols.

Generally speaking, density functional theory (DFT) studies are a family of methodologies for calculating the electronic structure of quantum mechanical systems that can be used to calculate the electronic structure of organic and main group molecules as well as more complex systems without adding extra computation time [231]. Density functional theory (DFT), which is one of several theoretical calculation techniques, is thought to be the best way for determining the antioxidant capabilities of medium-sized and big flavonoids since it has a high degree of accuracy, costs little, and takes little time. The focus of the current section is on quantum calculations, particularly the density functional theory (DFT) approach, to survey antioxidant activity and the mechanisms of action of various antioxidants.

In the past ten years, the rise in computational power available to researchers has coincided with an increase in the number of computational studies on phenolic antioxidants. Numerous more thorough and precise analyses, including the entire DFT geometry optimization of quite large polyphenol molecules and their potential radical products, the use of extended basis sets [232, 233], higher level theory *Ab initio* calculations [234], and double-hybrid or highly parametrised density functionals in DFT calculations[235, 236] for a more precise determination of the studied parameters, and determination of the activation energies (EA) for various reaction pathways in various environments in order to expose the true

mechanisms and kinetics of radical scavenging by the polyphenols [237]were made available by this computer capacity.

The primary role of polyphenolic compounds is to directly inhibit free radicals, which is known as free radical scavenging activity. Antioxidants can work through a variety of chemical pathways, but the four most crucial ones are formal hydrogen atom transfer (HAT), sequential electron transfer proton transfer (SETPT), radical adduct formation (RAF), and sequential proton loss electron transfer (SPLET). Calculating each mechanism's molecular thermodynamic indicators, such as its bond dissociation enthalpy (BDE), proton dissociation enthalpy (PDE), ionisation potential (IP), electron transfer enthalpy (ETE), and proton affinity (PA), can help determine how feasible these mechanisms are [238].

The quantum chemical descriptors and associated research on phenolic antioxidants are of extraordinary significance in the study of antioxidant behaviour. Reactivity indices like electro-accepting/donation capacities ($\square+$ and $\square-$) and the -OH BDE values are crucial among these descriptors. In particular, where electron transfer processes like SET, SPLET, and SETPT are significant, the discovery of electron-donating ($\square-$) and electron-accepting ($\square+$) as well as the related Acceptor index (Ra) and Donor index (Rd) has caused a substantial effect in the analysis of antiradicals. This makes it simple to classify antiradicals according to anti-oxidant and anti-reductant properties as well as into the best, worst, and most effective antiradicals.

The donator-acceptor map (DAM) is a good option for performing quick and simultaneous assessments of the relative electron-donating and electron-accepting features of a set of species. It is predicated on the premise that a quadratic interpolation for the energy as a function of the number of electrons can accurately depict a molecule's response to an idealised environment that can either remove or donate charge in a straightforward charge-transfer model. Since DAM has both □+ and □- properties, it tends to act as an antioxidant in processes involving charge. The type of the interacting free radical can have such a big impact that it can even flip the relative importance of the free radical scavenging mechanisms, hence it has been taken into consideration by the development of the Full electron-donor-acceptor map (FEDAM), an upgraded version of DAM. With Na and F atoms serving as references once more, FEDAM is based on the relative values of the electron acceptance (REA) and electron donation (RIE) indices obtained from vertical ionization potential (IP) and vertical electron affinity (EA) [239].

Theoretical studies have been carried out by Ana Martinez et al. to assess the donor-acceptor behaviour of certain antioxidants, such as carotenoids, melatonin, and vitamins. They accomplish this by using DAM-FEDAM plots [240]. The antiradical characteristics and potential modes of action of the tautomers of curcumin, caffeic acid phenethyl ester (CAPE), and chicoric acid (CA) have been investigated using M06-2X functional with the 6–31+G* basis set by Brenda Manzanilla et al (DFT). DAM and FEDAM plots revealed the better antiradical property of curcumin (keto-enol curcumin (CKE) and

diketone curcumin (CDK) [241]. In this manner, the antiradical can be divided into anti-oxidants and anti-reductants.

Theoretically derived parameters that are helpful in describing and explaining the radical-scavenging activity of antioxidant phenols were initially put out, debated, and contested in computer research carried out in the 1990s. Extensive research into the theoretical parameters related to these physico-chemical properties (computed BDE and ionisation potentials, IP) was prompted by the correlation of experimentally determined phenolic OH bond dissociation enthalpies (BDE) and half-peak oxidation potentials (Ep/2) with the rate constants k4 or k5 of reactions of phenols with different free radicals. The identification of mechanisms of reactions other than HAT spurred the development of theoretical correlates for the rate-limiting factors SET and SPLET (proton dissociation enthalpies, PDE, proton affinity of phenoxide ion, PA, and electron transfer enthalpy, ETE).

For a broad collection of substituted mono- and polyphenols, Wright and colleagues used DFT-based quantum chemical calculations to determine BDE and adiabatic IP. For computations of the electronic properties of AM1-optimized geometries, B3LYP functional with a variety of basis sets (6-31G, 6-31G(d), 6-31G(d,p), and 6-31G(d',p')) was utilised. The BDE computations were performed using the locally dense basis sets (LDBS) methodology. The variations between the experimental and LDBS-calculated BDE values were within 3 kcal/mol. Based on these theoretical investigations, numerous new fully substituted catechol's structural variants were created *in silico*, synthesised, and demonstrated to be more potent antioxidants than -

tocopherol [242]. Klein and Luke confirmed the relationship between BDE and the empiric Hammett-Brown substituent's constants σ_p/σ_m using both experimental data and B3LYP/6-311++G**-optimized geometries of para- and meta- substituted phenols [243, 244].

The rapid expansion of studies using computer modelling to analyse natural polyphenolic compounds is one of the noteworthy trends. Ranking BDE, PDE, and adiabatic IP for the several hydroxyl groups in the polyphenol's structure (to distinguish between HAT, SET, and SPLET processes) offers important knowledge regarding the preferred first step in these compounds' interactions with free radicals [245-247].

A common class of phenolic chemicals that is a part of the vast flavonoid family are anthocyanins and anthocyanidins. In this regard, all of the major anthocyanidins show high antioxidant qualities when compared to the well-known antioxidant vitamin E, with delphinidin likely being the best of the bunch [248]. Rosa Guzmán used the B3LYP/6-31G(d,p) method to conduct dft studies in an effort to comprehend the antioxidant characteristics of some anthocyanidins. According to an analysis of the computed findings, the antioxidant capacity of those structures is ranked as follows: cyanidin > malvidin > aurantinidin > delphinidin $\geqslant$ peonidin > pelargonidin [249]. The anthocyanidins apigeninidin, pelargonidin, peonidin, and malvidin as well as the 3-, 4′-, 5-, or 7 flavylium ions and their phenoxyl radicals were studied using DFT, and certain details regarding their molecular planarity, charge distribution, and resonance stability of their radicals were discovered. Ring B orientation and compound planarity are

influenced by the presence and orientation of the 3-OH bond, whereas compounds and radicals without the 3-O-H link were discovered to be planar. With the exception of malvidin, where 4′-OH had less BDE than 5-OH bond due to the additional stability provided by the two o-OMe groups, the bond dissociation energy of O-H bonds in anthocyanidins was in the range of 3< 5< 4′< 7-OH bond. By resonating with the carbons 2, 5, 7, 9, and 4′, positive charge was stabilised. The 3-anthocyanidin radicals were stabilised through unpaired electron resonance with the 5, 7, or 4′ oxygen atom, whereas the 5, 7, or 4′ radicals were stabilised through resonance with the pyrylium or 3′ oxygen atom. The maximum spin density is maintained by radical oxygen, which also creates a carbonyl group (C=O) with a nearby carbon atom. Also seen was the unpaired electron's delocalization, which was more pronounced in planar radicals but also found in the three rings. A strong correlation between experimental radical scavenging activity and the charge and unpaired electron delocalization as reflected by the charge and unpaired electron density on radical oxygen has been discovered [250].

The capacity of pyranoanthocyanins, which are found in aged wine and result from the chemical transition that anthocyanins underwent, to scavenge free radicals was theoretically investigated by DFT/B3LYP methods, by Monica Leopoldini et al. The O-H bond dissociation energy (BDE) and ionisation potential (IP) parameters were determined in the gas phase as well as in water and benzene solutions. The two primary functioning mechanisms (H atom donation and single-electron transfer) were also examined. According to the

findings, systems with both the catechol functionality and the o-dimethoxy motif are excellent candidates to donate a H atom to the free radicals, rendering them inactive. Higher degrees of electron delocalization in compounds may allow them to function within the single-electron transfer mechanism [251].

The effect of pH on various hydroxyl flavones' antioxidant capabilities was studied computationally by Katarzyna and colleagues. By using the Trolox Equivalent Antioxidant Capacity (TEAC) assay, they established a Qualitative Structure Activity Relationship (QSAR) model to calculate the pKa values of hydroxyl flavones. They discovered that the TEAC value rises as a result of deprotonation. The best explanation for the radical-scavenging ability of hydroxyl flavones, they discovered, is the HAT mechanism. These findings are also supported by the study of the antioxidant capacities of hydroxyl flavones using the DFT-B3LYP/6-31+ G (d, p) model [252].

Huai Cao and coworkers interpreted the ability of rosmarinic acid to scavenge the radicals by its structure based on the geometry of the ground state molecule and its free radical, the HOMO and LUMO, the O-H bond dissociation energy (BDE), and the single electron density distribution of the radicals. According to them, the greater antioxidant activity of rosmarinic acid in comparison to flavonoids may be caused by the abstraction of hydrogen atoms from the ortho-position hydroxyls on the rings A and B. The radical created by the H-abstraction of the ring A was more stable than the radical created by the H-abstraction of the ring B, but the ring B is a stronger electron donor than the ring A. They also discovered a strong correlation

between the unpaired electron delocalization, which is used to demonstrate the stability of the parent molecule, and the BDE, which measures the stability of the free radical [253].

The structural characteristics and electronic properties of two naturally occurring flavonoid compounds, apigenin and scutellarein, were clarified by K. Sadasivam and colleagues using the B3LYP/6-311G(d,p) theoretical technique. According to calculations using density functional theory, apigenin's B-ring plays a major role in its antioxidant property, whereas scutellarein's A-ring plays that role. This shows that in the absence of the o-dihydroxy pattern in the B-ring, the hydroxyl substituents in a catechol structure on the A-ring are what determine the flavonoid's antiradical action. The planar structure impacts the characteristics of the HOMO in the adiabatic ionisation potential situation and lowers the energy needed to remove a single electron. The ionisation potentials of these two compounds are discovered to be in the same range as that of synthetic food additives, with scutellarein (160.69 kcal/mol) having a lower ionisation potential than apigenin (172.91 kcal/mol) [254].

The antioxidative effects of quercetin and its glucosides in the gas, ethanol, and water phases were explored from a theoretical perspective by Yan-Zhen Zheng and colleagues. The enthalpies of charged species are significantly altered by solvents, which has a major impact on SET-PT and SPLET, particularly the value of PAs. Therefore, the surroundings can change the thermodynamically favoured mechanism of the antioxidative progression for quercetin and its glucosides. HAT is the thermodynamically dominating mechanism

for the antioxidative process in the gas phase, while SPLET is more preferred in the ethanol and water environments. According to the computed results, OH groups in the B-ring and C-ring contribute more than OH groups in the A-ring to the antioxidative actions of quercetin and glucosides [255].

By using the computational approach B3LYP/6-31+G(d, p), two valuable flavonoids with strong biological qualities, calycopetrin (Cal) and xanthomicrol (Xan), were thoroughly examined to gain structural and electronic information in both the gas phase and water. The 1HNMR and 13CNMR experimental data used to test the computational method showed high agreement between the computational and experimental chemical shifts. The reaction of Cal and Xan with oxygen radicals such HO•, HOO•, and O_2•- demonstrated their potent antioxidant abilities. The stability of the radicals created by the conjugate system in their structure is the primary cause of this feature. Cal has better antioxidant capabilities than Xan because the methoxy group acts as an electron donor group on the pyrene ring. Analysis of the examined compounds' reactivity with oxygen radicals revealed that OH• may react with these compounds to extract the hydrogen radical [256].

Pinocembrin, isosakuranetin, and eriodictyol were examined for their antioxidative properties by Aban Erdoan and co-workers. According to the results, HAT is a potential route for antioxidant action in the gas phase, while SPLET is a competing mechanism in the aqueous phase. The most active locations of eriodictyol, isosakuranetin, and pinocembrin for scavenging OH˙ in the gas phase

are 4', 5, and 7, respectively [257]. Chrysoeriol and hispidulin, two naturally occurring flavonoid compounds, have been studied for their structural characteristics as well as their antioxidant activity using the B3LYP/6-311G(d,p) theoretical technique. Chrysoeriol and hispidulin flavonoid compounds exhibit planar structure, according to the theoretical conclusions that were computed. 4′-OH is the most stable radical species in both compounds' gas phase. The B-ring plays a substantial role in both flavonoid molecules, according to this theoretical calculation. Chrysoeriol and hispidulin both have low BDE values for the B-ring, 84.4 kcal/mol and 84.1 kcal/mol, respectively, indicating that the B-ring is more reactive than the A-ring in both flavonoids [258].

Lingling Wang and coworkers investigated the antioxidant activity of (+)-Catechin (CAT) and its two derivatives, substituted by the electron-donating group -N(CH3)2 (CAT-DA) and electron-withdrawing group -CF3 (CAT-TF), in gas and solvent phases using the density functional theory approach. The obtained BDE, IP, and PA values indicate that the antioxidant reaction of these three compounds favours the HAT mechanism in the gas phase with the lowest BDE values of 75.2 kcal/mol, 74.4 kcal/mol, and 78.6 kcal/mol for CAT, CAT-DA, and CAT-TF, respectively and SPLET mechanism in solvents like methanol, ethanol, and water. Additionally, as solvent polarity increases, the expression of the SET-PT mechanism is favored while the SPLET mechanism is suppressed. And when compared to the other two solvents, the three compounds would exhibit the maximum antioxidant activity in the ethanol phase [259].

The radical scavenging mechanisms of curcumin and its structural counterparts (hispolon, halfcurcumin, and polyhydroxy curcumin) have been compared using density functional theory in both gas and aqueous phases. Similar findings were shown by the relative Gibbs free energy associated with the hydrogen atom transfer mechanism for OH• and OOH• scavenging by antioxidant molecules in both gas and aqueous environments. Based on the thermodynamic information, it is projected that the molecules will react with OH• more readily than with OOH•. When compared to curcumin in both the gas and solvent phases, half curcumin demonstrated almost identical activity. The numerous hydroxyl groups are organised in ortho dihydroxy form, enabling increased radical stability through internal H bonds and making the hispolon and polyhydroxycurcumin better radical scavengers than curcumin [260].

Using the DFT approach, Yan-Zhen Zheng et al. investigated multiple free radical scavenging responses for five flavonoids: ampelopsin, dihydro orobol, eriodictyol, hesperetin, and taxifolin. The studies showed that, the hydroxyl groups that operate as hydrogen-bond donors (5OH, 3OH, and 3'OH) have less antioxidant activity while hydroxyl groups that act as acceptors (4'OH), which has more antioxidant activity due to intramolecular hydrogen bonding interaction [261]. Gabriel L. C. de Souzaa et al reported a comparative study on the O–H bond dissociation enthalpies (BDEs) and ionization potential (IP) for the antioxidant polyphenol gallic acid in both the gas-phase and water under DFT, MP2, and coupled cluster approaches using 6-311++G(df,p), cc-pVDZ, aug-cc-pVDZ, cc-pVTZ, and aug-cc-

pVTZ basis sets. They came to the conclusion that, when compared to the corresponding CCSD(T)/aug-cc-pVTZ results, M06-2X provided the best agreement for the BDEs. M06-2X was also found to be the most suitable for probing the IP for the protonated forms of GA, while LC-PBE was the most reliable in the case of deprotonated GA [232].

18 polyphenol structures (13 hydrolyzable tannins, 4 flavonoids, and ellagic acid) and their molecular characteristics (volume, area, dipole moment, polarisability, LogP, EHOMO, ELUMO, and ELUMO-EHOMO gap) were studied by Suzana C. Santos et al. using the M062X/6-311 + G (d,p) level of theory. The experimental antioxidant activities determined by the ORAC and DPPH assays and molecular and lipophilic parameters were correlated using the multivariate regression tree (MRT) and canonical redundancy analysis (RDA). Following a gradient of increasing antioxidant activity, a multivariate regression tree divided compounds into four clusters; the cluster with the highest antioxidant activity was primarily made up of monomeric and dimeric ellagitannins [262].

Antioxidative mechanism of chlorogenic acid is very complex in aqueous solution. By combining the theoretical M06-2X approach with the 6-311++G(d,p) basis set, Jelena Tošović and co-workers studied the behaviour of the monoanion and dianion of chlorogenic acid in a simple aqueous solution. The research demonstrated that because all of dianion's antioxidative reactions are diffusion regulated, its role in scavenging HO• is roughly equivalent to that of monoanion, which is far more prevalent. Interestingly their calculated overall rate constant value of $4.83 \times 109 M^{-1} s^{-1}$ is in perfect accord with the

experimental value of $3.34 \pm 0.19 \times 10^9 \, \mathrm{M^{-1} \, s^{-1}}$. They also came to the conclusion that anionic forms of 5CQA only undergo HAT mechanism with the CH3OO• and that these reactions are slower than those with HO• [263].

Three flavonoid compounds from the Arbutus unedo L. plant were examined by L. Messaadia et al for their antioxidant properties. The order of the antioxidant capacity of the title compounds in various conditions was Fisetin > Catechin > Apigenin, based on the lowest BDE values which is in good agreement with the experimental test. According to their findings, HAT mechanism is the most advantageous thermodynamic mechanism for explaining free radical scavenging in the gas phase and in benzene, a non-polar solution and SPLET mechanism in polar media like water and methanol. The 4′-position hydroxyl group has lower values in the gas phase and solvents than the other OH groups [264].

A substantial amount of information on the mechanisms of reactions between phenolic compounds and free radicals has been obtained through quantum chemistry research. These studies which outline a number of features having a critical function for phenolics' capacity and activity to scavenge radicals. In quantitative structure-activity relationship (QSAR) investigations, the resulting quantum chemical parameters and other molecular descriptors were used to create novel, more potent phenolic antioxidants and to identify the most beneficial naturally occurring phenolic antioxidants.

1.5 Molecular docking and molecular dynamic simulation as powerful tools for studying the pharmacological activity of polyphenols

A methodical approach is required to increase the probability of discovering new drugs, to take advantage of the chances presented by potential new drug targets emerging from genomic and proteomic initiatives, and from the vast libraries of small compounds that are currently easily accessible through combinatorial chemistry. Despite a rocky beginning, computer-aided drug design techniques can now be useful for cutting costs and accelerating drug discovery. This pleasing result is due to the creation of more precise and trustworthy algorithms, the application of more carefully thought-through application techniques, and significantly greater computing power that enables research with the required reliability to be carried out. The molecular docking and thermodynamic-based molecular dynamics (MD) simulation are the two prominent toolboxes for *in silico* drug discovery. Molecular docking makes use of the atomic-level interactions between tiny molecules or large molecules and protein receptors to determine how they connect to one another. A substantial complement to docking is provided by MD simulation approaches. A protein-ligand, protein-protein, protein-nucleic acid, and protein-peptide complex's structural characteristics can be evaluated well using these methods. This session is organised to guide the reader from the quick and affordable docking algorithms used to scan enormous chemical libraries and shrink them to the more precise but more expensive MD simulations that can be utilised when only a few carefully chosen ligand candidates are left [265].

Molecular docking is an important tool in structural molecular biology and computer-aided drug design. It is a structure-based drug design technique that simulates the molecular interaction and predicts the binding mechanism and affinity between receptors and ligands, where the receptor is often a protein or a nucleic acid molecule (DNA or RNA), and the ligand is either a tiny molecule or another protein. Another way to describe it is as a simulation process where a ligand position in a projected or pre-established binding site is estimated. This method has been extensively employed in the field of drug design research in recent years. It has been significantly made easier by the rapid increase in computer power and availability, as well as the expanding accessibility of small molecule and protein databases. Molecular docking has a wide range of uses and applications in drug discovery, such as structure-activity studies, lead optimization, locating potential leads through virtual screening, providing binding hypotheses to facilitate predictions for mutagenesis studies, assisting x-ray crystallography in the fitting of substrates and inhibitors to electron density, chemical mechanism studies, and combinatorial library design [266].

Through the use of docking validation techniques, which compare in silico protein-ligand or protein-protein conformations to structures discovered through X-ray crystallography or nuclear magnetic resonance, molecular docking simulations can be used to replicate experimental findings. Additionally, docking is a key technique for virtual screening processes, where a library of several compounds is "docked" against a single therapeutic target to determine

which hit is most likely to be successful. Over 50,000 protein structures can be found in structure databases like Protein Data Bank (PDB) and Worldwide Protein Data Bank (wwPDB), and many of these structures could serve as potential therapeutic targets. In addition, there are numerous databases for small molecules, including ZINC, PubChem, ChemDB, and Drug Bank, which have more than one million deposited structures of possible ligands [267].

One of the most flexible and often used computer methods for analysing biological macromolecules is molecular dynamics simulation. They are highly useful for comprehending how proteins behave dynamically at various timescales, including quick internal motions, gradual conformational changes, and even the processes of protein folding. The study of molecular dynamics, which simulates the motions of a system of particles and is applied to biological macromolecules like proteins and DNA, reveals variations in the relative positions of atoms over time. Understanding these motions can help us better understand a variety of biological processes, including how flexibility affects ligand binding. Molecular dynamics is also used to determine protein structures from NMR, to improve protein X-ray crystal structures more quickly from less accurate starting models, time-averaged properties of the biomolecular system, such as density, conductivity, and dipolar moment, various thermodynamic parameters, such as interactions energies and entropies, and to investigate the impact of explicit solvent molecules on protein structure and stability [265, 268].

In order to anticipate protein-ligand complexes more accurately, fast and affordable docking processes can be paired with precise but more expensive MD approaches. The complementarity of their skills and weaknesses is what makes this combination effective. On the one hand, docking techniques are utilised to quickly explore the wide conformational space of ligands, allowing for the cost-effective examination of sizable libraries of drug-like molecules. The two main flaws are the protein's lack of flexibility, or low flexibility, which prevents it from changing its conformation upon ligand binding, and the lack of a distinctive scoring function that is generally applicable and required to produce a trustworthy ranking of the final complexes. However, MD simulations have the flexibility to handle both ligand and protein in a flexible manner, enabling an induced fit of the receptor-binding site around the newly added ligand. Additionally, highly precise binding free energies can be measured, allowing for direct study of the impact of specified water molecules. The system can become stuck in local minima, which is one of the fundamental issues of MD simulations, in addition to their time-consuming nature. Consequently, it makes sense to combine the two methods in a protocol where docking is used for quick screening of large libraries and MD simulations are then used to investigate protein receptor conformations, optimise the structures of the final complexes, and calculate precise energies. This will help the drug-design process [265].

In the search for natural inhibitors, researchers are becoming more interested in the naturally occurring active components found in

plants. Among the alternatives, polyphenols have demonstrated a potential inhibitory impact. The potential for quercetin to suppress tyrosinase activity has been well examined as a representative flavonoid molecule. It has been demonstrated that cinnamic acid has an inhibitory effect on the expression of enzymes related to melanin. Additionally, it has been discovered that isorhamnetin may act as a tyrosinase inhibitor [269]. Several polyphenols, including catechins [(−)-epigallocatechin-3-gallate, (−)-epigallocatechin, (−)-epicatechin-3-gallate], flavones (kaempferol, kaempferol-3-glucoside, quercetin, naringenin) and hydroxycinnamic acids (rosmarinic acid, caffeic acid, p-coumaric acid), were examined for their ability to bind to bovine serum albumin (BSA) by Mihaela Skrt. High binding energies for (-)-epicatechin-3-gallate and (-)-epigallocatechin-3-gallate were predicted by molecular docking for the binding site on BSA close to Trp213. The data show that the polyphenol structures have a substantial impact on the binding process. Glycosylation and a reduction in the amount of hydroxyl groups on the second aromatic ring often result in a decrease in binding affinity [270].

Since starch is the principal source of exogenous glucose in the human diet, amylase is crucial for starch digestion. Potential management and/or therapeutic strategies for type II diabetes include slowing the digestion of starchy meals by blocking α-amylase in the digestive tract. Polyphenols' ability to inhibit α-amylase is due to their ability to bind with both the enzyme and polyphenols. An essential role for polyphenols is played by the galloyl moiety. Since the inhibition is likely to depend on the formation of hydrogen bonds between -OH

groups of phenolics and side chains of amino acids (such as Asp197 and Glu233) at the active site of α-amylase, hydroxyl (-OH) groups are crucial for the inhibitory activity of flavonoid compounds against α-amylase. The likelihood of flavonoids being efficient inhibitors of α-amylase is higher for those without substitution of $-OCH_3$ at -OH in their molecular structures than for those with such substitution patterns. Flavonoids' inhibitory effect is also somewhat influenced by the 2,3-double bond in ring C. It has been proposed that the benzopyrone system (rings A and C) can form a highly stable conjugated - system with the indole ring of Trp59 at the active site of α-amylase, promoting its binding to -amylase and decreasing the catalytic activity. In addition to weakening conjugation, hydrogenation of the 2,3-double bond in flavonoids changes the molecules' near-planar molecular shape (flavonol and flavone) into a more flexible, non-planar stereochemical structure (flavanone and flavanols), which hinders their capacity to bind to α-amylase [271].

A diverse set of haematological illnesses known as leukaemia are distinguished by the unchecked and abnormal proliferation of leukocytes. Hamza Mechchate et al. investigated the anticancer potential of polyphenols like catechin, epicatechin, epigallocatechin, gallocatechin, oleuropein, rutin, chlorogenic acid, and vanillic acid against four receptors as targets (ABL kinase, ABL1, BCL2, and FLT3) of high interest in antileukemic research and therapy to reveal their potential mechanism of action through receptor-ligand analysis. Among the selected components, they noted that epicatechin exhibited the best affinity for the ABL kinase; epicatechin gallate was the most

active for ABL1 and Bcl-2; and catechin demonstrated the highest affinity for the FLT3. For majority of the studied receptors, rutin had good affinity [272].

The discovery of novel, more focused, and less harmful chemo preventive medicines has been made possible by our growing understanding of the molecular underpinnings of carcinogenesis. In order to investigate the potential molecular targets and to confirm the experimental activity testing for 28 plant-derived compounds, Narumol Phosrithong *et al.,* performed docking using various enzymes and receptor proteins involved with cell cycle, cell growth, and DNA replication (cyclin-dependent protein kinase 2 (CDK-2), CDK-6, DNA topoisomerases I and II, B-cell lymphoma 2 (Bcl-2), and vascular endothelial). According to the docking studies, lupeol has a greater binding interaction with CDK-2 and Bcl-2 than the established CDK-2 and Bcl-2 inhibitors. In comparison to other known CDK-6 inhibitors, epigallocatechin gallate (EGCG) was discovered to bind to CDK-6 with a tighter association. Quercetin demonstrated very high binding association with telomere: G-quadruplex, while green tea catechin docked best with topoisomerase II and VEGFR-2. The correlation between the docking energy-derived inhibition constant (Ki) against Bcl-2 and the experimentally determined Ki was strong. They came to the further conclusion that the computed Ki might be utilised as a preliminary tool for Bcl-2 inhibitor screening before undertaking experimental activity assay [273].

Numerous carcinomas are caused by β-catenin, which functions as a co-activator and is often found in combination with trans acting

TCFs or LEF-1. By preventing the transcriptional activation of β-catenin/TCF target genes, inhibition of this complex may operate as a therapeutic agent. Hira Iftikhar and coworkers investigated the structural features of flavonoids to understand the molecular basis of β-catenin/TCF4 inhibition. Isorhamnetin, fisetin, genistein, and silibinin, known inhibitors, had binding energies that ranged from -5.68 to -4.98 kcal/mol, whereas novel inhibitors (catechin, luteolin, coumestrol, and -naphthoflavone) had binding energies that ranged from -6.50 to -5.22 kcal/mol [274].

Alzheimer's disease is one of the leading causes of death in developed nations and is causally connected to the accumulation of amyloid-peptide. Najmeh Mahmoodabadi et al. used quantitative structure-activity relationship (QSAR), molecular docking, and molecular dynamics simulation to compare the inhibitory impact of amyloid- β aggregation in the presence of 25 polyphenolic substances. The findings demonstrated that luteolin, transilitin, and maritimetin were recognised as highly effective inhibitors of Aβ aggregation and MD simulation revealed that these compounds reduced protein aggregation and unfold enzyme structure [275]. A flavanone called naringenin (Nag) is well known for its neuroprotective properties. Treatment for neurodegenerative illnesses that lowers free iron is possible by inhibiting human transferrin (hTf). By using molecular docking analyses, Shama Khan and colleagues were able to determine how Nag binds to hTf with a high affinity through metal coordination bonding. To comprehend the dynamics of the hTf-Nag complex, 200 ns all-atom molecular dynamic simulation studies were conducted.

Nag's binding to hTf does not result in any noticeable structural changes, indicating the stability of the hTf-Nag complex. Experimental techniques also supported computational investigations [276].

Using multi-spectroscopic, molecular docking, and molecular dynamics modelling techniques, Xiaoge Zhang explored the simultaneous binding of resveratrol (RES) and curcumin (CUR) with bovine -lactoglobulin (β-LG, PDB: 3NPO). The lowest binding affinities were determined using docking analysis to be β-LG/CUR (7.2 kcal/mol) > β-LG/RES-CUR (6.7 kcal/mol) > β-LG/RES (6.6 kcal/mol) > β-LG/CUR-RES (6.1 kcal/mol). RES was found on the top surface of the β-LG and complexes were maintained by hydrophobic effects with neighbouring amino acids Pro38, Leu39, Val41, Leu 58, Lys69, Ile71, Ile84, Asn88, Asn90, Met107, Glu108, Asn109, Ser116, and Leu117. Due to the two polyphenols' competitive binding sites and the interaction forces of hydrogen bonds, hydrophobic effects, and pi-cation bonds, the larger CUR molecule initially occupied the binding site on top, and RES was transferred to a nearby location with interacting amino acids of Asp11, Ile12, Gln13, Pro50, Glu51, Gly52, Lys75, Thr76, Lys77, Ile 78, Pro79, Val81, and Phe82. According to a molecular dynamics simulation during 100ns, the ternary system with the addition of CUR and then RES had the least spacing between the start structure and equilibrium structure for both RES and CUR [277].

The most prevalent polyphenolic substances in the human diet are flavonoids, which have been shown to have a variety of neuroprotective effects. In-depth research has been done on the polyphenols naringenin and quercetin, which have a wide spectrum of

therapeutic possibilities for everything from cancer to neurological diseases. Structure-based docking of quercetin and naringenin with human ferritin was carried out by Anas Shamsi. In order to identify the stable poses, it was first necessary to evaluate the binding affinities of quercetin and naringenin for ferritin. The docking investigation was then accompanied by all-atom 100 ns MD simulations, principal component analysis, and free energy landscape analysis. Dynamic experiments were used to better understand how ferritin interacts with quercetin and naringenin in terms of conformational dynamics, structural stability, and interaction mechanism. According to their MD study, quercetin and naringenin's binding to ferritin stabilises during the course of the simulation and results in fewer conformational variations [278].

Molecular docking analysis was performed by Ifedayo Victor Ogungbe et al. to investigate possible Leishmania protein targets of antiprotozoal polyphenolic compounds obtained from plants. A total of 352 phenolic phytochemicals, including 10 aurones, six cannabinoids, 34 chalcones, 20 chromenes, 52 coumarins, 92 flavonoids, 41 isoflavonoids, 52 lignans, 25 quinones, eight stilbenoids, nine xanthones, and three other phenolic compounds, were used in the virtual screening study with 24 Leishmania enzymes (52 different protein structures from the Protein Data Bank). They identified several compounds as prospective therapeutic candidates deserving of additional research, including two aurones, one chalcone, five coumarins, six flavonoids, one isoflavonoid, three lignans, and one

stilbenoid based on their in-silico examination of antiparasitic polyphenolics [279].

The displacement reaction of ligands from their protein binding sites is the primary mechanism underlying drug-drug interactions. A model protein for studying drug/ligand binding and changes in the spectrophotometric and molecular docking properties of drug/ligand is serum albumin, which is the predominant protein in plasma and is involved in the disposition of many medications. Nawaf A. Alsaif et al. investigated the effects of the widely available plant flavonoids quercetin and rutin on the displacement of the anticancer medication sorafenib from the binding site on human blood albumin. Sorafenib was reported to have been displace from its binding site in HSA-sorafenib according to the binding experiments in the presence of quercetin and rutin [280].

One alternate method for reducing postprandial hyperglycemia is to inhibit -glucosidase, which slows down the absorption of absorbable monosaccharides from carbohydrates. Gallic acid and catechin, two polyphenols from faba beans, were investigated for their ability to inhibit -glucosidase using molecular docking and molecular dynamic studies by Dhiraj Kumar Choudhary and colleagues. Gallic acid and catechin molecular docking experiments on α-glucosidase suggested successful binding modes with binding energies of 6.58 and 7.25 kcal/mol and an appropriate amount of hydrogen bonds. A-glucosidase's Tyr63, Arg197, Asp198, Glu233, Asn324, and Asp326 took involvement in binding processes with gallic acid and catechin. Both complexes, gal:α-glucosidase and cat:α-glucosidase, as well as

the apo state of α-glucosidase, were subjected to molecular dynamics simulation studies, which demonstrated stable systems during the simulation [281].

Severe Acute Respiratory Syndrome Coronavirus-2 (SARS-CoV-2) is a zoonotic pathogenic virus that is responsible for the global outbreak of highly contagious deadly pneumonia known as Coronavirus Disease-2019 (COVID-19). Numerous research has been done to date; however, none have been successful in creating an antiviral medication for COVID-19. Protease inhibitors may be particularly successful in controlling, according to *in silico* studies to find and introduce COVID-19 antiviral medicines. There is a substantial virtual screening for polyphenols against COVID-19, due to the antiviral effects that polyphenols have been demonstrated to have. Epigallocatechin gallate (EGCG), epicatechingallate, and gallocatechin-3-gallate, polyphenols found in green tea, interact strongly with one or both of the catalytic residues of the SARS-CoV-2 Mpro, according to research by Ghosh *et al* [282]. They also showed that six polyphenols from the plant Broussonetia papyrifera inhibit the catalytic activity of M^{pro}. A strong interaction between EGCG and M^{pro} was also discovered by Khan et al. The binding energies of EGCG for the 6y2e, 6vw1, 6vww, 6lxt, 6vsb, 6lu7, and 6lvn proteins of SARS-CoV-2 were 9.30, -8.66, -8.38, -7.57, -7.26, -6.99, and -4.90 kcal/mole, respectively [283]. Lutein had a greater affinity for PL^{pro} than the FDA-approved antiviral medication Remdesivir, according to research by Ansari et al. Lutein formed potent hydrogen bonds with Val49, Gly130, Ile131, Pro125, and Ala154 amino acid residues in the active

sites necessary for enzyme inhibition to show the maximum binding affinity (-9.37 kcal/mole) towards papain-like protease (6wo2). Furthermore, Lutein demonstrated significant binding energies (-7.22 kcal/mole for 6y2e and -7.08 kcal/mole for 6mo3) through the formation of hydrogen bonds with Met165, Ser144, and Gly143 amino acid residues of 6vyo enzyme as well as Thr25, Gln143, Cys145, and Met165 amino acid residues for 6mo3 enzyme, and was subsequently discovered to be significantly active against 3C-like proteinase enzymes of main protease [284].

A massive virtual screening for more than 400 polyphenols to bind to SARS-CoV-2 M^{pro} (PDB ID: 7BRP) and PL^{pro} (PDB ID: 6W9C) was carried out by Yifei Wu. The top polyphenols bound to PL^{pro} include Kaempferol 3-O-sophoroside 7-O-glucoside, Cyanidin 3-O-sambubioside 5-O-glucoside, and Malvidin 3-O-(6″-p-coumaroyl-glucoside) (respectively, 87.97 kcal/mol, 87.33 kcal/mol, and 85.70 kcal/mol). Petunidin 3-O-(6″-p-coumaroyl-glucoside), Malvidin 3,5-O-diglucoside, and Cyanidin 3-O-(6″-p-coumaroyl-glucoside) are the components which possessed high binding affinity with M^{pro} whose energy values being −101.21 kcal/mol, −95.07 kcal/mol, and −90.17 kcal/mol, respectively [285]. In order to explore the binding properties of polyphenols, Rajesh Ghosh et al. docked them against the SARS CoV-2 Mpro along with two repurposed medicines (lopinavir and darunavir; having binding affinities between 7.3 and 7.4 kcal/mol). Only six polyphenols, broussoflavan A, papyriflavonol A, 3'-(3-methylbut-2-enyl)-3',4',7-trihydroxyflavane, kazinol F, and kazinol J, interacted with both the catalytic residues (His41 and Cys145) of M^{pro}

(PDB ID: 6LU7) and shown good binding affinity (between 7.6 and 8.2 kcal/mol). All M^{pro}-polyphenol complexes are more stable, conformationally less varied, slightly less compact, and slightly enlarged than M^{pro}-darunavir/lopinavir complex, according to molecular dynamic simulations (100 ns) [286].

160 natural polyphenols were analysed by Nada H. Aljarba et al. using *in-silico* approach to find the most promising druggable HITs against COVID protease enzyme (PDB id 6LU7) that can be exploited in the drug discovery process. Galangin, nalsudaldain and rhamnezine were identified as lead compounds with docking score −7.704, −6.51, −4.212 respectively. MD simulation over a 100 ns of galangin, nalsudaldain and rhamezine showed the RMSD values 2.9 Å, 7.6 Å and 9.5 Å and binding free energies (ΔG) of compounds with protein were found to be −49.8, −56.45, −62.87 kJ/mole respectively [287]. According to molecular docking and dynamic simulation studies, polyphenols from plants like the citrus and curcuma species inhibit SARS-CoV-2 infection by interacting with the S protein RBD. In comparison to the standard antiviral drug nafamostat, a study has found that the polyphenols from Curcuma spp. (curcumin and derivatives) and Citrus spp. (tangeretin, hesperetin, and hesperidin) had better interactions with the S protein [288].

A computational model of the SARS-CoV-2 spike protein interacting with the human ACE2 receptor was used in a molecular docking study, and it was discovered that among 77 candidates, eriodictyol, a flavanone found in yerba santa (Eriodictyon californicum), had one of the highest binding affinities for the human

ACE2 receptor portion of the interface. Another computational work shown that the flavonoids curcumin and catechin interact with ACE2 through π-σ interactions, carbon-hydrogen bonds, and hydrogen bonds, with binding affinities of -7.8 and -8.9 kcal/mol and respectively [288]. By using computational approaches, the polyphenolic agonist of the β2-adrenergic receptor fenoterol, the naturally occurring flavone baicalin from Scutellaria baicalensis, and a number of xanthones from Swerti apseudochinensis were found as possible SARS-CoV-2 RdRp inhibitors [289]. Epigallocatechin gallate, myricetin, quercetagetin, and other polyphenols recently showed substantial binding affinity towards the RdRp of both SARS-CoV and SARS-CoV-2, according to another in silico investigation [290].

Wet lab drug discovery and commercialization are challenging, costly, and time-consuming processes and development of new drugs for various diseases are highly recommended. The development of *in silico* techniques throughout the past century has raised the calibre of healthcare investigations by offering accurate forecasts. Numerous studies have provided evidence that polyphenols have a wide range of biological functions. The literature assessment shown above shows the importance of *in silico* studies on polyphenols' putative pharmacological actions. A mechanistic understanding of the inhibitory actions of polyphenols on a variety of proteins could be helpful in the pharmacological basis of drug discovery and development in near future.

1.6 Computer modelling explorations of polyphenols as highly effective corrosion inhibitor

Almost every industry is negatively impacted by the corrosion of metals and alloys, which causes significant financial and safety losses. The use of corrosion inhibitors of various types is one of the most popular corrosion prevention techniques. Finding efficient "green" solutions to stop metal and alloy corrosion that have little to no impact on environmental pollution has become an issue of increasing economic, social, and environmental importance in recent years. The efficacy of certain polyphenols for copper and mild steel has been evaluated in theoretical quantum chemistry and molecular dynamics investigations. These investigations' findings made it possible to advance our understanding of the polyphenols' inhibitory action as well as the processes that lead to their atomic-level adsorption on various metal surfaces.

Theoretically, Xianghong Li *et al.,* used molecular dynamics (MD) to examine the adsorption mechanism of four main chemicals from the extract of Dendrocalamus brandisii leaves (DBLE), including rutin, vientin, isovientin, and orientin on the surface of Fe (001). Each flavonoid has a lesser inhibitory effect than DBLE and acts in the following order: rutin > vientin > isovientin > orientin based on the parameters of E_{ads} and E_{bin} obtained from MD simulation. Additionally, they came to the conclusion that the substitution -OH is an extra centre of adsorption, leading to more adsorption centres and, hence, higher inhibitory efficiency [291]. Citrullus lanatus fruit (CLF) extract's polyphenols, hesperetin, and resveratrol were theoretically

investigated by Ali Dehghani *et al.* for their potential to lessen the corrosion of mild steel specimens. The results of MC and MD indicate that the aromatic rings of hesperetin and resveratrol were parallel to the surface of the iron. The adsorption energies of both neutral and protonated, hesperetin (-179.09 and -210.10 kcal/mol), and resveratrol (-132.76 and -154.95 kcal/mol), are negative, further supporting the claim that the selected compounds can bind to iron [292].

The effectiveness of polyphenols derived from Artemisia Herba alba (AHA) in preventing mild steel corrosion in a 1 M HCl solution was examined by Zerroug Meriem *et al.* The LC-MS analysis of the Artemisia Herba Alba hydroalcoholic extract has revealed a number of phenolic compounds, and according to the subtended regions of the peaks, the most prevalent organic components in the AHA extract are primarily "Dicaffeoylquinic acids" (DCQA). Dicaffeoylquinic acid is a naturally occurring polyphenolic molecule which is made up of two caffeic acid molecules are connected to one quinic acid molecule *via* ester bonds. Six Dicaffeoylquinic acid isomers' electronic characteristics were predicted by a quantum chemistry analysis, which might be used to forecast how reactive the isomer will be on steel surfaces. Utilizing the DMol3 module found in Material Studio 2017TM Software, theoretical calculations were performed in order to better understand the results of the experimental corrosion tests [293]. Amina Belakhdar investigated the effects of the Rosmarinus officinalis (RO) extract on the prevention of corrosion in XC48 steel. Quantum chemical calculations reveal that carnosic acid, one of the most prevalent substances found in the RO extract, has a higher inhibitor

potential than carnosol. A strong (monotonically increasing with the absolute value of the adsorption energy), quick, and firm adsorption on the surface of the iron in HCl solution is indicated by the negative adsorption energies of these two molecules. They also be deduced that the adsorption force of the inhibitors on the surface of the iron revealed to be stronger at higher HCl concentrations. The outcomes demonstrated that more carnosic acid than carnosol is absorbed [294].

D.K.Verma and colleagues investigated three plant extracts, namely Glycine max leaves (GMLE), Cuscuta reflexa roxb. (CRRE), and Spirogyra algae (SGAE), which have been evaluated as green corrosion inhibitors for mild steel corrosion in acidic solution of 1 M HCl using chemical, electrochemical, surface, and density functional theory (DFT) methods. It's vital to note that coumarin and flavone are the key phytochemical components of BPLE extract, bergenin and quercetin are the main phytochemical components of CRRE extract, and genistein and glycitein are the main phytoconstituents of GMLE extract. According to dft investigations, coumarin, flavone, bergenin, quercetin, genistein, and glycitein are linked to relatively low values for electronegativity, hardness, and band gap suggested that they are very reactive and prefer to form meta-inhibitor bonding when they come into touch with metallic surfaces [295]. Through detailed-level modelling, including molecular/atomic-level simulations, or MD/MC combined by DFT, Ali Dehghani et al. thoroughly investigated the protective behaviour of quercetin in HCl acidic conditions (containing 1 M). DFT calculations showed that a donor-acceptor interfacial mechanism might be used by the Quercetin/iron complexations to

interact with the target metallic adsorbent. Through the MC/MD techniques, iron surface adsorption of metal-organic complexes was assured [296].

For the purpose of reducing the corrosion of mild steel, BaominFan et al. examined green components that were isolated from Passiflora edulia Sims shell (PESE). Isoorientin (IRT), schaftoside (SAS), and apigenin (AGN), which together make up the majority of PESE's percentage content, were found through phytochemical screening on PESE using the GC-MS method. Due to their low global and local reactivity, hydroxypyran moieties on IRT and SAS were hardly ever engaged in electron donation/acceptance during PESE adsorption. MD models also revealed interactions between distinct components *via* potential hydrogen bonding. Therefore, they came to the conclusion that strong adsorption, chelation with corroded species, and inter-component synergy led to the PESE's good anticorrosion performance for M-steel in HCl medium [297]. The adsorption and corrosion-inhibiting effects of Punica granatum (PNG) aqueous extracts on mild steel in 1 M HCl were examined by Maduabuchi A. Chidiebere et al. They used theoretical calculations to simulate the electrical and adsorption structures of some important phytochemical components of PNG extract, including as pelargonidin (an anthocyanin plant pigment) and two phenolic acids (gallic acid and ellagic acid). Gallic acid was followed by perlagonidin, and ellagic acid in the decreasing sequence of molecular size, which demonstrates the molecules' propensity to work *via* a geometric blocking action. Accordingly, pelargonidin should be the substance that is most

strongly adsorbed based on electronic structure considerations, but ellagic acid should be the substance based on molecular size considerations. Additionally, they employed forcite quench molecular dynamics to sample a wide range of low energy adsorption patterns of these compounds on Fe. The trend of binding energy on Fe(110) surface (perlagonidin<ellagic acid<gallic acid) supports the notion that electrical interactions dominate pelargonidin adsorption [227].

By combining electrochemical and computational approaches, Mohammad Ramezanzadeh and co-workers analysed the synergistic corrosion inhibition function of many components in Mangifera indica L. extract (M.i-L) and zinc cations. To get a fundamental understanding of the active sites of the organic-inorganic corrosion-inhibiting compounds, modelling studies utilising *Ab initio* quantum chemistry methods were employed. These compounds include divalent zinc cations (Zn^{2+}) and organic gallic acid, iriflophenone, and mangiferin. The adsorption at the interface of the organic-inorganic zinc-gallic acid/iriflophenone/mangiferin species and iron (110) adsorbent was investigated using theoretical MC and MD modelling techniques. According to MD simulations, the adsorption energies for dissolved compounds are -173.19, -326.96, and -394.33 kcal/mol for zinc-gallic acid, zinc-iriflophenone, and zinc-mangiferin, respectively. To further investigate the local reactivity of created organic-inorganic coordination compounds, the Fukui indices representing the electrophilic/nucleophilic character of corrosion inhibiting complexes were examined [298].

Frontier orbital and inhibitor adsorption theories have been used by Jéssica V. Nardeli *et al.,* to investigate the principles of tannin's inhibitive mechanism. The HOMO orbitals on the double bond of the first ring and the oxygen heteroatom of the primary flavan-3-ol of tannin they used indicate that adsorption happens vertically towards the surface *via* one alone electron pair located at the polar group (OH) immediately attached to the first ring [299]. Through the use of both experimental and theoretical methods, S. Abdelaziz explored the green corrosion inhibition of leaves extract of Arbutus unedo L. plant on mild steel in HCl solution. The pKa analysis showed that in the acidic environment, the neutral form of the two key components of leaves extract quercetin and catechin predominates. The most active locations of these primary elements are heteroatoms and conjugated double bonds of aromatic rings, according to Mulliken charges analysis and Fukui functions. According to a molecular dynamics simulation, the quercetin molecule (binding energy = 613.265kJ/mol) was spontaneously adsorbed in parallel to the metal surface, resulting in a powerful contact that covered the entire surface [300].

Pigeon pea seed (PPS) extract is abundant in bioactive components like cajanin and cajanol and exhibits promising corrosion inhibition potential. Okechukwu Dominic Onukwuli *et al.* showed by FMO analysis that the hydroxyl group and lone pair electrons of oxygen atoms greatly enhance the binding mechanism and boost the adsorption centres of these inhibitors. They also came to the conclusion that cajanol had a lower adsorption energy than cajanin (188 kJ/mol) and that this indicated that cajanol had a physical

adsorption process, whereas cajanin had a chemical adsorption mechanism [301]. Abhradip Pal *et al.,* used density functional theory to evaluate the corrosion inhibition ability of two key chemicals termed cyaniding-3-glucoside (C3G) and peonidin-3-glucoside (P3G) of purple rice bran (DFT). According to theoretical research, P3G has a higher dipole moment than C3G but a smaller energy gap which in turn indicate P3G has more potential as inhibitor [302].

Ali Dehghani used ziziphora leaf extract as a new, eco-friendly green inhibitor for mild steel (MS) corrosion brought on by acidic environments. The inhibition activity of different phytochemicals found in the aqueous extract of Ziziphora leaves, such as acacetin, chrysin, and thymonin, was investigated using theoretical tools such as classical simulations like, molecular dynamics, MD connected with Mote Carlo, MC (in Fe(110)), and quantum chemical computations like,density functional theory, DFT, in order to learn the fundamental electronic/atomic-scale information about the extract compounds' adsorption on the target metal and their active sites. According to dft analysis, single ring ethylene bonds and atomic oxygen centres in specific neutral aromatic cycles of acacetin, chrysin, and thymonin appeared as electrophilic locations, suggesting that charges from these local regions were shared with electrophiles attacking the inhibitors. The C atoms in the ring and the nearby heteroatoms that are immediately linked to the ring are the local sites of charged or protonated acacetin, chrysin, and thymonin that are most vulnerable to electrophilic assaults. Additionally, in both charged and neutral species, the majority of backbone atoms (i.e., C and O), particularly

those with the carbonyl moiety (C = O), are most susceptible to nucleophilic type interactions and consequently presumably accept electronic charges that can be provided by occupied (i.e., filled) orbitals of metal atoms. According to MC, the absolute values of the calculated adsorption energies for both neutral and charged states varied in the following order: thymonin > acacetin > chrysin, indicating that the thymonin molecule has the strongest surface attachment capacity among the investigated green molecules. The adsorption energies (in kcal/mol) of neutral acacetin, chrysin, and thymonin were estimated to be -202.38, -164.37, and -231.85, and respectively, according to MD configurations. Additionally, the mono-protonated acacetin, chrysin, and thymonin adsorption energies of -250.12, -238.37, and -274.63 kcal/mol, respectively, were measured [303].

Significant strides in corrosion research have been made over time thanks to the use of theoretical simulations. Due to their affordability, accessibility, non-toxicity, and renewability, green corrosion inhibitors have been the subject of numerous studies in the field of anti-corrosion methods for metals [234]. The aforementioned session extensively covered the use of theoretical and computational methods, particularly DFT quantum calculations, Fukui indices, Molecular Dynamics simulation, and Monte Carlo simulation, as a crucial tool to assess the metal-polyphenol (inhibitor) interaction and adsorption behaviour of inhibitor molecules in an aqueous corrosive solution.

In the next session, the molecules investigated in the frame of this thesis will be introduced one by one.

1.7 Molecules under study

1.7.1 Coumestrol

Coumestrol (3,9-Dihydroxy-6-benzofuran [3,2-c] chromenone) is a phytoestrogen found in plants that is a member of the coumestan family, polyphenolic compounds. The fascinating pharmacological features of coumestrol, such as its ability to prevent breast cancer and its estrogen-like activity, have received a lot of interest recently. Its structure is comparable to that of estradiol and isoflavones. Its chemical structure is distinguished by a fused ring system made up of coumarin and benzofuran moieties as well as the presence of two hydroxyl groups. Clover, alfalfa, soy beans, peas, brussels sprouts, spinach, strawberries, and various legumes are among the plants that are high in coumestrol. Bickoff *et al.,* extracted coumestrol for the first time from alfalfa, strawberry, Lucerne, and ladino clover in the 1950s. According to reports, the amount of cholesterol in plant material varies depending on the type of plant, where it is in the growth cycle, whether it was cut, whether it has a disease, and whether it has been attacked by insects or fungi. Plants, like alfalfa, may create coumestrol or 4′-methoxycoumestrol as phytoalexins as a result of insect and fungus attacks. Plants benefit from phytoalexins, a wide family of substances that are frequently secondary metabolites created as a result of damage or disturbance, and which shield them against pests including insects, bacteria, and viruses [304].

It is not surprising that coumestrol has estrogenic activity because its structure mirrors that of the well-known (E)-4,4′-dihydroxystilbene derivatives, which have strong pharmacological activity. In addition to being stable to cross cell membranes due to their stable structure and low molecular weight, coumestrol has been found to interact with enzymes and receptors [305]. Coumestrol has become of concern as several reports indicate it may have a beneficial effect on health. The antioxidant activity of coumestrol revealed intriguing antioxidant capabilities. Its two hydroxyl groups, which are present and have an orientation similar to that of estradiol, are what give it both its antioxidant and estrogenic qualities. Mitchell et al. used electron spin resonance spectroscopy, plasma's capacity to reduce ferric, and trolox's equivalent antioxidant capacity to assess the antioxidant effectiveness of coumestrol. Additionally, they noted that coumestrol had about half the action of quercetin, a well-researched flavonoid, but more than two times the ability to reduce ferric iron compared to isoflavones [306]. Using quantum chemistry techniques, Houssem Boulebd assessed the kinetics and mechanism of the peroxyl radical (ROO•) scavenging activity of coumestrol. It has been demonstrated that the environment and the ROO• radical's characteristics affect the antioxidant activity of coumestrol [307].

Coumestrol has a strong affinity for the ERα and notably the ERβ receptors due to its hydrocarbon rings (analogue to natural hormones and their active metabolites). Because both receptors are expressed in the skin and regulate the amount of collagen, coumestrol is a promising preventative measure against skin photoaging. The

binding affinities of coumestrol for ERβ are higher than those of other phytoestrogens. By acting as an anti-estrogen at the ERβ, coumestrol exposure may affect ERβ-dependent processes. The mode of action may be tissue-specific, or the effects may be changed by the metabolism of dietary coumestrol [308]. After 10 minutes of total brain ischemia, Cibele Canal Castro et al. showed that coumestrol shielded mice from long-term neuronal degeneration in the CA1 hippocampal layer. These results point to the possibility that this substance obstructs the early and late phases of neuronal injury. According to the study, transient global ischemia insult in female rats causes delayed neuronal cell death in the hippocampus, which can be considerably reduced by acute coumestrol injection. The mechanisms behind the neuroprotective effects of coumestrol appear to involve, at least in part, oestrogen receptor activation, antioxidant activity, and activation of additional membrane receptors that facilitate estradiol's neuroprotective effects [309].

Coumestrol produces selective apoptotic action against breast cancer MCF-7 cells and the cell death is caused by the redox cycling of nuclear Cu(II) ions for intracellular ROS generation and pro-oxidant cell death. The importance of employing coumestrol to treat breast cancer lies in the drug's ability to selectively kill cancer cells with high copper levels through cytotoxicity [310]. It was discovered that coumestrol inhibits CKII's phosphotransferase activity towards β-casein, which gives rise to an anti-cancer action. It was discovered that coumestrol had an IC50 of roughly 50 μM, which led to a 50% suppression of MCF-7 human breast cancer cells. CK2 overexpression

is associated with a number of human malignancies, making it a possible target for cancer treatment. Coumestrol has been shown to be a potent inhibitor of CK-2.4'-Methoxycoumestrol has been shown to partially inhibit the growth of cancer cells by decreasing CK2-specific Akt phosphorylation [311].

Haspin kinase governs cell proliferation, hence haspin kinase inhibitors have been designed as anti-cancer medications. Coumestrol's dose-dependent lowering effect on recombinant haspin kinase activity supports this claim [312]. Through effects mediated by the PI3K/AKT, ERK1/2, and JNK MAPK cell signalling pathways, coumestrol can slow the evolution of prostate cancer and may represent a potential chemotherapeutic drug for the treatment of prostate cancer [313].

Coumestrol stimulated the sirtuin family of proteins, which in turn caused mitochondrial biogenesis in skeletal muscle. *In vitro* differentiation of preadipocytes toward adipogenesis may be inhibited by coumestrol. According to Sang-Nam Kim and co-workers, coumestrol enhances anti-obesity benefits by increasing and activating the metabolism of brown adipose tissue [314]. Biomedical research into the treatment of a variety of illnesses, such as HIV, cancer, and type II diabetes mellitus, has put -glucosidase inhibitors in the spotlight. According to Heung Joo Yuk *et al.,* coumestrol has an IC50 value of 6.0 μM and can function as a strong α-glucosidase inhibitor [315]. The effects of coumestrol on the production of melanin in healthy melan-a mouse melanocytes were examined by Jeong Ah Hwang et al. Coumestrol could be employed as an effective skin-whitening component for the treatment of hyperpigmentation, as

shown by the whitening impact of coumestrol employing several assessment systems, including human skin equivalent [316].

Coumestrol is a prospective target for enhancing drought responses as well as a possible biomarker for drought. According to earlier studies, coumestrol promotes mycorrhizal colonisation, and mycorrhizal plants are better able to withstand dryness under some circumstances [317]. Coumestrol has been shown to promote bone mineralization and prevent bone resorption *in vitro* [318]. The condition known as neonatal hypoxia-ischemia (HI) is a leading cause of morbidity and mortality and is frequently linked to both short- and long-term neurologic and cognitive deficits. Coumestrol protects against experimental neonatal brain hypoxia-ischemia by early regulation of mitochondrial activity, at least in part [319].

The metabolic enzymes acetylcholinesterase (AChE), butyrylcholinesterase (BChE), carbonic anhydrase II (CA II), and α-glycosidase were studied by Lokman Durmaz *et al.,* for Coumestrol's inhibitory actions against them. These enzymes are linked to various common disorders like Alzheimer's disease (AD), glaucoma, and diabetes. Coumestrol exhibited Ki values of 10.25 1.94, 5.99 1.79, 25.41 1.10, and 30.56 3.36 nM towards these enzymes, respectively. They came to the conclusion that coumestrol has anti-diabetic, anticholinergic, and anti-glaucoma effects and can be used to treat diseases like glaucoma, T2DM, and AD [320]. Coumestrol is a significant chemical with numerous biological activities that are still being investigated.

1.7.2 Herbacetin

Herbacetin (3,4′,5,7,8-pentahydroxyflavone) is a yellow bioactive flavonoid produced from 5,7,8-trihydroxyflavone ($C_{15}H_{10}O_5$) with a molecular weight of 302.23 g/mol, a density of 1.799, and a melting point of 284 °C is soluble in a variety of organic solvents, including methanol, ethanol, and dimethylsulfoxide (DMSO).it is a constituent of various herbs such as Ephedra sinica Stapf (Ephedraceae), Sedum roseum (L.). Scop. (Crassulaceae), and Linum usitatissimum Linn. (Linaceae) has multiple pharmacological activities. Neelakantam et al. (1935) first isolated it from the Malvaceae plant Gossypium herbaceum L. [321].

Oxidative stress can disrupt and harm DNA, proteins, lipids, and cell structures, which can result in diseases including cancer, diabetes, atherosclerosis, and neurological disorders. Herbacetin (10– 100 M) was shown by Qiao and Liu (2013) to have potent anti-free radical action and the ability to suppress protein oxidation. Additionally, it has been demonstrated to act as a concentration-dependent inhibitor of the carbonylation and oxidative damage brought on by 2,2′-azobis (2-methylpropionamidine) dihydrochloride (AAPH) or Cu^{2+}-H_2O_2 [321]. Herbacetin may also be helpful for conditions that cause inflammatory bone loss. Osteoblast-mediated bone creation and osteoclast-induced bone resorption are the two primary components of the bone remodelling process. Inflammatory stimuli can promote osteoclastic bone resorption and prevent osteoblasts from differentiating. Herbacetin dramatically reduced the inflammatory bone loss caused by LPS in the mouse model, according to Li et al.

(2016). Herbacetin also decreased the expression of the osteoclastogenic transcription factor c-Fos and calcineurin/nuclear factor of activated T cells c1 (NFATc1) in RAW264.7 cells and bone marrow-derived macrophages (BMMs), which are both involved in RANKL-mediated osteoclastogenesis. These effects were achieved by inhibiting the mitogen-activated protein kinases (MAPK) and NF-κB signalling pathways [322, 323].

In insulin resistant rats with obesity, herbacetin dramatically decreased body weight, plasma glucose, plasma insulin, and HOMA-IR activity (OIR). Aside from that, giving OIR mice herbacetin considerably decreased their total cholesterol, triglycerides, and free fatty acid levels in both their plasma and their livers. In addition, compared to OIR control mice, herbacetin significantly enhanced the altered hepatic lipid metabolising and lipid-regulating enzymes, including SREBP-1c, and 2, fatty acid synthase (FAS), fatty acid -oxidation (-oxidation), malic enzyme, glucose 6-phosphate dehydrogenase (G6PD), and carnitine palmitoyltransferase (CPT). Herbacetin lowers lipid droplets in the liver tissue, according to a histopathological analysis. This strongly suggests that herbacetin, which has anti-hyperglycaemic and anti-hyperlipidemic capabilities through the modulation of hepatic lipid metabolising and lipid-regulating enzymes, offers significant protection against the negative consequences of chronic high-fat diet consumption [324].

Herbacetin has been shown to have anticancer properties that inhibit the metastasis of tumour cells, induce apoptosis, and demonstrate cytotoxicity. Ornithine decarboxylase (ODC), a rate-

limiting enzyme involved in the production of polyamines, is linked to tumour development and cell growth. Herbacetin, was discovered to be a novel ODC inhibitor utilising computer docking modelling and an in vitro ODC enzyme assay by Dong Joon Kim and co-workers. In colon cancer cell lines expressing high amounts of ODC, herbacetin demonstrated powerful anticancer action. In a mouse model of APC-driven colon cancer (ApcMin/+), intraperitoneal or oral injection of herbacetin significantly decreased the number and size of polyps while also inhibiting the growth of the HCT116 xenograft tumour [325]. According to Hyuga et al. (2013), herbacetin (0.66, 3.3, or 16.5 μM) could reduce the motility of MDA-MB-231 human breast cancer cells caused by hepatocyte growth factor (HGF) without compromising the viability of the cells. Higher quantities of herbacetin (33, 66, and 132 μM) were also able to lower cell viability. Herbacetin has been demonstrated to inhibit c-Met tyrosine kinase activity in vitro in a concentration-dependent manner (IC50 = 15.7 M), which is consistent with these findings [326]. Additionally, herbacetin decreased the B-cell lymphoma 2 (Bcl-2)/Bcl-2 associated x-protein (Bax) ratio, increased caspase-3 cleavage, and inhibited the phosphatidylinositol-3 kinase (PI3K)/Akt pathway to cause HepG2 cells to apoptose in a mitochondrial-dependent manner [327]. Herbacetin has been demonstrated to prevent cutaneous squamous cell carcinoma (SCC), melanoma cell proliferation, and 12-O-tetradecanoylphorbol 13-acetate (TPA)-induced neoplastic transformation of JB6 mouse epidermal cells [328]. Herbacetin (100 or 500 nmol) administered topically reduced the growth of skin cancers brought on by solar UV exposure and TPA in mice in vivo. In a xenograft mouse model, intraperitoneal

administration of 0.2 or 1 mg/kg herbacetin dramatically slowed the growth of melanoma. Additionally, malignant melanoma angiogenesis mediated by matrix metalloproteinase 9 (MMP9) could be inhibited by herbacetin [329].

Herbacetin has the potential to be developed as an antiviral agent due to its antiviral properties. Herbacetin was shown to be more effective the H1N1 (A/PR/8/34) and H9N2 (A/Chicken/Korea/MS96/96) induced cytopathic effects (CPEs) in Madin-Darby canine kidney cells with EC50 values of 35.0 μM against H1N1 and 23.0 μM against H9N2, than Tamiflu (EC50 = 8.3 μM against H1N1 and 6.25 μM against H9N2) [330]. Herbacetin was shown by Jo et al. (2020) to bind to the His41 and Gln189 residues at the S2 site and inhibit the enzymatic activity of the viral protease SARS-CoV 3CLpro (IC50 = 53.90 M) [331]. Additionally, it has been found that herbacetin inhibits SARS-CoV-2 3CL's ability to proteolyze [332]. Herbacetin was found to inhibit MERS-CoV 3CLpro in a different investigation (IC50 = 40.95 M), which suggests that its 8-OH group forms a hydrogen bond with His41 in the S1 site of MERS-CoV 3CLpro [333]. These results imply that herbacetin's antiviral activity may result from its direct interaction with viral proteases, which would inhibit the primary viral proteases and negate the antiviral effects of viral peptides. These results imply that herbacetin's antiviral activity may result from its direct interaction with viral proteases, which would inhibit the primary viral proteases and negate the antiviral effects of viral peptides. Adenophora adenophora and Nerium oleander are two other herbacetin-rich plants that exhibit antibacterial properties.

Herbacetin-3-O-L-rhamnopyranosyl-8-O-D- lyxopyranoside has been shown to be antibacterial in vitro by Xu et al. (2015) [334].

Cholinergic pathways are linked to several neurodegenerative illnesses, including Alzheimer's disease. Using electrostatic interactions and hydrogen bonds to bind the enzyme, herbacetin and its glycosides rhodionin and rhodiosin have been found to inhibit acetylcholinesterase in vitro in a dose-dependent way. Rhodionin, 49.03 nM, and rhodiosin had inhibitory constants of 1.37 μM, 43.45 nM, and 103.34 nM, respectively, while galanthamine, the positive control, had a constant of 103.34 nM [335]. This suggests that herbacetin may one day be used to treat neurodegenerative illnesses.

This demonstrates that herbacetin has a wide range of pharmacological effects and has a great deal of potential as a new medicine. Future studies should concentrate on increasing its bioavailability, learning more about its pharmacological mechanism, assessing its toxicity and ideal dose, and conducting clinical evaluations.

1.7.3 Gossypetin

Gossypetin, 3,5,7,8,3',4'-hexahydroxy flavone is present in various flowers, including hibiscus. GTIN has a pair of para hydroxyls at positions 5 and 8 as well as two pairs of ortho hydroxyls at locations 7, 8, and 3′, 4′. It was initially isolated from Hibiscus vitifolius (tropical rose mallow, commonly known as Japa or Karupatti) and H. furcatus (Panchavam in Malayalam). These plants' extracts have historically been used to treat inflammation, jaundice, and diabetes.

Additionally, GTIN was discovered in the leaves of Bruckenthallia speciliforum, Loiseluria procumbens, LeiophyIlum buxifolium, Menziesia lasiophylla, and the calyx of Hibiscus sabdariffa (Roselle). Because two o-quinone and one p-quinone intermediates could potentially exist, it is oxidizable, which makes it an excellent free radical scavenger. It has a number of pharmacological effects, including antioxidant, antibacterial, and anticancer effects. According to earlier research, eating foods like Hibiscus sabdariffa, which are high in gossypetin and quercetin, can help to reduce oxidative stress and atherosclerosis [336].

Gossypetin has recently been demonstrated to have anticancer properties by inducing apoptosis and autophagic cell death in prostate cancer cells [337] and inhibiting the papilloma virus E6-dependent degradation of p53 in cervical cancer cells [338]. According to Xiaomeng Xie, gossypetin can prevent oesophageal cancer cells from growing in both an anchorage-dependent and an anchorage-independent manner. Their research showed that the gossypetin is a new MKK3 and MKK6 inhibitor with anticancer activities in *ex vivo, in vitro, and in vivo* [339].

Oxidized low-density lipoprotein (ox-LDL) causes damage to vascular endothelial cells, which aids in the aetiology of atherosclerosis. Hui-Hsuan Lin investigated the atheroprotective function of gossypetin in endothelial cells. Gossypetin's protective action against ox-LDL-induced damage to human umbilical vein endothelial cells (HUVECs) was discovered at a concentration of 0.1–0.5 M. According to morphological and biochemical characteristics,

such as the creation of apoptotic bodies, distribution of the hypodiploid phase, and activation of caspase-3, gossypetin demonstrated potential in lowering ox-LDL-dependent apoptosis. Gossypetin promoted the activation of autophagy-related genes (LC3 and Beclin-1) and the ox-LDL-induced production of acidic vesicular organelles. A rise in the level of LC3-II under pretreatment conditions with an autophagy inhibitor, chloroquine, provided additional confirmation of the gossypetin-triggered autophagic flux (CQ). Beclin-1 silencing also prevented the protective effects of gossypetin as well as the autophagic process. The use of a class III PI3K inhibitor, 3-methyladenine (3-MA), and a PTEN inhibitor, SF1670, suggested that the autophagic impact of gossypetin may be mediated *via* the class III PI3K/Beclin-1 and PTEN/class I PI3K/Akt signalling cascades. Finally, gossypetin reduced endothelial damage and atherosclerotic lesions *in vivo* [340].

A viable model for causing cognitive damage is chronic unexpected stress (CUS). The activation of the kynurenine (KYN) pathway is associated with stress-related memory impairment. Recently, Nikita Patil Samant investigated how gossypetin works on the kynurenine pathway to shield neurons from the cognitive damage caused by CUS. According to the findings, gossypetin treatment significantly improved the behavioural pattern in mice exposed to CUS. When compared to CUS-exposed mice, gossypetin (10 and 20 mg/kg, i.p.) treated mice showed significantly lower corticosterone levels and oxidative stress. Furthermore, gossypetin therapy was observed to boost levels of serotonin, norepinephrine, and brain-derived neurotrophic factor [341].

Gossypetin has been shown in several studies to have protective effects against nephrotoxicity. Gossypetin also shown strong anti-inflammatory action in kidney mesangial cells, providing additional evidence in favour of using natural substances to treat nephritis. Due to its potential as an antioxidant, gossypetin's significance for avoiding kidney damage has also been underlined. Gossypetin had a higher docking score against NF-κB and sEH, according to in silico research. According to docking experiments, gossypetin inhibits the conversion of xanthine to uric acid by surrounding the active sites of xanthine oxidase [342]. The results of a molecular docking investigation demonstrated the biological significance of the AChE and BuChE enzymes in brain related diseases [343]. Amyloidosis is a fatal condition characterised by the deposition of amyloidogenic immunoglobulin light chain secreted from clonal plasma cells. Daisuke Takahashi et al. identified gossypetin as a novel Wil amyloid inhibitor through *in vitro* studies, and looked into the molecular mechanism by which fibril formation was inhibited [344].

The medicinal value and pharmacological activities of gossypetin were discovered through literature data analysis of recent scientific research projects in the field of biological sciences, which highlighted their protective role in a number of diseases.

1.7.4 Rhodiola rosea

Rhodiola rosea L. (Crassulaceae, syn. Sedum rhodiola - DC. Sedum rosea - (L.) Scop cop, is renowned by the common names Rhodiola, Roseroot, Rosenroot, Golden Root, Arctic Root, Orpin Rose,

and Rhodiole Rougeatre) and has a lengthy tradition as a valuable medicinal plant that has appeared in the Materia Medica of several European countries. It grows in abundance at high altitudes in the Arctic and hilly areas of Europe and Asia. It has a reputation for energising the neurological system, lowering despair, improving work performance, eradicating exhaustion, and preventing high altitude sickness, making it a well-liked plant in traditional medical systems in Eastern Europe and Asia. Russian researchers have classified Rhodiola rosea as an adaptogen because of its documented capacity to boost resilience to a range of chemical, biological, and physical stimuli [345]. Rhodiola rosea has been used in folk medicine as ethanolic macerates for a long time [346].

An old book of useful plants from Icelandstates the following about Rhodiola: "Infusion of stone crop eaten dries and astringes, heals mouth discomfort, heals kidneys from sand which forms stones, stops diarrhoea and cures headache and also strengthens head and also hair growth in the head is washed with it. Some accounts claim that Rhodiola rosea was used by the Vikings as a medication and for its energising effects on hard labour. The rose root is advised for the treatment of headaches, "hysteria," hernias, discharges, and as an astringent in Linne's Materia Medica. Additionally, the root might be effective for severe skin disorders. When ground, pressed, and combined with butter, it is thought to reduce back pain, joint discomfort, and other painful conditions as well as swellings, especially when heat is administered. The dried root has been used for head strengthening, to treat swellings, and to get rid of freckles. The

plant Rhodiola rosea is described as having stimulant activity, vasoconstrictive, and hemostatic properties on haemorrhoids [347].

CNS stimulating, neuro-, cardio-, and hepato-protective effects, lifespan extension, MOA inhibitory, immunotropic, antiviral, anti-inflammatory, and antibacterial activities have all been shown by R.rosea in various *in vitro* and *in vivo* studies on animals. It has been established that Rhodiola's beneficial stress-protective activity is connected to the hypothalamic-pituitary-adrenal axis and the control of important stress response mediators like cortisol, nitric oxide, betta-endorphine, and molecular chaperones like stress-activated c-Jun N-terminal protein kinase 1 (JNK1) and Forkhead box O (FOXO) transcription. Rhodiola's ability to combat depression can be attributed to both its effects on monoamine oxidase A and the stress response system, specifically on cortisol release and JNK-mediated effects on glucocorticoid receptors [347].

The roots and above-ground sections of Rhodiola rosea have yielded total of 86 compounds. Numerous biologically active compounds, including as organic acids, flavonoids, tannins, and phenolic glycosides, are present in its roots. Rhodiola rosea rhizomes of wild origins seemed to underly great variability in chemical composition dependent on grow site. Phenolic and/or cyanogenic glycosides, which have antidepressive, anti-fatigue, cognitive-enhancing, anti-anoxia, hepatoprotective, anti-allergy, and anti-inflammatory characteristics, are examples of biologically active substances. p-Tyrosol and the phenolic glycoside rhodioloside, two substances isolated from the roots of Rhodiola rosea, were formerly

thought to be responsible for the plant's stimulating and adaptogenic effects. Rhodioloside was later revealed to share structural similarities with the well-known glycoside salidroside, which is present in a variety of different plant species. Rhodioloside, salidroside, and rhodosin are terms that are frequently used to refer to this substance and are thought to be synonyms. Rhodioniside, Rhodiolin, Rosin, Rosavin, Rosarin, and Rosiridin are further glycosides isolated from the root are believed be essential for the plant's apparent adaptogenic characteristics. It was discovered that rosiridin inhibits monoamine oxidases A and B in vitro, suggesting that it may have a positive impact on senile dementia and depression. p-tyrosol, organic acids (gallic acid, caffeic acid, and chlorogenic acid), and flavonoids (catechins andproanthocyanidins) are among the antioxidant substances found in Rhodiola rosea (catechins andproanthocyanidins). Alcohol and water extracts of Rhodiola sp. have been shown to have significant free-radical scavenging action, which is linked to the plant's range of antioxidant compounds. After an oral dose, it has been demonstrated that p-tyrosol is quickly and dose-dependently absorbed. It also appears to have substantial antioxidant8 and minor 5-lipoxygenase inhibitory activity *in vivo*. The most important plant components required for therapeutic efficacy are believed to be salidroside (rhodioloside) and salidroside-like glycoside compounds (rhodiolin, rosin, rosavin, rosarin, and rosiridin) [348].

R.rosea might be appealing for usage as a safe treatment due to its lack of interactions with other medications and negative effects during clinical studies. In conclusion, strong traditional and scientific

evidence supports the use of *R.rosea* in the treatment of a number of disorders.

1.7.5 Cocculus hirsutus

Cocculus hirsutus (Menispermaceae) is a perennial climber primarily found in tropical and subtropical areas. It is also known by a number of names in regional tongues, including Broom creeper (English); Huyer (Bengali); Farid buti, Jamti ki bel (Hindi); Kaage Mari (Kannada); Farid buti (Urdu); Paathaalagarudakkoti (Malayalam), Kaanse laharo (Nepali); Garudi, Patalagarudi (Sanskrit), Chipuru-tiga (Telegu); Kattu-k-koti (Tamil). Different plant components of *C. hirsutus* are frequently used in South Asia to treat fever, rheumatism, skin conditions, visceral ailments, and as a diuretic. The Tsonga people use leaves as a key herb in their diet. Regarding assessments of their pharmacological effects, extracts made from C. hirsutus plant sections have demonstrated strong diuretic, laxative, analgesic, and anti-inflammatory properties. Clinical research to assess the effectiveness and safety of tablets containing an aqueous extract of *C. hirsutus* (AQCH) in treating coronavirus infection has begun in India, according to Clinical Trials Registry-India (CTRI Number: CTRI/2020/05/025397, registered on May 28, 2020) [349, 350].

Additionally, leaves of *C. hirsutus* are used to treat eye diseases, fever, leucorrhoea, dysentery, diarrhoea, and acute gonorrhoea. The roots of *C. hirsutus* are used to cure a variety of conditions, including fever, skin irritation, rheumatism, gout, syphilitic cachexia, and stomachaches in youngsters. As a sedative, hypotensive,

cardiotonic, and spasmolytic, the extract of the stems and roots is utilised. In order to alleviate stomach discomfort, the root is ground into a paste, combined with water, and administered orally [350].

The anti-mycobacterial activity of the aqueous extract of *C. hirsutus* was tested by Jethva et al. on Mycobacterium tuberculosis H37Rv, and the extract demonstrated strong anti-mycobacterial activity with an inhibition percentage of 80.26%. Devi et al. tested the antibacterial activity of methanol, ethanol, and an aqueous extract of *C. hirsutus* leaves (at concentrations of 25, 50, 75, and 100 µL) using clinical bacterial isolates of Escherichia coli, Salmonella typhi, Micrococcus luteus, Staphylococcus aureus, Acetobacter laffi, Proteus mirabilis, and Bacillus cere demonstrated strong antibacterial properties. Different extracts from the roots of *C. hirsutus* were tested for their in-vitro antimalarial effects against the 3D7 (a strain that is sensitive to chloroquine) and K1 strains of Plasmodium falciparum by Brahmam and Sunita (chloroquine resistance strain). Both the chloroform and methanol extracts exhibited strong anti-both strain activities. The in vitro anti-cancer studies of *C. hirsutus* against breast (MCF7), melanoma (UACC62) and renal (TK10) cell lines by De Wet et al., and HeLa cell line by Thavamani et al, showed its potential anti-cancer effect. The plant has greater antioxidant activity as evidenced by its potent DPPH free radical scavenging activity, ABTS free radical scavenging activity, nitric oxide scavenging activity, reducing power, suppression of lipid peroxidation, and metal chelating activity assay ascorbic acid. In mice with diabetes induced by alloxan, Badole et al.

explored the anti-hyperglycemic efficacy of an aqueous extract of *C. hirsutus* leaves [350].

The plant has alkaloids, which are a crucial component, along with FL ginnol, sitosterol, glycosides, sterols, and others. The plant contains flavonoids (rutin, quercetin, liquiritin) alkaloids (trilobine, coclaurin, isotrilobine, magnoflorin, jamtinine, haiderine, hirsutine, Cohirsitin, Cohirsitinine, Cohirsine, Cohirsinine, Coclaurine, Shaheenine), sitosterol, glycosides, sterols, and ginnol [351]. It is crucial to critically evaluate and comprehend the available scientific information about the chemical components and pharmacological activities of a medicinal plant species that has been widely used in traditional medicines and is also being considered as a source for the development of therapeutic agents for a variety of diseases.

References

1. Rasouli H, Farzaei MH, Khodarahmi R: **Polyphenols and their benefits: A review**. *Int J Food Prop* 2017, **20**(sup2):1700-1741.

2. Naghdi T, Faham S, Mahmoudi T, Pourreza N, Ghavami R, Golmohammadi H: **Phytochemicals toward green (bio) sensing**. *ACS sensors* 2020, **5**(12):3770-3805.

3. Koche D, Shirsat R, Kawale M: **An overerview of major classes of phytochemicals: their types and role in disease prevention**. *Hislopia Journal* 2016, **9**:1-11.

4. Kabera JN, Semana E, Mussa AR, He X: **Plant secondary metabolites: biosynthesis, classification, function and pharmacological properties**. *J Pharm Pharmacol* 2014, **2**(7):377-392.

5. Koche D, Shirsat R, Kawale M: **An overerview of major classes of phytochemicals: their types and role in disease prevention**. *Hislopia Journal* 2016, **9**(1/2):0976-2124.

6. Panche A, Diwan A, Chandra S: **CAS: 528: DC% 2BC1cXlsVCmsLc% 3D: Flavonoids: an overview. vol. 5**. *J Nutr Sci* 2016.

7. Pietta P-G: **Flavonoids as antioxidants**. *J Nat Prod* 2000, **63**(7):1035-1042.

8. Cassidy: **Potential risks and benefits of phytoestrogen-rich diets**. *Int J Vitam Nutr Res* 2003, **73**(2):120-126.

9. Tuohy P: **Soy infant formula and phytoestrogens**. *J Paediatr Child Health* 2003, **39**(6):401-405.

10. Eden JA: **Phytoestrogens for menopausal symptoms: a review**. *Maturitas* 2012, **72**(2):157-159.

11. Michel T, Halabalaki M, Skaltsounis A-L: **New concepts, experimental approaches, and dereplication strategies for the discovery of novel phytoestrogens from natural sources**. *Planta Med* 2013, **79**(07):514-532.

12. Hajirahimkhan A, Dietz BM, Bolton JL: **Botanical modulation of menopausal symptoms: mechanisms of action?** *Planta Med* 2013, **79**(07):538-553.

13. Reinli K, Block G: **Phytoestrogen content of foods—a compendium of literature values**. *Nutr Cancer* 1996, **26**(2):123-148.

14. Tham DM, Gardner CD, Haskell WL: **Potential health benefits of dietary phytoestrogens: a review of the clinical, epidemiological, and mechanistic evidence**. *The Journal of Clinical Endocrinology & Metabolism* 1998, **83**(7):2223-2235.

15. Singh S, Sharma B, Kanwar SS, Kumar A: **Lead phytochemicals for anticancer drug development**. *Frontiers in plant science* 2016, **7**:1667.

16. Vladimir-Knežević S, Blažeković B, Bival Štefan M, Babac M: **Plant polyphenols as antioxidants influencing the human health**: IntechOpen; 2012.

17. Ratnam DV, Ankola D, Bhardwaj V, Sahana DK, Kumar MR: **Role of antioxidants in prophylaxis and therapy: A pharmaceutical perspective**. *Journal of controlled release* 2006, **113**(3):189-207.

18. Scalbert A, Johnson IT, Saltmarsh M: **Polyphenols: antioxidants and beyond**. *The American journal of clinical nutrition* 2005, **81**(1):215S-217S.

19. Fraga CG, Galleano M, Verstraeten SV, Oteiza PI: **Basic biochemical mechanisms behind the health benefits of polyphenols**. *Mol Aspects Med* 2010, **31**(6):435-445.

20. Binsack R, Boersma BJ, Patel RP, Kirk M, White CR, Darley-Usmar V, Barnes S, Zhou F, Parks DA: **Enhanced antioxidant activity after chlorination of quercetin by hypochlorous acid**. *Alcoholism: Clinical and Experimental Research* 2001, **25**(3):434-443.

21. Korkina LG, Afanas' Ev IB: **Antioxidant and chelating properties of flavonoids**. *Adv Pharmacol* 1996, **38**:151-163.

22. Cotelle N, Bernier J-L, Catteau J-P, Pommery J, Wallet J-C, Gaydou EM: **Antioxidant properties of hydroxy-flavones**. *Free Radical Biol Med* 1996, **20**(1):35-43.

23. Pan Y, Qin R, Hou M, Xue J, Zhou M, Xu L, Zhang Y: **The interactions of polyphenols with Fe and their application in Fenton/Fenton-like reactions**. *Sep Purif Technol* 2022:121831.

24. Nijveldt RJ, Van Nood E, Van Hoorn DE, Boelens PG, Van Norren K, Van Leeuwen PA: **Flavonoids: a review of probable mechanisms of action and potential applications**. *The American journal of clinical nutrition* 2001, **74**(4):418-425.

25. Dreosti IE: **Bioactive ingredients: antioxidants and polyphenols in tea**. *Nutr Rev* 1996, **54**(11):S51-S58.

26. El Gharras H: **Polyphenols: food sources, properties and applications–a review**. *Int J Food Sci Tech* 2009, **44**(12):2512-2518.

27. Lachman J, Šulc M, Faitová K, Pivec V: **Major factors influencing antioxidant contents and antioxidant activity in grapes and wines**. *Int J Wine Res* 2009, **1**:101-121.

28. Li H, Xia N, Förstermann U: **Cardiovascular effects and molecular targets of resveratrol**. *Nitric Oxide* 2012, **26**(2):102-110.

29. Spanier G, Xu H, Xia N, Tobias S, Deng S, Wojnowski L, Forstermann U, Li H: **Resveratrol reduces endothelial oxidative stress by modulating the gene expression of superoxide dismutase 1 (SOD1), glutathione peroxidase 1 (GPx1) and NADPH oxidase subunit (Nox4)**. *J Physiol Pharmacol* 2009, **60**(Suppl 4):111-116.

30. Maleyki MA, Ismail A: **Antioxidant properties of cocoa powder**. *J Food Biochem* 2010, **34**(1):111-128.

31. Quiñones M, Miguel M, Aleixandre A: **Beneficial effects of polyphenols on cardiovascular disease**. *Pharmacol Res* 2013, **68**(1):125-131.

32. Uddin MS, Hossain MF, Al Mamun A, Shah MA, Hasana S, Bulbul IJ, Sarwar MS, Mansouri RA, Ashraf GM, Rauf A: **Exploring the multimodal role of phytochemicals in the modulation of cellular signaling pathways to combat age-related neurodegeneration**. *Sci Total Environ* 2020, **725**:138313.

33. Velmurugan BK, Rathinasamy B, Lohanathan BP, Thiyagarajan V, Weng C-F: **Neuroprotective role of phytochemicals**. *Molecules* 2018, **23**(10):2485.

34. Begum M, Islam A, Begum R, Uddin M, Rahman M, Alam S, Akter W, Das M, Imon A: **Ethnopharmacological inspections of organic extract of Oroxylum indicum in rat models: a promising natural gift**. *Evid Based Complement Alternat Med* 2019, **2019**.

35. Hashimoto M, Hossain S: **Neuroprotective and ameliorative actions of polyunsaturated fatty acids against neuronal diseases: beneficial effect of docosahexaenoic acid on cognitive decline in Alzheimer's disease**. *J Pharmacol Sci* 2011, **116**(2):150-162.

36. Uddin MS, Kabir MT: **Emerging signal regulating potential of genistein against Alzheimer's disease: a promising molecule of interest**. *Frontiers in Cell and Developmental Biology* 2019, **7**:197.

37. Uddin MS, Kabir MT, Tewari D, Mathew B, Aleya L: **Emerging signal regulating potential of small molecule biflavonoids to combat neuropathological insults of Alzheimer's disease**. *Sci Total Environ* 2020, **700**:134836.

38. de Oliveira DM, Ferreira Lima RM, El-Bachá RS: **Brain rust: recent discoveries on the role of oxidative stress in neurodegenerative diseases**. *Nutr Neurosci* 2012, **15**(3):94-102.

39. Srivastava N, Chauhan AS, Sharma B: **Isolation and characterization of some phytochemicals from Indian traditional plants**. *Biotechnology research international* 2012, **2012**.

40. Naoi M, Shamoto-Nagai M, Maruyama W: **Neuroprotection of multifunctional phytochemicals as novel therapeutic strategy for neurodegenerative disorders: Antiapoptotic and antiamyloidogenic activities by modulation of cellular signal pathways**. *Future Neurol* 2019, **14**(1):FNL9.

41. Chu KO, Chan S-O, Pang CP, Wang CC: **Pro-oxidative and antioxidative controls and signaling modification of polyphenolic phytochemicals: contribution to health promotion and disease prevention?** *J Agric Food Chem* 2014, **62**(18):4026-4038.

42. Ighodaro O, Akinloye O: **First line defence antioxidants-superoxide dismutase (SOD), catalase (CAT) and glutathione peroxidase (GPX): Their fundamental role in the entire antioxidant defence grid**. *Alexandria journal of medicine* 2018, **54**(4):287-293.

43. Mao X, Gu C, Chen D, Yu B, He J: **Oxidative stress-induced diseases and tea polyphenols**. *Oncotarget* 2017, **8**(46):81649.

44. Pauff JM, Hille R: **Inhibition studies of bovine xanthine oxidase by luteolin, silibinin, quercetin, and curcumin**. *J Nat Prod* 2009, **72**(4):725-731.

45. Wang Y, Zhang G, Pan J, Gong D: **Novel insights into the inhibitory mechanism of kaempferol on xanthine oxidase**. *J Agric Food Chem* 2015, **63**(2):526-534.

46. Sakthivel K, Guruvayoorappan C: **Amentoflavone inhibits iNOS, COX-2 expression and modulates cytokine profile, NF-κB signal transduction pathways in rats with ulcerative colitis**. *International immunopharmacology* 2013, **17**(3):907-916.

47. Kumar D, Shahid M: **Natural materials and products from insects: chemistry and applications**: Springer; 2020.

48. Hwang S-L, Yen G-C: **Modulation of Akt, JNK, and p38 activation is involved in citrus flavonoid-mediated cytoprotection of PC12 cells challenged by hydrogen peroxide**. *J Agric Food Chem* 2009, **57**(6):2576-2582.

49. Vauzour D, Vafeiadou K, Rice-Evans C, Williams RJ, Spencer JP: **Activation of pro-survival Akt and ERK1/2 signalling pathways underlie the anti-apoptotic effects of flavanones in cortical neurons**. *J Neurochem* 2007, **103**(4):1355-1367.

50. Qin S, Deng F, Wu W, Jiang L, Yamashiro T, Yano S, Hou D-X: **Baicalein modulates Nrf2/Keap1 system in both Keap1-dependent and Keap1-independent mechanisms**. *Arch Biochem Biophys* 2014, **559**:53-61.

51. Hossain M, Uddin M, Uddin G, Sumsuzzman DM, Islam M, Barreto GE, Mathew B, Ashraf GM: **Melatonin in Alzheimer's disease: a latent endogenous regulator of neurogenesis to mitigate Alzheimer's neuropathology**. *Mol Neurobiol* 2019, **56**(12):8255-8276.

52. Mori T, Koyama N, Guillot-Sestier M-V, Tan J, Town T: **Ferulic acid is a nutraceutical β-secretase modulator that improves behavioral impairment and alzheimer-like pathology in transgenic mice**. *PLoS One* 2013, **8**(2):e55774.

53. Kostomoiri M, Fragkouli A, Sagnou M, Skaltsounis LA, Pelecanou M, Tsilibary EC, Tzinia AK: **Oleuropein, an anti-oxidant polyphenol constituent of olive promotes α-secretase cleavage of the amyloid precursor protein (AβPP)**. *Cell Mol Neurobiol* 2013, **33**(1):147-154.

54.   Asensi M, Ortega A, Mena S, Feddi F, Estrela JM: **Natural polyphenols in cancer therapy**. *Crit Rev Clin Lab Sci* 2011, **48**(5-6):197-216.

55.   Pratheeshkumar P, Son Y-O, Korangath P, Manu KA, Siveen KS: **Phytochemicals in cancer prevention and therapy**. In*.*, vol. 2015: Hindawi; 2015.

56.   Heo B-G, Park Y-J, Park Y-S, Bae J-H, Cho J-Y, Park K, Jastrzebski Z, Gorinstein S: **Anticancer and antioxidant effects of extracts from different parts of indigo plant**. *Industrial Crops and Products* 2014, **56**:9-16.

57.   Wen L, Wu D, Jiang Y, Prasad KN, Lin S, Jiang G, He J, Zhao M, Luo W, Yang B: **Identification of flavonoids in litchi (Litchi chinensis Sonn.) leaf and evaluation of anticancer activities**. *J Funct Foods* 2014, **6**:555-563.

58.   Girish C, Pradhan SC: **Drug development for liver diseases: focus on picroliv, ellagic acid and curcumin**. *Fundam Clin Pharmacol* 2008, **22**(6):623-632.

59.   Heber D: **Multitargeted therapy of cancer by ellagitannins**. *Cancer letters* 2008, **269**(2):262-268.

60.   Rocha A, Wang L, Penichet M, Martins-Green M: **Pomegranate juice and specific components inhibit cell and molecular processes critical for metastasis of breast cancer**. *Breast Cancer Res Treat* 2012, **136**(3):647-658.

61.   Zhang H-M, Zhao L, Li H, Xu H, Chen W-W, Tao L: **Research progress on the anticarcinogenic actions and mechanisms of ellagic acid**. *Cancer biology & medicine* 2014, **11**(2):92.

62.   Vanella L, Di Giacomo C, Acquaviva R, Barbagallo I, Cardile V, Kim DH, Abraham NG, Sorrenti V: **Apoptotic markers in a prostate cancer cell line: Effect of ellagic acid**. *Oncol Rep* 2013, **30**(6):2804-2810.

63.   Imran M, Aslam Gondal T, Atif M, Shahbaz M, Batool Qaisarani T, Hanif Mughal M, Salehi B, Martorell M, Sharifi-Rad J: **Apigenin as an anticancer agent**. *Phytother Res* 2020, **34**(8):1812-1828.

64.   Chen J, He Z-M, Wang F-L, Zhang Z-S, Liu X-z, Zhai D-D, Chen W-D: **Curcumin and its promise as an anticancer drug: An**

analysis of its anticancer and antifungal effects in cancer and associated complications from invasive fungal infections. *Eur J Pharmacol* 2016, **772**:33-42.

65.   Liu H-T, Ho Y-S: **Anticancer effect of curcumin on breast cancer and stem cells**. *Food science and human wellness* 2018, **7**(2):134-137.

66.   Serra D, Paixão J, Nunes C, Dinis TC, Almeida LM: **Cyanidin-3-glucoside suppresses cytokine-induced inflammatory response in human intestinal cells: comparison with 5-aminosalicylic acid**. *PLoS One* 2013, **8**(9):e73001.

67.   Lall RK, Adhami VM, Mukhtar H: **Dietary flavonoid fisetin for cancer prevention and treatment**. *Mol Nutr Food Res* 2016, **60**(6):1396-1405.

68.   Rengarajan T, Yaacob NS: **The flavonoid fisetin as an anticancer agent targeting the growth signaling pathways**. *Eur J Pharmacol* 2016, **789**:8-16.

69.   Stanisic D, Costa A, Fávaro W, Tasic L, Seabra A: **Anticancer activities of hesperidin and hesperetin**. In.: vivo; 2018.

70.   Adan A, Baran Y: **The pleiotropic effects of fisetin and hesperetin on human acute promyelocytic leukemia cells are mediated through apoptosis, cell cycle arrest, and alterations in signaling networks**. *Tumor Biol* 2015, **36**(11):8973-8984.

71.   Li Q-S, Li C-Y, Li Z-L, Zhu H-L: **Genistein and its synthetic analogs as anticancer agents**. *Anti-Cancer Agents in Medicinal Chemistry (Formerly Current Medicinal Chemistry-Anti-Cancer Agents)* 2012, **12**(3):271-281.

72.   Nafees S, Zafaryab M, Mehdi SH, Zia B, Rizvi MA, Khan MA: **Anti-cancer effect of gingerol in cancer prevention and treatment**. *Anti-Cancer Agents in Medicinal Chemistry (Formerly Current Medicinal Chemistry-Anti-Cancer Agents)* 2021, **21**(4):428-432.

73.   Radhakrishnan E, Bava SV, Narayanan SS, Nath LR, Thulasidasan AKT, Soniya EV, Anto RJ: **[6]-Gingerol induces caspase-dependent apoptosis and prevents PMA-induced proliferation in colon cancer cells by inhibiting MAPK/AP-1 signaling**. *PLoS One* 2014, **9**(8):e104401.

74. Wang X, Yang Y, An Y, Fang G: **The mechanism of anticancer action and potential clinical use of kaempferol in the treatment of breast cancer**. *Biomed Pharmacother* 2019, **117**:109086.

75. Lee J, Kim JH: **Kaempferol inhibits pancreatic cancer cell growth and migration through the blockade of EGFR-related pathway in vitro**. *PLoS One* 2016, **11**(5):e0155264.

76. Hossan MS, Rahman S, Bashar A, Jahan R, Al-Nahain A, Rahmatullah M: **Rosmarinic acid: A review of its anticancer action**. *World J Pharm Pharm Sci* 2014, **3**(9):57-70.

77. Ahmadi R, Ebrahimzadeh MA: **Resveratrol–A comprehensive review of recent advances in anticancer drug design and development**. *Eur J Med Chem* 2020, **200**:112356.

78. Varoni EM, Lo Faro AF, Sharifi-Rad J, Iriti M: **Anticancer molecular mechanisms of resveratrol**. *Frontiers in nutrition* 2016, **3**:8.

79. Medzhitov R: **Origin and physiological roles of inflammation**. *Nature* 2008, **454**(7203):428-435.

80. Zhao R, Liang H, Clarke E, Jackson C, Xue M: **Inflammation in chronic wounds**. *International journal of molecular sciences* 2016, **17**(12):2085.

81. Bengmark S: **Acute and "chronic" phase reaction—a mother of disease**. *Clin Nutr* 2004, **23**(6):1256-1266.

82. Middleton E, Kandaswami C, Theoharides TC: **The effects of plant flavonoids on mammalian cells: implications for inflammation, heart disease, and cancer**. *Pharmacol Rev* 2000, **52**(4):673-751.

83. Scalbert A, Manach C, Morand C, Rémésy C, Jiménez L: **Dietary polyphenols and the prevention of diseases**. *Crit Rev Food Sci Nutr* 2005, **45**(4):287-306.

84. Yoon J-H, Baek SJ: **Molecular targets of dietary polyphenols with anti-inflammatory properties**. *Yonsei Med J* 2005, **46**(5):585-596.

85. Santangelo C, Varì R, Scazzocchio B, Di Benedetto R, Filesi C, Masella R: **Polyphenols, intracellular signalling and inflammation**. *Annali-istituto superiore di sanita* 2007, **43**(4):394.

86. French JA, Koepp M, Naegelin Y, Vigevano F, Auvin S, Rho JM, Rosenberg E, Devinsky O, Olofsson PS, Dichter MA: **Clinical studies and anti-inflammatory mechanisms of treatments**. *Epilepsia* 2017, **58**:69-82.

87. Ponder A, Long MD: **A clinical review of recent findings in the epidemiology of inflammatory bowel disease**. *Clin Epidemiol* 2013, **5**:237.

88. Calixto JB, Otuki MF, Santos AR: **Anti-inflammatory compounds of plant origin. Part I. Action on arachidonic acid pathway, nitric oxide and nuclear factor κ B (NF-κB)**. *Planta Med* 2003, **69**(11):973-983.

89. John CM, Sandrasaigaran P, Tong CK, Adam A, Ramasamy R: **Immunomodulatory activity of polyphenols derived from Cassia auriculata flowers in aged rats**. *Cell Immunol* 2011, **271**(2):474-479.

90. Karasawa K, Uzuhashi Y, Hirota M, Otani H: **A matured fruit extract of date palm tree (Phoenix dactylifera L.) stimulates the cellular immune system in mice**. *J Agric Food Chem* 2011, **59**(20):11287-11293.

91. Biasutto L, Mattarei A, Zoratti M: **Resveratrol and health: the starting point**. *ChemBioChem* 2012, **13**(9):1256-1259.

92. Mohar DS, Malik S: **The sirtuin system: the holy grail of resveratrol?** *J Clin Exp Cardiolog* 2012, **3**(11).

93. Capiralla H, Vingtdeux V, Venkatesh J, Dreses-Werringloer U, Zhao H, Davies P, Marambaud P: **Identification of potent small-molecule inhibitors of STAT 3 with anti-inflammatory properties in RAW 264.7 macrophages**. *The FEBS journal* 2012, **279**(20):3791-3799.

94. Leiherer A, Mündlein A, Drexel H: **Phytochemicals and their impact on adipose tissue inflammation and diabetes**. *Vascul Pharmacol* 2013, **58**(1-2):3-20.

95. Marchiani A, Rozzo C, Fadda A, Delogu G, Ruzza P: **Curcumin and curcumin-like molecules: from spice to drugs**. *Curr Med Chem* 2014, **21**(2):204-222.

96. Noorafshan A, Ashkani-Esfahani S: **A review of therapeutic effects of curcumin**. *Curr Pharm Des* 2013, **19**(11):2032-2046.

97. Akyol S, Ozturk G, Ginis Z, Armutcu F, Yigitoglu MR, Akyol O: **In vivo and in vitro antıneoplastic actions of caffeic acid phenethyl ester (CAPE): therapeutic perspectives**. *Nutr Cancer* 2013, **65**(4):515-526.

98. Domitrovic R: **The molecular basis for the pharmacological activity of anthocyans**. *Curr Med Chem* 2011, **18**(29):4454-4469.

99. Bae J-S: **Role of high mobility group box 1 in inflammatory disease: focus on sepsis**. *Arch Pharmacal Res* 2012, **35**(9):1511-1523.

100. Boissier M-C, Assier E, Biton J, Denys A, Falgarone G, Bessis N: **Regulatory T cells (Treg) in rheumatoid arthritis**. *Joint Bone Spine* 2009, **76**(1):10-14.

101. Robinson DS, Larché M, Durham SR: **Tregs and allergic disease**. *The Journal of clinical investigation* 2004, **114**(10):1389-1397.

102. Sakaguchi S, Miyara M, Costantino CM, Hafler DA: **FOXP3+ regulatory T cells in the human immune system**. *Nature Reviews Immunology* 2010, **10**(7):490-500.

103. Wong CP, Nguyen LP, Noh SK, Bray TM, Bruno RS, Ho E: **Induction of regulatory T cells by green tea polyphenol EGCG**. *Immunol Lett* 2011, **139**(1-2):7-13.

104. Yang J, Yang X, Li M: **Baicalin, a natural compound, promotes regulatory T cell differentiation**. *BMC Complement Altern Med* 2012, **12**(1):1-7.

105. Wang H-K, Yeh C-H, Iwamoto T, Satsu H, Shimizu M, Totsuka M: **Dietary flavonoid naringenin induces regulatory T cells via an aryl hydrocarbon receptor mediated pathway**. *J Agric Food Chem* 2012, **60**(9):2171-2178.

106. Wang J, Pae M, Meydani SN, Wu D: **Green tea epigallocatechin-3-gallate modulates differentiation of naïve CD4+ T cells into specific lineage effector cells**. *J Mol Med* 2013, **91**(4):485-495.

107. Yang J, Yang X, Chu Y, Li M: **Identification of Baicalin as an immunoregulatory compound by controlling TH17 cell differentiation**. *PLoS One* 2011, **6**(2):e17164.

108.   Murray PJ, Wynn TA: **Protective and pathogenic functions of macrophage subsets**. *Nature reviews immunology* 2011, **11**(11):723-737.

109.   González R, Ballester I, López-Posadas R, Suárez M, Zarzuelo A, Martínez-Augustin O, Medina FSD: **Effects of flavonoids and other polyphenols on inflammation**. *Crit Rev Food Sci Nutr* 2011, **51**(4):331-362.

110.   Wang K, Ping S, Huang S, Hu L, Xuan H, Zhang C, Hu F: **Molecular mechanisms underlying the in vitro anti-inflammatory effects of a flavonoid-rich ethanol extract from Chinese propolis (poplar type)**. *Evid Based Complement Alternat Med* 2013, **2013**.

111.   Park K-I, Kang S-R, Park H-S, Lee DH, Nagappan A, Kim JA, Shin SC, Kim EH, Lee WS, Chung H-J: **Regulation of proinflammatory mediators via NF-κB and p38 MAPK-dependent mechanisms in RAW 264.7 macrophages by polyphenol components isolated from Korea Lonicera japonica THUNB**. *Evid Based Complement Alternat Med* 2012, **2012**.

112.   Lai Z-R, Ho Y-L, Huang S-C, Huang T-H, Lai S-C, Tsai J-C, Wang C-Y, Huang G-J, Chang Y-S: **Antioxidant, anti-inflammatory and antiproliferative activities of Kalanchoe gracilis (L.) DC stem**. *The American journal of Chinese medicine* 2011, **39**(06):1275-1290.

113.   Comalada M, Ballester I, Bailon E, Sierra S, Xaus J, Gálvez J, de Medina FS, Zarzuelo A: **Inhibition of pro-inflammatory markers in primary bone marrow-derived mouse macrophages by naturally occurring flavonoids: analysis of the structure–activity relationship**. *Biochem Pharmacol* 2006, **72**(8):1010-1021.

114.   Crouvezier S, Powell B, Keir D, Yaqoob P: **The effects of phenolic components of tea on the production of pro-and anti-inflammatory cytokines by human leukocytes in vitro**. *Cytokine* 2001, **13**(5):280-286.

115.   Bitler CM, Viale TM, Damaj B, Crea R: **Hydrolyzed olive vegetation water in mice has anti-inflammatory activity**. *The Journal of nutrition* 2005, **135**(6):1475-1479.

116.   Chen J-C, Ho F-M, Chao P-DL, Chen C-P, Jeng K-CG, Hsu H-B, Lee S-T, Wu WT, Lin W-W: **Inhibition of iNOS gene expression by quercetin is mediated by the inhibition of IκB kinase, nuclear factor-kappa B and STAT1, and depends on heme oxygenase-1**

induction in mouse BV-2 microglia. *Eur J Pharmacol* 2005, **521**(1-3):9-20.

117. García-Lafuente A, Guillamón E, Villares A, Rostagno MA, Martínez JA: **Flavonoids as anti-inflammatory agents: implications in cancer and cardiovascular disease**. *Inflammation Res* 2009, **58**(9):537-552.

118. Leifert WR, Abeywardena MY: **Cardioprotective actions of grape polyphenols**. *Nutr Res* 2008, **28**(11):729-737.

119. Zalba G, Fortuño A, San José G, Moreno MU, Beloqui O, Díez J: **Oxidative stress, endothelial dysfunction and cerebrovascular disease**. *Cerebrovasc Dis* 2007, **24**(Suppl. 1):24-29.

120. Andriambeloson E, Kleschyov AL, Muller B, Beretz A, Stoclet JC, Andriantsitohaina R: **Nitric oxide production and endothelium-dependent vasorelaxation induced by wine polyphenols in rat aorta**. *Br J Pharmacol* 1997, **120**(6):1053-1058.

121. Perez-Vizcaino F, Duarte J, Andriantsitohaina R: **Endothelial function and cardiovascular disease: effects of quercetin and wine polyphenols**. *Free Radical Res* 2006, **40**(10):1054-1065.

122. Li H-F, Chen S-A, Wu S-N: **Evidence for the stimulatory effect of resveratrol on Ca2+-activated K+ current in vascular endothelial cells**. *Cardiovasc Res* 2000, **45**(4):1035-1045.

123. Abu-Amsha R, Croft KD, Puddey IB, Proudfoot JM, Beilin LJ: **Phenolic content of various beverages determines the extent of inhibition of human serum and low-density lipoprotein oxidation in vitro: identification and mechanism of action of some cinnamic acid derivatives from red wine**. *Clin Sci* 1996, **91**(4):449-458.

124. Ridker PM, Brown NJ, Vaughan DE, Harrison DG, Mehta JL: **Established and emerging plasma biomarkers in the prediction of first atherothrombotic events**. *Circulation* 2004, **109**(25_suppl_1):IV-6-IV-19.

125. Renaud Sd, de Lorgeril M: **Wine, alcohol, platelets, and the French paradox for coronary heart disease**. *The Lancet* 1992, **339**(8808):1523-1526.

126. Ou H-C, Chou F-P, Sheen H-M, Lin T-M, Yang C-H, Sheu WH-H: **Resveratrol, a polyphenolic compound in red wine, protects**

against oxidized LDL-induced cytotoxicity in endothelial cells. *Clin Chim Acta* 2006, **364**(1-2):196-204.

127. Ursini F, Zamburlini A, Cazzolato G, Maiorino M, Bon GB, Sevanian A: **Postprandial plasma lipid hydroperoxides: a possible link between diet and atherosclerosis**. *Free Radical Biol Med* 1998, **25**(2):250-252.

128. Elbaz M, Alves A, Andriantsithohaina R, Roul G: **ProvinolsTM, a polyphenolic extract of red wine inhibits in-stent neointimal growth in cholesterol-fed rabbit**. In: *Eur Heart J: 2005*. OXFORD UNIV PRESS GREAT CLARENDON ST, OXFORD OX2 6DP, ENGLAND: 236-236.

129. Arranz S, Chiva-Blanch G, Valderas-Martínez P, Medina-Remón A, Lamuela-Raventós RM, Estruch R: **Wine, beer, alcohol and polyphenols on cardiovascular disease and cancer**. *Nutrients* 2012, **4**(7):759-781.

130. Kurosawa T, Itoh F, Nozaki A, Nakano Y, Katsuda S-i, Osakabe N, Tsubone H, Kondo K, Itakura H: **Suppressive effects of cacao liquor polyphenols (CLP) on LDL oxidation and the development of atherosclerosis in Kurosawa and Kusanagi-hypercholesterolemic rabbits**. *Atherosclerosis* 2005, **179**(2):237-246.

131. Auger C, Gérain P, Laurent-Bichon F, Portet K, Bornet A, Caporiccio B, Cros G, Teissédre P-L, Rouanet J-M: **Phenolics from commercialized grape extracts prevent early atherosclerotic lesions in hamsters by mechanisms other than antioxidant effect**. *J Agric Food Chem* 2004, **52**(16):5297-5302.

132. Sakakura K, Nakano M, Otsuka F, Ladich E, Kolodgie FD, Virmani R: **Pathophysiology of atherosclerosis plaque progression**. *Heart, Lung and Circulation* 2013, **22**(6):399-411.

133. Cirillo G, Iemma F: **Antioxidant polymers: Synthesis, properties, and applications**: John Wiley & Sons; 2012.

134. Riahi E: **Effect of high pressure treatment on the kinetics of enzyme inactivation and microbial destruction in apple juice**. 2003.

135. Wenzel U, Daniel H: **Polypenols and gene expression**. *Recent Adv Polyphen Res, Oxford, UK: Wiley-Blackwell* 2009:359-377.

136. Coimbra S, Lage S, Brandizzi L, Yoshida V, Da Luz P: **The action of red wine and purple grape juice on vascular reactivity is independent of plasma lipids in hypercholesterolemic patients**. *Braz J Med Biol Res* 2005, **38**:1339-1347.

137. Kim J-E, Son JE, Jung SK, Kang NJ, Lee CY, Lee KW, Lee HJ: **Cocoa polyphenols suppress TNF-α-induced vascular endothelial growth factor expression by inhibiting phosphoinositide 3-kinase (PI3K) and mitogen-activated protein kinase kinase-1 (MEK1) activities in mouse epidermal cells**. *Br J Nutr* 2010, **104**(7):957-964.

138. Di Pietro N, Baldassarre MPA, Cichelli A, Pandolfi A, Formoso G, Pipino C: **Role of polyphenols and carotenoids in endothelial dysfunction: An overview from classic to innovative biomarkers**. *Oxid Med Cell Longev* 2020, **2020**.

139. Covas M-I, Nyyssönen K, Poulsen HE, Kaikkonen J, Zunft H-JF, Kiesewetter H, Gaddi A, de la Torre R, Mursu J, Bäumler H: **The effect of polyphenols in olive oil on heart disease risk factors: a randomized trial**. *Ann Intern Med* 2006, **145**(5):333-341.

140. Anhê FF, Desjardins Y, Pilon G, Dudonné S, Genovese MI, Lajolo FM, Marette A: **Polyphenols and type 2 diabetes: A prospective review**. *PharmaNutrition* 2013, **1**(4):105-114.

141. Seeram NP: **Berry fruits: compositional elements, biochemical activities, and the impact of their intake on human health, performance, and disease**. In., vol. 56: ACS Publications; 2008: 627-629.

142. Hanhineva K, Törrönen R, Bondia-Pons I, Pekkinen J, Kolehmainen M, Mykkänen H, Poutanen K: **Impact of dietary polyphenols on carbohydrate metabolism**. *International journal of molecular sciences* 2010, **11**(4):1365-1402.

143. Ahn J, Lee H, Kim S, Ha T: **Resveratrol inhibits TNF-α-induced changes of adipokines in 3T3-L1 adipocytes**. *Biochem Biophys Res Commun* 2007, **364**(4):972-977.

144. Chuang C-C, Martinez K, Xie G, Kennedy A, Bumrungpert A, Overman A, Jia W, McIntosh MK: **Quercetin is equally or more effective than resveratrol in attenuating tumor necrosis factor-α– mediated inflammation and insulin resistance in primary human**

adipocytes. *The American journal of clinical nutrition* 2010, **92**(6):1511-1521.

145.   Montopoli M, Ragazzi E, Froldi G, Caparrotta L: **Cell-cycle inhibition and apoptosis induced by curcumin and cisplatin or oxaliplatin in human ovarian carcinoma cells**. *Cell Prolif* 2009, **42**(2):195-206.

146.   Muraoka K, Shimizu K, Sun X, Tani T, Izumi R, Miwa K: **Flavonoids exert diverse inhibitory effects on the activation of NF-κB**. In: *Transplant Proc: 2002*. 1335-1340.

147.   Park J-Y, Kawada T, Han I-S, Kim B-S, Goto T, Takahashi N, Fushiki T, Kurata T, Yu R: **Capsaicin inhibits the production of tumor necrosis factor α by LPS-stimulated murine macrophages, RAW 264.7: a PPARγ ligand-like action as a novel mechanism**. *FEBS Lett* 2004, **572**(1-3):266-270.

148.   Penumetcha M, Santanam N: **Nutraceuticals as ligands of PPAR**. *PPAR research* 2012, **2012**.

149.   Guo H, Ling W, Wang Q, Liu C, Hu Y, Xia M, Feng X, Xia X: **Effect of anthocyanin-rich extract from black rice (Oryza sativa L. indica) on hyperlipidemia and insulin resistance in fructose-fed rats**. *Plant Foods Hum Nutr* 2007, **62**(1):1-6.

150.   Jayaprakasam B, Olson LK, Schutzki RE, Tai M-H, Nair MG: **Amelioration of obesity and glucose intolerance in high-fat-fed C57BL/6 mice by anthocyanins and ursolic acid in Cornelian cherry (Cornus mas)**. *J Agric Food Chem* 2006, **54**(1):243-248.

151.   Prior RL, E. Wilkes S, R. Rogers T, Khanal RC, Wu X, Howard LR: **Purified blueberry anthocyanins and blueberry juice alter development of obesity in mice fed an obesogenic high-fat diet**. *J Agric Food Chem* 2010, **58**(7):3970-3976.

152.   Brownlee M: **Biochemistry and molecular cell biology of diabetic complications**. *Nature* 2001, **414**(6865):813-820.

153.   Diepvens K, Westerterp KR, Westerterp-Plantenga MS: **Obesity and thermogenesis related to the consumption of caffeine, ephedrine, capsaicin, and green tea**. *American journal of physiology-Regulatory, integrative and comparative physiology* 2007.

154. Lee MS, Kim CT, Kim IH, Kim Y: **Effects of capsaicin on lipid catabolism in 3T3-L1 adipocytes**. *Phytother Res* 2011, **25**(6):935-939.

155. Lee YM, Choi JS, Kim MH, Jung MH, Lee YS, Song J: **Effects of dietary genistein on hepatic lipid metabolism and mitochondrial function in mice fed high-fat diets**. *Nutrition* 2006, **22**(9):956-964.

156. Kole PL, Jadhav HR, Thakurdesai P, Nagappa AN: **Cosmetic potential of herbal extracts**. 2005.

157. de Lima Cherubim DJ, Buzanello Martins CV, Oliveira Fariña L, da Silva de Lucca RA: **Polyphenols as natural antioxidants in cosmetics applications**. *J Cosmet Dermatol* 2020, **19**(1):33-37.

158. Bose B, Choudhury H, Tandon P, Kumaria S: **Studies on secondary metabolite profiling, anti-inflammatory potential, in vitro photoprotective and skin-aging related enzyme inhibitory activities of Malaxis acuminata, a threatened orchid of nutraceutical importance**. *J Photochem Photobiol B: Biol* 2017, **173**:686-695.

159. Cuelho CHF, Alves GdAD, Lovatto MO, Bonilha IF, Barbisan F, da Cruz IBM, Oliveira SM, Fachinetto R, do Canto GS, Manfron MP: **Topical formulation containing Ilex Paraguariensis extract increases metalloproteinases and myeloperoxidase activities in mice exposed to UVB radiation**. *J Photochem Photobiol B: Biol* 2018, **189**:95-103.

160. Ratz-Lyko A, Arct J, Pytkowska K: **Methods for evaluation of cosmetic antioxidant capacity**. *Skin Res Technol* 2012, **18**(4):421-430.

161. Leopoldini M, Russo N, Toscano M: **The molecular basis of working mechanism of natural polyphenolic antioxidants**. *Food Chem* 2011, **125**(2):288-306.

162. Ng T, Liu F, Wang Z: **Antioxidative activity of natural products from plants**. *Life Sci* 2000, **66**(8):709-723.

163. Reuter J, Merfort I, Schempp CM: **Botanicals in dermatology**. *Am J Clin Dermatol* 2010, **11**(4):247-267.

164. Ribeiro AS, Estanqueiro M, Oliveira MB, Sousa Lobo JM: **Main benefits and applicability of plant extracts in skin care products**. *Cosmetics* 2015, **2**(2):48-65.

165. Barbulova A, Colucci G, Apone F: **New trends in cosmetics: By-products of plant origin and their potential use as cosmetic active ingredients**. *Cosmetics* 2015, **2**(2):82-92.

166. Basile A, Sorbo S, Giordano S, Ricciardi L, Ferrara S, Montesano D, Cobianchi RC, Vuotto M, Ferrara L: **Antibacterial and allelopathic activity of extract from Castanea sativa leaves**. *Fitoterapia* 2000, **71**:S110-S116.

167. Calliste C-A, Trouillas P, Allais D-P, Duroux J-L: **Castanea sativa Mill. leaves as new sources of natural antioxidant: an electronic spin resonance study**. *J Agric Food Chem* 2005, **53**(2):282-288.

168. Almeida IF, Maleckova J, Saffi R, Monteiro H, Góios F, Amaral MH, Costa PC, Garrido J, Silva P, Pestana N: **Characterization of an antioxidant surfactant-free topical formulation containing Castanea sativa leaf extract**. *Drug Dev Ind Pharm* 2015, **41**(1):148-155.

169. Isman MB, Koul O, Luczynski A, Kaminski J: **Insecticidal and antifeedant bioactivities of neem oils and their relationship to azadirachtin content**. *J Agric Food Chem* 1990, **38**(6):1406-1411.

170. Vanka A, Tandon S, Rao S, Udupa N, Ramkumar P: **The effect of indigenous Neem Azadirachta indica [correction of (Adirachta indica)] mouth wash on Streptococcus mutans and lactobacilli growth**. *Indian journal of dental research: official publication of Indian Society for Dental Research* 2001, **12**(3):133-144.

171. Anton R, Jiang Y, Weniger B, Beck J, Rivier L: **Pharmacognosy of Mimosa tenuiflora (willd.) poiret**. *J Ethnopharmacol* 1993, **38**(2-3):145-152.

172. Choi SW, Son BW, Son YS, Park YI, Lee SK, Chung MH: **The wound-healing effect of a glycoprotein fraction isolated from aloe vera**. *Br J Dermatol* 2001, **145**(4):535-545.

173. Olsen DL, Raub W, Bradley C, Johnson M, Macias JL, Love V, Markoe A: **The effect of aloe vera gel/mild soap versus mild soap alone in preventing skin reactions in patients undergoing radiation therapy**. In: *Oncol Nurs Forum: 2001*.

174.   Rajeswari R, Umadevi M, Rahale CS, Pushpa R, Selvavenkadesh S, Kumar KS, Bhowmik D: **Aloe vera: the miracle plant its medicinal and traditional uses in India**. *Journal of Pharmacognosy and Phytochemistry* 2012, **1**(4):118-124.

175.   Leung AY: **Encyclopedia of common natural ingredients used in food, drugs, and cosmetics**: Wiley; 1980.

176.   Patel M, Sahu A, Rajak R: **Solid Waste Management in Textile Industry**. In: *Handbook of Solid Waste Management*. Springer; 2022: 1225-1256.

177.   Thakker AM, Sun D: **Sustainable plant-based bioactive materials for functional printed textiles**. *The Journal of the Textile Institute* 2021, **112**(8):1324-1358.

178.   Saxena S, Raja A: **Natural dyes: sources, chemistry, application and sustainability issues**. In: *Roadmap to sustainable textiles and clothing*. Springer; 2014: 37-80.

179.   Mishra A, Gautam S: **Application of natural dyes for herbal textiles**. *Chemistry and technology of natural and synthetic dyes and pigments* 2020:123-150.

180.   Kim S: **Biopolyphenolics in textile**. *Advances in Textile Biotechnology* 2019:159-183.

181.   Dabas D: **Polyphenols as colorants**. *Adv Food Technol Nutr Sci Open J* 2016:S1-S6.

182.   Wang F, Gong J, Ren Y, Zhang J: **Eco-dyeing with biocolourant based on natural compounds**. *Royal Society Open Science* 2018, **5**(1):171134.

183.   Wang F, Gong J, Zhang X, Ren Y, Zhang J: **Preparation of biocolorant and eco-dyeing derived from polyphenols based on laccase-catalyzed oxidative polymerization**. *Polymers* 2018, **10**(2):196.

184.   Thakker AM: **Sustainable processing of cotton fabrics with plant-based biomaterials Sapindus mukorossi and Acacia concinna for health-care applications**. *The Journal of The Textile Institute* 2021, **112**(5):718-726.

185.   Sanda MD, Badu M, Awudza J, Boadi N: **Development of TiO 2-based dye-sensitized solar cells using natural dyes extracted from**

some plant-based materials. *Chemistry International* 2021, **7**(1):9-20.

186.   Hussain SA: **Development of dye sensitized solar cells using Botuje green leaves (Jathopha Curcas Linn)**. *Science Journal of Physics* 2013, **2013**.

187.   Calogero G, Di Marco G: **Red Sicilian orange and purple eggplant fruits as natural sensitizers for dye-sensitized solar cells**. *Sol Energy Mater Sol Cells* 2008, **92**(11):1341-1346.

188.   Calogero G, Di Marco G, Cazzanti S, Caramori S, Argazzi R, Di Carlo A, Bignozzi CA: **Efficient dye-sensitized solar cells using red turnip and purple wild Sicilian prickly pear fruits**. *International journal of molecular sciences* 2010, **11**(1):254-267.

189.   Dai Q, Rabani J: **Photosensitization of nanocrystalline TiO2 films by pomegranate pigments with unusually high efficiency in aqueous medium**. *Chem Commun* 2001(20):2142-2143.

190.   Dai Q, Rabani J: **Photosensitization of nanocrystalline TiO2 films by anthocyanin dyes**. *J Photochem Photobiol A: Chem* 2002, **148**(1-3):17-24.

191.   Smestad GP, Gratzel M: **Demonstrating electron transfer and nanotechnology: a natural dye-sensitized nanocrystalline energy converter**. *J Chem Educ* 1998, **75**(6):752.

192.   Tennakone K, Kumara G, Kottegoda I, Wijayantha K: **The photostability of dye-sensitized solid state photovoltaic cells: factors determining the stability of the pigment in a nanoporous n-/cyanidin/p-CuI cell**. *Semicond Sci Technol* 1997, **12**(1):128.

193.   Cherepy NJ, Smestad GP, Grätzel M, Zhang JZ: **Ultrafast electron injection: implications for a photoelectrochemical cell utilizing an anthocyanin dye-sensitized TiO2 nanocrystalline electrode**. *The Journal of Physical Chemistry B* 1997, **101**(45):9342-9351.

194.   Calogero G, Yum J, Sinopoli A, Di Marco G: **tzel, MK Nazeeruddin**. *Solar Energy* 2012, **86**:1563-1575.

195.   Brockington SF, Walker RH, Glover BJ, Soltis PS, Soltis DE: **Complex pigment evolution in the Caryophyllales**. *New Phytol* 2011, **190**(4):854-864.

196. Hao S, Wu J, Huang Y, Lin J: **Natural dyes as photosensitizers for dye-sensitized solar cell**. *Solar energy* 2006, **80**(2):209-214.

197. Narayan MR: **Dye sensitized solar cells based on natural photosensitizers**. *Renewable and sustainable energy reviews* 2012, **16**(1):208-215.

198. Zhou H, Wu L, Gao Y, Ma T: **Dye-sensitized solar cells using 20 natural dyes as sensitizers**. *J Photochem Photobiol A: Chem* 2011, **219**(2-3):188-194.

199. Hug H, Bader M, Mair P, Glatzel T: **Biophotovoltaics: natural pigments in dye-sensitized solar cells**. *Applied Energy* 2014, **115**:216-225.

200. Coleman WF: **Molecular models of indicators**. In.: ACS Publications; 2008.

201. Devarayan K, Kim B-S: **Reversible and universal pH sensing cellulose nanofibers for health monitor**. *Sensors Actuators B: Chem* 2015, **209**:281-286.

202. Zhang X, Lu S, Chen X: **A visual pH sensing film using natural dyes from Bauhinia blakeana Dunn**. *Sensors Actuators B: Chem* 2014, **198**:268-273.

203. Shukla V, Kandeepan G, Vishnuraj MR, Soni A: **Anthocyanins based indicator sensor for intelligent packaging application**. *Agricultural research* 2016, **5**(2):205-209.

204. Meng Q, Han T, Wang G, Zheng N, Cao C, Xie S: **Preparation of a natural dye doped Ormosil coating for the detection of formaldehyde in the optical gas sensor**. *Sensors Actuators B: Chem* 2014, **196**:238-244.

205. da Silva HM, Mageste AB, e Silva SJB, Ferreira GMD, Ferreira GMD: **Anthocyanin immobilization in carboxymethylcellulose/starch films: A sustainable sensor for the detection of Al (III) ions in aqueous matrices**. *Carbohydrate polymers* 2020, **230**:115679.

206. Yang S, Yin B, Xu L, Gao B, Sun H, Du L, Tang Y, Jiang W, Cao F: **A natural quercetin-based fluorescent sensor for highly sensitive and selective detection of copper ions**. *Analytical Methods* 2015, **7**(11):4546-4551.

207. Okello VA, Osonga FJ, Knipfing MT, Bushlyar V, Sadik OA: **Reactivity, characterization of reaction products and immobilization of lead in water and sediments using quercetin pentaphosphate**. *Environmental Science: Processes & Impacts* 2016, **18**(3):306-313.

208. Bai R, Zhang X, Yong H, Wang X, Liu Y, Liu J: **Development and characterization of antioxidant active packaging and intelligent Al3+-sensing films based on carboxymethyl chitosan and quercetin**. *International journal of biological macromolecules* 2019, **126**:1074-1084.

209. Normaya E, Fazli M, Ahmad MN, Bulat KHK: **COSMO-RS and DFT studies on development and optimization of quercetin as a chemosensor for Fe3+ recognition in aqueous medium**. *J Mol Struct* 2019, **1184**:538-545.

210. Alshammari AH, Alqahtani Z, Suah FBM, Nizar SA, Dunbar A, Grell M: **Low cost, high sensitivity detection of waterborne Al3+ cations and F− anions via the fluorescence response of a morin derivative dye**. *Anal Chim Acta* 2020, **1105**:1-10.

211. Li C, Zhao J, Chen Y, Wang X, Sun X, Pan W, Yu G, Yan Z, Wang J: **A carbon dots/rutin system for colorimetric and fluorimetric dual mode detection of Al 3+ in aqueous solution**. *Analyst* 2018, **143**(22):5467-5473.

212. Yang S, Jiang W, Zhao F, Xu L, Xu Y, Gao B, Sun H, Du L, Tang Y, Cao F: **A highly sensitive and selective fluorescent sensor for detection of copper ions based on natural isorhamnetin from Ginkgo leaves**. *Sensors Actuators B: Chem* 2016, **236**:386-391.

213. Cao Y, Wu X, Wang M: **Silver nanoparticles fluorescence enhancement effect for determination of nucleic acids with kaempferol–Al (III)**. *Talanta* 2011, **84**(4):1188-1194.

214. Zhang G, Guo J, Zhao N, Wang J: **Study of interaction between kaempferol–Eu3+ complex and DNA with the use of the Neutral Red dye as a fluorescence probe**. *Sensors Actuators B: Chem* 2010, **144**(1):239-246.

215. Zhang X, Guo X, Yuan H, Jia X, Dai B: **One-pot synthesis of a natural phenol derived fluorescence sensor for Cu (II) and Hg (II) detection**. *Dyes and Pigments* 2018, **155**:100-106.

216. Singh G, Arora A, Rani S, Kalra P, Kumar M: **A Click-Generated Triethoxysilane Tethered Ferrocene-Chalcone-Triazole Triad for Selective and Colorimetric Detection of Cu2+ Ions**. *ChemistrySelect* 2017, **2**(13):3637-3647.

217. Sun Y, Chen H, Cao D, Liu Z, Chen H, Deng Y, Fang Q: **Chalcone derivatives as fluorescence turn-on chemosensors for cyanide anions**. *J Photochem Photobiol A: Chem* 2012, **244**:65-70.

218. Liu H, Guo C, Guo S, Fan J, Wang L, Shi D: **Chalcone-analogue fluorescent probes for detecting thiophenols in seawater samples**. *Talanta* 2019, **201**:301-308.

219. Luo Z, Liu B, Qin T, Zhu K, Zhao C, Pan C, Wang L: **Cyclization of chalcone enables ratiometric fluorescence determination of hydrazine with a high selectivity**. *Sensors Actuators B: Chem* 2018, **263**:229-236.

220. Alrefaee SH, Rhee KY, Verma C, Quraishi M, Ebenso EE: **Challenges and advantages of using plant extract as inhibitors in modern corrosion inhibition systems: Recent advancements**. *J Mol Liq* 2021, **321**:114666.

221. Darling D, Rakshpal R: **Green chemistry applied to corrosion and scale inhibitors**. In: *CORROSION 98: 1998*. OnePetro.

222. Marzorati S, Verotta L, Trasatti SP: **Green corrosion inhibitors from natural sources and biomass wastes**. *Molecules* 2018, **24**(1):48.

223. El-Etre A: **Inhibition of acid corrosion of carbon steel using aqueous extract of olive leaves**. *Journal of Colloid and Interface Science* 2007, **314**(2):578-583.

224. Prabakaran M, Kim S-H, Hemapriya V, Chung I-M: **Evaluation of polyphenol composition and anti-corrosion properties of Cryptostegia grandiflora plant extract on mild steel in acidic medium**. *Journal of Industrial and Engineering Chemistry* 2016, **37**:47-56.

225. Abdallah M, Asghar BH, Zaafarany I, Fouda A: **The inhibition of carbon steel corrosion in hydrochloric acid solution using some phenolic compounds**. *Int J Electrochem Sci* 2012, **7**(1):282-304.

226. Tan KW, Kassim MJ: **A correlation study on the phenolic profiles and corrosion inhibition properties of mangrove tannins (Rhizophora apiculata) as affected by extraction solvents**. *Corrosion Science* 2011, **53**(2):569-574.

227. Chidiebere MA, Ogukwe CE, Oguzie KL, Eneh CN, Oguzie EE: **Corrosion inhibition and adsorption behavior of Punica granatum extract on mild steel in acidic environments: Experimental and theoretical studies**. *Industrial & Engineering Chemistry Research* 2012, **51**(2):668-677.

228. Mitra I, Saha A, Roy K: **Exploring quantitative structure–activity relationship studies of antioxidant phenolic compounds obtained from traditional Chinese medicinal plants**. *Mol Simul* 2010, **36**(13):1067-1079.

229. Kabanda MM, Mammino L, Murulana LC, Mwangi HM, Mabusela WT: **Antioxidant radical scavenging properties of phenolic pent-4-en-1-yne derivatives isolated from Hypoxis rooperi. A DFT study in vacuo and in solution**. *Int J Food Prop* 2015, **18**(1):149-164.

230. Indira Priyadarsini K: **Chemical and structural features influencing the biological activity of curcumin**. *Curr Pharm Des* 2013, **19**(11):2093-2100.

231. Van Mourik T, Bühl M, Gaigeot M-P: **Density functional theory across chemistry, physics and biology**. In., vol. 372: The Royal Society Publishing; 2014: 20120488.

232. de Souza GL, Peterson KA: **Benchmarking antioxidant-related properties for gallic acid through the use of DFT, MP2, CCSD, and CCSD (T) approaches**. *The Journal of Physical Chemistry A* 2021, **125**(1):198-208.

233. Barsberg S: **Evaluation of recent scaling free methods to predict phenol and phenoxyl radical vibrational properties—Guidelines for more complex models of lignin or protein moieties**. *Int J Quantum Chem* 2009, **109**(7):1531-1546.

234. Donkor S, Song Z, Jiang L, Chu H: **An overview of computational and theoretical studies on analyzing adsorption performance of phytochemicals as metal corrosion inhibitors**. *J Mol Liq* 2022:119260.

235. Truong DH, Nhung NTA, Dao DQ: **Iron ions chelation-based antioxidant potential vs. pro-oxidant risk of ferulic acid: A DFT study in aqueous phase**. *Computational and Theoretical Chemistry* 2020, **1185**:112905.

236. Madala NE, Kabanda MM: **LC-MS based validation and DFT investigation on the antioxidant properties of clovamide:• OH**

and• **OOH scavenging and Cu (II) chelation mechanisms**. *J Mol Struct* 2021, **1236**:130349.

237.   Tošović J, Bren U: **Antioxidative action of ellagic acid—A kinetic DFT study**. *Antioxidants* 2020, **9**(7):587.

238.   Boulebd H, Khodja IA: **A detailed DFT-based study of the free radical scavenging activity and mechanism of daphnetin in physiological environments**. *Phytochemistry* 2021, **189**:112831.

239.   Spiegel M: **Current Trends in Computational Quantum Chemistry Studies on Antioxidant Radical Scavenging Activity**. *J Chem Inf Model* 2022.

240.   Martínez A, Rodríguez-Gironés MA, Barbosa A, Costas M: **Donator acceptor map for carotenoids, melatonin and vitamins**. *The Journal of Physical Chemistry A* 2008, **112**(38):9037-9042.

241.   Manzanilla B, Robles J: **Antiradical properties of curcumin, caffeic acid phenethyl ester, and chicoric acid: a DFT study**. *J Mol Model* 2022, **28**(3):1-14.

242.   Alov P, Tsakovska I, Pajeva I: **Computational studies of free radical-scavenging properties of phenolic compounds**. *Curr Top Med Chem* 2015, **15**(2):85-104.

243.   Klein E, Lukeš V: **DFT/B3LYP study of the substituent effect on the reaction enthalpies of the individual steps of sequential proton loss electron transfer mechanism of phenols antioxidant action: Correlation with phenolic CO bond length**. *Journal of Molecular Structure: THEOCHEM* 2007, **805**(1-3):153-160.

244.   Klein E, Lukeš V: **DFT/B3LYP study of O–H bond dissociation enthalpies of para and meta substituted phenols: Correlation with the phenolic C–O bond length**. *Journal of Molecular Structure: THEOCHEM* 2006, **767**(1-3):43-50.

245.   Mikulski D, Molski M: **A quantum chemical study on the antioxidant activity of bioactive polyphenols from peanut (Arachis hypogaea) and the major metabolites of trans-resveratrol**. *Computational and Theoretical Chemistry* 2012, **981**:38-46.

246.   Lu L, Qiang M, Li F, Zhang H, Zhang S: **Theoretical investigation on the antioxidative activity of anthocyanidins: A DFT/B3LYP study**. *Dyes and pigments* 2014, **103**:175-182.

247.   Boulebd H: **Theoretical insights into the antioxidant activity of moracin T**. *Free Radical Res* 2020, **54**(4):221-230.

248.   Sinopoli A, Calogero G, Bartolotta A: **Computational aspects of anthocyanidins and anthocyanins: A review**. *Food Chem* 2019, **297**:124898.

249.   Guzmán R, Santiago C, Sánchez M: **A density functional study of antioxidant properties on anthocyanidins**. *J Mol Struct* 2009, **935**(1-3):110-114.

250.   Ali HM, Ali IH: **A DFT and QSAR study of the role of hydroxyl group, charge and unpaired-electron distribution in anthocyanidin radical stabilization and antioxidant activity**. *Med Chem Res* 2017, **26**(10):2666-2674.

251.   Leopoldini M, Rondinelli F, Russo N, Toscano M: **Pyranoanthocyanins: a theoretical investigation on their antioxidant activity**. *J Agric Food Chem* 2010, **58**(15):8862-8871.

252.   Lemańska K, Szymusiak H, Tyrakowska B, Zieliński R, Soffers AE, Rietjens IM: **The influence of pH on antioxidant properties and the mechanism of antioxidant action of hydroxyflavones**. *Free Radical Biol Med* 2001, **31**(7):869-881.

253.   Cao H, Cheng W-X, Li C, Pan X-L, Xie X-G, Li T-H: **DFT study on the antioxidant activity of rosmarinic acid**. *Journal of Molecular Structure: THEOCHEM* 2005, **719**(1-3):177-183.

254.   Sadasivam K, Kumaresan R: **A comparative DFT study on the antioxidant activity of apigenin and scutellarein flavonoid compounds**. *Mol Phys* 2011, **109**(6):839-852.

255.   Zheng Y-Z, Deng G, Liang Q, Chen D-F, Guo R, Lai R-C: **Antioxidant activity of quercetin and its glucosides from propolis: A theoretical study**. *Sci Rep* 2017, **7**(1):1-11.

256.   Jalezadeh A, Mirjafary Z, Rouhani M, Saeidian H: **Investigation of structural, electronic, and antioxidant properties of calycopetrin and xanthomicrol as two polymethoxylated flavones using DFT calculations**. *Struct Chem* 2022:1-10.

257.   Erdoğan Ş, Özbakır Işın D: **A DFT study on OH radical scavenging activities of eriodictyol, Isosakuranetin and pinocembrin**. *J Biomol Struct Dyn* 2021:1-10.

258.   Sadasivam K, Kumaresan R: **Theoretical investigation on the antioxidant behavior of chrysoeriol and hispidulin flavonoid compounds–A DFT study**. *Computational and Theoretical Chemistry* 2011, **963**(1):227-235.

259.   Wang L, Yang Q, Li Y, Wang S, Yang F, Zhao X: **How the functional group substitution and solvent effects affect the antioxidant activity of (+)-catechin?** *J Mol Liq* 2021, **327**:114818.

260.   Purushothaman A, Rose KT, Jacob JM, Varatharaj R, Shashikala K, Janardanan D: **Curcumin analogues with improved antioxidant properties: A theoretical exploration**. *Food Chem* 2022, **373**:131499.

261.   Zheng Y-Z, Deng G, Zhang Y-C: **Multiple free radical scavenging reactions of flavonoids**. *Dyes and Pigments* 2022, **198**:109877.

262.   Santos SC, Fortes GA, Camargo LT, Camargo AJ, Ferri PH: **Antioxidant effects of polyphenolic compounds and structure-activity relationship predicted by multivariate regression tree**. *LWT* 2021, **137**:110366.

263.   Tošović J, Marković S: **Antioxidative activity of chlorogenic acid relative to trolox in aqueous solution–DFT study**. *Food Chem* 2019, **278**:469-475.

264.   Messaadia L, Bekkar Y, Benamira M, Lahmar H: **Predicting the antioxidant activity of some flavonoids of Arbutus plant: A theoretical approach**. *Chemical Physics Impact* 2020, **1**:100007.

265.   Alonso H, Bliznyuk AA, Gready JE: **Combining docking and molecular dynamic simulations in drug design**. *Med Res Rev* 2006, **26**(5):531-568.

266.   Morris GM, Lim-Wilby M: **Molecular docking**. In: *Molecular modeling of proteins*. Springer; 2008: 365-382.

267.   Dias R, de Azevedo J, Walter F: **Molecular docking algorithms**. *Curr Drug Targets* 2008, **9**(12):1040-1047.

268.   Singh A, Vanga SK, Orsat V, Raghavan V: **Application of molecular dynamic simulation to study food proteins: A review**. *Crit Rev Food Sci Nutr* 2018, **58**(16):2779-2789.

269.   Yu Q, Fan L, Duan Z: **Five individual polyphenols as tyrosinase inhibitors: Inhibitory activity, synergistic effect, action**

mechanism, and molecular docking. *Food Chem* 2019, **297**:124910.

270.   Skrt M, Benedik E, Podlipnik Č, Ulrih NP: **Interactions of different polyphenols with bovine serum albumin using fluorescence quenching and molecular docking**. *Food Chem* 2012, **135**(4):2418-2424.

271.   Sun L, Warren FJ, Gidley MJ: **Natural products for glycaemic control: Polyphenols as inhibitors of alpha-amylase**. *Trends Food Sci Technol* 2019, **91**:262-273.

272.   Mechchate H, Costa de Oliveira R, Es-Safi I, Vasconcelos Mourão EM, Bouhrim M, Kyrylchuk A, Soares Pontes G, Bousta D, Grafov A: **Antileukemic activity and molecular docking study of a polyphenolic extract from coriander seeds**. *Pharmaceuticals* 2021, **14**(8):770.

273.   Phosrithong N, Ungwitayatorn J: **Molecular docking study on anticancer activity of plant-derived natural products**. *Med Chem Res* 2010, **19**(8):817-835.

274.   Iftikhar H, Rashid S: **Molecular docking studies of flavonoids for their inhibition pattern against β-catenin and pharmacophore model generation from experimentally known flavonoids to fabricate more potent inhibitors for Wnt signaling pathway**. *Pharmacogn Mag* 2014, **10**(Suppl 2):S264.

275.   Mahmoodabadi N, Ajloo D: **QSAR, docking, and Molecular dynamic studies on the polyphenolic as inhibitors of β-amyloid aggregation**. *Med Chem Res* 2016, **25**(10):2104-2118.

276.   Khan S, Alhumaydhi FA, Khan MS, Sharaf SE, Al Abdulmonem W, Hassan MI, Shamsi A, Yadav DK: **Exploring binding mechanism of naringenin to human transferrin using combined spectroscopic and computational methods: Towards therapeutic targeting of neurodegenerative diseases**. *J Mol Liq* 2022, **356**:119001.

277.   Zhang X, Lu Y, Zhao R, Wang C, Wang C, Zhang T: **Study on simultaneous binding of resveratrol and curcumin to β-lactoglobulin: Multi-spectroscopic, molecular docking and molecular dynamics simulation approaches**. *Food Hydrocolloids* 2022, **124**:107331.

278. Shamsi A, Shahwan M, Khan MS, Husain FM, Alhumaydhi FA, Aljohani AS, Rehman MT, Hassan MI, Islam A: **Elucidating the interaction of human ferritin with quercetin and naringenin: Implication of natural products in neurodegenerative diseases: Molecular docking and dynamics simulation insight**. *ACS omega* 2021, **6**(11):7922-7930.

279. Ogungbe IV, Erwin WR, Setzer WN: **Antileishmanial phytochemical phenolics: molecular docking to potential protein targets**. *J Mol Graphics Modell* 2014, **48**:105-117.

280. Alsaif NA, Wani TA, Bakheit AH, Zargar S: **Multi-spectroscopic investigation, molecular docking and molecular dynamic simulation of competitive interactions between flavonoids (quercetin and rutin) and sorafenib for binding to human serum albumin**. *International Journal of Biological Macromolecules* 2020, **165**:2451-2461.

281. Choudhary DK, Chaturvedi N, Singh A, Mishra A: **Characterization, inhibitory activity and mechanism of polyphenols from faba bean (gallic-acid and catechin) on α-glucosidase: Insights from molecular docking and simulation study**. *Prep Biochem Biotechnol* 2020, **50**(2):123-132.

282. Ghosh R, Chakraborty A, Biswas A, Chowdhuri S: **Evaluation of green tea polyphenols as novel corona virus (SARS CoV-2) main protease (Mpro) inhibitors–an in silico docking and molecular dynamics simulation study**. *J Biomol Struct Dyn* 2021, **39**(12):4362-4374.

283. Khan M, Khan M, Khan Z, Ahamad T, Ansari W: **Identification of dietary molecules as therapeutic agents to combat COVID-19 using molecular docking studies**. 2020.

284. Ansari WA, Ahamad T, Khan MA, Khan ZA, Khan MF: **Luteolin: a dietary molecule as potential anti-COVID-19 agent**. 2020.

285. Wu Y, Pegan SD, Crich D, Desrochers E, Starling EB, Hansen MC, Booth C, Mullininx LN, Lou L, Chang KY: **Polyphenols as alternative treatments of COVID-19**. *Computational and structural biotechnology journal* 2021, **19**:5371-5380.

286. Ghosh R, Chakraborty A, Biswas A, Chowdhuri S: **Identification of polyphenols from Broussonetia papyrifera as SARS CoV-2 main protease inhibitors using in silico docking and molecular**

dynamics simulation approaches. *J Biomol Struct Dyn* 2021, **39**(17):6747-6760.

287. Aljarba NH, Hasnain MS, Bin-Meferij MM, Alkahtani S: **An In-silico investigation of potential natural polyphenols for the targeting of COVID main protease inhibitor**. *Journal of King Saud University-Science* 2022, **34**(7):102214.

288. Paraiso IL, Revel JS, Stevens JF: **Potential use of polyphenols in the battle against COVID-19**. *Current Opinion in Food Science* 2020, **32**:149-155.

289. Wu C, Liu Y, Yang Y, Zhang P, Zhong W, Wang Y, Wang Q, Xu Y, Li M, Li X: **Analysis of therapeutic targets for SARS-CoV-2 and discovery of potential drugs by computational methods**. *Acta Pharmaceutica Sinica B* 2020, **10**(5):766-788.

290. Singh S, Sk MF, Sonawane A, Kar P, Sadhukhan S: **Plant-derived natural polyphenols as potential antiviral drugs against SARS-CoV-2 via RNA-dependent RNA polymerase (RdRp) inhibition: an in-silico analysis**. *J Biomol Struct Dyn* 2021, **39**(16):6249-6264.

291. Li X, Deng S, Li N, Xie X: **Inhibition effect of bamboo leaves extract on cold rolled steel in Cl3CCOOH solution**. *Journal of materials research and technology* 2017, **6**(2):158-170.

292. Dehghani A, Bahlakeh G, Ramezanzadeh B, Ramezanzadeh M: **A combined experimental and theoretical study of green corrosion inhibition of mild steel in HCl solution by aqueous Citrullus lanatus fruit (CLF) extract**. *J Mol Liq* 2019, **279**:603-624.

293. Meriem Z, Hana F, Souad D, Abderrazak B, Amin MA, Leila R, Belakhdar A, Jeon B-H, Boulechfar C, Benguerba Y: **Experimental and theoretical evaluation of the adsorption process of some polyphenols and their corrosion inhibitory properties on mild steel in acidic media**. *Journal of Environmental Chemical Engineering* 2021, **9**(6):106482.

294. Belakhdar A, Ferkous H, Djellali S, Sahraoui R, Lahbib H, Amor YB, Erto A, Balsamo M, Benguerba Y: **Computational and experimental studies on the efficiency of Rosmarinus officinalis polyphenols as green corrosion inhibitors for XC48 steel in acidic medium**. *Colloids Surf Physicochem Eng Aspects* 2020, **606**:125458.

295. Verma D, Khan F, Bahadur I, Salman M, Quraishi M, Verma C, Ebenso EE: **Inhibition performance of Glycine max, Cuscuta reflexa and Spirogyra extracts for mild steel dissolution in acidic**

medium: density functional theory and experimental studies. *Results in Physics* 2018, **10**:665-674.

296. Dehghani A, Mostafatabar AH, Bahlakeh G, Ramezanzadeh B, Ramezanzadeh M: **Detailed-level computer modeling explorations complemented with comprehensive experimental studies of Quercetin as a highly effective inhibitor for acid-induced steel corrosion**. *J Mol Liq* 2020, **309**:113035.

297. Fan B, Zhao X, Liu Z, Xiang Y, Zheng X: **Inter-component synergetic corrosion inhibition mechanism of Passiflora edulia Sims shell extract for mild steel in pickling solution: Experimental, DFT and reactive dynamics investigations**. *Sustainable Chemistry and Pharmacy* 2022, **29**:100821.

298. Ramezanzadeh M, Bahlakeh G, Ramezanzadeh B: **Study of the synergistic effect of Mangifera indica leaves extract and zinc ions on the mild steel corrosion inhibition in simulated seawater: computational and electrochemical studies**. *J Mol Liq* 2019, **292**:111387.

299. Nardeli JV, Fugivara CS, Taryba M, Pinto ER, Montemor M, Benedetti AV: **Tannin: A natural corrosion inhibitor for aluminum alloys**. *Prog Org Coat* 2019, **135**:368-381.

300. Abdelaziz S, Benamira M, Messaadia L, Boughoues Y, Lahmar H, Boudjerda A: **Green corrosion inhibition of mild steel in HCl medium using leaves extract of Arbutus unedo L. plant: An experimental and computational approach**. *Colloids Surf Physicochem Eng Aspects* 2021, **619**:126496.

301. Onukwuli OD, Anadebe VC, Nnaji PC, Okafor NA, Abeng FE, Chidiebere MA, Chukwuike VI, Uwaleke CC, Guo L: **Effect of pigeon pea seed (isoflavone) molecules on corrosion inhibition of mild steel in oilfield descaling solution: electro-kinetic, DFT modeling and optimization studies**. *Journal of the Iranian Chemical Society* 2021, **18**(11):2983-3005.

302. Pal A, Das C: **New eco-friendly anti-corrosion inhibitor of purple rice bran extract for boiler quality steel: Experimental and theoretical investigations**. *J Mol Struct* 2022, **1251**:131988.

303. Dehghani A, Bahlakeh G, Ramezanzadeh B, Ramezanzadeh M: **Potential role of a novel green eco-friendly inhibitor in corrosion inhibition of mild steel in HCl solution: Detailed macro/micro-scale experimental and computational explorations**. *Construction and Building Materials* 2020, **245**:118464.

304. Ososki AL, Kennelly EJ: **Phytoestrogens: a review of the present state of research**. *Phytotherapy Research: An International Journal Devoted to Pharmacological and Toxicological Evaluation of Natural Product Derivatives* 2003, **17**(8):845-869.

305. Kutuk O, Basaga H: **Phytoestrogens in cell signaling**. In: *Phytoestrogens in functional foods*. CRC Press; 2019: 123-152.

306. Montero G, Arriagada F, Günther G, Bollo S, Mura F, Berríos E, Morales J: **Phytoestrogen coumestrol: Antioxidant capacity and its loading in albumin nanoparticles**. *Int J Pharm* 2019, **562**:86-95.

307. Boulebd H: **DFT analysis of peroxyl radical scavenging capacity of Coumestrol: insights into kinetics and reaction mechanisms**. *J Phys Org Chem*:e4421.

308. Patisaul HB, Whitten PL, Young LJ: **Regulation of estrogen receptor beta mRNA in the brain: opposite effects of 17β-estradiol and the phytoestrogen, coumestrol**. *Mol Brain Res* 1999, **67**(1):165-171.

309. Castro CC, Pagnussat AS, Orlandi L, Worm P, Moura N, Etgen AM, Netto CA: **Coumestrol has neuroprotective effects before and after global cerebral ischemia in female rats**. *Brain Res* 2012, **1474**:82-90.

310. Zafar A, Singh S, Naseem I: **Cytotoxic activity of soy phytoestrogen coumestrol against human breast cancer MCF-7 cells: Insights into the molecular mechanism**. *Food Chem Toxicol* 2017, **99**:149-161.

311. Tanwar AK, Dhiman N, Kumar A, Jaitak V: **Engagement of phytoestrogens in breast cancer suppression: Structural classification and mechanistic approach**. *Eur J Med Chem* 2021, **213**:113037.

312. Kim J-E, Lee S-Y, Jang M, Choi H-K, Kim JH, Chen H, Lim T-G, Dong Z, Lee KW: **Coumestrol epigenetically suppresses cancer cell proliferation: Coumestrol is a natural haspin kinase inhibitor**. *International journal of molecular sciences* 2017, **18**(10):2228.

313. Lim W, Jeong M, Bazer FW, Song G: **Coumestrol inhibits proliferation and migration of prostate cancer cells by regulating AKT, ERK1/2, and JNK MAPK cell signaling cascades**. *J Cell Physiol* 2017, **232**(4):862-871.

314. Kim S-N, Ahn S-Y, Song H-D, Kwon H-J, Saha A, Son Y, Cho YK, Jung Y-S, Jeong HW, Lee Y-H: **Antiobesity effects of coumestrol**

through expansion and activation of brown adipose tissue metabolism. *J Nutr Biochem* 2020, **76**:108300.

315. Yuk HJ, Lee JH, Curtis-Long MJ, Lee JW, Kim YS, Ryu HW, Park CG, Jeong T-S, Park KH: **The most abundant polyphenol of soy leaves, coumestrol, displays potent α-glucosidase inhibitory activity**. *Food Chem* 2011, **126**(3):1057-1063.

316. Hwang JA, Park NH, Na YJ, Lee HK, Lee JH, Kim YJ, Lee CS: **Coumestrol down-regulates melanin production in melan-a murine melanocytes through degradation of tyrosinase**. *Biological and Pharmaceutical Bulletin* 2017, **40**(4):535-539.

317. Tripathi P, Rabara RC, Reese RN, Miller MA, Rohila JS, Subramanian S, Shen QJ, Morandi D, Bücking H, Shulaev V: **A toolbox of genes, proteins, metabolites and promoters for improving drought tolerance in soybean includes the metabolite coumestrol and stomatal development genes**. *BMC Genomics* 2016, **17**(1):1-22.

318. TSUTSUMI N: **Effect of coumestrol on bone metabolism in organ culture**. *Biological and Pharmaceutical Bulletin* 1995, **18**(7):1012-1015.

319. Anastacio JBR, Sanches EF, Nicola F, Odorcyk F, Fabres RB, Netto CA: **Phytoestrogen coumestrol attenuates brain mitochondrial dysfunction and long-term cognitive deficits following neonatal hypoxia–ischemia**. *Int J Dev Neurosci* 2019, **79**:86-95.

320. Durmaz L, Erturk A, Akyüz M, Polat Kose L, Uc EM, Bingol Z, Saglamtas R, Alwasel S, Gulcin İ: **Screening of Carbonic Anhydrase, Acetylcholinesterase, Butyrylcholinesterase, and α-Glycosidase Enzyme Inhibition Effects and Antioxidant Activity of Coumestrol**. *Molecules* 2022, **27**(10):3091.

321. Wei X, Zhao Z, Zhong R, Tan X: **A comprehensive review of herbacetin: From chemistry to pharmacological activities**. *J Ethnopharmacol* 2021, **279**:114356.

322. Li L, Sapkota M, Kim S-w, Soh Y: **Herbacetin inhibits inducible nitric oxide synthase via JNK and nuclear factor-κB in LPS-stimulated RAW264. 7 cells**. *Eur J Pharmacol* 2015, **765**:115-123.

323. Li L, Sapkota M, Kim S-w, Soh Y: **Herbacetin inhibits RANKL-mediated osteoclastogenesis in vitro and prevents inflammatory bone loss in vivo**. *Eur J Pharmacol* 2016, **777**:17-25.

324. Veeramani C, Alsaif MA, Al-Numair KS: **Herbacetin, a flaxseed flavonoid, ameliorates high percent dietary fat induced insulin resistance and lipid accumulation through the regulation of**

hepatic lipid metabolizing and lipid-regulating enzymes. *Chem Biol Interact* 2018, **288**:49-56.

325. Kim DJ, Roh E, Lee M-H, Oi N, Lim DY, Kim MO, Cho Y-Y, Pugliese A, Shim J-H, Chen H: **Herbacetin is a novel allosteric inhibitor of ornithine decarboxylase with antitumor activity**. *Cancer Res* 2016, **76**(5):1146-1157.

326. Hyuga S, Hyuga M, Yoshimura M, Amakura Y, Goda Y, Hanawa T: **Herbacetin, a constituent of ephedrae herba, suppresses the HGF-induced motility of human breast cancer MDA-MB-231 cells by inhibiting c-Met and Akt phosphorylation**. *Planta Med* 2013, **79**(16):1525-1530.

327. Qiao Y, Xiang Q, Yuan L, Xu L, Liu Z, Liu X: **Herbacetin induces apoptosis in HepG2 cells: Involvements of ROS and PI3K/Akt pathway**. *Food Chem Toxicol* 2013, **51**:426-433.

328. Kim DJ, Lee M-H, Liu K, Lim DY, Roh E, Chen H, Kim S-H, Shim J-H, Kim MO, Li W: **Herbacetin suppresses cutaneous squamous cell carcinoma and melanoma cell growth by targeting AKT and ODC**. *Carcinogenesis* 2017, **38**(11):1136-1146.

329. Li L, Fan P, Chou H, Li J, Wang K, Li H: **Herbacetin suppressed MMP9 mediated angiogenesis of malignant melanoma through blocking EGFR-ERK/AKT signaling pathway**. *Biochimie* 2019, **162**:198-207.

330. Jeong HJ, Ryu YB, Park S-J, Kim JH, Kwon H-J, Kim JH, Park KH, Rho M-C, Lee WS: **Neuraminidase inhibitory activities of flavonols isolated from Rhodiola rosea roots and their in vitro anti-influenza viral activities**. *Biorg Med Chem* 2009, **17**(19):6816-6823.

331. Jo S, Kim S, Kim DY, Kim M-S, Shin DH: **Flavonoids with inhibitory activity against SARS-CoV-2 3CLpro**. *J Enzyme Inhib Med Chem* 2020, **35**(1):1539-1544.

332. Jo S, Kim S, Shin DH, Kim M-S: **Inhibition of SARS-CoV 3CL protease by flavonoids**. *J Enzyme Inhib Med Chem* 2020, **35**(1):145-151.

333. Jo S, Kim H, Kim S, Shin DH, Kim MS: **Characteristics of flavonoids as potent MERS-CoV 3C-like protease inhibitors**. *Chem Biol Drug Des* 2019, **94**(6):2023-2030.

334. Xu K, Zhang S, Li Q: **Preventive and treatment effect of composite Rhodiolae on acute lung injury in patients with severe pulmonary hypertension during extracorporeal circulation**. *Zhongguo Zhong xi yi jie he za zhi Zhongguo Zhongxiyi Jiehe Zazhi=*

Chinese Journal of Integrated Traditional and Western Medicine 2003, **23**(9):648-650.

335. Li F-j, Liu Y, Yuan Y, Yang B, Liu Z-m, Huang L-q: **Molecular interaction studies of acetylcholinesterase with potential acetylcholinesterase inhibitors from the root of Rhodiola crenulata using molecular docking and isothermal titration calorimetry methods**. *International Journal of Biological Macromolecules* 2017, **104**:527-532.

336. Khan A, Manna K, Bose C, Sinha M, Das DK, Kesh SB, Chakrabarty A, Banerji A, Dey S: **Gossypetin, a naturally occurring hexahydroxy flavone, ameliorates gamma radiation-mediated DNA damage**. *Int J Radiat Biol* 2013, **89**(11):965-975.

337. Lee MS, Tsai CW, Wang CP, Chen JH, Lin HH: **Anti-prostate cancer potential of gossypetin via inducing apoptotic and autophagic cell death**. *Mol Carcinog* 2017, **56**(12):2578-2592.

338. Malecka KA, Fera D, Schultz DC, Hodawadekar S, Reichman M, Donover PS, Murphy ME, Marmorstein R: **Identification and characterization of small molecule human papillomavirus E6 inhibitors**. *ACS Chem Biol* 2014, **9**(7):1603-1612.

339. Xie X, Liu K, Liu F, Chen H, Wang X, Zu X, Ma X, Wang T, Wu Q, Zheng Y: **Gossypetin is a novel MKK3 and MKK6 inhibitor that suppresses esophageal cancer growth in vitro and in vivo**. *Cancer letters* 2019, **442**:126-136.

340. Lin H-H: **In vitro and in vivo atheroprotective effects of gossypetin against endothelial cell injury by induction of autophagy**. *Chemical Research in Toxicology* 2015, **28**(2):202-215.

341. Samant NP, Gupta GL: **Gossypetin-based therapeutics for cognitive dysfunction in chronic unpredictable stress-exposed mice**. *Metab Brain Dis* 2022, **37**(5):1527-1539.

342. Patel DK, Patel K: **P0174 NEPHROPROTECTIVE ACTIVITY OF GOSSYPETIN THROUGH INHIBITORY EFFECT ON XANTHINE OXIDASE, NUCLEAR FACTOR KAPPA B (NF-KB) AND SOLUBLE EPOXIDE HYDROLASE (SEH): IN-VITRO AND IN-SILICO EXPERIMENT**. *Nephrology Dialysis Transplantation* 2020, **35**(Supplement_3):gfaa142. P0174.

343. Patel DK, Patel K: **P-MD005. Neuroprotective effects of gossypetin in alzheimer's disease: Therapeutic approaches to evaluate the acetylcholinesterase and butyl cholinesterase inhibitory potential**. *Clin Neurophysiol* 2021, **132**(8):e97-e98.

344.   Takahashi D, Matsunaga E, Yamashita T, Caaveiro JM, Abe Y, Ueda T: **Compound screening identified gossypetin and isoquercitrin as novel inhibitors for amyloid fibril formations of Vλ6 proteins associated with AL amyloidosis**. *Biochem Biophys Res Commun* 2022, **596**:22-28.

345.   Marchev AS, Dinkova-Kostova AT, György Z, Mirmazloum I, Aneva IY, Georgiev MI: **Rhodiola rosea L.: from golden root to green cell factories**. *Phytochem Rev* 2016, **15**(4):515-536.

346.   Alperth F, Turek I, Weiss S, Vogt D, Bucar F: **Qualitative and quantitative analysis of different Rhodiola rosea rhizome extracts by UHPLC-DAD-ESI-MSn**. *Sci Pharm* 2019, **87**(2):8.

347.   Panossian A, Wikman G, Sarris J: **Rosenroot (Rhodiola rosea): traditional use, chemical composition, pharmacology and clinical efficacy**. *Phytomedicine* 2010, **17**(7):481-493.

348.   Adaptogen APP: **Rhodiola rosea: a possible plant adaptogen**. *Altern Med Rev* 2001, **6**(3):293-302.

349.   Ganapaty S, Dash G, Subburaju T, Suresh P: **Diuretic, laxative and toxicity studies of Cocculus hirsutus aerial parts**. *Fitoterapia* 2002, **73**(1):28-31.

350.   Logesh R, Das N, Adhikari-Devkota A, Devkota HP: **Cocculus hirsutus (L.) W. Theob.(Menispermaceae): A review on traditional uses, phytochemistry and pharmacological activities**. *Medicines* 2020, **7**(11):69.

351.   Panda N, Mishra B, Kar NR, Panigrahi SP, Dash RN, Gangopadhyay A: **Phytochemical Constituent And Its Pharmacological Application Of Various Types Of Chemical Compounds Present In Cocculus Hirsutus (L.) Diels**. *Journal of Positive School Psychology* 2022, **6**(8):992-1000.

Chapter 2

Computational Methodology

2.1 Introduction

Computational chemistry alternatively sometimes called theoretical chemistry or molecular modelling is the study of chemical problems utilizing quantum mechanics on a computer with the aid of appropriate computer programs. Although the adjectives "precise" and "perfect" cannot be used in this context, practically all parameters can be predicted qualitatively or quantitatively. Computational chemistry has particular relevance in the field of study in numerous disciplines, just as all spectra are not totally resolvable but are extremely valuable for forecasting suitable findings. The majority of the computations are based on approximations. To begin, a computational chemist must be familiar with approximation methods; second, powerful computers and appropriate software are required; and third, mathematical descriptions must be implemented on these computers [1].

Although it has taken more than 30 years to create miniature quantum computers, recent advancements in quantum hardware, such as ion traps, superconducting, and photonic systems, suggest that we may soon be able to test Feynman's hypothesis. It is anticipated that by employing quantum systems as our simulation platform, we would be able to solve unsolvable issues in physics, materials science, and chemistry. Classical computational techniques are now crucial research tools in fields like high-temperature superconductivity and transition metal catalysis. Classical simulations give us the ability to explain experimental findings, validate physical hypotheses, and comprehend system characteristics. However, the computing complexity of realistic models frequently prevents them from serving as design guides. It is

believed that as quantum computers become more proficient at simulating quantum systems, this would lead to a more accurate knowledge of current models as well as the capacity to simulate more complicated (and hence more realistic) models. This might result in a deeper comprehension that we can use to progress fields as various as chemistry, biology, medicine, and materials science [2]. The majority of the experimental data can be computed with a high degree of precision and in a short amount of time. The molecular bonding data were not achieved by any experimental means; instead, they were derived through computational computations. As a result, most experimental researchers in various disciplines are required to use computational simulations in order to obtain a clear molecular picture of the substance they have created. We can't argue that the computational calculations are straightforward because only a professional can fully comprehend and explain all of the obtained findings [1, 3].

When Walter Heitler and Fritz London launched their first theoretical calculations in 1927, a new age of computational chemistry began. However, the requirement for good computer technology remained unanswered [4]. As a result, by 1940, the solution of complicated wave equations for complex atomic systems had become a simple process, thanks to the advancement of computer technology. There is no other field other than computational chemistry that is both young and ancient; it can be termed old because the basis was laid from the development of quantum mechanics in the twentieth century. While it is new, no other technology in human history has progressed at the

rate that digital computers have over the last 35 years or so. The computational chemist's tool is regarded to be digital computers. The primary principle of computational chemistry is to calculate molecular properties and modifications, to impart simulations to macromolecular systems, and to immediately apply the development of this to the real chemical system [5]. There is no other field other than computational chemistry that is both young and ancient; it can be termed old because the basis was laid from the development of quantum mechanics in the twentieth century.

The applications of computers in chemistry are manifold. Computer use in chemistry has long been accepted practise. It is primarily used in the fields of molecular geometry, molecule energies and transition states, chemical reactivity, IR, UV, and NMR spectra, substrate-enzyme interactions, physical properties of the substance, multipoles, polarizability, atomic charges, electrostatic potential, magnetic properties, and vibrational frequencies, among others. Then there's the issue of combining the clubbing experiment with theory. For interpreting unclear or contradictory results, computational or theoretical methods can be applied. If a real-time examination of the progress of an experimental process is required, a computational method can be employed to optimise the data. Not all processes can be carried out experimentally, but computational tools make it possible. Computational approaches can easily be used to study difficult or harmful experiments. Early on, it became clear that solving chemical issues by algorithms that mimic human intelligence in terms of decision-making and inductive reasoning would be difficult. It sparked

research in a field that is now linked to the phrase "artificial intelligence" [6].

Science's most fundamental concept is energy. All of the computational experts are calculating the most stable (lowest energy) conformer possible. Kinetic and potential energy are both possible forms of energy. A reference system with zero energy is required for researching energetics. For example, in *Ab initio* and Density Functional Theory (DFT), which simulate all of the electrons in a system, zero energy corresponds to all nuclei and electrons at an infinite distance from each other. The Semi Empirical (SE) approaches, on the other hand, rely on valance energy, which is calculated by removing valence electrons and the resultant ions from an infinite distance. Chemical standard states or stainless molecules are treated as zero energy in Molecular Mechanics (MM). However, all of these total energy numbers in relation to the associated zero energy are frequently incorrect. This occurs as a result of a systemic error. However, the energy difference can be precise, resulting in exceedingly accurate energy differences between conformers, bond dissociation energies (BDE), and so on [1]. The following are the basic computational chemistry tools:

2.2 MM Mechanics

Molecular mechanics is based on Newtonian mechanics, which is a branch of classical physics. Each atom is treated and stimulated as a single particle in this method. Electrons are not explicitly addressed in the computation of potential energy using a force field, and atoms

are treated as spheres with a net charge. As a result, a physical model can be created that can be converted into computer programmes. Hook's law, which is used to describe the parabolic potential for stretching a chemical bond, van der Waals interaction, and electrostatic contact, is the main theory that molecular mechanics relies on. The position of the electron is fixed in this case, whereas it is variable in nuclei and can be calculated.

In terms of hardware needs, MM is light and speedy. It's also known as the ball and stick model since it believes atoms to be balls and bonds to be sticks/springs. We can determine the energy of molecules like steroid molecules in a short amount of time if we know the spring lengths and angles linking them [7]. Electronic properties can't be calculated because it ignores electrons. The optimized structures from MM can be utilized as inputs for *Ab initio*, SE, or DFT computations to minimize calculation time, despite their low accuracy, due to their speed and availability of parameters for practically all elements. This is one of MM's key advantages. Molecular mechanics, rather than quantum mechanics, uses parameters determined from experimental or *Ab initio* data. The energies of the system are predicted using information such as bond stretching, bond bending, torsions, electrostatic interaction, van der Waals force, and hydrogen bonding. The energy associated with a specific type of bond is applied throughout the molecule to simplify the calculation. However, the energy derived from molecular mechanics is used to characterise the difference between various conformations rather than having any physical value. When the zero-point energy is taken into consideration,

molecular mechanics can also be used to determine the heat of formation. Molecular mechanics is considered significantly better than any other method for larger systems such as enzymes and systems with no creating or breaking of bonds. However, molecular mechanics has significant drawbacks, such as the fact that, while each force field method produces outstanding results, it is only applicable to a limited class of molecules [8].

If a compound is optimized with MM, the compound's IR spectral calculation by the same MM can be correct. Atoms are regarded to be in a force field in MM, and mathematical study of these force fields yields the atom's energy expressed in geometrical parameters. As a result, the method is also known as the force field method. MM calculates electronic properties by analogy using this force field parameterization, which may or may not be accurate. MM is deafeningly silent on the subject of electrons, orbital shapes, and related features. The force fields for one class of compounds might not be accurate for another. It is impossible to transfer parameters from one force field to another.

The optimized structures in MM could be a global minimum or not. The force fields and characteristics can be wrong at times. Electronic correlations or polar molecules cannot be examined with MM since solvation and adjacent ions are ignored. Potential energy is calculated in MM as a sum of bond stretching, angle bending, dihedral angles, and non-bonded interactions. Creating a forcefield entails providing these words specific mathematical representations, and parameterizing the field entails assigning actual numbers to the

constants in the field. The main uses of MM are biomolecular calculations [9]. Molecular docking and molecular dynamics are two methods based on molecular mechanics.

2.3 Molecular docking

The demands of structural molecular biology and structure-based drug discovery have propelled the development of the discipline of molecular docking over the past three decades. The tremendous increase in computer power and availability, as well as the expanding accessibility of small chemical and protein databases, have considerably aided in this process. The goal of automated molecular docking software is to understand and predict molecular recognition, both structurally, finding likely binding modes, and energetically, predicting binding affinity. Molecular docking is usually performed between a small molecule and a target macromolecule. This is often referred to as ligand protein docking, but there is growing interest in protein–protein docking. Chemical mechanism studies, lead optimization, virtual screening for potential leads, providing binding hypotheses to facilitate predictions for mutagenesis studies, assisting x-ray crystallography in the fitting of substrates and inhibitors to electron density, structure-activity studies, and combinatorial library design are just a few of the many uses and applications for molecular docking in drug discovery [10].

In docking simulations, accuracy and speed are essential components for achieving a successful outcome. The primary goal of developing a docking algorithm is to provide a quick technique that can

find the innovative lead molecule (in virtual screening) or replicate the experimental conformation (for confirmation using experimental data) with the highest degree of accuracy. Numerous docking applications exist, including DOCK, AUTODOCK, GOLD, FLEXX, ZDOCK, M-ZDOCK, MSDOCK, Surflex, and MCDOCK. A particular search technique, such as Incremental Construction (IC), Genetic Algorithm (GA), or Monte Carlo, forms the foundation of any docking application (MC). The docking programme can look for the best fit between two or more molecules while taking into account a number of parameters, such as geometric complementarity, atomic VDW radius and charge, receptor or ligand structure flexibility, or interatomic interactions like hydrogen bonds and hydrophobic contacts. These parameters are obtained from the receptor and ligand input coordinates [11].
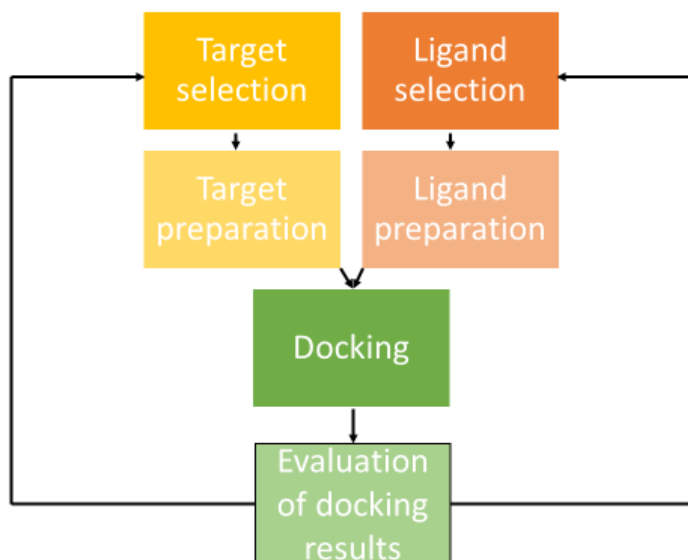
Fig. 2.1. Flow chart of docking

The key steps that all docking approaches share are shown in this flowchart. The target macromolecule and small molecule 3D structures must be chosen before each structure is produced in accordance with the docking method's requirements. The results of docking must be analysed in order to determine which binding modes have the highest scores. The process of docking involves identifying the most beneficial binding mode(s) of a ligand to the target of interest. The state variables of a ligand can be used to specifically describe its binding mode with respect to the receptor. These comprise the ligand's position (x, y, and z translations), orientation (Euler angles, axis-angle, or quaternion), and conformation (the torsion angles for each rotatable bond), if the ligand is flexible. The bounds of each of these state variables, which each represent one degree of freedom in a multidimensional search space, establish the parameters of the search. All docking methods need a scoring system to evaluate the many different binding modes and a search mechanism to investigate the state variables. Scoring criteria may be empirical, force field-based, or knowledge-based, and there are two categories of search methods: systematic and stochastic. Deterministic systematic search techniques sample the search space periodically. The search result swings because stochastic search strategies repeatedly apply random changes to state variables up until a user-defined termination condition is met [12].

2.4 Molecular dynamics

Molecular dynamics simulations replicate the time-dependent behaviour of a molecule, which is also referred to as motion, dynamics, vibrations, or trajectory. It enables the analysis of the dynamic

behaviour of a group of thousands of dispersed molecules. Currently, biomolecular dynamics simulations are used mostly in three fields. First, MD simulation is used to give biomolecular structures life and reveal information about the natural dynamics of biomolecules in solution on various timeframes. Second, MD simulation provides molecular property thermal averages. The ergodic hypothesis states that by simulating a single molecule in its environment over time, one can obtain time-averaged molecular properties that are close to the ensemble averages that can be measured empirically. For instance, this is used to compute the bulk characteristics of fluids and the variations in free energy for chemical processes like ligand binding. Thirdly, MD can investigate which molecular or complex conformations are thermally accessible. This method is applied, for instance, in ligand-docking applications to explore conformational space [13].

The fundamental concept of an MD simulation (**Fig. 2.2**) is simple. One may determine the force applied on each atom by the other atoms in a biomolecular system by knowing the locations of all the atoms (for instance, a protein surrounded by water and possibly a lipid bilayer). Thus, it is possible to anticipate each atom's spatial position as a function of time using Newton's equations of motion. To be more specific, one calculates the forces on each atom repeatedly while stepping through time, updating each atom's position and velocity using those forces. In essence, the generated trajectory is a three-dimensional movie that depicts the system's atomic-level configuration at each point during the simulated time period. A model called a molecular mechanics force field, which is often suited to the outcomes of some

experimental observations and the results of quantum mechanical computations, is used to determine the forces in an MD simulation. A typical force field, for instance, includes terms that mimic the preferred length of each covalent bond, words that capture a variety of additional interatomic interactions, and terms that capture electrostatic (Coulombic) interactions between atoms. Such force fields are by their very nature illustrative. Furthermore, no covalent bonds form or break in a traditional MD simulation. Researchers frequently use quantum mechanics/molecular mechanics (QM/MM) simulations to study reactions involving changes to covalent bonds or that are triggered by the absorption of light. In these simulations, a small portion of the system is modelled using quantum mechanical calculations and the remaining portion by MD simulation [14, 15].
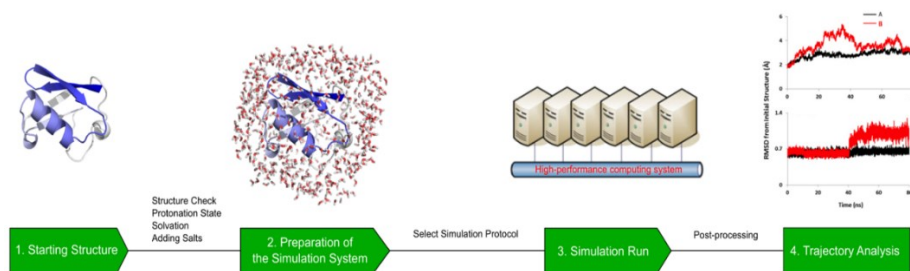
Fig. 2.2. Flow chart of MD simulation

In the late 1950s, the first MD simulations of simple gases were carried out. In the late 1970s, the first MD simulation of a protein was conducted, and the foundational work that made these simulations possible was one of the accomplishments honoured by the 2013 Nobel Prize in Chemistry. In recent years, molecular dynamics (MD) simulations have had a significant increase on influence in molecular

biology and drug development. These simulations completely capture the atomic level details and extremely fine temporal resolutions of the behaviour of proteins and other biomolecules. The appeal of biomolecular modelling to experimentalists has expanded as a result of significant advancements in simulation speed, accuracy, and accessibility, as well as the abundance of experimental structural data—a development that is particularly apparent in, but not limited to, neurology. The understanding of the workings of proteins and other biomolecules, the discovery of the structural underpinnings of disease, and the design and optimization of small molecules, peptides, and proteins have all benefited from simulations. Based on a general model of the physics driving interatomic interactions, molecular dynamics (MD) simulations forecast how each atom in a protein or other molecular system will move over time. With femtosecond temporal precision, these simulations may disclose the positions of all the atoms during a wide range of crucial biomolecular processes, including conformational change, ligand binding, and protein folding. Importantly, these simulations can also forecast how biomolecules will react to alterations like mutations, phosphorylation, protonation, or the addition or removal of ligands at the atomic level. A wide range of experimental structural biology methods, such as X-ray crystallography, cryo-electron microscopy, nuclear magnetic resonance, electron paramagnetic resonance, and Förster resonance energy transfer, are frequently combined with MD simulations [16].

Over the past few years, MD simulations have significantly improved in both power and accessibility. The majority of high-impact

MD simulation work until recently required a supercomputer. Powerful simulations may be done locally at a low cost because to recently developed computer hardware, especially graphics processing units (GPUs). Software programmes used to run MD simulations have improved in usability and support for non-experts. The physical models that underlie MD simulations are naturally approximations, but they have significantly improved in accuracy. The time steps in an MD simulation must be minimal, often only a few femtoseconds (10–15 s) each, to ensure numerical stability. On durations of nanoseconds, microseconds, or longer, the majority of biochemically interesting events, such as structural changes in proteins that are crucial for their functional properties, occur. Thus, there are millions or billions of time steps in a typical simulation. Simulations are exceedingly computationally intensive due to this feature and the millions of interatomic interactions that are routinely analysed during a single time step [14].

2.5 *Ab initio* Method

In the past three decades, *Ab initio* quantum chemistry has advanced to the point that it is now a crucial tool for studying atoms and molecules as well as, more and more, for modelling complex systems that arise in fields like biology and materials science. These are based on the Schrödinger equation, which is the most fundamental physical equation, with no empirical changes. They employ some quantum chemical approximations, which, if not very severe for the task at hand, could yield correct results [17].

This method is slower than MM computations, but it is more accurate. Through trial-and-error approaches or experience, the levels of theory for a particular application can be obtained with considerable accuracy. Because empirical parameters are not required, *Ab initio* calculations can be applied to any type of system, including transition states and non-stationary points, rather than just species for which empirical data are available, which is a significant benefit. *Ab initio* computations have the advantages of reliability and generality, but they are slower than other computational methods.

Ab initio computations, unlike MM calculations, necessitate the use of hardware. The level of calculations increases the computer resource needs, but these are overcome through the use of supercomputers. Hartree-Fock (HF) is the simplest *Ab initio* approach, in which the wave function is represented by a Slater determinant made of occupied spin orbitals. We might acquire the HF equations by writing the molecular energy as expectation values and solving the associated Schrödinger equation, then differentiating the energy with regard to the spin orbitals that make up the wave function. These are approximated as a linear combination of basis functions, which can be any mathematical functions that yield an acceptable wave function, in order to employ them in practical applications.

The HF approach has a major flaw in that it ignores electron correlations. Each electron in HF is assumed to have the same potential as the other ions. In practice, however, one electron perceives the other as a moving particle, and they change their behavior to reduce the interaction repulsion energy. Electron correlation, on the other hand, is

investigated in Post-HF calculations such as Moller-Plessel (MP), Configuration interaction (CI), and Couple Cluster (CC). These strategies reduce electron correlation energy by allowing electrons to fill not only readily occupied molecular orbitals, but also virtual molecular orbitals, which are formally vacant molecular orbitals.

The *Ab initio* approach can be used to calculate energy, IR-UV-NMR spectra, electron affinity, ionization enthalpy, dipole moments, and other properties. *Ab initio* calculations are necessary because the majority of the enzyme-substrate interaction is influenced by shape, charge distribution, and other factors, which are influenced by electronic characteristics and energy differences.

2.6 Semi Empirical Methods

Semi empirical methods use empirical modifications to increase performance and are simplified versions of Hartree-Fock theory. They're crucial in computational chemistry for dealing with big molecules where the complete Hartree–Fock method is too expensive without the approximations. The inclusion of electron correlation effects in the approaches appears to be possible thanks to the use of empirical parameters. The most straightforward application of electronic structure theory is quantum chemical semiempirical approaches, which involve integral approximations and parameterizations that reduce their accuracy but increase their efficiency and enable realistic modelling of huge molecules.

They begin with *Ab initio* or first principles formalism and then make some pretty extreme assumptions in order to speed up the

computations, usually by ignoring many of the less relevant terms in the underlying equations. Empirical parameters are included into the formalism and calibrated against valid experimental or theoretical reference data to compensate for the mistakes produced by these approximations. These are faster than DFT and *Ab initio*. The accuracy suffers as a result of the increased speed. Semi-empirical calculations, on the other hand, are sufficient for comparative research, particularly for organic compounds.

The Huckel -electron method, which creates MOs essentially from a molecule's connectivity matrix and offers insightful qualitative information about the structure, stability, and spectroscopy of unsaturated compounds, was one of the earliest semiempirical methodologies in quantum chemistry. Numerous qualitative investigations of inorganic and organometallic compounds have used Hoffmann's extended Huckel theory, which incorporates all valence electrons. Because they helped shape qualitative MO theory, which is frequently used to explain chemical events in terms of orbital interactions, these early semiempirical approaches had a lasting influence on chemical thought.

The most often used approaches (MNDO, AM1, and PM3) all use the Neglect of Differential Diatomic Overlap (NDDO) integral approximation, although older methods use simpler integral schemes like CNDO and INDO. All three methods are part of the Zero Differential Overlap (ZDO) method family, which ignores all two-electron integrals with two-center charge distributions. To speed up calculations, a variety of additional approximations are used, as well as

parameterized adjustments to account for the approximate quantum mechanical model. The semi empirical technique is defined by how parameterization is done. The parameterization for MNDO, AM1, and PM3 is done so that the computed energy is expressed as heats of formations rather than total energies. MNDO/d and PM3(tm) are new versions of the NDDO methods that contain d-Orbitals for second-row and higher elements. PM5 is a significantly extended and reparameterized version of PM3 that was just released. The semiempirical techniques described above are conceptually condensed *Ab initio* MO procedures [18].

2.7 Density Functional theory

Unlike other quantum mechanical methods, these are based on electron density rather than wave function. DFT is based on the Hohenberg and Kohn theorem and offers information about atoms and molecules' energetics, structure, and characteristics at a far lower cost than standard *Ab initio* wave function approaches [19]. DFT is widely used in a variety of fields of study, including material sciences, chemical sciences, and biological sciences, among others. The presence of variational principles explains the similarities across the various applications of DFT. For transition metal complexes, DFT produces better results than *Ab initio* approaches. Higher basis sets and functions produce better outcomes in this case. DFT is primarily concerned with the ground state, but its application to higher states is being explored [20].

In all sectors where DFT is used, the energy that is not tied to an external potential is a universal functional (it is the same for all external potentials). However, the functionals used here are based on multiple approximations, and the correct functional is unknown and unpredictable in nature. A functional's best decision is always linked to some insight, scientific aptitude, and a mix of numerical, test, and investigative fittings. The Hohenberg-Kohn hypothesis and Kohn-Sham techniques are the most common electronic properties estimated using DFT. The most current use of DFT is the creation of Schrödinger conditions for electronic frameworks, which is the most precise first principle approach of calculating energy of chemical interest [21].

The wave function-based procedures and density-based tactics are two notable approaches to dealing with the Schrödinger wave equation. Both methods represent the many-body framework as a set of single-molecule equations. DFT focuses on the Slater approach, which relies on the densities of electronic frameworks rather than directly inferring the wave function. A framework's energy is conveyed as a function of electronic density, which is a function of three spatial directions and so referred to as a functional. Hohenberg and Kohn established in 1964 that the electron density can be used to characterize any ground state attribute.

In the Kohn- Sham (KS) method, the nature of exchange-correlation functional is a difficulty. To obtain the best-fitting functional, it must be estimated in several ways, resulting in the local, gradient-corrected, or hybrid functional. The most well-known exchange-correlation functional is based on Local Density

Approximations (LDA), in which the functional is dependent on the electron density locally.

Density functional theory is being used more and more in chemistry and materials science to explain and predict complicated system behaviour at the atomic level. DFT computational approaches are used for synthesis-related systems and processing parameters in particular. Experimental research in such systems is frequently hampered by inconsistent results and non-equilibrium situations. The influence of dopants on phase transformation behaviour in oxides, magnetic behaviour in dilute magnetic semiconductor materials, and the study of magnetic and electronic behaviour in ferroelectrics and dilute magnetic semiconductors are all examples of current DFT uses [22, 23]. It has also been demonstrated that DFT is effective in predicting the sensitivity of some nanostructures to contaminants such as sulphur dioxide [24] or acrolein [25], as well as mechanical properties [26].

There have been numerous attempts to simplify the many electron problem and avoid a direct solution of the Schrodinger equation due to its complexity. The following section discuss the same;

2.7.1 Thomas- Fermi model (first DFT)

Independently, Thomas and Fermi proposed a method based on electron charge density. They reasoned that the necessity to solve for the wave function is eliminated by electron density. They have a big advantage because wave functions cannot be directly measured in quantum theory because they are not observable in quantum mechanics.

This model, which is thought to be the first DFT, was put forth in 1927 [27]. According to then the total electronic energy of a system is given by,

$$E_T = \frac{3}{10} \frac{\hbar^2 \left(3\pi^2\right)^{\frac{2}{3}}}{m} \int \left[n(\vec{r})^{\frac{5}{3}} \right] d^3r + \int V_{ext} n(\vec{r}) d^3r + \int n(\vec{r}) V_H(\vec{r}) d^3r \quad (1)$$

Where, m, $n\left(\vec{r}\right)$, V_{ext}, V_H corresponds to the mass of electron, electron density and fixed external potential and Hartree potential respectively. the first term in this equation is related to the kinetic energy, second term corresponds to electronic interaction with external potential which is independent on electron density, and the third term indicate electrostatic interaction which depends on electron density.

2.7.2 The Kohn-Sham equations

Kohn and Sham proposed an equation in 1965 to obtain a good approximation to kinetic energy because the Thomas-Fermi model's approximation for kinetic energy is not well-accepted. They claim that the kinetic energy is represented by;

$$T_s = \frac{1}{2} \sum_i^N \left\langle \psi_i \left| \nabla^2 \right| \psi_i \right\rangle \quad (2)$$

where ψ_i denotes the non-interacting system's orbitals. Ts, on the other hand, is not the system's exact or actual kinetic energy. Another functional F[ρ] is introduced by Kohn and Sham as;

$$f[\rho] = T_s[\rho] + J[\rho] + Exc[\rho] \qquad (3)$$

where $Exc[\rho]$ is the exchange-correlation energy.

The well-known KohnSham (KS) equations are constructed following a lengthy succession of mathematical salvation techniques and the application of the variational principle.

$$\left(-\frac{1}{2}\nabla^2 + \left[\frac{\rho(\vec{r}_2)}{r_{12}} + V_{XC}(\vec{r}_1) - \sum_A^M \frac{Z_A}{r_{1A}}\right]\right)\psi_i = \left(-\frac{1}{2}\nabla^2 + V_S(\vec{r}_1)\right)\psi_i = \varepsilon_i\psi_i$$

4)

From this equation, the ground state energy and density can be obtained.

Molecular docking

2.8 Basis Set

A basis set is a collection of estimated atomic orbitals that simulates the actual wave function determined by the more complex numerical method. Atomic orbitals are combined in a linear fashion. The molecular orbitals are produced using a collection of functions that are expanded into a linear combination with undetermined coefficients. These functions have frequently been concentrated on atoms, but they have also occasionally been centred on bonds or lone pairs. It expresses electronic wave functions in the density functional theory in order to convert the model's partial differential equations into algebraic equations that can be efficiently implemented on a computer. It

illustrates how atomic orbitals actually work. The degree of approximation employed in a particular computation is determined by the characteristics of the chosen basis set. Basis sets are only necessary for the *Ab initio* technique and density functional theory. The accuracy of the outcome depends on the basis set selection made. The size of the basis sets affects how reliable a quantum chemical calculation is [28].

The Schrödinger equation solution, polynomial-based functions, Slater functions, and Gaussian functions (**Fig. 2.3**) are just a few of the approaches one may take to address the electron distribution around an atom. Slater-type orbitals (STOs), which are solutions to the Schrödinger equation of hydrogen-like atoms and decrease exponentially away from the nucleus, are the most physically motivated basis set. They are naturally good bases for molecular orbitals since they have direct physical interpretation. However, because to the mathematical complexity, computing integrals using STOs is computationally difficult. Later on, Frank Boys demonstrated that STOs might alternatively be approximated as linear combinations of Gaussian-type orbitals (GTOs).

A number of GTOs are utilized in place of STOs to make the calculations with STOs easier. However, one GTO's precision is lower than that of STO. As a result, we must use multiple GTOs for a single STO. GTOs are basic mathematical functions that are used to imitate a STO. GTO is easier to evaluate than STO, although it is not as good as STO.
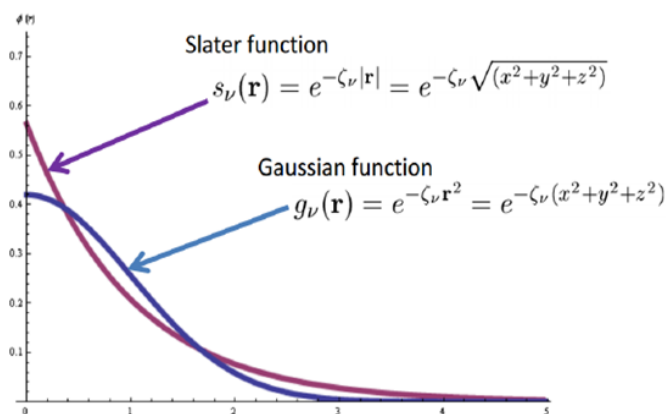
Fig. 2.3. Slater versus Gaussian type functions

2.8.1 B3LYP

In density functional theory, hybrid functionals are a set of approximations to the exchange correlation energy functional (DFT). It combines a part of exact exchange from Hartree-Fock theory with the balance of the exchange correlation energy from *Ab initio* or empirical resources. The precise exchange energy functional is known as an implicit density functional since it is represented in terms of the Kohn-Sham orbitals rather than density. B3LYP is one of the most regularly utilized variants (Becke, 3-parameter, Lee-Yang-Parr).

Axel Becke introduced the hybrid approach to constructing density functional approximations in 1993[30]. The Hartree-Fock exact exchange functional is combined with any number of exchange and correlation explicit density functions to form a hybrid exchange correlation function. The weight of each particular functional is normally determined by comparing its prediction to experimental or

properly calculated thermochemical data[31].For example in the case of B3LYP exchange correlation functional is

$$E_{xc}^{B3LYP} = (1-\alpha)E_x^{LSDA} + a\ E_x^{HF} + b\Delta E_x^{B} + (1-c)E_c^{LSDA} + cE_C^{LYP} \qquad (5)$$

Where a = 0.20, b = 0.72, and c = 0.81, and ExB is a generalized gradient approximation: the Becke 88 exchange functional and the Lee, Yang, and Parr correlation functional for B3LYP, and EcLSDA is the VWN local spin density approximation to the correlation functional, and EcLSDA is the VWN local spin density approximation to the correlation functional. Becke's original fitting of the comparable B3PW91 functional to a set of atomization energies, ionization potentials, proton affinities, and total atomic energies yielded the three parameters that define B3LYP.

2.8.2 M06

Minnesota Functionals M06 is a functional that is a component of Minnesota Functionals. Minnesota Functionals (Myz) are a class of highly parameterized approximate exchange-correlation energy functionals in density functional theory (DFT). Prof. Donald Truhlar and his team at the University of Minnesota are the masterminds behind the invention of this feature. Because kinetic energy density terms are incorporated in these functionals, they are based on the meta-GGA approximation (generalized gradient approximation), and the factor that makes it adaptable is that it is based on sophisticated functional forms, frame-worked on high-quality benchmark databases. These functionals are more commonly employed in both quantum and solid-state chemistry.

When we try to independently analyse the strength and limitations of the Minnesota functionals based on various chemical properties, we run into a problem with accuracy. These functionals, on the other hand, make every effort to provide a fair account of both main group and transition metal chemistry. So, in order to improve the accuracy of the functional, only main group chemistry performance is taken into account, as it works better for main group chemistry than transition metal chemistry. Some research, particularly those published in 2007, revealed that these functionals operate poorly at atomic densities. However, recent investigations have shown that Minnesota functionals, which are widely used for computing energy numbers, have emerged by correcting all flaws in atomic densities and energetics. They are praised for the replication of chemically relevant Fukui functions and perform better for diatomic densities than atomic densities.

The functional is framed to satisfy the uniform-electron-gas limit and is designed to capture the major dependency of the exchange-correlation energy on local spin density, spin density gradient, and spin kinetic energy density. Geometries and vibrational frequencies are also predicted using it. The proposed functional should be particularly beneficial for many applications in chemistry, especially for simulations on moderate-sized or large systems and when long time scales must be addressed, due to the computing advantages of local functionals.

2.9 Computational software

Some software that is utilised to carry out all the computations is the basis of this study. So, the most significant software employed in this study is explained in depth in this part.

2.9.1 Molecular modelling software

2.9.1.1 Gaussian software

Gaussian is a computer program used by chemists, biochemists, chemical engineers, physicists and other scientists. It works under the laws of quantum mechanics. It is used for predicting energies, molecular structures, spectroscopic data and other advanced calculations. It is used for predicting energies, molecular structures, spectroscopic data and other advanced calculations.

John Pople and his research group at Carnegie Mellon University created the Gaussian 09 software package in the early 1970s under the moniker Gaussian 70. Since then, the software has been regularly upgraded, and for our project, we used the Gaussian 09 version. The Gaussview-5.0 graphical user interface is used to create the input structures, which are then passed to the Gaussian 09 software package for output. The software includes a variety of computational tools, including simple molecular mechanics (such as Amber force field), semi-empirical methods (such as CNDO), Hartree-Fock (restricted and unrestricted), MPn (Mollar-Plesset perturbation theory of order n = 2,3, 4), CI (Configuration-Interaction), CC (Coupled-Cluster), Multiconfigurational SCF (such as CAS-SCF) and various

DFT methods are incorporated in the software. Gaussian 16 is the latest version of Gaussian series of programs. New and enhanced method of algorithms is used in this version.

The electronic structure and quantum chemistry computations are aided by Gaussian software. This software can be used to study variety of spectra including IR, NMR, UV/Visible, Vibrational circular dichroism, optical rotatory dispersion, *etc*. It can also be used to gain information about reaction pathways, thermo chemical quantities, solvent effects, photochemistry, *etc*. Gaussian is a widely used computational software among scientists from a variety of areas, including physics, chemistry, and biology.

2.9.1.2 Auto Dock Vina

The Scripps Research Institute's Molecular Graphics Lab creates Autodock-Vina software, an open-source platform with multi-core capability, high performance, and improved accuracy for drug discovery, molecular docking, and virtual screening. Autodock Vina's results are simple to understand. Auto-dock Vina is a revolutionary molecular docking and virtual screening application. It works well for docking proteins and ligands. Docking in terms of accuracy and performance, Vina is the successor of Auto dock. Auto-docking Vina can be performed with the assistance of Auto dock tools. It uses a novel scoring function to measure binding affinity and a new search algorithm to forecast feasible binding modes to create an efficient optimization algorithm. Rather of giving the customer a choice of search algorithm, Autodock Vina employs an iterated Local search

global optimizer [29]. Partial charges, solvation settings, and other characteristics are not required for Autodock Vina. AutoDock is a company that sells interactive graphics software that may be used to prepare receptors and ligands for molecular docking.

2.9.1.3 Maestro

All programmes from Schrödinger use Maestro as their user interface. Compound analysis, design, generation, and long-term visualisation are all possible with it. Organizing and analysing chemical data by researchers is also made easier by this. With Maestro, molecules and protein-ligand complexes can be seen in 3D and as 2D line diagrams in this thesis.

2.9.1.4 Desmond

Simulations can be carried out on time scales that provide light on these crucial dynamic processes using a high-performance MD algorithm and rapidly improving computer hardware technology. To accomplish these objectives, Desmond package, a recently created MD code made by D. E. Shaw Research, offers parallel scalability, simulation throughput, and scientific precision.

2.9.2 Molecular editing and visualization tools

2.9.2.1 Open Babel

Open Babel is a free and open-source chemical toolset that understands a variety of chemical data languages. This software allows for the conversion of chemical structures between different formats. It

can convert between 110 different formats. Open Babel can also generate 3D and 2D images. It aids in the search, concealment, analysis, and storage of data from a variety of chemistry domains.[30] .

2.9.2.2 GaussView

The graphical user interface for Gaussian is called GaussView. It facilitates the generation of Gaussian input files, enables the execution of Gaussian operations *via* a graphical user interface rather than through a command-line interface, and facilitates the interpretation of Gaussian output. This study generated inputs for the optimization of complex geometry using GaussView. The present study uses both GaussView 5 and GaussView 6

2.9.2.3 CORINA

CORINA is a powerful and quick piece of software used to create accurate three-dimensional chemical structures. When compared to other tools, this online 3D drawing tool is relatively simple to use. To construct a model of a small or stiff molecule, they employ built-in data of typical bond lengths and angles. You can store the three-dimensional structure in PDB or Mol format [31].

2.9.2.4 Data warrior

Data Warrior is a free, interactive programme that is simple to download. It combined cutting-edge cheminformatics algorithms in a single setting. Since 2014, it has being used by research organisations, the government, and business. An all-purpose programme for data analysis and visualisation is called Data Warrior. It can be used for

interactive visualisation, toxicity investigations, and cheminformatic computations, among other things [32].

2.9.2.5 Auto Dock tools

Auto Dock Tools is the free graphical user interface (GUI) for Auto Dock (ADT). It can be used to set up, operate, and analyse auto dock docking. Proteins and ligands can be prepared using the Auto dock tools. The active site of a protein can be surrounded by a grid using auto docking technology. Auto dock accepts PDBQT as an input format, therefore files may be saved in that format. The same research team that produced Auto Dock also produced this. The grid box's visual depiction of the grid box can be used to set up the auto dock grid parameter file, observe molecules in 3D, rotate them, add all hydrogen or non-polar hydrogens, apply partial atomic charge, and add hydrogen to any position [33].

2.9.2.6 Discovery studio

Discovery studio is a program that allows you to analyze and model molecular structures and sequences. ADME, QSAR, Structure based drug design, pharmacophore modelling, and simulations are some of the applications included in Discovery Studio. Both Windows and Linux are supported by the software. It's a great way to see molecular structures [34].

2.9.2.7 Material studio

Materials Studio is a comprehensive modelling and simulation environment created to help researchers in the fields of materials

science and chemistry forecast and comprehend how a material's atomic and molecular structure affects its characteristics and behaviour. Researchers from a variety of sectors can design better performing materials of all kinds using Materials Studio, including drugs, catalysts, polymers, composites, metals, alloys, batteries, fuel cells, and more.

2.9.2.8 VMD

A molecular visualisation programme called VMD uses 3-D graphics and built-in scripting to show, animate, and analyse massive biomolecular systems. VMD supports MacOS X, Unix, and Windows PCs, is freely available, and comes with source code.

2.9.3 Online softwares

2.9.3.1 PubChem

PubChem, a component of the Molecular Libraries Roadmap Initiatives of the US National Institutes of Health, was established in 2004 as a public repository for data on chemical compounds and their biological activity. It is now a well-developed research information resource. Substance, molecule, and Bioassay are all interconnected databases in PubChem. Chemical information can be found in the substance data base, chemical structures may be found in the compound data base, and bioassay data is stored in the bioassay database [35] .

2.9.3.2 Protein Data Bank

The only global repository for structural information on biological macromolecules is the Protein Data Bank (PDB;

http://www.rcsb.org/pdb/). Since 1971, this database has served as a repository for 3D models of proteins, nucleic acids, and complex assemblies for the benefit of the global research community. Cryo-electron microscopy, NMR spectroscopy, X-ray crystallography, and other techniques are frequently used to obtain the data that is stored. It is a publicly available online database.

2.9.3.3 SwissADME

SwissADME is a web tool that offers free access to a collection of quick but reliable predictive models for physicochemical properties, pharmacokinetics, drug-likeness, and medicinal chemistry friendliness, including in-house effective techniques like the BOILED-Egg, iLOGP, and Bioavailability Radar. Through the login-free website http://www.swissadme.ch, simple, effective entry and interpretation are guaranteed thanks to a user-friendly interface. The critical parameters for a group of chemicals can be predicted quickly by experts in computational chemistry or cheminformatics as well as non-experts, supporting their efforts to find new drugs.

2.10 Computational methodology

2.10.1 Potential energy scanning

The PES defines a system's potential energy as a function of the locations of its atomic nuclei. An intuitive understanding of a number of chemical concepts is provided by a graphical depiction of the PES: Geometry optimization can find these zones, which are concave up in all local directions and correspond to stable molecules or phases on the

PES. On the other hand, a first-order saddle point on the PES is concave up in all local directions but concave down in just one local direction; the properties of this saddle-point region might give insight into the rate of chemical reaction or phase change, for example *via* transition-state theory. In normal-mode analysis, the vibrational entropy of the corresponding stable configuration is most closely approximated by the curvature of the potential well at the local minimum. In *Ab initio* molecular dynamics, the PES calculated in the context of quantum mechanics predicts that the system would change over time in a classical manner. As a result, a thorough investigation of system dynamics requires an accurate representation of the PES. In fact, the accuracy of the PES determines the entire validity of investigations like reaction dynamics, vibrational analysis, and molecular dynamics [36].

2.10.2 Optimization

According to some computational models of chemical bonding, geometry optimization, (also referred to as energy optimization, geometry minimization, or energy minimization) is the process of finding a spatial arrangement of atoms where the net inter-atomic force on each atom is acceptable close to zero and the position on the potential energy surface (PES) is a stationary point. The group of atoms may be included in a single molecule, an ion, a condensed phase, a transition state, or a combination of any of these. The best shape for a system is the one that places the least amount of strain on it. A local or global energy minimum is intended to be reflected in an atom arrangement, and this method seeks to identify its geometrical characteristics. Optimizing to a transition state, such as a saddle point

on the potential energy surface, rather than a global energy minimum, may be preferable. Optimized structures frequently closely resemble natural substances, and the geometry of such a structure can be employed in a number of experimental and theoretical studies in chemical structure, thermodynamics, chemical kinetics, spectroscopy, and other domains.

2.10.3 Frontier Molecular Orbitals

The highest occupied molecular orbital (HOMO) and lowest unoccupied molecular orbital (LUMO), sometimes known as FMOs, are particularly important in predicting molecule reactivity. The nucleophilic ability of molecules is determined by the HOMO orbital, whereas the electrophilic ability is determined by the LUMO orbital. The energy difference between these two orbitals is used to determine stability. The stability will be higher if the energy gap is minimal. As a result, the molecule's chemical reactivity can be predicted. When the HOMO-LUMO energy gap widens, a molecule's flexibility, polarizability, and electron mobility are hampered. The ionization enthalpy (I) is represented by the HOMO energy, whereas the electron affinity (A) is represented by the LUMO energy [37].

The orbitals HOMO and LUMO are the most likely to be engaged in chemical reaction. The production and destruction of bonds, oxidation, reduction, and other chemical reactions all require the redistribution of electrons. Because the HOMO is the highest-energy orbital that is still filled, it is the easiest to remove electrons from this orbital energetically. This can be as simple as contributing electron

density to form a link and acting as a Lewis base, or it can be as complex as oxidation. Because the LUMO is the lowest lying vacant orbital, it is the easiest to add extra electrons to this orbital and act as Lewis acid or reduction energetically. Chemical reactivity isn't usually caused by the HOMO and/or LUMO. Aspects of symmetry are also important. It's possible that the HOMO-1 or LUMO+1 is involved in the reaction if the HOMO or LUMO isn't of the correct symmetry.

2.10.4 Molecular Electrostatic Potential

The net electrostatic potential at a given position in space is represented by the overall charge distribution of the molecular system in a molecular electrostatic potential map. The MESP surface is a valuable tool for visualizing a molecule's relative polarity in electrophilic and nucleophilic processes, as well as hydrogen bonding interactions. The MESP map clearly shows that structural similarities between two compounds will not be reflected in their electrophilic or nucleophilic reactivities. The surface map help to estimate the size, shape, charge density and reactive sites of the molecule as this is basically electron density mapped against electrostatic potential surface. The surface map, which is basically electron density projected against an electrostatic potential surface, aids in estimating the size, shape, charge density, and reactive sites of the molecule. The electrostatic potential values at the surface are represented by three colors: red, blue, and green. The most electronegative electrostatic potential is represented by the red shaded area of the map, while the most positive electrostatic potential is represented by the blue color, and the zero potential, or neutral region, is represented by the green

color. The order of increasing electrostatic potential is red<orange<yellow<green[38] according to colored regions.

2.10.5 TD-DFT

Hohenberg, Kohn, and Sham's classic density-functional theory (DFT) formalism was developed on the premise that calculations of the electronic structure of the ground stationary state can be performed using the mathematically simpler 1-electron charge density instead of the complex N-electron wave function. As a result, neither excited electronic states nor time-dependent (TD) problems can be handled by standard DFT. Time-dependent density functional theory (TD-DFT) is a time-dependent extension of density functional theory (DFT). Runge and Gross were the ones who first proposed it. Casida expands on this by developing an effective linear-response (LR) formalism for TD-DFT, allowing for the rapid and efficient determination of the TD-DFT equations for molecules. It's a method for calculating not only transition energies but also excited-state features like dipole moments and emission geometries. The most extensively used *Ab initio* technique for modeling the electronic spectra of organic and inorganic molecules is TD-DFT, which may be extended to include environmental effects using either a bulk environment model or a number of quantum mechanical or molecular mechanical approaches. Actual TD-DFT implementations necessitate the selection of an exchange correlation functional (XCF) that concentrates the model's approximations. The selection of an exchange correlation function is a difficult undertaking since it has a considerable impact on accuracy [39].

The quality of the acquired data is fundamentally functionally dependent, which is a major shortcoming of TD-DFT. The choice of exchange-correlation function has a considerable impact on the results' reliability.

2.10.6 Natural Bond Orbital Analysis

Chemists can use Natural Bond Orbital Analysis to get an intuitive image of both electron orbitals and population analysis. It provides a comprehensive understanding of the intramolecular and intermolecular orbital interactions in molecules between filled donor and empty acceptor NBOs, allowing us to make a quantitative assessment and draw a qualitative conclusion about the donor-acceptor properties of substituents. The charge distribution of the atoms is employed in natural bond orbital (NBO) analysis is used to understand electronic structure and chemical reactivity and also a convenient platform for studying charge transfer and conjugative interactions in molecular systems. The optimised structures were subjected to NBO analysis in order to identify the electronic charges on the atoms at the centre of the complexes as well as to estimate the key donor-acceptor interactions [40].

2.10.7 Antioxidant activity

According to the literature, polyphenolic anti-oxidants' reaction pathways for scavenging free radicals are primarily divided into three types: (1) hydrogen atom transfer (HAT); (2) single electron transfer followed by proton transfer (SET-PT); and (3) sequential proton loss electron transfer (SPLET). Free radicals react with phenolic hydroxyl

groups to form phenolic compounds (ArOH) and phenolic radicals (ArO·) lowering reactive oxygen species' oxidation activity. To assess oxidation activity, the following markers will be used: BDE stands for bond dissociation enthalpy, IP stands for ionisation potential, PDE stands for proton dissociation enthalpy, PA stands for proton affinity, and ETE stands for electron transfer enthalpy (ETE). The enthalpies of anti-oxidant (ArOH), neutral radical (ArO·), anion (ArO), radical cation (ArOH•+), proton (H+), hydrogen atom (H•), and electron (e) are represented by H(ArOH), H(ArO•), H(ArO-), H(ArOH•+), HH+, HH, and He, respectively. The gas phase enthalpy of a hydrogen atom is computed using the B3LYP/6-31G method is 0.49764hartree. The gas phase enthalpies of proton(0.002363hartree) and electron (0.001198 hartree) were obtained from literature [41]. For these indicators, the precise reaction pathways and calculation equations are as follows:

HAT mechanism

In general, hydrogen atom transfer is a significant field of chemistry that has received a lot of attention (combustion, halogenation, oxidation – antioxidant action, and other processes). Hydrogen atom transfer (HAT) from the antioxidant molecule to the reactive radical intermediate is the initial step in primary antioxidants terminating reactive radicals.

$$\text{ArOH} + \text{R}\bullet \rightarrow \text{ArO}\bullet + \text{RH} \tag{6}$$

$$\text{BDE} = \text{H(ArO}\bullet) + \text{H(H}\bullet) - \text{H(ArOH)} \tag{7}$$

A hydrogen atom is extracted from the phenolic anti-oxidant (ArOH) by homolytic cleavage to the free radical (R•) in the HAT process. BDE (ArO–H) can be used to assess ArOH's anti-oxidant reactivity, with the lower the BDE value, the higher the predicted activity.

SET-PT mechanism

However, reactions frequently entail the stepwise transfer of an electron and a proton, with the initial electron or proton transfer. In the case of initial electron transfer, the first step is to generate the appropriate radical cation, which is then deprotonated.

$$ArOH + R• \rightarrow ArOH•+ + R– \tag{8}$$
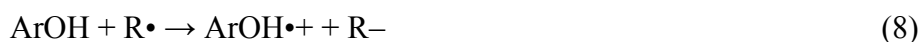
$$ArOH•+ \rightarrow ArO• + H+ \tag{9}$$

$$IP = H(ArOH•+) + H(e) - H(ArOH) \tag{10}$$

$$PDE = H(ArO•) + H(H+) - H(ArOH•+) \tag{11}$$

The SET-PT mechanism has two steps: first, the electron is extracted from ArOH and transferred to the free radical R•, and then the proton is transferred from the cation ArOH•+ to the anion R–. The first and second stages' reaction enthalpy changes can be evaluated using ionisation potential (IP) and proton dissociation enthalpy (PDE) values[57]. Likewise, the lower the numbers, the greater the antioxidant activity.

SPLET mechanism

The SPLET (sequential proton loss electron transfer) mechanism may also be important in solution-phase.

$$ArOH \rightarrow ArO\text{-} + H\text{+} \qquad (11)$$

$$ArO\text{-} + R\cdot + H\text{+} \rightarrow ArO\bullet + RH \qquad (12)$$

$$PA = H(ArO\text{-}) + H(H\text{+}) - H(ArOH) \qquad (13)$$

$$ETE = H(ArO\bullet) + H(e) - H(ArO\text{-}) \qquad (14)$$

SPLET is the third key mechanism, and it involves two phases. ArOH will first dissociate its acidic moiety to generate an anion (ArO-), which will then undergo electron transfer to form ArO•. Proton affinity (PA) and electron transfer enthalpy (ETE), respectively, could be used to quantify the reaction enthalpy changes in the two phases.

2.10.8 Atoms in Molecules (AIM)

The "Atoms in Molecules" (AIM) theory is an interpretive theory that seeks to extract chemical knowledge from contemporary high-resolution electron densities. These densities could be generated from *Ab initio* wave functions or come from experimental data. The atom and the bond are two crucial pillars of chemistry that are defined by AIM [42]. The Lewis model from the 1900s, the Heitler-London-Pauling Valence Bond model from the 1930s, or the Hund-Mulliken Molecular Orbital from the 1960s are still the most common models used by chemists today. A full, coherent, and consistent theory to bridge the gap between contemporary solutions of the Schrodinger

equation and chemical understanding is still elusive, despite the fact that many of these early conceptions have been examined and their flaws are widely documented. AIM is a top contender to accomplish that goal, nevertheless. Instead of being a comprehensive and thorough theory based on quantum physics, this theory is sometimes misunderstood to be another atomic population analysis [43].

As part of a larger system, such as a molecule or crystal, QTAIM precisely describes a number of atom-level characteristics as well as the chemical connections that connect them. The topological examination of the electron density leads to the simultaneous and coherent emergence of the properties of atoms and bonds. These characteristics fall into three categories in general: (1) The atomic attributes including atomic energy, atomic charge, and atomic electric multipoles are integrated with respect to atomic basin [44]; (2) Integrated interatomic characteristics, including the delocalization index [45] or the interacting quantum atoms (IQA) interaction energy component [46], which are derived from integrals over the basins of pairs of atoms; (3) Bond properties [44] can be further divided into those that are locally determined at the bond critical point (BCP), such as the electron density or the energy density evaluated at the BCP, or integrated along the bond path, such as the bond path length, or integrated over the interatomic zero-flux surface, such as the integrated electron density over the interatomic surface.

Current applications of AIM include high-resolution crystallography [47], surface science [48], solid state physics [49], biological chemistry [50], organometallic chemistry [51], noble gas

chemistry [52], physical organic chemistry [53], transition metal complex chemistry [54], boron chemistry [55], lithium chemistry [56], and other fields. Numerous concepts have been reinterpreted with the aid of the AIM theory, including bond energy, hydrogen bonding, the VSEPR model, the Ligand Close Packing (LCP) model, nucleophilic addition, atomic volume, strain energy, chemical reactivity, acid and base promoted hydrolysis, polarizabilities, molecular similarity, atomic charges, semi-empirical valence electron distributions, non-bonded charge concentrations (lone-pairs), (hyper)conjugation, the characterisation of atomic interactions, F centres, electron delocalisation, aromaticity, origin of molecular dipole moments, structural stability, and magnetic properties [42].

2.10.9 Electron Localisation Function (ELF)

The use of theoretical notions in chemistry is significant, and fundamental qualitative concepts like the chemical bond first emerged in the literature relatively early on. One of the key ideas in chemistry for describing and comprehending molecular structure and chemical reactivity is the chemical bond. Different types of bonding analysis methods are based on the topology of scalar fields, and various applications have already been reported in the literature. Topological analysis is a useful tool to characterise intra- and intermolecular interactions. Topological research of the ELF is now gaining interest as a means of characterising chemical bonding in systems ranging from clusters in the gas phase to solids [57].

A formulation with a similar idea to ELF was first presented by Artmann. In quantum mechanics, a probability density is represented by the sum of squares of the N-particle wave function. He therefore looked for the maximum of this quantity and discovered that it occurs where the chemist imagines the bonds to be. For example, in the case of the methane molecule, he discovered four valence electron pairs arranged tetrahedrally around the carbon atom. While extremely interesting, sum of the squares analyses of the wave function are challenging to carry out in real life [58]. Lennard-Jones realised that the work of Artmann could be greatly simplified by using only two electrons with identical spin and, consequently, only two coordinates to examine the Pauli principle. According to the Pauli principle, space is divided into regions, as demonstrated by Lennard-Jones. The other electron avoids a certain location if an electron resides there. After integrating over each coordinate of the remaining N-2 electrons, Lennard-Jones quantitatively reduced the probability density of two electrons. The resulting quantity (the pair density) is a function of the coordinates of two electrons, a six-dimensional function that is too complex for our three-dimensional understanding of the chemical bond. Consider the electron density is the only way to simplify the analysis of a single electron [59].

The electron localization function (ELF), which Becke and Edgecombe first presented for the Hartree-Fock theory and which Savin later expanded to the Kohn-Sham density-functional theory (DFT), has had great success as a tool for comprehending and visualising chemical bonding. Understanding bonding in atoms,

molecules, clusters, and solid-state structures has been greatly aided by the ELF. More details on bonding in a particular system can be found by conducting a topological analysis of ELF in the vein of Bader's atoms-in-molecules approach, though interpretations based on this study should be approached with some caution [57].

According to Becke and Edgecombe, the ELF focused on Hartree–Fock theory and the same-spin pair density and relative ELF measure is given by:

$$f_{ELF,\sigma}(r) = \frac{1}{1 + \left[D_{\sigma}(r)/D_{\sigma}^{0}(r) \right]^{2}} \tag{15}$$

Where D_{σ} as a measure of electron localization

$$D_{\sigma} = \tau_{\sigma} - \frac{1}{4} \frac{(\nabla \rho_{\sigma})^{2}}{\rho_{\sigma}} \tag{16}$$

And D_{σ}^{0} is the corresponding quantity for a homogeneous electron gas

$$D_{\sigma}^{0}(r) = 2^{\frac{5}{3}} c_{F} \rho_{\sigma}(r)^{\frac{5}{3}} \tag{17}$$

$$c_{F} = \frac{3}{10}(3\pi^{2})^{2} \tag{18}$$

The overlap function between the hole and electron distribution is given by,

$$\text{Sm index} = \int \min\left[\rho^{hole}(r), \rho^{ele}(r) \right] dr \tag{19}$$

$$\text{Sr index} = \int \sqrt{\rho^{hole}(r)\rho^{ele}(r)} \tag{20}$$

Where ρ^{hole} and ρ^{ele} represent the hole distribution and electron distribution respectively

The quantity D-index specifies the distance between the centroid of the electron and the hole in respective directions which is given by,

$$D_x = \left| X_{ele} - X_{hole} \right|, D_y = \left| Y_{ele} - Y_{hole} \right|, D_z = \left| Z_{ele} - Z_{hole} \right| \tag{21}$$

$$\text{D index} = |D| = \sqrt{D_x^{\,2} + D_y^{\,2} + D_z^{\,2}} \tag{22}$$

In which X_{ele}, Y_{ele}, Z_{ele} is the *X, Y, and Z* coordinates of the centroid of the electron and X_{hole}, Y_{hole}, Z_{hole} is the *X, Y, and Z* coordinates of the centroid of the hole respectively.

H index is an overall measure of the average degree of the spatial extension of hole and electron distribution

$$\text{H index} = \frac{\left(\left| \sigma_{ele} \right| + \left| \sigma_{hole} \right| \right)}{2} \tag{23}$$

σ_{ele}, σ_{hole} measures the RMSD of electron and hole respectively.

$$\text{t index} = \text{D index} - \text{H}_{CT} \tag{24}$$

H_{CT} measures the average degree of the spatial extension of hole and electron distribution in the CT direction. If the t index is less than zero, charge transfer does not significantly separate the hole from

the electron. A positive t index must match a distinct separation of the hole and electron distributions [60].

This definition of the ELF makes it a dimensionless quantity between 0 and 1. The upper limit of $f_{ELF,\sigma}(r) = 1$ denotes perfect localization, whereas $f_{ELF,\sigma}(r) = 0.5$ denotes behaviour that is comparable to that of a uniform gas with the same density [61].

The ELF as proposed for Hartree–Fock theory depends on the conditional pair-density, for the interacting system. This parameter is not accessible in the same way in Kohn-Sham DFT because the determinantal wave function is then employed to describe a system of electrons that are not interacting rather than to mimic the actual system. The ELF can then be seen as a measure of localization that accounts for changes brought about by the electrons' fermionic nature and the Pauli principle's fulfilment. The Fermi-correlation (exchange) effects between electrons with the same spin are often orders of magnitude larger as a result of the Pauli principle than those between electrons with the opposite spin (dynamical correlation). As a result, same-spin interaction interpretation, such as that used in ELF, can be a helpful qualitative tool for interpretation.

$$f_{ELF}(r) = \frac{1}{1 + \left(\dfrac{\tau_\alpha^{Pauli}(r) + \tau_\beta^{Pauli}(r)}{\tau_\alpha^{UEG}(r) + \tau_\beta^{UEG}(r)} \right)^2} \qquad (25)$$

Where $\tau^{Pauli}(r)$ represents the Pauli kinetic energy density and $\tau^{UEG}(r)$ indicate the spin-dependent parts of the kinetic energy density

of the spin-polarized homogeneous electron gas. According to the Pauli principle, the ELF formula relates to the kinetic energy needed for the distribution of all electrons (regardless of spin). ELF values are restricted to the range of 0 (poor localization) and 1. (high localization) [62].

2.10.10 Localized orbital locator (LOL)

As a result of the success of density functional theory (DFT) of electronic structure, new descriptors for long-standing chemical bonding issues, like the electron localization function (ELF) proposed by Becke and Edgecombe, have been developed. One of the key elements of the nature of the chemical bond is the issue of electron localization and delocalization [57]. Different partitioning strategies, primarily based on topological methods, have been presented that specifically address this issue for density-based representations of chemical bonding. Through a topological analysis of the Laplacian distribution of the underlying density, Bader's quantum theory of atoms in molecules (QTAIM) analyses the gradient field of the one-electron density and determines the nature of a chemical bond. The topology of the function L, where $L = - \nabla^2(\rho)$, in particular, offers important details on the nature of the chemical bond. Schmider and Becke remarked that LOL provides straightforward, recognisable patterns in conventional chemical bonds and stated their hope that "LOL will prove useful in comprehending the structures of exotic materials, as well as the conventional examples of freshman chemistry texts as well [63]." LOL shows the useful interpretation of the structures of strange materials and offers basic, observable patterns in typical chemical bonds. The

greatest localised orbital overlap is being explained by the localised orbital locator (LOL), which focuses on the topology characteristics of kinetic energy density [64].

The kinetic-energy density upon which the localization descriptor LOL is based is given by:

$$\tau = \frac{1}{2} \sum_i \Delta \psi_i . \Delta \psi_i^* \qquad (26)$$

Kinetic energy plays a significant part in the description of a chemical bond since the primary mechanism underlying covalent bonding is an orbital-sharing-induced decrease in the quantum kinetic-energy density. It is preferable to utilise a measure of the local kinetic energy as a sign of bond effects because the contributions to the kinetic energy from the bond regions typically decrease. High charge density regions frequently dominate to the point where important bonding characteristics are obscured. The kinetic-energy density (τ), is compared with a suitable reference value (τ_o), in order to get around this issue. Both ELF and LOL use a homogeneous spin-neutral electron gas with electron density and

$$\tau_o = \left(\frac{3}{10}\right)\left(3\pi^2\right)^{\frac{2}{3}} \rho^{\frac{5}{3}} \qquad (27)$$

as their reference. The dimensionless variable (t), is then defined through LOL analysis as:

$$t = \frac{\tau_o}{\tau} \qquad (28)$$

The local orbital locator v is defined as the measure of t in a mapping onto the finite range [0, 1] and is given by:

$$v = \frac{t}{1+t} \qquad (29)$$

Schmider and Becke assert that the mapping $t \rightarrow v$ preserves the topological characteristics of t because it is monotonically rising. The region where the local kinetic energy of electrons is equal to that of a uniform electron gas with the local density corresponds to the value of t = 1, which is transferred onto v=1/2. Electrons that are "quick" and have a higher kinetic energy than would be predicted by their local density are indicated by values of v<1/2. Areas with higher values of are defined by electrons that move comparatively slowly. A covalent bond is represented in v as a local maximum between the bound centres. In many bonds, the form of the v = 1/2 surface that encloses the maximum becomes more concave. The localized-orbital locator reaches high values (over 1/2) in places where a single localised orbital dominates the electron density. Lone electron pairs are resolved as local maxima in the middle of a v=1/2 surface with a distinctive form [63].

The electron localization function, ELF, which similarly depends on the kinetic-energy density, has a chemical composition comparable to that of the localized-orbital locator, LOL. The gradients of localised orbitals are maximised when localised orbitals overlap, whereas ELF is based on taking the electron pair density into account. Additionally, LOL always falls to zero asymptotically and has a

simpler meaning in terms of the fast and slow electron zones, whereas ELF does not necessarily [65].

2.10.11 In-silico ADME and drug-likeness prediction

The ADME analysis is a crucial step in weeding out a few interesting chemical entities from a vast chemical dataset [66]. The ADME profile of the herbacetin molecule could thus be predicted using an internet accessible web tool: SwissADME, which is publically available at http://www.swissadme.ch. Lipophilicity, water solubility, pharmacokinetics, and drug-likeness qualities, as well as Lipinski's rule of five, were all described. The SwissADME is well-liked by scientists because of its quick forecasting power and simple interpretation. In addition, a number of properties such as the n-octanol and water (log Po/w) partition coefficient or lipophilicity, molar solubility in water, BBB permeability, skin permeation, human gastrointestinal absorption (HIA) capability, and other important medicinal chemistry properties were examined in order to select the best BACE1 inhibitors for further evaluation.\

2.10.12 Full Electron Donor Acceptor Map (FEDAM)

To understand how different molecules can scavenge radicals, it's necessary to look at the one-electron-transfer process while simultaneously considering their ability to receive electrons. The most obvious qualities to evaluate for this purpose are ionisation energy(I) and electron affinity(A) [67]. FEDAM, is a graphical technique based on vertical ionization energies (VI) and vertical electron affinities (VA) and it is an easy way to evaluate the relative viability of

contributing, or accepting, charges [68]. Low-I-value compounds are the easiest to oxidize, and as a result, they are the most effective antiradicals in terms of electron donating capacity. High and positive A values indicate that a substance's ability to receive electrons is greater. Compounds with high positive A values are the easiest to reduce, and as a result, they are the most effective antiradicals in terms of electron accepting capacity [69]. According to the following equations, electron donating and accepting indexes of the coumestrol derivatives were calculated with respect to the parent molecule,

$$RI = I_D / I_{Cou} \tag{30}$$

$$RA = A_D / A_{Cou} \tag{31}$$

I_D and I_{Cou} represents the ionisation potential whereas A_D and A_{Cou} indicates the electron affinity of coumestrol derivative and coumestrol respectively.

2.10.13 Donor Acceptor Map (DAM)

DAM offers a valuable method for qualitative material comparison of molecules in terms of their electron acceptance and donation power [70]. It also provided details about the anti-radical potential of molecules, as well as a base for anti-oxidant studies [69, 71]. Ga'zquez et al [72] proposed an alternative quadratic interpolation for the energy as a function of the number of electrons to characterize a molecule's response to charge acceptance or withdrawal in terms of electron affinity and ionisation potential. According to this

approximation, the tendency to donate charge, or electron donating power (ω-), may be defined as;

$$\omega^- = (3I + A)^2/16(I - A) \qquad (32)$$

whereas, the tendency to accept a charge, or electron accepting power, may be defined as;

$$\omega^+ = (I + 3A)^2/16(I - A) \qquad (33)$$

ω^- and ω^+ refer to fractional charges. The compound would have a strong tendency to donate electrons as ω^- decreases, while the high value of ω^+ indicates a strong tendency to accept electrons [73]. The electron donation (Rd) and acceptance (Ra) index for every derivative were calculated from the electron donating and accepting powers of the molecules**.** In order to compare the radical scavenging ability of the derivatives with the coumestrol molecule, the Ra and Rd for each of the derivatives were calculated in terms of electron accepting power (ω^+_{Cou}) and electron donating power (ω^-_{Cou}) of coumestrol.

For any molecule D the electron acceptance index Ra is given as

$$Ra = \omega^+_D / \omega^+_D \qquad (34)$$

If Ra=1, then $\omega^+_D = \omega^+_{Cou}$, and D represents as effective of an electron acceptor as coumestrol. If Ra > 1, then $\omega^+_D > \omega^+_{Cou}$, and D represents a more effective electron acceptor than coumestrol. If Ra < 1, then $\omega^+_D < \omega^+_{Cou}$, and D represents a less effective electron acceptor than coumestrol.

$$Rd = \omega^-_D / \omega^-_{Cou} \tag{35}$$

If Rd =1, then $\omega^-_D = \omega^-_{Cou}$, and D is as effective of an electron donor as coumestrol. If Rd > 1, then $\omega^-_D > \omega^-_{Cou}$, and D is a less effective electron donor than coumestrol. If Rd < 1, then $\omega^-_D < \omega^-_{Cou}$, and D is a more effective electron donor than coumestrol.

2.10.14 Hole-electron excitation

Deep insight into all different forms of electron transfer features can be gained by hole-electron excitation analysis. It is an extremely useful technique for revealing the nature of electron excitations. The overlap function between the hole and electron distribution is given by,

$$Sm \quad index \quad = \int min\left[\rho^{hole}(r), \rho^{ele}(r) \right] dr \tag{36}$$

$$Sr \ index = \int \sqrt{\rho^{hole}(r)\rho^{ele}(r)} \tag{37}$$

Where ρ^{hole} and ρ^{ele} represent the hole distribution and electron distribution respectively

The quantity D-index specifies the distance between the centroid of the electron and the hole in respective directions which is given by,

$$D_x = \left| X_{ele} - X_{hole} \right|, D_y = \left| Y_{ele} - Y_{hole} \right|, D_z = \left| Z_{ele} - Z_{hole} \right| \tag{38}$$

$$D \ index = \left| D \right| = \sqrt{D_x^2 + D_y^2 + D_z^2} \tag{39}$$

In which X_{ele}, Y_{ele}, Z_{ele} is the *X, Y, and* Z coordinates of the centroid of the electron and X_{hole}, Y_{hole}, Z_{hole} is the *X, Y, and* Z coordinates of the centroid of the hole respectively.

H index is an overall measure of the average degree of the spatial extension of hole and electron distribution

$$H \text{ index} = \frac{\left(\left|\sigma_{ele}\right| + \left|\sigma_{hole}\right|\right)}{2} \tag{40}$$

σ_{ele}, σ_{hole} measures the RMSD of electron and hole respectively.

$$t \text{ index} = D \text{ index} - H_{CT} \tag{41}$$

H_{CT} measures the average degree of the spatial extension of hole and electron distribution in the CT direction. If the t index is less than zero, charge transfer does not significantly separate the hole from the electron. A positive t index must match a distinct separation of the hole and electron distributions [60].

References

1.   Young DC: **A practical guide for applying techniques to real-world problems**. *Computational Chemistry, New York* 2001, **9**:390.

2.   McArdle S, Endo S, Aspuru-Guzik A, Benjamin SC, Yuan X: **Quantum computational chemistry**. *Reviews of Modern Physics* 2020, **92**(1):015003.

3.   長谷川淳也: **EG Lewars, Computational Chemistry; Introduction to the Theory and Applications of Molecular and Quantum Mechanics 2nd edition, Springer-Verlag, Berlin, 2011, xvi+ 664p, 24× 16cm, 159.9€,[専門・大学院向], ISBN978-90-481-3860-9 (新著紹介)**. *日本物理学会誌* 2013, **68**(8):560-561.

4.   Gavroglu K, Simões A: **Neither physics nor chemistry: A history of quantum chemistry**: MIT Press; 2011.

5.   Young D: **Computational chemistry: a practical guide for applying techniques to real world problems**: John Wiley & Sons; 2004.

6.   Ugi I, Bauer J, Brandt J, Friedrich J, Gasteiger J, Jochum C, Schubert W: **New applications of computers in chemistry**. *Angewandte Chemie International Edition in English* 1979, **18**(2):111-123.

7.   Allinger NL: **Molecular structure: understanding steric and electronic effects from molecular mechanics**: John Wiley & Sons; 2010.

8.   Lewars EG: **Molecular mechanics**. In: *Computational Chemistry.* Springer; 2016: 51-99.

9.   Huang N, Kalyanaraman C, Bernacki K, Jacobson MP: **Molecular mechanics methods for predicting protein–ligand binding**. *PCCP* 2006, **8**(44):5166-5177.

10. Gschwend DA, Good AC, Kuntz ID: **Molecular docking towards drug discovery**. *Journal of Molecular Recognition: An Interdisciplinary Journal* 1996, **9**(2):175-186.

11. Dias R, de Azevedo J, Walter F: **Molecular docking algorithms**. *Curr Drug Targets* 2008, **9**(12):1040-1047.

12. Morris GM, Lim-Wilby M: **Molecular docking**. In: *Molecular modeling of proteins.* Springer; 2008: 365-382.

13. Hansson T, Oostenbrink C, van Gunsteren W: **Molecular dynamics simulations**. *Curr Opin Struct Biol* 2002, **12**(2):190-196.

14. Hollingsworth SA, Dror RO: **Molecular dynamics simulation for all**. *Neuron* 2018, **99**(6):1129-1143.

15. Rapaport DC, Rapaport DCR: **The art of molecular dynamics simulation**: Cambridge university press; 2004.

16. Karplus M, Petsko GA: **Molecular dynamics simulations in biology**. *Nature* 1990, **347**(6294):631-639.

17. Friesner RA: **Ab initio quantum chemistry: Methodology and applications**. *Proceedings of the National Academy of Sciences* 2005, **102**(19):6648-6653.

18. Thiel W: **Semiempirical quantum–chemical methods**. *Wiley Interdisciplinary Reviews: Computational Molecular Science* 2014, **4**(2):145-157.

19. Hohenberg P, Kohn W: **Inhomogeneous electron gas**. *Physical review* 1964, **136**(3B):B864.

20. Zhao Y, Truhlar DG: **Density functionals with broad applicability in chemistry**. *Acc Chem Res* 2008, **41**(2):157-167.

21. Balbuena PB, Seminario JM: **Density functional theory: Further applications**. In: *Theoretical and Computational Chemistry*. vol. 2: Elsevier; 1995: 383-401.

22. Assadi MHN, Hanaor DA: **Theoretical study on copper's energetics and magnetism in TiO2 polymorphs**. *J Appl Phys* 2013, **113**(23):233913.

23. Segall M, Lindan PJ, Probert Ma, Pickard CJ, Hasnip PJ, Clark S, Payne M: **First-principles simulation: ideas, illustrations and the CASTEP code**. *J Phys: Condens Matter* 2002, **14**(11):2717.

24. Rastegar SF, Hadipour NL, Soleymanabadi H: **Theoretical investigation on the selective detection of SO 2 molecule by AlN nanosheets**. *J Mol Model* 2014, **20**(9):1-6.

25. Rastegar SF, Hadipour NL, Tabar MB, Soleymanabadi H: **DFT studies of acrolein molecule adsorption on pristine and Al-doped graphenes**. *J Mol Model* 2013, **19**(9):3733-3740.

26. Music D, Geyer RW, Schneider JM: **Recent progress and new directions in density functional theory based design of hard coatings**. *Surface and Coatings Technology* 2016, **286**:178-190.

27. Kohn W: **Density functional theory**. *Introductory Quantum Mechanics with MATLAB: For Atoms, Molecules, Clusters, and Nanocrystals* 2019.

28. Boese AD, Martin JM, Handy NC: **The role of the basis set: Assessing density functional theory**. *The Journal of chemical physics* 2003, **119**(6):3005-3014.

29. Tang S, Chen R, Lin M, Lin Q, Zhu Y, Ding J, Hu H, Ling M, Wu J: **Accelerating AutoDock Vina with GPUs**. *Molecules* 2022, **27**(9):3041.

30. O'Boyle NM, Banck M, James CA, Morley C, Vandermeersch T, Hutchison GR: **Open Babel: An open chemical toolbox**. *J Cheminform* 2011, **3**(1):1-14.

31. Sadowski J, Gasteiger J, Klebe G: **Comparison of automatic three-dimensional model builders using 639 X-ray structures**. *J Chem Inf Comput Sci* 1994, **34**(4):1000-1008.

32. Sander T, Freyss J, von Korff M, Rufener C: **DataWarrior: an open-source program for chemistry aware data visualization and analysis**. *J Chem Inf Model* 2015, **55**(2):460-473.

33. Huey R, Morris GM, Forli S: **Using AutoDock 4 and AutoDock vina with AutoDockTools: a tutorial**. *The Scripps Research Institute Molecular Graphics Laboratory* 2012, **10550**:92037.

34. Studio D: **Discovery studio**. *Accelrys [21]* 2008.

35. Kim S, Thiessen PA, Bolton EE, Chen J, Fu G, Gindulyte A, Han L, He J, He S, Shoemaker BA: **PubChem substance and compound databases**. *Nucleic Acids Res* 2016, **44**(D1):D1202-D1213.

36. Khorshidi A, Peterson AA: **Amp: A modular approach to machine learning in atomistic simulations**. *Comput Phys Commun* 2016, **207**:310-324.

37. Bradley J, Gerrans G: **Frontier molecular orbitals. A link between kinetics and bonding theory**. *J Chem Educ* 1973, **50**(7):463.

38. Singh I, El-Emam AA, Pathak SK, Srivastava R, Shukla VK, Prasad O, Sinha L: **Experimental and theoretical DFT (B3LYP, X3LYP, CAM-B3LYP and M06-2X) study on electronic structure, spectral features, hydrogen bonding and solvent effects of 4-methylthiadiazole-5-carboxylic acid**. *Molecular Simulation* 2019, **45**(13):1029-1043.

39. Marques MA, Ullrich CA, Nogueira F, Rubio A, Burke K, Gross EK: **Time-dependent density functional theory**, vol. 706: Springer Science & Business Media; 2006.

40. Weinhold F: **Natural bond orbital analysis: a critical overview of relationships to alternative bonding perspectives**. *J Comput Chem* 2012, **33**(30):2363-2379.

41. Wang G, Xue Y, An L, Zheng Y, Dou Y, Zhang L, Liu Y: **Theoretical study on the structural and antioxidant properties of some recently synthesised 2, 4, 5-trimethoxy chalcones**. *Food Chem* 2015, **171**:89-97.

42. Popelier PLA, Aicken F, O'Brien S: **Atoms in molecules**, vol. 188: Prentice Hall Manchester; 2000.

43. Bader R: **From Schrodinger to atoms in molecules**. *Pure Appl Chem* 1988, **60**(2):145-155.

44. Bader RF: **Atoms in molecules**. *Acc Chem Res* 1985, **18**(1):9-15.

45. Fradera X, Austen MA, Bader RF: **The Lewis model and beyond**. *The Journal of Physical Chemistry A* 1999, **103**(2):304-314.

46. Blanco M, Martín Pendás A, Francisco E: **Interacting quantum atoms: a correlated energy decomposition scheme based on the quantum theory of atoms in molecules**. *J Chem Theory Comput* 2005, **1**(6):1096-1109.

47. Mallinson PR, Woźniak K, Smith GT, McCormack KL: **A charge density analysis of cationic and anionic hydrogen bonds in a "proton sponge" complex**. *Journal of the American Chemical Society* 1997, **119**(47):11502-11509.

48. Aray Y, Bader R: **Requirements for activation of surface oxygen atoms in MgO using the Laplacian of the electron density**. *Surf Sci* 1996, **351**(1-3):233-249.

49. Zou P, Bader R: **A topological definition of a Wigner–Seitz cell and the atomic scattering factor**. *Acta Crystallogr Sect A: Found Crystallogr* 1994, **50**(6):714-725.

50. Becke A: **The quantum theory of atoms in molecules: from solid state to DNA and drug design**: John Wiley & Sons; 2007.

51. Calhorda MJ, Lopes PE: **An 'atoms in molecules'(AIM) analysis of the dihydrogen bond in organometallic compounds**. *J Organomet Chem* 2000, **609**(1-2):53-59.

52. MacDougall PJ, Schrobilgen GJ, Bader RF: **Properties of atoms in molecules: krypton and xenon and their bonds to nitrogen and fluorine in hydrogen cyanide complexes with noble gas fluorides, HCN-NgF+, NgF+ and NgF2 (Ng= noble gas)**. *Inorg Chem* 1989, **28**(4):763-769.

53. Bader RF, Chang C: **Properties of atoms in molecules: electrophilic aromatic substitution**. *The Journal of Physical Chemistry* 1989, **93**(8):2946-2956.

54.   Matito E, Solà M: **The role of electronic delocalization in transition metal complexes from the electron localization function and the quantum theory of atoms in molecules viewpoints**. *Coordination Chemistry Reviews* 2009, **253**(5-6):647-665.

55.   Bader R, Legare D: **Properties of atoms in molecules: Structures and reactivities of boranes and carboranes**. *Can J Chem* 1992, **70**(2):657-676.

56.   Ritchie JP, Bachrach SM: **Bond paths and bond properties of carbon-lithium bonds**. *Journal of the American Chemical Society* 1987, **109**(20):5909-5916.

57.   Andrés J, González-Navarrete P, Safont VS, Silvi B: **Curly arrows, electron flow, and reaction mechanisms from the perspective of the bonding evolution theory**. *PCCP* 2017, **19**(43):29031-29046.

58.   Putz MV: **Electron Localization Function**. In: *New Frontiers in Nanochemistry*. Apple Academic Press; 2020: 133-142.

59.   Savin A, Nesper R, Wengert S, Fässler TF: **ELF: The electron localization function**. *Angewandte Chemie International Edition in English* 1997, **36**(17):1808-1832.

60.   Zhang Y, Shen C, Lu X, Mu X, Song P: **Effects of defects in g-C3N4 on excited-state charge distribution and transfer: potential for improved photocatalysis**. *Spectrochimica Acta Part A: Molecular and Biomolecular Spectroscopy* 2020, **227**:117687.

61.   Becke AD, Edgecombe KE: **A simple measure of electron localization in atomic and molecular systems**. *The Journal of chemical physics* 1990, **92**(9):5397-5403.

62.   Kohout M, Savin A: **Atomic shell structure and electron numbers**. *Int J Quantum Chem* 1996, **60**(4):875-882.

63.   Jacobsen H: **Localized-orbital locator (LOL) profiles of chemical bonding**. *Can J Chem* 2008, **86**(7):695-702.

64.   Sarala S, Geetha S, Muthu S, Irfan A: **Computational investigation, comparative approaches, molecular structural, vibrational spectral, non-covalent interaction (NCI), and electron excitations analysis of benzodiazepine derivatives**. *J Mol Model* 2021, **27**(9):1-34.

65.   Prasana JC, Muthu S, Abraham CS: **Molecular docking studies, charge transfer excitation and wave function analyses (ESP, ELF, LOL) on valacyclovir: a potential antiviral drug**. *Comput Biol Chem* 2019, **78**:9-17.

66. Gombar VK, Silver IS, Zhao Z: **Role of ADME characteristics in drug discovery and their in silico evaluation: in silico screening of chemicals for their metabolic stability**. *Curr Top Med Chem* 2003, **3**(11):1205-1225.

67. Martínez A, Vargas R, Galano A: **What is important to prevent oxidative stress? A theoretical study on electron-transfer reactions between carotenoids and free radicals**. *The Journal of Physical Chemistry B* 2009, **113**(35):12113-12120.

68. Vinduja P, Muraleedharan K: **Theoretical Studies on Anti-Oxidant Activity of the Phytochemical, Coumestrol and Its Derivatives**. In: *Functional Foods-Phytochemicals and Health Promoting Potential.* IntechOpen; 2021.

69. Martinez A: **Donator acceptor map of psittacofulvins and anthocyanins: are they good antioxidant substances?** *The Journal of Physical Chemistry B* 2009, **113**(14):4915-4921.

70. Alfaro RAD, Gomez-Sandoval Z, Mammino L: **Evaluation of the antiradical activity of hyperjovinol-A utilizing donor-acceptor maps**. *J Mol Model* 2014, **20**(7):1-11.

71. Martínez A: **Donator− acceptor map and work function for linear polyene-conjugated molecules. A density functional approximation study**. *The Journal of Physical Chemistry B* 2009, **113**(10):3212-3217.

72. Gázquez JL, Cedillo A, Vela A: **Electrodonating and electroaccepting powers**. *The Journal of Physical Chemistry A* 2007, **111**(10):1966-1970.

73. Martínez A, Rodríguez-Gironés MA, Barbosa A, Costas M: **Donator acceptor map for carotenoids, melatonin and vitamins**. *The Journal of Physical Chemistry A* 2008, **112**(38):9037-9042.

Chapter 3

Theoretical Probing to the Reactivity and Biological Effects of the Phytochemical, Coumestrol and its Derivatives

Abstract

Coumestrol, a pytochemical, has been shown to have anti-inflammatory, neuroprotective, anti-oxidant, and anti-cancer properties. Herein, the effect of substitution at various positions of the coumestrol molecule was systematically investigated using density functional theory (DFT) calculations. Full electron donor acceptor maps (FEDAM) and donor acceptor maps (DAM) identified the radical scavenging ability of these molecules. The derivative prepared by substituting the 15th position of coumestrol with -NH_2 group even outperformed coumestrol in terms of its powerful anti-oxidant character. This effect of -NH_2 substitution is attributed to the low O-H bond dissociation enthalpy. Moreover, most of the derivatives exhibited significantly higher interaction with cancer causing kinase proteins compared to the parent molecule, as evident by the in silico molecular docking and thereby revealing potential anti-cancer applications. Coumestrol and its derivatives obey Lipinski's rule of five, showing that they are safe for oral consumption, implying their application as future   drugs.

3.1. Introduction

Bioactive components are found in food that has the potential to modulate one or more metabolic processes or pathways in the human body, resulting in health and well-being benefits [1]. A large number of phytochemicals have been discovered in plants during the last four decades and received great attention due to their low toxicity and wide spectrum of biological activities such as anti-oxidant, anti-microbial, anti-viral, anti-mutagenic, anti-cancer activity, or their use in pathologies such as Alzheimer's and cardiometabolic disorders have received a lot of attention in recent years [2-5]. As a result, traditional medicine makes extensive use of herbs, herbal extracts, and single phytochemicals as foods, medications, and remedies [6]. The antioxidant properties, as well as their cancer-fighting properties of phyochemicals, are now widely recognized [7-10]. As a factor, research into natural additives has gained a foothold, as they are thought to pose no health risk to consumers [11].

Coumestrol, a coumestan is containing a 6H-benzofuro- [3,2-c][1]benzopyran-6-one skeleton [12], isolated from different clovers, alfalfa and other leguminous plants that are source of food for human and animals [13]. Coumestrol has become of concern as several reports indicate its multi-pharmacological activities, including anti-inflammatory, neuroprotective, osteoblast differentiation, and anticancer [14-16]. Coumestrol is a coumarin like compound whose structure is more resemble to stilbestrol and normal estrogen, estradiol

[17]. Both its antioxidant and estrogenic properties are attributed to the presence of two hydroxyl groups in its chemical structure, which have an orientation similar to estradiol [18]. It also has been shown to have receptor-dependent anti-estrogenic activity[19], and its impermissibility has lowered the risk of breast cancer [16, 20], prostate cancer [21-23], heart disease [24], and a decline in menopausal symptoms [24].

In phytochemical research, there has been a notable increase in the use of computational techniques, artificial intelligence, and mathematical modeling, particularly in screening plant materials, plant metabolomics, and prediction of pharmacological and toxicological properties (virtual screening or in silico studies). The present work is mainly focussed on computer-aided studies on the reactivity and biological effects of the phytochemical coumestrol and its derivatives.

Computational chemistry, a quantum mechanical approach, deals with the problems numerically based on fundamental law of physics. Green computing approaches are less time-consuming, and it opens up new frontiers for chemists to research chemical processes by running computer-based calculations instead of experimentally investigating reactions and compounds. The notable impact of DFT methods, close to the ab-initio method in several respects, is very important due to the advancement of chemical quantity measurement [25]. Compared to other computational methods, DFT is not based on wave function but rather on electron density function [26]. Until moving into the specifics of anticancer studies, a clear understanding of the structure of the molecules under study is necessary. The

geometrical parameters and global descriptive properties of coumestrol and its derivatives were studied here through DFT calculations. The phenolic profile and antioxidant ability of coumestrol and its derivatives were investigated in this research, which was motivated by the under appreciated biological potential of coumestrol.

Furthermore, one of the primary goals of this research was to explore the general anticancer activity of coumestrol and its derivatives and found that inhibition of cancer causing kinases by coumestrol led to the suppression of tumerous cell proliferation. We also investigated the toxic effect of the derivative models through ADME analysis. Previous reports are concentrated mainly on the impact of coumestrol on breast cancer [27] and prostate cancer [21]. To our knowledge, this computational work is the first to examine the anticancer activity of coumestrol and its derivatives on various cancer-causing kinases.

3.2. Materials and Methodology

3.2.1. Materials

The research is carried out by means of computational methods. The structure of coumestrol (CID:5281707) was downloaded from PubChem software in SDF format. It was then converted to Gaussian Job File (GJF) as input files with the aid of the Open Babel application. Gaussview-5.0 graphical user interface was used to draw the structure of coumestrol derivatives. All the structures were optimised and their global descriptive parameters were calculated using Gaussian 09 software package. Toxicity study of all the compounds were done by using SwissADME. The 3D

structures of kinase proteins were downloaded from the protein data bank in PDB format. Output Gaussian files of optimized coumestrol derivatives were converted into PDB files using Open Babel tool. The structure of the protein and ligands were edited using the software, AutoDock tools and saved as PDBQT format. Anticancer studies were performed using AutoDock Vina and protein-ligand interactions were studied with the help of discovery studio.

3.2.2 Computational methodology

All the DFT calculations were done by setting B3LYP as the level of theory and 6–31+ G (2d,2p) as the basis set using the Gaussion09 software package. In order to obtain the stable structure of the parent molecule, coumestrol, potential energy scanning was done. For the subsequent studies, the minimum energy conformer was then used. The derivatives were prepared by attaching electron donating (-OH, $-NH_2$, $-OCH_3$, CH_3, -Ph, -OCOR and -NHCOR) as well as electron withdrawing (-F, -Cl, -CN, $-NO_2$, -CHO, -COR, -COCl, -COOR and -COOH) substituents (where 'R' is a methyl group) on C-15, C-16, C-17 and C-19 position of coumestrol.

3.2.2.1 Molecular Docking

Molecular docking of coumestrol and its derivatives is performed using the AutoDock Vina program. AutoDock Vina program is used to obtain the scoring functions which represents the binding affinity between protein and ligand. The protein structures obtained may contain water molecules and other ligands. They are removed and hydrogen atoms are added to the proteins using

AutoDock tools. Set grid around the active site and the structure of proteins in the pdb format is then converted to pdbqt format. Coumestrol and its derivatives are used as ligands. The selected kinase proteins, corresponding PDB id and their grid dimensions are given in the **Table 3.1**. Both 2D as well as 3D structures of the protein-ligand complex can be obtained using the discovery studio. The binding affinities are tabulated and the types of interactions are studied.

Table 3.1 Name of kinase proteins along with their PDB id and grid dimensions

PROTEIN	PDB ID	DIMENSION (X, Y, Z)	CENTERED ON
BRAF	5CSX	42x42x42	20.17, -77.1, 90.434
Aurora A	3H0Y	40x40x40	48.222,11.748,25.827
JAK3	4HVD	30x30x30	-0.423, -16.670, -3.977
VEGFR2	4ASE	40x40x40	-23.138, 0.251, -9.480
MCL-1	3KJ0	18x18x18	-3.507, -13.459, 24.775
LCK	3MPM	40x40x40	26.132, 12.570, 52.905
MEK1	3ZLW	20x20x20	-18.966, 27.056, -3.156
MMP3	1HY7	50x50x50	0.888, 48.032, 55.449

Inorder to compare the reactivity difference between the parent coumestrol molecule and the optimized derivatives, global descriptive parameters were calculated. DAM and FEDAM plots were obtained revealing radical scavenging activities of the molecules under study. The anti-oxidant mechanism of coumestrol and its derivatives were

analysed. As a potential application, anti cancer activity of the derivatives was studied using molecular docking and most of them outperformed the parent molecule. Derivatives obtained by substitution at the 15th position of coumestrol molecule are presented in the main text for clarity, and the data related to the rest are shown in the supporting information. Detailed description of DAM, FEDAM, and anti-oxidant mechanisms can be seen in chapter 2.

3.3 Optimisation of coumestrol and its derivatives

The potential energy surface (PES) scan with the theoretical approximations level B3LYP/6-31+G(2d, 2p) was carried out to identify the stable conformer of coumestrol. The preliminary search of low energy structures are carried out for the dihedral angles 19,20,5,28 and 15,10,4,27, which are the appropriate coordinate for conformational flexibility within the molecule. The minimum energy conformer (**Fig. 3.1**) was used for further studies. Optimized bond length (in Å) and bond angle(^{0}) of coumestrol using B3LYP/6-31+G(2d,2p) and M06/6-31+G(2d,2p) and B3LYP-D3/6-31+G(2d,2p) are given **Table 3.2** and **Table 3.3** reapectively. The derivatives were prepared and optimized using the same theoretical level of approximation.
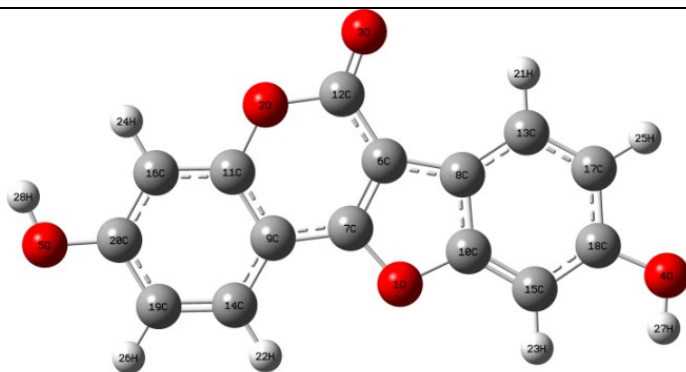
Fig. 3.1. Optimized lowest energy conformer of coumestrol

Table 3.2 Optimized bond length (in Å) of coumestrol using B3LYP/6-31+G(2d,2p) and M06/6-31+G(2d,2p) and B3LYP-D3/6-31+G(2d,2p)

Bonds	Bond length (Å)		
	B3LYP	M06	B3LYP+D3
R(1,7)	1.3598	1.3503	1.3604
R(1,10)	1.3828	1.3743	1.3839
R(2,11)	1.3634	1.3548	1.3641
R(2,12)	1.4059	1.3948	1.4060
R(3,12)	1.2046	1.1988	1.2047
R(4,18)	1.3673	1.3573	1.3676
R(4,27)	0.9631	0.9607	0.963
R(5,20)	1.3614	1.3515	1.3616
R(5,28)	0.9638	0.9616	0.9636
R(6,7)	1.3742	1.3678	1.3738
R(6,8)	1.4439	1.4387	1.4421
R(6,12)	1.4398	1.4352	1.4389
R(7,9)	1.4227	1.4184	1.4213
R(8,10)	1.4034	1.398	1.4035
R(8,13)	1.3999	1.3952	1.399
R(9,11)	1.4109	1.4043	1.4114
R(9,14)	1.4065	1.401	1.4057
R(10,15)	1.3852	1.3807	1.3847

R(11,16)	1.3936	1.3885	1.393
R(13,17)	1.3893	1.3838	1.3895
R(13,21)	1.0822	1.0844	1.0821
R(14,19)	1.3822	1.3769	1.3823
R(14,22)	1.083	1.0855	1.0829
R(15,18)	1.3977	1.3916	1.3982
R(15,23)	1.0838	1.0856	1.0834
R(16,20)	1.3928	1.3878	1.3932
R(16,24)	1.0841	1.0864	1.0837
R(17,18)	1.4071	1.402	1.4074
R(17,25)	1.0828	1.085	1.0826
R(19,20)	1.4055	1.4005	1.4056
R(19,26)	1.0823	1.0844	1.0821

Table 3.3 Optimized bond angle (in ^{0}) of coumestrol using B3LYP/6-31+G(2d,2p) and M06/6-31+G(2d,2p) and B3LYP-D3/6-31+G(2d,2p)

Angles	Bond angle (^{0})		
	B3LYP	M06	B3LYP-D3
A(7,1,10)	106.0523	105.9457	105.9457
A(11,2,12)	124.0664	124.3550	124.3550
A(18,4,27)	110.0722	110.2208	110.2208
A(20,5,28)	110.1736	110.2988	110.2988
A(7,6,8)	106.5024	106.3948	106.3948
A(7,6,12)	121.0144	121.1175	121.1175
A(8,6,12)	132.4831	132.4877	132.4877
A(1,7,6)	111.8728	112.1004	112.1004
A(1,7,9)	124.3044	124.2022	124.2022
A(6,7,9)	123.8228	123.6974	123.6974
A(6,8,10)	104.7178	104.5036	104.5036
A(6,8,13)	136.6489	136.8677	136.8677
A(10,8,13)	118.6333	118.6287	118.6287
A(7,9,11)	114.2270	114.1066	114.1066
A(7,9,14)	126.9853	126.9244	126.9244
A(11,9,14)	118.7877	118.9690	118.9690
A(1,10,8)	110.8547	111.0556	111.0556

A(1,10,15)	124.9725	124.7043	124.7043
A(8,10,15)	124.1727	124.2401	124.2401
A(2,11,9)	122.4675	122.5086	122.5086
A(2,11,16)	116.698	116.7253	116.7253
A(9,11,16)	120.8346	120.7661	120.7661
A(2,12,3)	117.6234	117.9393	117.9393
A(2,12,6)	114.4019	114.2149	114.2149
A(3,12,6)	127.9747	127.8457	127.8457
A(8,13,17)	118.6637	118.5934	118.5934
A(8,13,21)	120.4131	120.5402	120.5402
A(17,13,21)	120.9232	120.8664	120.8664
A(9,14,19)	120.7329	120.6454	120.6454
A(9,14,22)	119.0359	118.9129	118.9129
A(19,14,22)	120.2312	120.4417	120.4417
A(10,15,18)	116.0054	115.9075	115.9075
A(10,15,23)	121.7031	121.7374	121.7374
A(18,15,23)	122.2915	122.3551	122.3551
A(11,16,20)	119.1769	119.122	119.122
A(11,16,24)	119.0592	118.9853	118.9853
A(20,16,24)	121.7639	121.8926	121.8926
A(13,17,18)	121.1038	121.1536	121.1536
A(13,17,25)	120.8362	121.0607	121.0607
A(18,17,25)	118.06	117.7857	117.7857
A(4,18,15)	122.0533	122.0844	122.0844
A(4,18,17)	116.5256	116.4389	116.4389
A(15,18,17)	121.4211	121.4767	121.4767
A(14,19,20)	119.6249	119.5722	119.5722
A(14,19,26)	121.4162	121.7460	121.7460
A(20,19,26)	118.9589	118.6818	118.6818
A(5,20,16)	122.3272	122.2827	122.2827
A(5,20,19)	116.8298	116.7919	116.7919
A(16,20,19)	120.8430	120.9253	120.9253

3.4 Global descriptive parameters

The global descriptive parameters (ionisation potential, electron affinity, electronegativity, softness, hardness, chemical potential, and electrophilic index) of coumestrol and all its derivatives were calculated according to both Koopman's and vertical energy methods in order to compare the reactivity difference. The high ionisation potential and electron affinity of a molecule indicate that removing an electron from the molecule is more difficult, than accepting one[28]. Electronegativity (χ) is a relevant quantum chemical reactivity descriptor that describes a molecule's ability to attract electrons [29]. The electrophilicity index (ω) expresses a molecule's stabilization energy when it receives electrons . It represents a molecule's electrophilicity or nucleophilicity, with larger values of ω indicating stronger electrophiles[30]. A molecule's resistance to electron density distortion is measured by its hardness (h)[31]. When interacting with another molecule, it is a crucial property that expresses a molecule's tendency to give non-bonding electrons. According to the hard-soft acid-base (HSAB) theory[32], molecules with a high hardness tend to give electrons less frequently, making them less reactive. Soft molecules (those with a lower hardness) have a higher ability to donate electrons, whereas hard molecules (those with a higher hardness) have a lower capacity[30].
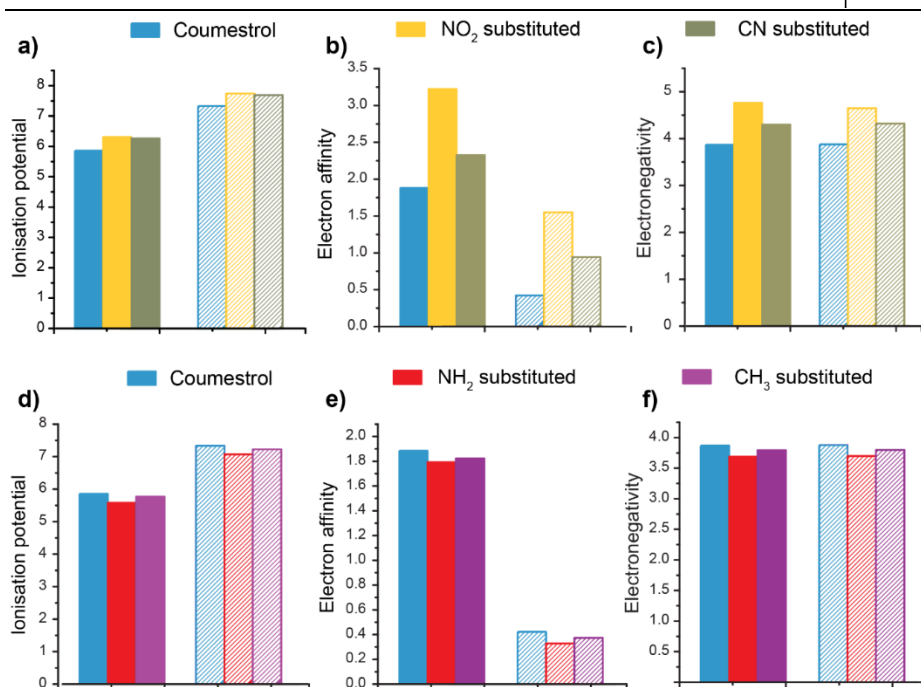
Fig. 3.2. a), b), and c) The ionization potential, electron affinity, and electronegativity when coumestrol is substituted at C 15th position by electron withdrawing groups, NO₂ and CN. **d), e), and f)** The same parameters obtained when coumestrol is substituted at C 15th position by electron releasing groups, NH₂ and CH₃. The solid bars in the figure indicate the values calculated using Koopman's theorem and the patterned bars indicate the ones calculated using energy vertical method

The effect of substitution of different electron withdrawing groups and electron releasing groups at various positions of coumestrol was revealed through these calculations. In general, substitution of coumestrol with all the electron withdrawing groups studied, resulted in the increase of ionisation potential, electron affinity, electronegativity, softness, and electrophilic index compared to the parent molecule. The hardness and chemical potential in these cases were found to be lesser than the parent molecule. On the other hand, if

the coumestrol molecule is substituted with electron releasing groups, the ionisation potential, electron affinity, electronegativity, and hardness are found to decrease. The other parameters such as softness, electrophilic index, and chemical potential tend to increase. Interestingly, the same trend was obtained irrespective of the method used, i.e., the Koopman's method and energy vertical method resulted in the same trend. The data obtained from these calculations are presented in **Tables 3.4-3.11**. In the main text, the substitutions that resulted in significant decrease/increase (compared to coumestrol) in ionisation potential, electron affinity, and electron negativity are presented in **Fig. 3.2**. The electron withdrawing groups such as -NO_2, and -CN indicated the best increase in such parameters (see **Figs. 3.2a,b,and c**). The electron releasing groups like -NH_2, and -CH_3 indicated the best decrease in the same parameters (see **Figs. 3.2d,e,and f**).

Table 3.4 Global descriptive parameters of derivatives of coumestrol and derivatives substituted at C-15th position under DFT/B3LYP/6–31+ G (2d,2p) according to Koopman's method

Molecules	I	A	η	χ	S	μ	ω
Coumestrol	5.8556	1.8844	3.9712	3.87	0.1259	-3.9700	1.8857
15-F	6.0086	2.0074	2.0006	4.008	0.2499	-4.0080	4.0144
15-Cl	6.014	2.0218	1.9961	4.0179	0.2505	-4.0179	4.0440
15-CN	6.2641	2.3282	1.968	4.2962	0.2541	-4.2962	4.6900
15-NO$_2$	6.3052	3.2226	1.5413	4.7639	0.3244	-4.7639	7.3622
15-CHO	6.1315	2.5791	1.7762	4.3553	0.2815	-4.3553	5.3397
15-COR	6.0336	2.3633	1.8352	4.1984	0.2724	-4.1984	4.8015
15-COCl	6.2121	2.7369	1.7376	4.4745	0.2878	-4.4745	5.7621
15-COOR	5.9495	2.1290	1.9102	4.0392	0.2618	-4.0392	4.2713
15-COOH	6.0268	2.2485	1.8892	4.1376	0.2647	-4.1376	4.5311
15-OH	6.0306	2.4360	1.7973	4.2333	0.2782	-4.2333	4.9856
15-NH$_2$	5.5824	1.7930	1.8947	3.6877	0.2639	-3.6877	3.5886
15-OCH$_3$	5.7982	1.9070	1.9456	3.8526	0.2570	-3.8526	3.8123
15-CH$_3$	5.7683	1.8226	1.9728	3.7954	0.2534	-3.7954	3.6510
15-Ph	5.7778	1.8324	1.9649	3.8142	0.2546	-3.8142	3.7045
15-OCOR	5.8891	1.9081	1.9905	3.8986	0.2512	-3.8986	3.8178
15-NHCOR	6.0709	2.0871	1.9919	4.079	0.251	-4.079	4.1765

Table 3.5 Global descriptive parameters of derivatives of coumestrol substituted at C-15th position DFT/B3LYP/6–31+ G (2d,2p) according to energy vertical method

Molecules	I	A	η	χ	S	μ	ω
Coumestrol	7.3311	0.4221	3.4545	3.8766	0.1447	-3.8766	2.1751
15-F	7.4814	0.5350	3.4732	4.0082	0.1440	-4.0082	2.3128
15-Cl	7.4558	0.5799	3.4380	4.0178	0.1454	-4.0178	2.3477
15-CN	7.6973	0.9410	3.3781	4.3191	0.1480	-4.3191	2.7612
15-NO$_2$	7.7380	1.5498	3.0941	4.6439	0.1616	-4.6439	3.4850
15-CHO	7.5668	1.0888	3.2390	4.3278	0.1544	-4.3278	2.8914
15-COR	7.4587	0.9611	3.2488	4.2099	0.1539	-4.2099	2.7277
15-COCl	7.6323	1.2592	3.1866	4.4457	0.1569	-4.4457	3.1012
15-COOR	7.3715	0.7635	3.3040	4.0675	0.1513	-4.0675	2.5037
15-COOH	7.4595	0.8511	3.3042	4.1553	0.1513	-4.1553	2.6128
15-OH	7.5079	0.9399	3.2840	4.2239	0.1523	-4.2239	2.7164
15-NH$_2$	7.0677	0.3277	3.3700	3.6977	0.1484	-3.6977	2.0286
15-OCH$_3$	7.2513	0.4517	3.3998	3.8515	0.1471	-3.8515	2.1816
15-CH$_3$	7.2211	0.3721	3.4245	3.7966	0.1460	-3.7966	2.1045
15-Ph	7.1617	0.5017	3.3300	3.8317	0.1501	-3.8317	2.2045
15-OCOR	7.3237	0.4753	3.4242	3.8995	0.1460	-3.8995	2.2204
15-NHCOR	7.4954	0.6631	3.4161	4.0792	0.1464	-4.0792	2.4356

Table 3.6 Global descriptive parameters of derivatives of coumestrol substituted at C-16th position DFT/B3LYP/6–31+ G (2d,2p) according to Koopman's method

Position & groups attached	I	A	η	X	S	μ	ω
16-F	5.9920	2.0300	1.9810	4.0110	0.2524	-4.0110	4.0606
16-Cl	5.9903	2.0466	1.9718	4.0184	0.2536	-4.0184	4.0950
16-CN	6.2015	2.4324	1.8846	4.3170	0.2653	-4.3170	4.9443
16-NO$_2$	6.2243	3.2050	1.5096	4.7146	0.3312	-4.7146	7.3617
16-CHO	6.0877	2.6520	1.7178	4.3698	0.2911	-4.3698	5.5586
16-COR	6.0023	2.4077	1.7973	4.2050	0.2782	-4.2050	4.9191
16-COCl	6.1607	2.6610	1.7498	4.4108	0.2857	-4.4108	5.5592
16-COOR	5.8951	2.0988	1.8981	3.9969	0.2634	-3.9969	4.2082
16-COOH	5.9664	2.2316	1.8674	4.0990	0.2678	-4.0990	4.4987
16-OH	5.879	1.9369	1.9710	3.9080	0.2537	-3.9080	3.8746
16-NH$_2$	5.8148	1.8591	1.9779	3.8369	0.2528	-3.8369	3.7217
16-OCH$_3$	5.833	1.871	1.9810	3.8520	0.2524	-3.8520	3.7452
16-CH$_3$	5.7974	1.8109	1.9932	3.8042	0.2508	-3.8042	3.6302
16-Ph	5.7849	1.824	1.9804	3.8044	0.2525	-3.8044	3.5410
16-OCOR	6.07	2.142	1.9645	4.1055	0.2545	-4.1055	4.2899
16-NHCOR	6.0431	2.1162	1.9634	4.0797	0.2546	-4.0797	4.2394

Table 3.7 Global descriptive parameters of derivatives of coumestrol substituted at C-16th position DFT/B3LYP/6–31+ G (2d,2p) according to energy vertical method

Position & groups attached	I	A	η	χ	S	μ	ω
16-F	7.4689	0.5578	3.4556	4.0133	0.1447	-4.0133	2.3306
16-Cl	7.4425	0.6080	3.4173	4.0253	0.1463	-4.0253	2.3707
16-CN	7.6594	1.0007	3.3294	4.3300	0.1502	-4.3300	2.8157
16-NO$_2$	7.6796	1.5158	3.0819	4.5977	0.1622	-4.5977	3.4295
16-CHO	7.5348	1.1064	3.2142	4.3206	0.1556	-4.3206	2.9039
16-COR	7.4306	0.9353	3.2477	4.1830	0.1540	-4.1830	2.6939
16-COCl	7.6040	1.1919	3.2061	4.3980	0.1560	-4.3980	3.0165
16-COOR	7.3310	0.6910	3.3200	4.0110	0.1506	-4.0110	2.4229
16-COOH	7.4149	0.7913	3.3118	4.1031	0.1510	-4.1031	2.5418
16-OH	7.3332	0.4735	3.4298	3.9034	0.1458	-3.9034	2.2211
16-NH$_2$	7.2667	0.4105	3.4281	3.8386	0.1459	-3.8386	2.1491
16-OCH$_3$	7.2750	0.4329	3.4210	3.8539	0.1462	-3.8539	2.1708
16-CH$_3$	7.2491	0.3721	3.4385	3.8106	0.1454	-3.8106	2.1115
16-Ph	7.1791	0.4754	3.3519	3.8272	0.1492	-3.8272	2.1850
16-OCOR	7.5087	0.7162	3.3963	4.1124	0.1472	-4.1124	2.4898
16-NHCOR	7.4808	0.6957	3.3926	4.0882	0.1474	-4.0882	2.4633

Table 3.8 Global descriptive parameters of derivatives of coumestrol substituted at C-17th position DFT/B3LYP/6–31+ G (2d,2p) according to Koopman's method

Position & groups attached	I	A	η	X	S	μ	ω
17-F	5.986	2	1.9930	3.9930	0.2509	-3.9930	4.0004
17-Cl	6.0145	2.0365	1.9890	4.0255	0.2514	-4.0255	4.0738
17-CN	6.2929	2.298	1.9974	4.2954	0.2503	-4.2954	4.6182
17-NO$_2$	6.3462	2.5775	1.8844	4.4618	0.2653	-4.4618	5.2815
17-CHO	6.165	2.23	1.9675	4.1975	0.2541	-4.1975	4.4770
17-COR	6.0657	2.1519	1.9569	4.1088	0.2555	-4.1088	4.3134
17-COCl	6.2984	2.402	1.9482	4.3502	0.2566	-4.3502	4.8560
17-COOR	6.131	2.1089	2.0110	4.1200	0.2486	-4.1200	4.2201
17-COOH	6.0951	2.1434	1.9758	4.1193	0.2531	-4.1193	4.2940
17-OH	5.787	1.8498	1.9686	3.8184	0.2540	-3.8184	3.7032
17-NH$_2$	5.4978	1.754	1.8719	3.6259	0.2671	-3.6259	3.5118
17-OCH$_3$	5.6322	1.8038	1.9142	3.7180	0.2612	-3.7180	3.6109
17-CH$_3$	5.7724	1.827	1.9727	3.8000	0.2535	-3.8000	3.6593
17-Ph	5.8137	1.8996	1.9570	3.8567	0.2555	-3.8567	3.8000
17-OCOR	6.1171	2.1149	2.0011	4.1160	0.2498	-4.1160	4.2330
17- NHCOR	5.9582	2.0504	1.9539	4.0043	0.2559	-4.0043	4.1031

Table 3.9 Global descriptive parameters of derivatives of coumestrol substituted at C-17th position DFT/B3LYP/6–31+ G (2d,2p) according to energy vertical method

Positions & groups attached	I	A	η	χ	S	μ	ω
17-F	7.4566	0.5438	3.4564	4.0002	0.1447	-4.0002	2.3148
17-Cl	7.4444	0.6094	3.4175	4.0269	0.1463	-4.0269	2.3725
17-CN	7.7996	0.8160	3.4918	4.3078	0.1432	-4.3078	2.6573
17-NO$_2$	7.7759	1.1339	3.3210	4.4549	0.1506	-4.4549	2.9880
17-CHO	7.5931	0.8447	3.3742	4.2189	0.1482	-4.2189	2.6375
17-COR	7.4850	0.7812	3.3519	4.1331	0.1492	-4.1331	2.5482
17-COCl	7.7101	1.0498	3.3301	4.3799	0.1501	-4.3799	2.8804
17-COOR	7.5521	0.6939	3.4291	4.1230	0.1458	-4.1230	2.4786
17-COOH	7.5227	0.7553	3.3837	4.1390	0.1478	-4.1390	2.5314
17-OH	7.2470	0.3995	3.4238	3.8233	0.1460	-3.8233	2.1347
17-NH$_2$	6.9655	0.3150	3.3253	3.6402	0.1504	-3.6402	1.9925
17-OCH$_3$	7.0693	0.3630	3.3532	3.7162	0.1491	-3.7162	2.0592
17-CH$_3$	7.2189	0.3837	3.4176	3.8013	0.1463	-3.8013	2.1140
17-Ph	7.1430	0.5270	3.3080	3.8350	0.1511	-3.8350	2.2230
17-OCOR	7.5300	0.7025	3.4137	4.1162	0.1465	-4.1162	2.4817
17-NHCOR	7.3339	0.6471	3.3434	3.9905	0.1495	-3.9905	2.3815

Table 3.10 Global descriptive parameters of derivatives of coumestrol substituted at C-19th position DFT/B3LYP/6–31+ G (2d,2p) according to Koopman's method

Position & groups attached	I	A	η	χ	S	μ	ω
19-F	5.968	2.0648	1.9516	4.0164	0.2562	-4.0164	4.1329
19-Cl	5.992	2.0871	1.9524	4.0396	0.2561	-4.0396	4.1791
19-CN	6.2303	2.3679	1.9312	4.2991	0.2589	-4.2991	4.7850
19-NO$_2$	6.2796	2.8294	1.7251	4.5545	0.2898	-4.5545	6.01245
19-CHO	6.107	2.4000	1.8535	4.2535	0.2698	-4.2535	4.8813
19-COR	6.029	2.1769	1.9260	4.1030	0.2596	-4.1030	4.3703
19-COCl	6.1963	2.4256	1.8854	4.3110	0.2652	-4.3110	4.9287
19-COOR	5.9819	2.0615	1.9602	4.0217	0.2551	-4.0217	4.1260
19-COOH	6.1971	2.2961	1.9505	4.2466	0.2563	-4.2466	4.6228
19-OH	5.7949	1.8926	1.9512	3.8438	0.2562	-3.8438	3.7853
19-NH$_2$	5.5914	1.7613	1.9110	3.6804	0.2616	-3.6804	3.5435
19-OCH$_3$	5.6934	1.8174	1.9380	3.75540	0.258	-3.7554	3.6386
19-CH$_3$	5.7808	1.8204	1.9802	3.8006	0.2525	-3.8006	3.6473
19-Ph	5.8162	1.8882	1.9640	3.8522	0.2546	-3.8522	3.7779
19-OCOR	5.8983	1.9649	1.9667	3.9316	0.2542	-3.9316	3.9299
19-NHCOR	5.8262	1.9676	1.9293	3.8969	0.2592	-3.8969	3.9357

Table 3.11 Global descriptive parameters of derivatives of coumestrol substituted at C-19th position DFT/B3LYP/6–31+ G (2d,2p) according to energy vertical method

Position & groups attached	I	A	H	χ	S	μ	ω
19-F	7.4410	0.5962	3.4224	4.0186	0.1461	-4.0186	2.3593
19-Cl	7.4306	0.6554	3.3876	4.0430	0.1476	-4.0430	2.4126
19-CN	7.6805	0.9450	3.3678	4.3127	0.1485	-4.3127	2.7614
19-NO$_2$	7.7433	1.2538	3.2448	4.4985	0.1541	-4.4985	3.1184
19-CHO	7.5639	0.9432	3.3104	4.2535	0.1510	-4.2535	2.7327
19-COR	7.4749	0.7835	3.3457	4.1292	0.1494	-4.1292	2.5481
19-COCl	7.6423	1.0263	3.3080	4.3343	0.1511	-4.3343	2.8395
19-COOR	7.4203	0.6664	3.3770	4.0433	0.1481	-4.0433	2.4206
19-COOH	7.6697	0.8701	3.3998	4.2699	0.1471	-4.2699	2.6813
19-OH	7.2437	0.4386	3.4025	3.8411	0.1469	-3.8411	2.1682
19-NH$_2$	7.0137	0.3368	3.3385	3.6753	0.1498	-3.6753	2.0230
19-OCH$_3$	7.1118	0.3887	3.3616	3.7502	0.1487	-3.7502	2.0919
19-CH$_3$	7.2264	0.3886	3.4189	3.8075	0.1462	-3.8075	2.1201
19-Ph	7.1617	0.5291	3.3163	3.8454	0.1508	-3.8454	2.2294
19-OCOR	7.3362	0.5427	3.3967	3.9394	0.1472	-3.9394	2.2844
19-NHCOR	7.2190	0.5911	3.3139	3.9051	0.1509	-3.9051	2.3008

3.5. FEDAM and DAM Plot

The full-electron donor-acceptor map (FEDAM) is a valuable tool for evaluating the electron-transfer process between the molecules and free radicals, as shown in **Fig. 3.3a**. The FEDAM is a graphical representation of IE against EA that gives qualitative information about a molecule's electron-donor and electron-accepting potential [33]. Electrons will be moved from molecules in region 3 (good electron-donors) to those in region 1 (good electron-acceptors) (good acceptors) [34]. If a molecule's electron-accepting ability is lower than

that of a free radical, the molecule is expected to be in the good-electron-donors section of the map. However, some of these radical species, such as those with nitrogen and carbon in their structures (R-C and R-N, where R-indicates the radical character), are better electron-donors, instead of accepting electrons as in the previous reaction, are deactivated by donating to the molecule. A closer examination of the FEDAM reveals that both strategies for scavenging free radicals are possible, i.e., the molecule can lose or absorb electrons to prevent oxidative damage.
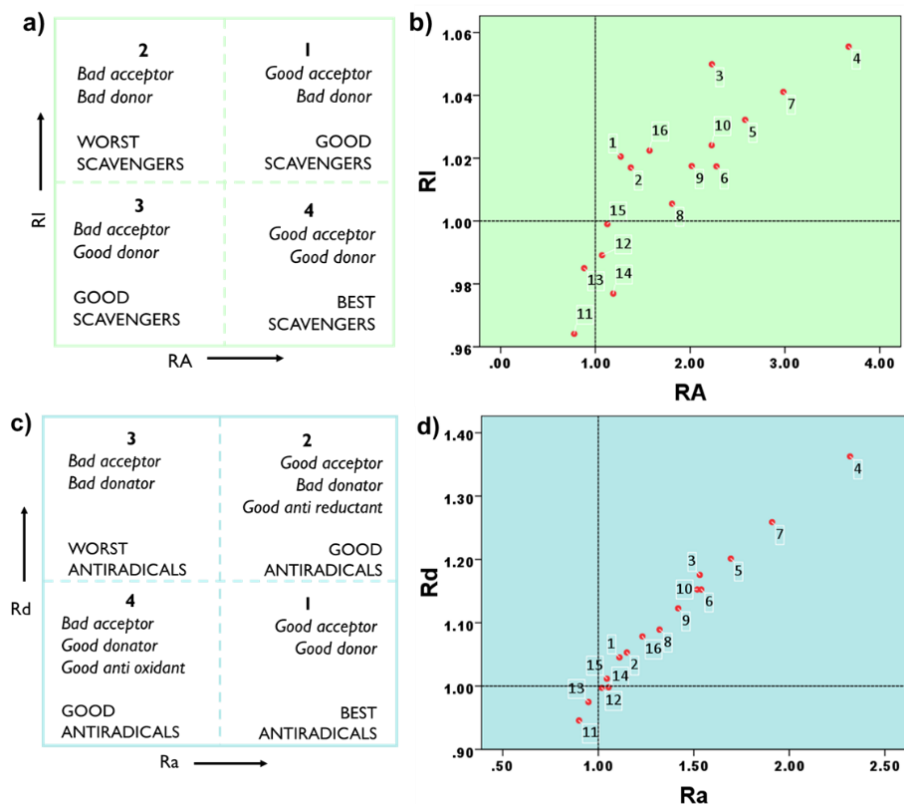
Fig. 3.3 a) and **b)** FEDAM plot of model and C-15 substituted coumestrol derivatives, respectively. **c)** and **d)** DAM plot of model and C-15 substituted coumestrol derivatives, respectively

The FEDAM plot of C-15th substituted coumestrol is shown in **Fig. 3.3b.** Each number in the plot corresponds to a particular derivative (the assignments of derivatives based on these numbers can found in **Table 3.12**. According to FEDAM plots, all the coumestrol derivatives were good radical scavengers. The derivatives substituted by electron donating groups such as -OCH3, -Ph, and –OCOR like showed the best radical scavenging capacity among the studied derivatives. Derivatives substituted with electron withdrawing groups, exhibited good electron accepting properties while electron donating groups showed good electron donating property. For example, 15-F C, 15-Cl C, 15-CN C, 15-NO$_2$C, , 15-CHO C, 15-COR C, 15-COCl C, 15-COOR C, 15-COOH C, 15-OH C, and 15-NHCOR C (where 'R' is a methyl group) were good electron acceptors in region one and 15-NH$_2$ C and 15-CH$_3$ C in region 3. FEDAM plots of all other derivatives are shown in **Figs. 3.4a, 3.4b and 3.4c**.

Table 3.12 Numbers and corresponding functional groups used in DAM and FEDAM plots

Label	Functional Group	
1	-F	
2	-Cl	
3	-CN	
4	-NO$_2$	
5	-CHO	
6	-COR	
7	-COCl	
8	-COOR	
9	-COOH	**R= -CH$_3$**
10	-OH	
11	-NH$_2$	
12	-OCH$_3$	
13	-CH$_3$	
14	-Ph	
15	-OCOR	
16	-NHCOR	
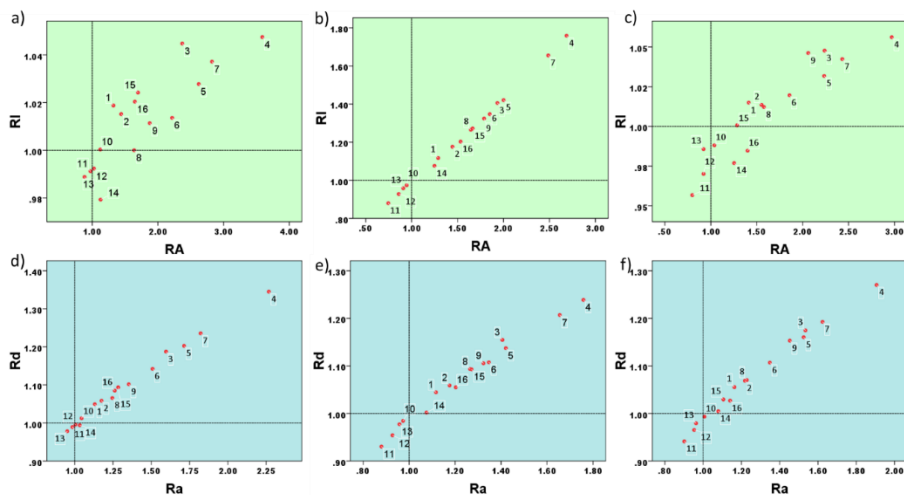
Fig. 3.4. a), b) and **c)** FEDAM plot of C-16 substituted coumestrol derivatives, and C-17 substituted coumestrol derivatives, and C-19 substituted coumestrol derivatives respectively. **c), e)** and **f)** DAM plot of C-16 substituted coumestrol derivatives, C-17substituted coumestrol derivatives, and C-19 substituted coumestrol derivatives respectively

FEDAM plot already helped to classify the derivates as electron donors or acceptors. When characterizing the charge transfer of antiradicals, electron donating ($\omega-$) and electro-accepting (ω^+) capacity provides further insights into the anti-oxidant or anti-reductant capacity of a molecule[35]. The molecule can serve as an antioxidant (an electron donor) or an anti-reductant depending on the direction of charge transfer (acceptor of an electron). The donator acceptor map (DAM) is analyzed to compare the anti-oxidant and anti-reductant capabilities of the derivatives with the parent coumestrol molecule[36]. A plot of Rd vs Ra (DAM) is divided into four sections (**Fig. 3.3c**): (1) the best antiradical zone, where ligand (L) is a good electron donor (Rd small) and a good electron acceptor (Ra large); (2) the worst antiradical zone, where L is a bad electron donor (Rd large) and a bad electron acceptor (Ra small); (3) the good anti-reductant sector (Ra and

217

Rd large), where L is a good electron acceptor and thus a good antiradical; and (4) the good antioxidant region (Ra and Rd small) where L is a good electron donor and hence also a good antiradical(separating lines are symbolic to help imagine). In short, three out of four zones in DAM plot point towards molecules with good anti-radical activity[37].

Fig. 3.3d shows the DAM plot of the derivatives obtained in gas phase, by substitution of the 15th position of coumestrol molecule. The results indicate that most of the derivatives (irrespective of the nature of substitution, i.e., whether electron withdrawing or electron donating) exhibited good anti-radical potential as they are mainly concentrated in 1st, 3rd and 4th zones of DAM plot. A low value of ω^{-} indicates a higher tendency to donate an electron, while a high value of ω^{+} indicates a higher susceptibility to accept an electron. For example, due to the low ionization potential (I) and low electron donating power (ω-), 15-NH$_2$ C showed better anti-oxidant character, whereas 15-NO$_2$ C with high electron affinity (A) and high electron accepting power (ω^{+}), showed better anti-reductant character. Analysis of the calculated electron donating (Rd) and accepting (Ra) indexes (with respect to coumestrol) indicated that, all the derivatives, except 15-NH$_2$ C, and15-CH$_3$ C exhibited better electron accepting efficiency than coumestrol. On the other hand, 15-NH$_2$ C, 15-OCH$_3$ C, 15-CH$_3$ C, and 15-Ph C, exhibited better electron donating capability than coumestrol. However, 15-NH$_2$ C and 15-NO$_2$ C gave the most impressive results compared to all other derivatives and can be considered as the best anti-radical scavengers. DAM plots of all other derivatives obtained

by substitution at other positions of coumestrol are shown in **Figs. 3.4d, 3.4e, 3.4f**. The parameters used to obtain both FEDAM and DAM plots of coumestrol and all its derivatives are provided in **Tables 3.13-3.16**.

Table 3.13 Ionisation potential (I), Electron affinity (A), Electron donation and acceptance (ω- and ω+)powers, Indexes (Rd and Ra), Relative I and A obtained for coumestrol and its derivatives substituted at C-15th position

Molecule	I	A	ω-	ω+	Rd	Ra	RI	RA
Coumestrol	7.3311	0.4221	4.5452	0.6686	1.0000	1.0000	1.0000	1.0000
15-F C	7.4814	0.5350	4.7510	0.7428	1.0453	1.1110	1.0205	1.2674
15-Cl C	7.4558	0.5799	4.7864	0.7686	1.0531	1.1495	1.0170	1.3737
15-CN C	7.6973	0.9410	5.3430	1.0238	1.1755	1.5313	1.0499	2.2294
15-NO$_2$ C	7.7380	1.5498	6.1937	1.5498	1.3627	2.3180	1.0555	3.6717
15-CHO C	7.5668	1.0888	5.4601	1.1323	1.2013	1.6935	1.0322	2.5796
15-COR C	7.4587	0.9611	5.2387	1.0288	1.1526	1.5388	1.0174	2.2771
15-COCl C	7.6323	1.2592	5.7224	1.2767	1.2590	1.9094	1.0411	2.9831
15-COOR C	7.3715	0.7635	4.9505	0.8829	1.0892	1.3205	1.0055	1.8088
15-COOH C	7.4595	0.8511	5.1035	0.9482	1.1228	1.4181	1.0175	2.0163
15- OH C	7.5079	0.9399	5.2389	1.0150	1.1526	1.5180	1.0241	2.2267
15- NH$_2$ C	7.0677	0.3277	4.2987	0.6010	0.9458	0.8989	0.9641	0.7762
15- OCH$_3$ C	7.2513	0.4517	4.5323	0.6808	0.9972	1.0182	0.9891	1.0700
15-CH$_3$ C	7.2211	0.3721	4.4309	0.6343	0.9749	0.9487	0.9850	0.8815
15-Ph C	7.1617	0.5017	4.5366	0.7049	0.9981	1.0542	0.9769	1.1885
15-OCOR C	7.3237	0.4753	4.5982	0.6987	1.0117	1.0449	0.9990	1.1260
15-NHCOR C	7.4954	0.6631	4.9022	0.8229	1.0785	1.2308	1.0224	1.5710

Table 3.14 Ionisation potential (I), Electron affinity (A), Electron donation and acceptance (ω- and ω+) powers, Indexes (Rd and Ra), Relative I and A obtained for derivatives substituted at C-16th position of Coumestrol

Molecule	I	A	ω-	ω+	Rd	Ra	RI	RA
16-F C	7.4689	0.5578	4.7692	0.7558	1.0493	1.1305	1.0188	1.3214
16-Cl C	7.4425	0.6080	4.8105	0.7853	1.0584	1.1744	1.0152	1.4404
16-CN C	7.6594	1.0007	5.3969	1.0669	1.1874	1.5956	1.0448	2.3707
16-NO$_2$ C	7.6796	1.5158	6.1136	1.5159	1.3451	2.2672	1.0475	3.5911
16-CHO C	7.5348	1.1064	5.4660	1.1454	1.2026	1.7131	1.0278	2.6212
16-COR C	7.4306	0.9353	5.1913	1.0083	1.1422	1.5080	1.0136	2.2159
16-COCl C	7.6040	1.1919	5.6163	1.2183	1.2356	1.8221	1.0372	2.8238
16-COOR C	7.3310	0.6910	4.8434	0.8324	1.0656	1.2450	1.0000	1.6371
16-COOH C	7.4149	0.7913	5.0073	0.9042	1.1017	1.3523	1.0114	1.8748
16- OH C	7.3332	0.4735	4.6015	0.6982	1.0124	1.0442	1.0003	1.1218
16-NH$_2$ C	7.2667	0.4105	4.4969	0.6583	0.9894	0.9846	0.9912	0.9724
16- OCH$_3$ C	7.2750	0.4329	4.5254	0.6715	0.9956	1.0043	0.9923	1.0256
16-CH$_3$ C	7.2491	0.3721	4.4466	0.6360	0.9783	0.9512	0.9888	0.8816
16-Ph C	7.1791	0.4754	4.5176	0.6904	0.9939	1.0325	0.9793	1.1262
16-OCOR C	7.5087	0.7162	4.9706	0.8581	1.0936	1.2834	1.0242	1.6966
16-NHCOR C	7.4808	0.6957	4.9315	0.8432	1.0850	1.2611	1.0204	1.6481

Table 3.15 Ionisation potential (I), Electron affinity (A), Electron donation and acceptance (ω- and ω+) powers, Indexes (Rd and Ra), Relative I and A obtained for derivatives substituted at C-17th position of Coumestrol

MOLECULE	I	A	ω-	ω+	Rd	Ra	RI	RA
17-F C	7.4566	0.5438	4.7469	0.7467	1.0444	1.1168	1.1168	1.2883
17-Cl C	7.4444	0.6094	4.8131	0.7862	1.0589	1.1759	1.1759	1.4438
17-CN C	7.7996	0.8160	5.2477	0.9398	1.1546	1.4056	1.4056	1.9333
17-NO$_2$ C	7.7759	1.1339	5.6306	1.1757	1.2388	1.7584	1.7584	2.6864
17-CHO C	7.5931	0.8447	5.1687	0.9498	1.1372	1.4206	1.4206	2.0011
17-COR C	7.4850	0.7812	5.0337	0.9006	1.1075	1.3470	1.3470	1.8508
17-COCl C	7.7101	1.0498	5.4866	1.1067	1.20710	1.6551	1.6551	2.4872
17-COOR C	7.5521	0.6939	4.9688	0.8458	1.0932	1.2650	1.2650	1.6439
17-COOH C	7.5227	0.7553	5.0239	0.8849	1.1053	1.3235	1.3235	1.7894
17- OH C	7.2470	0.3995	4.4743	0.6510	0.9844	0.9737	0.9737	0.9465
17-NH$_2$ C	6.9655	0.3150	4.2283	0.5881	0.9303	0.8795	0.8795	0.7462
17- OCH$_3$ C	7.0693	0.3630	4.3365	0.6203	0.9541	0.9277	0.9277	0.8600
17-CH$_3$ C	7.2189	0.3837	4.4419	0.6406	0.9773	0.9580	0.9580	0.9089
17-Ph C	7.1430	0.5270	4.5540	0.7190	1.0019	1.0754	1.0754	1.2486
17-OCOR C	7.5300	0.7025	4.9665	0.8503	1.0927	1.2716	1.2716	1.6643
17-NHCOR C	7.3339	0.6471	4.7946	0.8041	1.0549	1.2026	1.2026	1.5331

Table 3.16 Ionisation potential (I), Electron affinity (A), Electron donation and acceptance (ω- and ω+) powers, Indexes (Rd and Ra), Relative I and A obtained for derivatives substituted at C-19th position of Coumestrol

Molecule	I	A	ω-	ω+	Rd	Ra	RI	RA
19-F C	7.4410	0.5962	4.7964	0.7778	1.0553	1.1633	1.0150	1.4125
19-Cl C	7.4306	0.6554	4.8575	0.8145	1.0687	1.2182	1.0136	1.5526
19-CN C	7.6805	0.9450	5.3388	1.0260	1.1746	1.5345	1.0477	2.2387
19-NO$_2$ C	7.7433	1.2538	5.7733	1.2747	1.2702	1.9065	1.0562	2.9703
19-CHO C	7.5639	0.9432	5.2733	1.0197	1.1602	1.5251	1.0318	2.2345
19-COR C	7.4749	0.7835	5.0309	0.9017	1.1069	1.3486	1.0196	1.8563
19-COCl C	7.6423	1.0263	5.4201	1.0858	1.1925	1.6240	1.0424	2.4314
19-COOR C	7.4203	0.6664	4.8644	0.8210	1.0702	1.2280	1.0122	1.5787
19-COOH C	7.6697	0.8701	5.2412	0.9713	1.1531	1.4527	1.0462	2.0613
19- OH C	7.2437	0.4386	4.5140	0.6729	0.9931	1.0064	0.9881	1.0391
19-NH$_2$ C	7.0137	0.3368	4.2779	0.6027	0.9412	0.9014	0.9567	0.7979
19- OCH$_3$ C	7.1118	0.3887	4.3872	0.6370	0.9652	0.9527	0.9701	0.9208
19-CH$_3$ C	7.2264	0.3886	4.4512	0.6437	0.9793	0.9628	0.9857	0.9206
19-Ph C	7.1617	0.5291	4.5667	0.7213	1.0047	1.0788	0.9769	1.2535
19-OCOR C	7.3362	0.5427	4.6788	0.7393	1.0294	1.1057	1.0007	1.2858
19-NHCOR C	7.2190	0.5911	4.6676	0.7625	1.0269	1.1405	0.9847	1.4005

3.6 Anti-oxidant activity
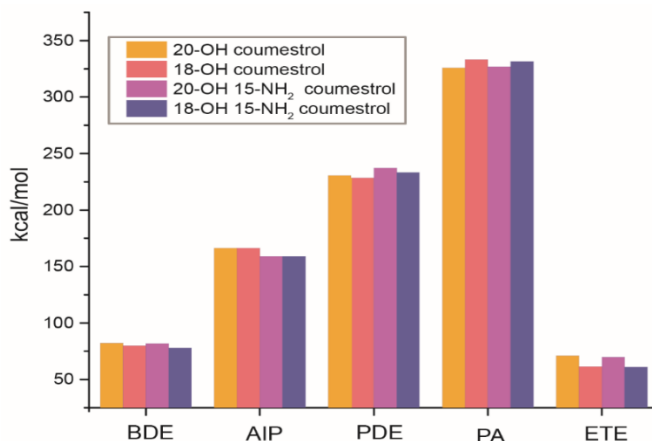
Fig. 3.5. Numerical parameters corresponding to all the possible antioxidant mechanism of coumestrol and 15-NH$_2$ C in gas phase

The anti-oxidant properties of coumestrol are due to the presence of two -OH groups in its structure. DAM plot showed that 15-NH_2 C can act as good anti-oxidant. The antioxidant pathways have been evaluated for radical scavenging activity of both coumestrol and 15-NH_2 C, then the most appropriate mechanism has been chosen. The kind of bond cleavage can be easily deduced from the examination of the antioxidant capacity mechanism. we have calculated all of the relevant parameters associated with the three antioxidant mechanisms of coumestrol and 15-NH_2 C, which are shown in **Fig. 3.5**.

BDEs, IPs, and PAs influence the mechanisms of HAT, SET-PT, and SPLET, respectively, and BDEs, IPs, and PAs can thus designate the thermodynamically preferable reaction pathway involved in the free radical scavenging strategy. Only when all the parameters connected with a mechanism are smallest then it is said to be suitable for a chemical. In this case, the HAT mechanism is linked to hydrogen atom transfer, whereas others are linked to electron transport. The initial step of SPLET involves a proton loss. According to the results, the measured IPs and PAs of coumestrol and its derivative in the gas phase are significantly higher than BDEs, making HAT the most attractive approach in the gas phase from a thermodynamic standpoint. BDE is a numerical parameter that describes hydroxyl group stability and is linked to the HAT process. The lower the BDE number, the less stable the O-H bond is, and the more antioxidant capability there is. Both coumestrol and 15-NH_2 C preferentially undergo homolytic fission of the -OH bond in the gaseous phase, forming stable radicals that neutralise reactive free radicals in the biological system.

Coumestrol has two hydroxyl groups that can transfer hydrogen to a free radical in biological systems. Among the two hydroxyl group the one attached to 18th carbon atom showes low BDE (79.89kcal/mol) hence high anti-oxidant capability than the hydroxyl group attached to 20th carbon (80.09kcal/mol) . According to the table, 15-NH$_2$ C processed a lower BDE value than its parent molecule, coumestrol. The OH group connected to the 18th carbon atom in 15-NH$_2$ coumestrol had a low BDE value (77.98kcal/mol), indicating that the same position generates the most stable radical. More specifically we can say that the derivative shows more anti-oxidant activity than coumestrol. Bond dissociation enthalpy values of phenolic groups of coumestrol calculated under B3LYP/6-31+G(2d,2p) and M06/6-31+G(2d,2p) and B3LYP-D3/6-31+G(2d,2p) are given in **Table 3.17**.

Table 3.17 Bond dissociation enthalpy values of phenolic groups of coumestrol calculated under B3LYP/6-31+G(2d,2p) and M06/6-31+G(2d,2p) and B3LYP-D3/6-31+G(2d,2p)

Phenolic group of coumestrol	BDE (kcal/mol)		
	B3LYP	M06	B3LYP-D3
20-OH	82.09	83.70	82.35
18-OH	79.89	81.37	80.14

3.7 Anticancer activity

To the best of our knowledge, no theoretical investigations have been conducted on the behaviour of protein-ligand adducts of cancer-causing kinases with coumestrol and its derivatives substituted by electron withdrawing and donating groups. AutoDock Vina was

used to analyse the models describing the docking molecules of all the compounds under study into the complex structure of proteins, including BRAF, Aurora A, VEGFR2, JAK3, MEK-1, MCL-1, LCK, and MMP3, and the results are shown in **Tables 3.18-3.21**.

Table 3.18 Docking score of coumestrol derivatives substituted at C-15th position with kinase proteins

MOLECULE	BRAF	Aurora A	VEGFR2	JAK3	MEK1	MCL-1	LCK	MMP3
15-F C	-9.3	-9.7	-9.9	-9.7	-9.3	-4.9	-9.8	-8.6
15-Cl C	-9.1	-9.6	-9.2	-9.9	-9.0	-4.9	-9.8	-8.1
15-CN C	-9.2	-10.0	-9.4	-10.1	-9.6	-5.1	-10.1	-7.9
15-NO$_2$ C	-9.1	-9.7	-9.2	-9.7	-9.3	-4.9	-9.9	-7.7
15-CHO C	-8.9	-9.5	-9.0	-9.9	-9.1	-4.9	-9.8	-8.2
15-COR C	-9.2	-9.9	-9.3	-10.0	-9.3	-5.0	-10.1	-7.8
15-COCl C	-9.2	-9.9	-8.3	-10.0	-9.3	-5.0	-10.1	-7.9
15-COOR C	-9.1	9.6	-8.1	-9.6	-9.2	-4.9	-10.0	-7.8
15-COOH C	-9.1	-9.6	-8.3	-9.8	-9.4	-5.1	-9.8	-7.7
15-OH C	-9.4	-9.3	-8.1	-9.4	-9.0	-4.9	-9.8	-9.0
15-NH$_2$ C	-9	-9.3	-9.2	-9.5	-9.0	-4.9	-9.4	-8.9
15-OCH$_3$ C	-8.6	-9.4	-8.9	-9.4	-9.1	-4.7	-9.5	-7.5
15-CH$_3$ C	-9.3	-9.8	-9.8	-10.2	-9.2	-5.0	-10.0	-7.8
15-Ph C	-10.2	-10.2	-9.8	-10.5	-8.8	-6.0	-11.2	-9.7
15-OCOR C	-9.4	-9.5	-9.0	-9.6	-9.3	-4.8	-9.8	-8.1
15-NHCOR C	-9.9	-9.7	-9.4	-10.3	-9.0	-5.2	-10.1	-8.2

Table 3.19 Docking score of coumestrol derivatives substituted at C-16th position with kinase proteins

Molecule	BRAF	Aurora A	VEGFR2	JAK3	MEK1	MCL-1	LCK	MMP3
16-F C	-9.5	-9.7	-9.6	-9.9	-9.3	-4.8	-9.9	-9.2
16-Cl C	-9.6	-9.5	-9.2	-10.0	-9.0	-4.8	-10.0	-8.9
16-CN C	-9.8	-9.6	-8.7	-10.4	-9.3	-5.0	-10.3	-8.9
16-NO$_2$ C	-9.4	-9.4	-8.0	-10.0	-8.9	-4.8	-9.8	-8.7
16-CHO C	-9.4	-9.5	-9.1	-9.9	-8.8	-4.9	-9.8	-9.0
16-COR C	-9.7	-9.3	-8.0	-9.6	-8.9	-4.8	-9.6	-8.6
16-COCl C	-9.7	-9.3	-8.1	-9.8	-8.9	-4.8	-9.6	-9.1
16-COOR C	-9.4	-9.1	-8.0	-10.1	-8.6	-4.6	-9.9	-8.3
16-COOH C	-9.4	-9.8	-8.7	-9.8	-9.0	-4.7	-10.2	-8.9
16-OH C	-9.1	-9.6	-7.8	-9.5	-9.1	-4.7	-9.8	-10.0
16-NH$_2$ C	-9.1	-9.7	-8.9	-9.5	-9.0	-4.7	-9.5	-8.8
16-OCH$_3$ C	-9.1	-8.9	-8.8	-9.2	-8.7	-4.6	-9.4	-8.6
16-CH$_3$ C	-9.8	-9.7	-9.4	-10.1	-9.2	-4.9	-10.1	-9.3
16-Ph C	-11.1	-10.5	-9.7	-10.2	-8.9	-5.9	-10.0	-9.9
16-OCOR C	-9.3	-9.3	-9.1	-9.6	-7.5	-4.9	-9.6	-8.5
16-NHCOR C	-9.8	-9.4	-8.5	-10.1	-7.3	-5.0	-10.1	-9.0

Table 3.20 Docking score of coumestrol derivatives substituted at C-17th position with kinase proteins

Molecule	BRAF	Aurora A	VEGFR2	JAK3	MEK1	MCL-1	LCK	MMP3
17-F C	-9.3	-9.5	-8.1	-9.5	-9.3	-4.8	-9.9	-8.9
17-Cl C	-9.4	-9.7	-9.6	-9.7	-8.9	-4.8	-10.0	-9.2
17-CN C	-9.7	-9.8	-8.3	-9.8	-9.4	-5.0	-10.2	-9.2
17-NO$_2$ C	-9.3	-9.7	-8.7	-9.9	-9.3	-4.8	-10.1	-9.3
17-CHO C	-9.1	-9.7	-9.4	-9.8	-8.8	-4.7	-9.9	-9.3
17-COR C	-9.0	-9.0	-8.8	-9.4	-6.9	-4.8	-9.4	-9.3
17-COCl C	-9.8	-9.5	-9.0	-9.9	-9.0	-5.0	-10.0	-9.4
17-COOR C	-9.4	-9.5	-9.3	-9.6	-9.0	-4.9	-9.7	-9.3
17-COOH C	-9.5	-9.9	-9.2	-10.2	-9.0	-4.7	-10.1	-9.3
17-OH C	-9	-9.5	-9.1	-9.4	-9.2	-4.7	-9.5	-8.7
17-NH$_2$ C	-9	-9.6	-9.1	-9.5	-9.2	-4.7	-9.5	-8.9
17-OCH$_3$ C	-9.1	-9.1	-8.4	-9.4	-8.1	-4.8	-9.7	-9.0
17-CH$_3$ C	-9.5	-9.9	-9.5	-9.8	-8.6	-4.8	-10.2	-8.9
17-Ph C	-11.1	-10.4	-11.1	-11.1	-8.2	-5.5	-11.1	-9.8
17-OCOR C	-9.4	-9.2	-9.6	-10	-8.7	-4.9	-9.9	-8.5
17-NHCOR C	-10.2	-10	-8.8	-10.1	-8.6	-5.2	-10.1	-9.6

Table 3.21 Docking score of coumestrol derivatives substituted at C-19th position with kinase proteins

Molecule	BRAF	Aurora A	VEGFR2	JAK3	MEK1	MCL-1	LCK	MMP3
19-F C	-9.4	-9.6	-8.2	-9.7	-9.3	-4.9	-9.7	-8.8
19-Cl C	-9.4	-9.6	-9.3	-9.8	-9.3	-5.0	-9.7	-8.8
19-CN C	-9.3	-9.9	-9.5	-10.2	-9.1	-5.1	-10.0	-8.9
19-NO2 C	-8.9	-9.7	-9.2	-9.9	-9.4	-4.9	-10.0	-8.7
19-CHO C	-9.2	-9.4	-9.1	-9.8	-9.1	-4.7	-9.8	-8.7
19-COR C	-9.7	-9.7	-9.4	-10.1	-9.0	-5.1	-10.1	-9.0
19-COCl C	-9.7	-9.7	-8.9	-10.0	-8.9	-5.2	-10.2	-9.2
19-COOR C	-9.4	-9.6	-9.2	-9.8	-9.0	-4.9	-9.9	-8.7
19-COOH C	-9.3	-9.5	-9.5	-9.9	-9.2	-4.9	-10.4	-9.4
19-OH C	-9.1	-9.4	-8.0	-9.6	-9.2	-4.7	-9.5	-9.0
19-NH2 C	-9	-9.5	-9.0	-9.5	-9.2	-4.7	-9.4	-9.0
19-OCH3 C	-9.2	-9.5	-9.1	-9.6	-9.2	-4.8	-9.6	-8.1
19-CH3 C	-9.4	-9.7	-9.7	-10.0	-9.3	-4.9	-9.9	-8.7
19-Ph C	-10.3	-10.3	-10.2	-11.0	-8.8	-6.0	-11.1	-10.3
19-OCOR C	-9.6	-9.7	-9.2	-9.8	-9.2	-4.9	-9.9	-8.5
19-NHCOR C	-9.9	-10.0	-9.4	-10.6	-9.6	-5.4	-9.8	-9.7

Fig. 3.6 shows the binding energy as well as the interaction of coumestrol and its derivatives that show highest binding affinity with the targets under study. Molecular docking was successful for coumestrol and most of its derivatives, and their binding affinity with all of the receptors was compared to corresponding in-built ligands

identified in each of the targets. in which black square, red circle, blue triangle and green triangle represents, coumestrol, 17-Ph C, 19-PhC, and 15-CN C respectively. The native ligand was retrieved and redocked toward the binding site of each protein for each of the selected protein-ligand complexes, and the corresponding binding energy values are shown in **Table 3.22**.
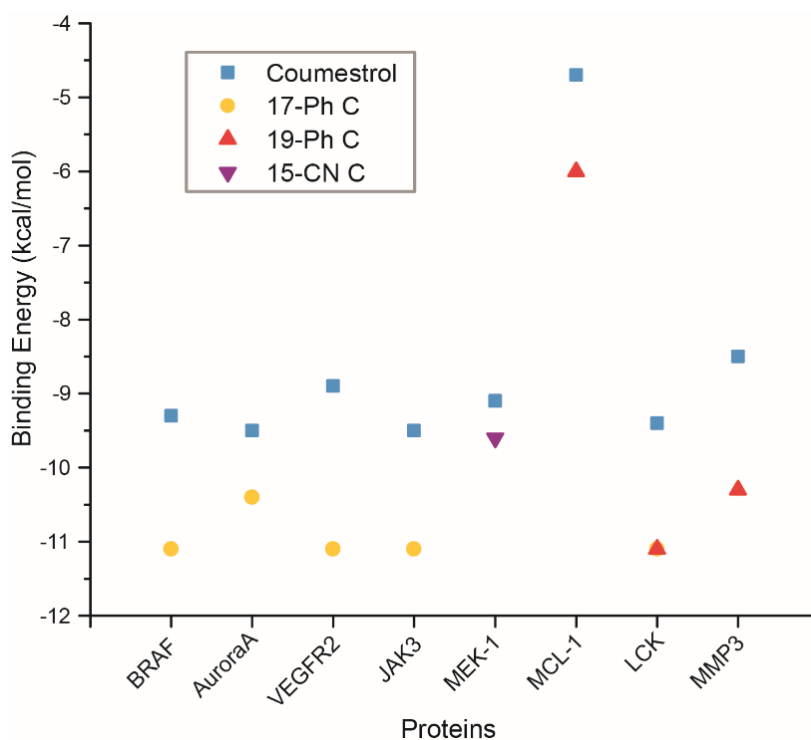
Fig. 3.6. Binding energy value(kcal/mol) of coumestrol and the derivatives which showed high binding affinity with selected protein obtained from molecular docking studies

Table 3.22 Docking scores of native ligands with corresponding kinase proteins

Protein kinases	Native ligand
BRAF	-8.6
Aurora A	-8.7
VEGFR2	-8.6
JAK3	-8.1
MEK1	-7.7
MCL-1	2.4
LCK	8.9
MMP3	-7.0

The binding energy values observed for the inbuilt ligands of the corresponding proteins are -8.6kcal/mol for BRAF, -8.7kcal/mol for Aurora A, -8.6kcal/mol for VEGFR2, -8.1kcal/mol for JAK3, -7.7kcal/mol for MEK-1, -2.4 kcal/mol for MCL-1, -8.9kcal/mol for LCK, -7.0kcal/mol for MMP3, respectively. Interestingly, coumestrol showed an even higher binding affinity value of -9.3, -9.5, -8.9, -9.5, -9.1, -4.7, -9.4 and -8.5kcal/mol with the same proteins (in the same order as in previous sentence). Molecular docking of coumestrol derivatives showed an even stronger docking with all the selected targets. Among the derivatives (as shown in **Fig. 3.6**), coumestrol substituted at 17th position by phenyl group(17-Ph C) showed the highest binding affinity with most of the targets and more surprisingly, those binding energy values (-11.1, -10.4, -11.1, -11.1, and -11.1kcal/mol with BRAF, Aurora A, VEGFR2, JAK3, and LCK, respectively) were much lower than that of coumestrol. 19-Ph C

exhibited a binding energy value of -6.0kcal/mol, -11.1kcal/mol, and -10.3kcal/mol with proteins MCL-1, LCK, and MMP3, respectively and 15-CN C showed a binding energy value -9.6kcal/mol with MEK1. From the results, it was clear that 17-Ph C, 19-Ph C and 15-CN C have lower binding energy values than coumestrol, so that these derivatives can be used as better kinase inhibitors thereby prevent various types of cancers.

Insights into interaction between the selected molecules (coumestrol and derivatives showing highest binding affinity) with the targets, were obtained from interaction analysis diagrams. The interaction diagrams of coumestrol with the different targets is shown in **Fig. 3.7**. The interaction of coumestrol with the BRAF protein demonstrates that the molecule interacted well with the surrounding amino acid residues of this kinase protein, such as ASP594, LEU597, ILE463, PHE583, GLU533, ILE527, THR529, LEU514 and GLN530, *via* van der Waals interaction. At the active site of BRAF, a typical hydrogen bond (H-bond) was identified between coumestrol and the amino acid residue CYS532. Other important interactions observed in the coumestrol-BRAF complex included pi-pi stacked, pi-pi T-shaped, pi-sigma, and pi-alkyl interactions. In the coumestrol-aurora A complex, two forms of hydrogen bonding interactions were observed: conventional H-bond and C-H bonding interactions. The keto and hydroxyl groups near the C-17th and C-15th positions of coumestrol formed conventional H-bonding with amino acid residues ALA213, and LYS162, of aurora A respectively. With amino acid residue TYR212, a C-H bonding interaction was identified. Within the active

site of aurora A, the molecule has van der Waals contacts, Pi-sigma interactions, and pi-alkyl interactions.
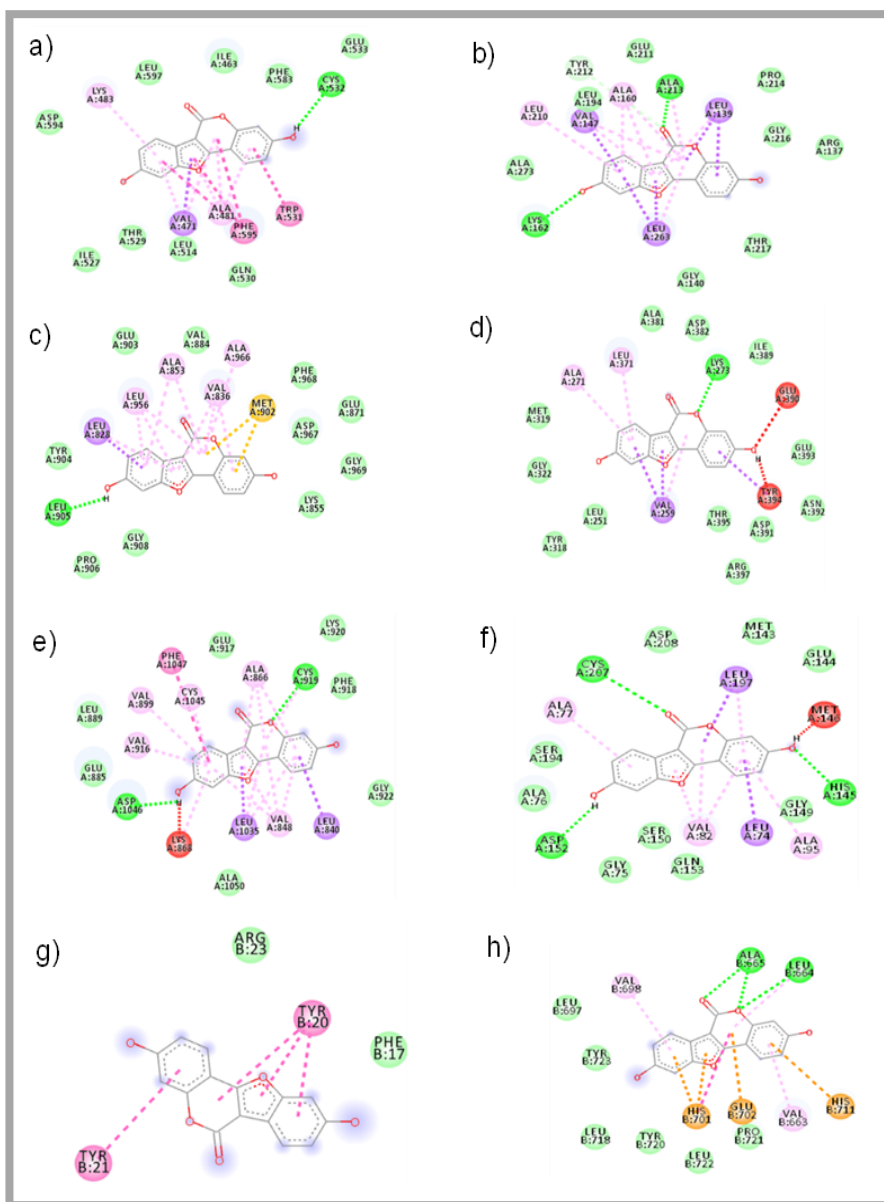
Fig. 3.7. Interaction of coumestrol with (a) BRAF, (b) Aurora A, (c) JAK3, (d) LCK, (e) VEGFR2, (f) MEK-1, (g) MCL-1, (h) MMP3

Coumestrol demonstrated van der Waals interactions with amino acid residues, such as LEU899, GLU885, GLU917, LYS920, PHE918, GLY922, and ALA1050 in the active region of VEGFR2. The hydroxyl group near the C-15t^h and C-17th position of coumestrol showed conventional H- bonding interaction with the protein's ASP1046 residue. The oxygen atom in the lactone ring of coumestrol showed conventional H-bonding with amino acid residue CYC919, and the hydroxyl group near the C-15th and C-17th position showed conventional H-bonding interaction. Coumestrol with PHE1047 in the active site demonstrated a pi-pi T-shaped interaction. Docking studies of the comestrol with JAK3 revealed a significant H-bond interaction between amino acid residues LEU905 and the hydroxyl group near the C-15th and C-17th positions.By van der Waals interaction, the molecule perfectly couples with surrounding aminoacids such as GLU903, VAL884, PHE968, ASP967, GLU871, GLY969, LYS855, GLY908, PRO906, and TYR904. The molecule also demonstrated a pi-sulfur interaction with JAK3 protein residue MET902.

Three H-bonding connections were identified in the coumesrol MEK-1 complex, two of which were between two hydroxyl groups of coumestrol with amino acid residues ASP152 and HIS145, while the other was shown by the keto group present in coumestrol with residue CYS207. These interactions demonstrated that the chemical fits well into MEK1's pocket. The van der Waals force of interaction with ASP208, MET143, GLU144, GLY149, GLN153, SER150, GLY75, ALA76, and SER194 was another important interaction in this complex. The amino acid residues ARG23 and PHE17, which are

found in the active site of the kinase protein MCL-1, demonstrated van der Waals interactions with Coumestrol. Coumestrol's interactions with MCL-1 included pi-pi stacked and pi-pi T shaped interactions. The oxygen atom of the lactone ring in the coumestrol developed a typical H- bonding contact with residue LYS273 when docked with LCK. Between coumestrol and the LCK protein, a pi-pi T-shaped interaction was also discovered.

The significant potential as an anticancer drug of coumestrol is also evident from its high binding affinity with MMP3. van der Waals interactions were observed between MMP3 amino acid residues LEU697, TYR723, LEU718, TYR720, LEU722, and PRO721. With residues HIS701, GLU702, and HIS711 in the active site target protein, coumestrol displayed pi-cation and pi-anion interactions. A pi-pi stacking interaction was also identified. With the residues ALA665 and LEU664, the keto group and oxygen atom of coumestrol's lactone ring displayed normal H-bonding interactions.

Coumestrol derivative, 17-Ph C, showed the highest binding affinity with most of the targets. **Fig. 3.8** depicts the interactions of 17-Ph C with kinase proteins such as BRAF, Aurora A, JAK3, LCK, and VEGFR2. This allows for a systematic comparison of different interactions of this derivative with different proteins. van der Waals, classical hydrogen bonds, stacked pi-pi, pi-pi T, pi-cation, pi-anion, pi-alkyl, pi-sulphur, and pi-sigma interactions are among the key interactions revealed by these stable complexes.
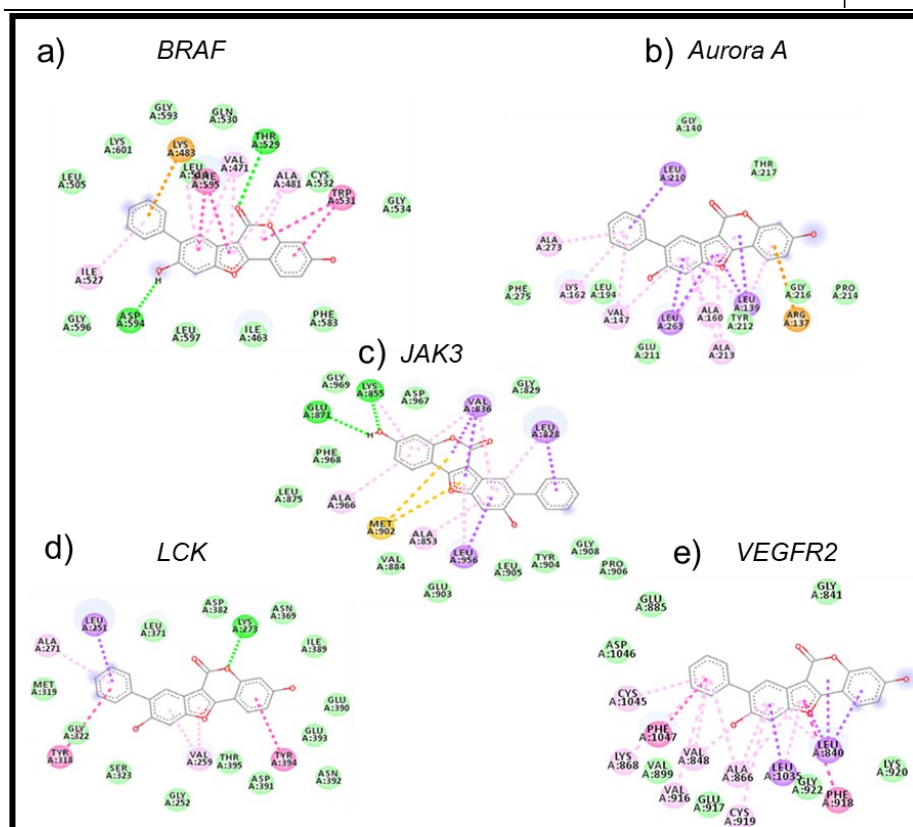
Fig. 3.8. Interaction of 17 Ph with (a) BRAF, (b) Aurora A, (c) JAK3, (d) LCK, (e) VEGFR2

Three conventional H-bonding interactions were observed in the 17-Ph C-BRAF complex, namely the OH group present in 17-Ph C near to the phenyl substitution with residue ASP594, OH in C-15 with ASP594, and the keto group of 17-Ph C with the residue, THR529. 17-Ph C showed, pi-cation interaction with LYS483; pi-pi stacked and pi-pi T shaped interactions with PHE595 and TRP531; and pi-alkyl interaction with amino acid residues such as VAL471, ILE527. It also exhibited van der Waals interactions with the surrounding amino acid residues like, LEU505, LYS593, GLN530, CYS532, GLY534,

GLY596, LEU597, ILE463 and PHE583. The binding site highly suits the active site cavity allowing numerous close contacts between the ligand 17-Ph C and residues like PHE275, LEU194, GLY140, THR217, GLU211, TYR212, GLY216, LEU210, LEU263, LEU139, ALA273, LYS162, VAL147, ALA160, ALA213 and PRO214 of kinase protein aurora A. The derivative 17 Ph C showed van der Waals interaction with amino acid residues PHE275, LEU194, GLY140, THR217, GLU211, TYR212, GLY216 and PRO214 of kinase protein aurora A. 17 Ph C also showed a pi-cation interaction with the amino acid residue ARG137, pi-sigma interaction with LEU210, LEU263 and LEU139 and pi-alkyl interaction with ALA273, LYS162, VAL147, ALA160 and ALA213.

The derivative 17 Ph C was found to be packed deeply inside the pocket by van der Waals interaction with amino acid residues, GLY969, ASP967, GLY829, LEU875, PHE968, VAL884, GLU903, LEU905, TYR904, GLY908, and PRO906 present in protein kinase, JAK3. Comparing with other ligand-protein complex, 17 Ph C showed pi-sulphur interaction with the amino acid residue MET902.The hydroxyl group present in 17 Ph C near to the C-16 & C-19 positions showed conventional H- bond with residues GLU871 and LYS855. Pi-sigma and pi-alkyl interactions were the other major interactions showed by 17 Ph C within the active site of the JAK3. 17 Ph C interacted with the amino acid residues VAL836, LEU828 and LEU956 and pi-alkyl interaction with residues ALA966 and ALA853 through pi-sigma interaction. The analysis of interaction of 17 Ph C with LCK, exhibited van der Waals interaction with residues, LEU371,

ASP382, ASN369, ILE389, GLU390, GLU393, ASN392, ASP391, THR395, GLY252, SER323, GLY322, and MET319. The oxygen atom present in the lactone ring structure near to the C-16 position of 17 Ph C showed conventional hydrogen bonding interaction with the residue LYS273. Few other interactions observed in 17 Ph C-LCK include, pi-pi stacked and pi-pi T Shaped interactions with TYR394 and TYR318; pi-sigma with LEU271; and pi-alkyl with VAL259 and ALA27. The derivative 17 Ph C interacted with the with the amino acid residues, GLU885, GLY841, ASP1046, VAL899, GLU917, GLY922 and LYS920 present in th protein kinase, VEGFR2 by van der Waals interaction. Pi-sigma, pi-pi stacked, and pi-alkyl were the other interactions showed by 17 Ph C with VEGFR2. 17 Ph C also offered pi-sigma interaction with LEU1035 and LEU840; pi-pi stacked interaction with PHE1047 and PHE918; pi-alkyl interaction with CYS1045, LYS868, VAL916, CYS919, VAL848 and ALA866 present in VEGFR2. In short, docking studies of coumestrol derivatives with selected proteins revealed that many of the derivatives were powerful inhibitors of cancer causing kinases than the parent molecule, coumestrol and are well connected to the amino acid residues present in the active site.

3.8 Toxicity prediction

The molecular characteristics for toxicity analysis of coumestrol and its derivatives were determined and displayed in **Tables 3.23-3.26** in supplementary materials. Ligands with logP below 5, molecular weight below 500g/mol, less than 5 numbers of hydrogen bond donors, less than 10 numbers of hydrogen bond acceptors,

positive drug similarity value and overall drug score represent traded qualities less harmful drug. Evidently, these compounds met Lipinski 's rule of five and ADME characteristics.

Table 3.23 ADME analysis of coumestrol and its derivatives substituted at C-15th position

Molecule	Molecular weight	No: of hydrogen donors	No: of hydrogen acceptors	log p	No: of violation
Coumestrol	268.22	2	5	2.46	0
15-F C	286.21	2	6	2.75	0
15-Cl C	302.67	2	5	2.97	0
15-CN C	293.23	2	6	2.33	0
15-NO$_2$ C	313.22	2	7	1.8	0
15-CHO C	296.23	2	6	2.22	0
15-COR C	310.26	2	6	2.59	0
15-COCl C	330.68	2	6	2.8	0
15-COOR C	326.26	2	7	2.5	0
15-COOH C	312.23	3	7	2.12	0
15-OH C	284.22	3	6	2.03	0
15-NH$_2$ C	283.24	3	5	1.88	0
15-OCH$_3$ C	298.25	2	6	2.44	0
15-CH$_3$ C	282.25	2	5	2.76	0
15-Ph C	344.32	2	5	3.79	0
15-OCOR C	326.26	2	7	2.38	0
15-NHCOR C	325.27	3	6	2.01	0

Table 3.24 ADME analysis of coumestrol derivatives substituted at C-16th position

Molecule	Molecular weight	No: of hydrogen donors	No: of hydrogen acceptors	log p	No: of violation
16-F C	286.21	2	6	2.74	0
16-Cl C	302.67	2	5	2.97	0
16-CN C	293.23	2	6	2.37	0
16-NO$_2$ C	313.22	2	7	1.81	0
16-CHO C	296.23	2	6	2.25	0
16-COR C	310.26	2	6	2.55	0
16-COCl C	330.68	2	6	2.89	0
16-COOR C	326.26	2	7	2.55	0
16-COOH C	312.23	3	7	2.1	0
16-OH C	284.22	3	6	2.04	0
16-NH$_2$ C	283.24	3	5	1.94	0
16-OCH$_3$ C	298.25	2	6	2.49	0
16-CH$_3$ C	282.25	2	5	2.83	0
16-Ph C	344.32	2	5	3.8	0
16-OCOR C	326.26	2	7	2.45	0
16-NHCOR C	325.27	3	6	2.05	0

Table 3.25 ADME analysis of coumestrol derivatives substituted at C-17th position

Molecule	Molecular weight	No: of hydrogen donors	No: of hydrogen acceptors	log p	No: of violation
17-F C	286.21	2	6	2.75	0
17-Cl C	302.67	2	5	2.96	0
17-CN C	293.23	2	6	2.32	0
17-NO$_2$ C	313.22	2	7	1.77	0
17-CHO C	296.23	2	6	2.21	0
17-COR C	310.26	2	6	2.6	0
17-COCl C	330.68	2	6	2.81	0
17-COOR C	326.26	2	7	2.56	0
17-COOH C	312.23	3	7	1.97	0
17-OH C	284.22	3	6	2.04	0
17-NH$_2$ C	283.24	3	5	1.86	0
17-OCH$_3$ C	298.25	2	6	2.46	0
17-CH$_3$ C	282.25	2	5	2.77	0
17-Ph C	344.32	2	5	3.8	0
17-OCOR C	326.26	2	7	2.36	0
17-NHCOR C	325.27	3	6	2.03	0

Table 3.26 ADME analysis of coumestrol derivatives substituted at C-19th position

Molecule	Molecular weight	No: of hydrogen donors	No: of hydrogen acceptors	log p	No: of violation
19-F C	268.21	2	6	2.79	0
19-Cl C	302.67	2	5	3.02	0
19-CN C	293.23	2	6	2.37	0
19-NO$_2$ C	313.22	2	7	1.64	0
19-CHO C	296.23	2	6	2.27	0
19-COR C	310.26	2	6	2.63	0
19-COCl C	330.68	2	6	2.77	0
19-COOR C	326.26	2	7	2.6	0
19-COOH C	312.23	3	7	2.19	0
19-OH C	284.22	3	6	2.04	0
19-NH$_2$ C	283.24	3	5	1.91	0
19-OCH$_3$ C	298.25	2	6	2.52	0
19-CH$_3$ C	282.25	2	5	2.82	0
19-Ph C	344.32	2	5	3.78	0
19-OCOR C	326.26	2	7	2.4	0
19-NHCOR C	325.27	3	6	2.08	0

Conclusion

The present study was undertaken to enumerate the reactivity and the dynamic range of bioactivity of coumestrol and its derivatives. Global descriptive parameters calculated for coumestrol and its derivatives, revealed that many of the derivates possess higher reactivity than the parent coumestrol molecule.. DAM plot of coumestrol substituted at C-15th position in gas phase showed that 15-NH$_2$ C showed better anti-oxidant character, while 15-NO$_2$ C exhibited

better anti-reductant character. The anti-oxidant activity as well as the mechanism of coumestrol was compared with its derivative, 15-NH_2 C using DFT analysis. According to FEDAM plots, all the coumestrol derivatives were good radical scavengers. The derivatives, 15th position substituted by -OCH3, -Ph, -CHCR2 and -OCOR groups showed best radical scavenging capacity among others. Molecular docking analysis revealed that most of the molecules under study are good inhibitors for cancer causing kinases.The binding affinity values of coumestrol with selected targets were even higher than that of corresponding inbuilt ligands which clearly indicates its high inhibition potential. Among the derivatives,17-Ph C processed the highest binding affinity value of -11.1, -10.4, -11.1, -11.1, and -11.1kcal/mol with BRAF, Aurora A, VEGFR2, JAK3, and, LCK respectively, which were much higher than that of coumestrol. The high binding affinity value of 19-Ph C with MCL-1, LCK, and, MMP3 indicated that it can act as a potent anticancer drug. Therefore these results include support of truffle health benefits that could be used in the pharmaceutical industries.

References

1.   Provenza FD, Villalba JJ: **The role of natural plant products in modulating the immune system: an adaptable approach for combating disease in grazing animals**. *Small Rumin Res* 2010, **89**(2-3):131-139.

2.   Abuajah CI, Ogbonna AC, Osuji CM: **Functional components and medicinal properties of food: a review**. *J Food Sci Technol* 2015, **52**(5):2522-2529.

3.   Coman V, Teleky B-E, Mitrea L, Martău GA, Szabo K, Călinoiu L-F, Vodnar DC: **Bioactive potential of fruit and vegetable wastes**. In: *Adv Food Nutr Res*. vol. 91: Elsevier; 2020: 157-225.

4.   Dey G, Sireswar S: **Emerging functional beverages: fruit wines and transgenic wines**. In: *Alcoholic beverages.* Elsevier; 2019: 471-514.

5.   Mondal S, Rahaman S: **Flavonoids: A vital resource in healthcare and medicine**. *Pharm Pharmacol Int J* 2020, **8**:91-104.

6.   Dillard CJ, German JB: **Phytochemicals: nutraceuticals and human health**. *J Sci Food Agric* 2000, **80**(12):1744-1756.

7.   Bakar MFA, Mohamed M, Rahmat A, Fry J: **Phytochemicals and antioxidant activity of different parts of bambangan (Mangifera pajang) and tarap (Artocarpus odoratissimus)**. *Food Chem* 2009, **113**(2):479-483.

8.   Dutt R, Garg V, Khatri N, Madan AK: **Phytochemicals in anticancer drug development**. *Anti-Cancer Agents in Medicinal Chemistry (Formerly Current Medicinal Chemistry-Anti-Cancer Agents)* 2019, **19**(2):172-183.

9.   Lako J, Trenerry VC, Wahlqvist M, Wattanapenpaiboon N, Sotheeswaran S, Premier R: **Phytochemical flavonols, carotenoids and the antioxidant properties of a wide selection of Fijian fruit, vegetables and other readily available foods**. *Food Chem* 2007, **101**(4):1727-1741.

10. Øverby A, Zhao C-M, Chen D: **Plant phytochemicals: potential anticancer agents against gastric cancer**. *Curr Opin Pharmacol* 2014, **19**:6-10.

11. Siro I, Kápolna E, Kápolna B, Lugasi A: **Functional food. Product development, marketing and consumer acceptance—A review**. *Appetite* 2008, **51**(3):456-467.

12. Kurzer MS, Xu X: **Dietary phytoestrogens**. *Annu Rev Nutr* 1997, **17**(1):353-381.

13. Price K, Fenwick G: **Naturally occurring oestrogens in foods—a review**. *Food Addit Contam* 1985, **2**(2):73-106.

14. Castro CC, Pagnussat AS, Moura N, da Cunha MJ, Machado FR, Wyse AT, Netto CA: **Coumestrol treatment prevents Na+, K+-ATPase inhibition and affords histological neuroprotection to male rats receiving cerebral global ischemia**. *Neurol Res* 2014, **36**(3):198-206.

15. You J-S, Cho I-A, Kang K-R, Oh J-S, Yu S-J, Lee G-J, Seo Y-S, Kim S-G, Kim CS, Kim DK: **Coumestrol counteracts interleukin-1β-induced catabolic effects by suppressing inflammation in primary rat chondrocytes**. *Inflammation* 2017, **40**(1):79-91.

16. Zafar A, Singh S, Satija YK, Saluja D, Naseem I: **Deciphering the molecular mechanism underlying anticancer activity of coumestrol in triple-negative breast cancer cells**. *Toxicol In Vitro* 2018, **46**:19-28.

17. Bickoff E, Booth A, Lyman R, Livingston A, Thompson C, Deeds F: **Coumestrol, a new estrogen isolated from forage crops**. *Science (Washington)* 1957, **126**:969-970.

18. Montero G, Arriagada F, Günther G, Bollo S, Mura F, Berríos E, Morales J: **Phytoestrogen coumestrol: Antioxidant capacity and its loading in albumin nanoparticles**. *Int J Pharm* 2019, **562**:86-95.

19. Jacob DA, Temple JL, Patisaul HB, Young LJ, Rissman EF: **Coumestrol antagonizes neuroendocrine actions of estrogen via the estrogen receptor α**. *Exp Biol Med* 2001, **226**(4):301-306.

20. Diel P, Olff S, Schmidt S, Michna H: **Effects of the environmental estrogens bisphenol A, o, p′-DDT, p-tert-octylphenol and coumestrol on apoptosis induction, cell proliferation and the expression of estrogen sensitive molecular parameters in the human breast cancer cell line MCF-7**. *The Journal of Steroid Biochemistry and Molecular Biology* 2002, **80**(1):61-70.

21.   Cho S-Y, Cho S, Park E, Kim B, Sohn EJ, Oh B, Lee E-O, Lee H-J, Kim S-H: **Coumestrol suppresses hypoxia inducible factor 1α by inhibiting ROS mediated sphingosine kinase 1 in hypoxic PC-3 prostate cancer cells**. *Bioorg Med Chem Lett* 2014, **24**(11):2560-2564.

22.   Lim W, Jeong M, Bazer FW, Song G: **Coumestrol inhibits proliferation and migration of prostate cancer cells by regulating AKT, ERK1/2, and JNK MAPK cell signaling cascades**. *J Cell Physiol* 2017, **232**(4):862-871.

23.   Reger MK, Zollinger TW, Liu Z, Jones JF, Zhang J: **Dietary intake of isoflavones and coumestrol and the risk of prostate cancer in the Prostate, Lung, Colorectal and Ovarian Cancer Screening Trial**. *Int J Cancer* 2018, **142**(4):719-728.

24.   Patisaul HB, Whitten PL, Young LJ: **Regulation of estrogen receptor beta mRNA in the brain: opposite effects of 17β-estradiol and the phytoestrogen, coumestrol**. *Mol Brain Res* 1999, **67**(1):165-171.

25.   Clementi E, André J-M, McCammon JA: **Theory and Applications in Computational Chemistry: The First Decade of the Second Millennium**: American Institute of Physics; 2012.

26.   Lewars E: **Computational chemistry**. *Introduction to the theory and applications of molecular and quantum mechanics* 2003:318.

27.   Lee Y-H, Yuk HJ, Park K-H, Bae Y-S: **Coumestrol induces senescence through protein kinase CKII inhibition-mediated reactive oxygen species production in human breast cancer and colon cancer cells**. *Food Chem* 2013, **141**(1):381-388.

28.   Sadasivam K, Kumaresan R: **Antioxidant behavior of mearnsetin and myricetin flavonoid compounds—a DFT study**. *Spectrochimica Acta Part A: Molecular and Biomolecular Spectroscopy* 2011, **79**(1):282-293.

29.   Iczkowski RP, Margrave JL: **Electronegativity**. *Journal of the American Chemical Society* 1961, **83**(17):3547-3551.

30.   Abdulazeez I, Khaled M, Al-Saadi AA: **Impact of electron-withdrawing and electron-donating substituents on the corrosion inhibitive properties of benzimidazole derivatives: a quantum chemical study**. *J Mol Struct* 2019, **1196**:348-355.

31.   Pearson RG: **The principle of maximum hardness**. *Acc Chem Res* 1993, **26**(5):250-255.

32.   Ayers PW: **The physical basis of the hard/soft acid/base principle**. *Faraday Discussions* 2007, **135**:161-190.

33.   Monego DL, da Rosa MB, do Nascimento PC: **Applications of computational chemistry to the study of the antiradical activity of carotenoids: A review**. *Food Chem* 2017, **217**:37-44.

34.   Martínez A, Vargas R, Galano A: **Citric acid: A promising copper scavenger**. *Computational and Theoretical Chemistry* 2018, **1133**:47-50.

35.   Johns JR, Platts JA: **Theoretical insight into the antioxidant properties of melatonin and derivatives**. *Org Biomol Chem* 2014, **12**(39):7820-7827.

36.   Martinez A: **Donator acceptor map of psittacofulvins and anthocyanins: are they good antioxidant substances?** *The Journal of Physical Chemistry B* 2009, **113**(14):4915-4921.

37.   Martínez A, Rodríguez-Gironés MA, Barbosa A, Costas M: **Donator acceptor map for carotenoids, melatonin and vitamins**. *The Journal of Physical Chemistry A* 2008, **112**(38):9037-9042.

Chapter 4

Theoretical insights into Zn^{2+}chelated metal complexes of herbacetin for the application in Alzheimer's disease

Abstract

Herbacetin is a potential phytochemical that is proposed to treat various diseases. In this study, density functional theory is used to characterize the metal-chelating ability of herbacetin, with Zn^{2+} metal ion in various solvents like DMSO, acetone, CCl$_4$, and toluene. In general, metal chelation improved the reactivity of herbacetin. Interaction energies suggest Zn^{2+} is preferably coordinated to O6 and O4 atoms of herbacetin and the higher affinity of herbacetin for Zn^{2+} is found in CCl$_4$ solvent. Efficient charge transfer occurs *via* the lone pair of oxygen atoms in herbacetin to the anti-bonding orbital of metal ions through non-covalent interactions, particularly electrostatic. The metal chelation enhanced the anti-oxidant activity of herbacetin for scavenging •OH and •OOH. Further, the anti-Alzheimer's property of herbacetin was explained using molecular docking technique. Our results suggest that herbacetin is a potential contender in chelation therapy for the treatment of Alzheimer's disease due to its metal chelating and antioxidant properties. More importantly, an outstanding bioactivity score of 0.55 was obtained for the herbacetin molecule.

4.14   Introduction

Alzheimer's disease is a neurodegenerative illness marked by the formation of intracellular neurofibrillary tangles, extracellular amyloid beta (A) plaques, together with a disruption of transition metal ion homeostasis in conjunction with oxidative stress [1]. It is a huge scientific challenge that has yet to be solved. This is the most frequent kind of dementia in the elderly, accounting for 60–80 percent of all dementia cases globally, which are currently estimated to number more than 45 million [2] and are expected to triple by 2050 due to increased life expectancy [3]. Despite massive efforts and financial investments targeted at developing new effective treatments for Alzheimer's disease, no new drugs have arrived on the market in recent years [4, 5]. Only a few anti-AD drugs, such as acetylcholinesterase inhibitors (donepezil, rivastigmine, and galantamine), and NMDA (N-methyl-D-aspartate) receptor antagonists (memantine) have been used clinically, with limited treatment effects and numerous side effects in AD patients [6]. As a result, one of the most pressing and sought-after jobs in medicinal chemistry is the study and development of novel anti-AD medications.

Neurodegenerative disorders like Alzheimer's disease (AD), Parkinson's disease (PD), and transmissible spongiform encephalopathies (TSEs) are all characterised by similar cellular and molecular pathways, such as protein aggregation and oxidative stress-induced damage [7]. Redox-active metal ions (e.g., Cu and Zn) play a key role in protein aggregation and are believed to offer a link between oxidative damage and protein aggregation [8-10]. Transition metal ions (M^{n+}) in lower oxidation states (n=1 or 2) can stimulate oxidative

reactions in living organisms by lowering their activation energy. On the other hand, this may result in the creation of extremely harmful reactive oxygen species, the most common of which are hydroxyl radicals (HO·), as well as reactive nitrogen species. According to Fenton chemistry, the oxidation of redox active metal ions in their reduced form reacts with H_2O_2 to produce radicals known to induce DNA damage, alteration of mitochondrial membrane potentials, and lipid peroxidation. Disruptions or changes in the redox potential of metal ion regulatory systems have therefore been linked to a variety of disease states, including neurodegenerative disorders such as Alzheimer's disease [1]. In short, the apparent involvement of such transition metal ions in both protein aggregation and oxidative stress makes chelation therapy an appropriate treatment for eliminating metal ions such as Zn^{2+} which is responsible for neurodegenerative diseases.

One of the important characteristics of an effective chelating agent is that it has a high affinity for the targeted metal ions, resulting in a stronger ability to scavenge the free active metal ions [11]. Natural polyphenols can really chelate metal ions, preventing the formation of harmful hydroxyl radicals. The hydroxyl, carbonyl, and carboxyl groups of these polyphenols typically bond to transition metal ions [12, 13]. This is accomplished through an acid-base reaction in which the metal ion serves as the Lewis acid and the polyphenol serves as the Lewis base. Many investigations have been conducted on the above-mentioned solutions for reducing transition metal ion excesses in living organisms [14]. Herbacetin is an yellow bioactive flavonoid derived from 5,7,8-trihydroxyflavone ($C_{15}H_{10}O_7$) found in various herbs like

Ephedra sinica Stapf (Ephedraceae) [15], Sedum roseum (L.). Scop. (Crassulaceae) [16] and Linum usitatissimum Linn. (Linaceae) [17]. The herbacetin molecule has a wide range of pharmacological activities which involve antioxidant, antiviral, anti-inflammatory, anticancer, anti-obesity, and anticholinesterase effects and it is also used to treat depression, fatigue and cardiovascular diseases [15, 17-23]. Herbacetin due to the presence of hetero atoms(oxygen) in its structure, can be a good option for a competitive chelate complexation process to scavenge neurotoxic transition metal ions as a chelating agent.

Herein a comparison of information from NMR spectroscopy (experimental part) and quantum mechanical (QM/NMR) calculations (predicted part) was undertaken to shed significant insight on the correct prediction of geometry [24] of herbacetin molecule as well as the selection of best basis set for further studies. The main goal of this study is the quantum mechanical evaluation of the phytochemical herbacetin for its scavenging ability with the transition metal ion Zn^{2+} (which have been implicated in Alzheimer's disease). Density functional theory is used to predict the structure, stability, and electronic properties of Zn^{2+} chelates of herbacetin molecule and the influence of solvents on metal chelation was explored. The study also focuses on the effect of Zn^{2+} ion on the anti-oxidant activity of herbacetin molecule in the gas and DMSO solvent phase. The last part of this paper is oriented towards the anti-AD potential of herbacetin molecule using in silico molecular docking studies against AChE2 and BChE targets. The drug-likeness and ADME properties of herbacetin

molecule were also analysed for developing herbacetin as a promising drug.

4.2 Computational methodology

4.2.1 DFT calculation

The present study uses a computational approach to the structural analysis of herbacetin and Zn^{2+} chelated herbacetin using Gaussian16 software package. To obtain the stable conformer, a potential energy scanning is first performed on the structure of herbacetin and the lowest energy conformer was optimized under B3LYP/6-31g, B3LYP/6-31+g(d,p), B3LYP/6-31++g(d,p), B3LYP/6-311g, B3LYP/6-311+g(d,p), B3LYP/6-311++g(d,p), B3LYP/6-31g', B3LYP/6-31+g(d',p'), B3LYP/6-31++g(d',p'), M06/6-31g, M06/6-31+g(d,p), M06/6-31++g(d,p), M06/6-311+g(d,p), M06/6-311+g(d,p), M06/6-311++g(d,p),   M06/6-31g', M06/6-31+g(d',p'), and M06/6-31++g(d',p') basis sets. In order to compare the results with those obtained experimentally, the estimated sets of NMR data coming from the various combinations of functional/basis sets (previously stated) were accounted. The basis set showing a maximum correlation in NMR data (B3LYP/6-31g) is used for further analysis. Three coordination binding sites were taken into consideration in order to study the formation of complexes between herbacetin and metal ion. In HER1-Zn^{2+}, the metal ion is coordinated to O6 and O4 atoms of herbacetin molecule. In HER2- Zn^{2+} and HER3- Zn^{2+} complexes, Zn^{2+} is coordinated to O5 and O2 atoms and O5 and O3 atoms of herbacetin respectively. The equilibrium geometries of HERN- Zn^{2+} (N=1,2,3

possible chelation sites) complexes were optimized using the DFT method B3LYP, which combines Becke's three (B3) parameter exchange functional with Lee, Yang, Parr's (LYP) gradient corrected correlation functional [25] and a mixed basis set 631g+LANL2DZ (631g for non-metal atoms and LANL2DZ [26] for Zn^{2+} metal ion. The usage of the effective core potential LanL2DZ basis set for transition-metal complexes have been found to attain a degree of precision comparable to that of the all-electron basis set for transition-metal complexes [27]. Harmonic – vibrational – frequency calculations have been performed at the same computational levels to confirm that the structures are at energetic minima on the potential energy surface (PES). Solvent effects have been taken into account by an implicit approach, namely, the polarisable continuum model (PCM) using the non-equilibrium version of the IEF-PCM model [28]. The interaction energy of metal-ligand complex (ΔE_{Int}) was calculated according to the following equation[29],

$$\Delta E_{Int} = E_{Complex} - (E_{Metal} + E_{ligand}) \qquad\qquad (1)$$

where $E_{Complex}$, E_{Metal} and E_{ligand} are the energy of complex, metal, and ligand respectively. The optimised structures were subjected to NBO analysis [30] in order to identify the electronic charges on the atoms of the complexes as well as to estimate the key donor-acceptor interactions. Bader's QTAIM analysis [31] was used to calculate the topological characteristics of electron density $\rho(r)$ and Laplacian of electron density $\nabla^2\rho(r)$ for the complexes [32]. The frontier molecular orbital (FMO) analysis was performed to find the reactivity of metal complex formed. Electron location function (ELF)[33] and localised

orbital locator (LOL) [34] were used to further understand the nature of the interaction between the metal and herbacetin. The Multiwfn 3.7 software was used to carry out the ELF, LOL, and QTAIM analyses [35, 36].

The enthalpy of a reaction is defined as the difference between the sums of the enthalpies of the reactant and product species. This concept is used to compute the numerical parameters associated to the anti-oxidant mechanisms. Let •OOH be the free radical scavenged by herbacetin molecule (ArOH) [37].

$$\Delta H_{BDE} = H\left(ArO^{\bullet}\right) + H\left(H_2O_2\right) - H\left({}^{\bullet}OOH\right) - H\left(ArOH\right) \qquad (2)$$

$$\Delta H_{IP} = H\left(ArO^{\bullet+}\right) + H\left(OOH^-\right) - H\left({}^{\bullet}OOH\right) - H\left(ArOH\right) \qquad (3)$$

$$\Delta H_{PDE} = H\left(ArO^{\bullet}\right) + H\left(H_2O_2\right) - H\left(ArO^{\bullet+}\right) - H\left(OOH^-\right) \qquad (4)$$

$$\Delta H_{PA} = H\left(ArO^-\right) + H\left(H_2O_2\right) - H\left(ArOH\right) - H\left(OOH^-\right) \qquad (5)$$

$$\Delta H_{ETE} = H\left(ArO^{\bullet}\right) + H\left(OOH^-\right) - H\left(ArO^-\right) - H\left({}^{\bullet}OOH\right) \qquad (6)$$

Where $H\left(ArO^{\bullet}\right)$, $H\left(H_2O_2\right)$, $H\left({}^{\bullet}OOH\right)$, and $H\left(ArOH\right)$ represents the sum of electronic and thermal enthalpy for $ArO^{\bullet}$, H_2O_2, ${}^{\bullet}OOH$ and $ArOH$ respectively.

4.2.2 Molecular docking

Molecular docking investigation was carried out to understand the anti-AD property of herbacetin. To get the score functions that represent the binding affinity between protein and ligand, the

AutoDock Vina tool is employed [38]. The crystal structures of human acetylcholinesterase (PDB ID: 3LII), human butyrylcholinesterase (PDB ID: 4BDS), were taken from the RCSB-Protein Data Bank (PDB). Using the AutoDock tool (ADT), polar hydrogen atoms and the appropriate amount of Gasteiger charges were added to the crystal structure of all the proteins in order to prepare them for molecular docking. The crystal structure of the protein was saved in .pdbqt format after water molecules, ligands, and other structures were removed. The grid box was chosen as 25x25x25, with the dimensions x: 132.994, y: 116.014, and z: 41.214 for AChE2 [39]. For BChE, a grid box of size 52x40x48 centred on X:91.443, Y:88.69, Z:-5.859 was selected. The previously specified information of the receptor, ligand, grid centre, and sizes was maintained within a configuration (.conf) file in order to execute molecular docking. During docking execution, a maximum of 8 binding modes were allowed to be generated for the ligand. For molecular docking, no extra special constraints were implied.

4.3 Basis set selection

The present study involves the potential energy scanning of herbacetin to get the lowest energy conformer. After completing potential energy scanning, the stable conformer was subjected to a geometry optimization step at the density functional theory (DFT) utilising multiple functional/basis sets combinations (see the computational methodology part), and corresponding ^{13}C NMR chemical shifts were determined. The analysis of all these data highlighted that by comparing each computational set of data against the experimental one (**Fig. 4.1.**), and the combination B3LYP/6-31g

showed best correlation. The obtained results prompted us to perform further studies using the same basis set.
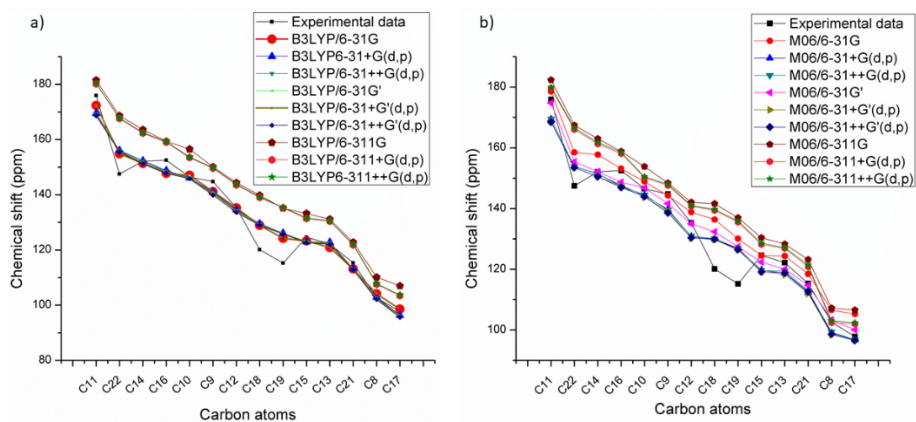
Fig. 4.1. ^{13}C NMR data comparison between experimental data and computational data obtained using level of theory a) B3LYP b) M06

4.4 Geometrical parameters
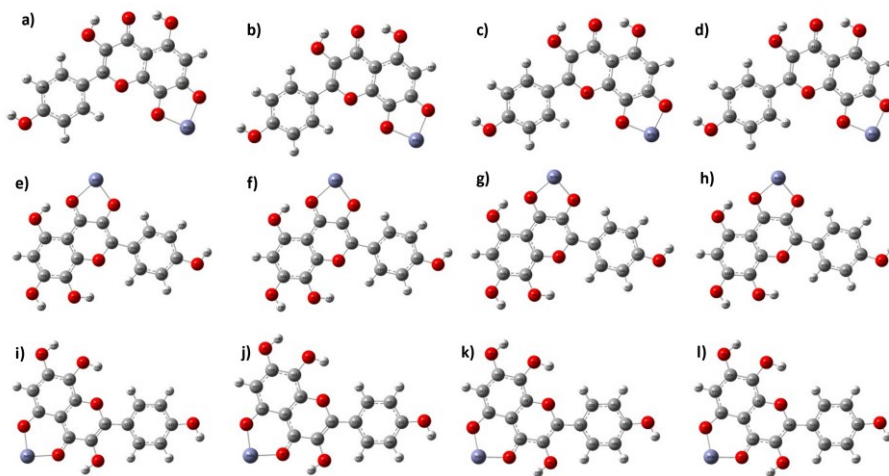
Fig. 4.2. Optimized geometry of HER1-Zn^{2+} in **a)** DMSO, **b)** acetone, **c)** CCl4, **d)** toluene, HER2-Zn^{2+} in **e)** DMSO, **f)** acetone, **g)** CCl4, **h)** toluene, and HER3-Zn^{2+} in **i)** DMSO, **j)** acetone, **k)** CCl4, **l)** toluene

The herbacetin molecule has mainly three possible metal chelation sites due to the presence of carbonyl and hydroxyl groups and the metal ion Zn^{2+} is coordinated to the oxygen atoms in these sites. In this work, herbacetin metal chelates of the form 1:1 are considered. The HERN- Zn^{2+} (where N=1, 2, and 3) complexes were fully optimised at the B3LYP/6-31g+LANL2DZ level of theory in in polar solvents like DMSO, and water, and non-polar solvents like CCl_4 and toluene to analyse the structure of HERN-Zn^{2+} chelates more realistically. **Fig. 4.2.** shows the optimized geometry of all the possible herbacetin-metal complexes and the corresponding geometrical parameters are given in **Tables 4.1-4.8** in the supplementary information.

Table 4.1. Optimized bond lengths of herbacetin molecule under DFT/B3LYP/631g

Bond	DMSO	Acetone	CCl_4	Toluene
R(1,9)	1.3868	1.3871	1.3891	1.389
R(1,10)	1.4038	1.4041	1.4063	1.4062
R(2,12)	1.3824	1.3823	1.3812	1.3813
R(2,28)	0.9893	0.9894	0.9901	0.9901
R(3,14)	1.3744	1.3741	1.3707	1.3709
R(3,29)	1.0014	1.0013	0.9998	0.9999
R(4,15)	1.3904	1.3907	1.3936	1.3934
R(4,30)	0.976	0.976	0.9755	0.9755
R(5,11)	1.2913	1.2911	1.289	1.2891
R(6,16)	1.3762	1.3761	1.3751	1.3752
R(6,31)	0.9816	0.9816	0.9812	0.9813
R(7,22)	1.3843	1.3843	1.385	1.385

R(7,32)	0.9777	0.9776	0.977	0.9771
R(8,9)	1.4094	1.4094	1.4096	1.4096
R(8,11)	1.4311	1.4311	1.4305	1.4305
R(8,14)	1.4216	1.4217	1.4226	1.4226
R(9,15)	1.388	1.3878	1.3863	1.3864
R(10,12)	1.3736	1.3734	1.3721	1.3722
R(10,13)	1.4581	1.4581	1.4583	1.4582
R(11,12)	1.4457	1.4459	1.4485	1.4484
R(13,18)	1.4147	1.4147	1.4141	1.4142
R(13,19)	1.4161	1.416	1.4156	1.4156
R(14,17)	1.3912	1.3913	1.3922	1.3922
R(15,16)	1.4036	1.4036	1.4041	1.4041
R(16,17)	1.4005	1.4004	1.3994	1.3994
R(17,23)	1.0814	1.0814	1.0811	1.0811
R(18,20)	1.3932	1.3933	1.3933	1.3933
R(18,24)	1.0803	1.0803	1.0804	1.0804
R(19,21)	1.3893	1.3893	1.3889	1.3889
R(19,25)	1.0812	1.0812	1.0814	1.0814
R(20,22)	1.4015	1.4015	1.4009	1.4009
R(20,26)	1.0854	1.0854	1.0861	1.0861
R(21,22)	1.4026	1.4025	1.4017	1.4018
R(21,27)	1.0835	1.0834	1.0833	1.0833

Table 4.2. Optimized bond angles of herbacetin molecule under DFT/B3LYP/631g

Angle	DMSO	Acetone	CCl$_4$	Toluene
A(9,1,10)	121.9841	121.9685	121.8045	121.8137
A(12,2,28)	106.7095	106.6862	106.3829	106.3983
A(14,3,29)	108.7794	108.8185	109.2269	109.205
A(15,4,30)	112.4157	112.3767	111.8815	111.9113
A(16,6,31)	110.4241	110.4123	110.2549	110.2625
A(22,7,32)	112.5269	112.5058	112.3003	112.3109
A(9,8,11)	118.5788	118.5765	118.5516	118.5532
A(9,8,14)	118.8106	118.8117	118.8103	118.8107
A(11,8,14)	122.6106	122.6118	122.6381	122.6361
A(1,9,8)	121.0633	121.0746	121.2061	121.1987
A(1,9,15)	117.4247	117.4217	117.3472	117.3529
A(8,9,15)	121.512	121.5037	121.4467	121.4484
A(1,10,12)	117.8574	117.8568	117.8623	117.861
A(1,10,13)	112.8059	112.8147	112.85	112.8473
A(12,10,13)	129.3367	129.3284	129.2877	129.2917
A(5,11,8)	123.5996	123.6188	123.8329	123.8199
A(5,11,12)	118.5755	118.5582	118.381	118.3919
A(8,11,12)	117.8249	117.8229	117.7861	117.7882
A(2,12,10)	122.4073	122.421	122.5712	122.5632
A(2,12,11)	114.9012	114.8784	114.6394	114.6516
A(10,12,11)	122.6915	122.7006	122.7894	122.7852
A(10,13,18)	121.5976	121.5832	121.482	121.487
A(10,13,19)	120.3165	120.3324	120.4297	120.4262
A(18,13,19)	118.0859	118.0844	118.0883	118.0867
A(3,14,8)	120.1065	120.1216	120.2778	120.2695
A(3,14,17)	119.7515	119.7397	119.6277	119.6329
A(8,14,17)	120.142	120.1387	120.0945	120.0976

A(4,15,9)	125.2575	125.2446	125.0415	125.0552
A(4,15,16)	116.2884	116.2855	116.336	116.33
A(9,15,16)	118.4541	118.47	118.6224	118.6149
A(6,16,15)	119.2957	119.2883	119.2311	119.2342
A(6,16,17)	119.0682	119.0836	119.2321	119.2237
A(15,16,17)	121.6361	121.6281	121.5368	121.5421
A(14,17,16)	119.4451	119.4478	119.4892	119.4862
A(14,17,23)	120.6294	120.6204	120.5251	120.5298
A(16,17,23)	119.9255	119.9318	119.9856	119.984
A(13,18,20)	120.8613	120.8551	120.7676	120.7739
A(13,18,24)	119.6833	119.6715	119.5734	119.578
A(20,18,24)	119.4554	119.4734	119.659	119.6481
A(13,19,21)	121.111	121.1183	121.1937	121.1898
A(13,19,25)	119.8249	119.8194	119.7042	119.7135
A(21,19,25)	119.0642	119.0623	119.1021	119.0966
A(18,20,22)	120.0119	120.0165	120.0823	120.0775
A(18,20,26)	119.6408	119.6344	119.5706	119.5734
A(22,20,26)	120.3473	120.3492	120.3471	120.349
A(19,21,22)	119.8898	119.8833	119.8091	119.8135
A(19,21,27)	120.9667	120.9923	121.2351	121.2223
A(22,21,27)	119.1435	119.1244	118.9558	118.9641
A(7,22,20)	123.0037	123.0063	123.0513	123.0492
A(7,22,21)	116.9561	116.9513	116.8896	116.8924
A(20,22,21)	120.0402	120.0424	120.0591	120.0584

Table 4.3. Optimized bond lengths of HER1-Zn^{2+} molecule under DFT/B3LYP/631g+LANL2DZ

Bond	DMSO	Acetone	CCl$_4$	toluene
R(1,9)	1.4038	1.4033	1.3939	1.3943
R(1,10)	1.3977	1.3977	1.3975	1.3975
R(2,12)	1.3947	1.3946	1.3922	1.3923
R(2,28)	0.9917	0.9917	0.9916	0.9916
R(3,14)	1.394	1.3932	1.3858	1.3862
R(3,29)	1.0053	1.0052	1.0032	1.0033
R(4,15)	1.3749	1.3763	1.3928	1.3919
R(4,31)	1.9703	1.9656	1.9166	1.919
R(5,11)	1.3077	1.3073	1.3012	1.3015
R(6,16)	1.3565	1.3582	1.3811	1.3798
R(6,31)	1.9831	1.9769	1.9269	1.9289
R(7,22)	1.396	1.3962	1.3974	1.3974
R(7,30)	0.9801	0.9801	0.9795	0.9795
R(8,9)	1.4305	1.4303	1.4239	1.4242
R(8,11)	1.4303	1.4307	1.4367	1.4364
R(8,14)	1.4286	1.4286	1.4294	1.4294
R(9,15)	1.3978	1.3978	1.3975	1.3975
R(10,12)	1.379	1.3789	1.379	1.379
R(10,13)	1.4678	1.4677	1.4664	1.4665
R(11,12)	1.4551	1.4549	1.4558	1.4558
R(13,18)	1.4198	1.4197	1.4185	1.4186
R(13,19)	1.4222	1.4221	1.4222	1.4222
R(14,17)	1.3933	1.3934	1.3959	1.3957
R(15,16)	1.4495	1.4488	1.4414	1.4417
R(16,17)	1.4202	1.4193	1.4136	1.4138
R(17,23)	1.0852	1.0851	1.084	1.084
R(18,20)	1.4025	1.4025	1.4025	1.4025
R(18,24)	1.0821	1.0822	1.0825	1.0825
R(19,21)	1.3989	1.3988	1.398	1.398
R(19,25)	1.084	1.084	1.0842	1.0842
R(20,22)	1.4098	1.4097	1.4093	1.4093
R(20,26)	1.0879	1.0879	1.0887	1.0887
R(21,22)	1.41	1.4099	1.409	1.409
R(21,27)	1.0858	1.0857	1.0856	1.0856

Table 4.4. Optimized bond angles of HER1-Zn^{2+} molecule under DFT/B3LYP/631g+LANL2DZ

Angle	DMSO	Acetone	CCl$_4$	toluene
A(9,1,10)	122.4451	122.4347	122.423	122.4254
A(12,2,28)	106.663	106.6447	106.6502	106.6477
A(14,3,29)	108.4166	108.4782	109.1186	109.0833
A(15,4,31)	106.9873	106.7296	103.2659	103.4639
A(16,6,31)	108.118	107.9088	104.549	104.7533
A(22,7,30)	112.7005	112.6657	112.4086	112.4191
A(9,8,11)	119.4078	119.3871	119.0452	119.0621
A(9,8,14)	118.6773	118.7114	118.8977	118.8897
A(11,8,14)	121.9149	121.9015	122.0571	122.0482
A(1,9,8)	119.4357	119.4661	120.0968	120.0631
A(1,9,15)	117.8215	117.8498	117.7041	117.7169
A(8,9,15)	122.7429	122.6841	122.1991	122.22
A(1,10,12)	118.7749	118.7838	118.6696	118.6764
A(1,10,13)	112.5509	112.5506	112.2759	112.2913
A(12,10,13)	128.6742	128.6656	129.0545	129.0323
A(5,11,8)	123.9683	123.9678	123.9164	123.9207
A(5,11,12)	118.0947	118.0966	118.311	118.2983
A(8,11,12)	117.937	117.9356	117.7726	117.781
A(2,12,10)	123.0382	123.0517	122.9783	122.984
A(2,12,11)	114.9622	114.9555	115.0289	115.0241
A(10,12,11)	121.9995	121.9927	121.9928	121.9919
A(10,13,18)	121.9753	121.951	121.9609	121.9576
A(10,13,19)	119.7578	119.7597	119.5611	119.5737
A(18,13,19)	118.2669	118.2893	118.478	118.4687
A(3,14,8)	119.781	119.8404	120.121	120.1075
A(3,14,17)	119.9745	119.9341	119.6919	119.7039
A(8,14,17)	120.2445	120.2255	120.1871	120.1886
A(4,15,9)	123.9179	123.85	122.1208	122.2235
A(4,15,16)	119.1949	119.2412	120.4494	120.374
A(9,15,16)	116.8871	116.9089	117.4298	117.4025

A(6,16,15)	117.6034	117.6267	118.2091	118.1658
A(6,16,17)	121.2096	121.1384	120.4933	120.5313
A(15,16,17)	121.187	121.2349	121.2976	121.303
A(14,17,16)	120.2612	120.2352	119.9886	119.9962
A(14,17,23)	120.3554	120.3397	120.2725	120.2766
A(16,17,23)	119.3834	119.4251	119.7389	119.7272
A(13,18,20)	120.8539	120.8361	120.6273	120.6385
A(13,18,24)	119.6416	119.634	119.5771	119.5796
A(20,18,24)	119.5045	119.53	119.7955	119.7818
A(13,19,21)	121.0873	121.0763	121.0239	121.0254
A(13,19,25)	119.3466	119.3221	119.1367	119.1465
A(21,19,25)	119.5661	119.6016	119.8394	119.8281
A(18,20,22)	119.8542	119.8569	119.9237	119.9201
A(18,20,26)	119.7764	119.7767	119.7517	119.7535
A(22,20,26)	120.3694	120.3664	120.3246	120.3264
A(19,21,22)	119.7315	119.7257	119.6595	119.6632
A(19,21,27)	121.002	121.0223	121.2516	121.2388
A(22,21,27)	119.2665	119.252	119.0888	119.098
A(7,22,20)	122.8196	122.8029	122.7854	122.7824
A(7,22,21)	116.9742	116.9813	116.9271	116.9334
A(20,22,21)	120.2062	120.2157	120.2875	120.2841
A(4,31,6)	88.0964	88.4937	93.5266	93.2431

Table 4.5. Optimized bond lengths of HER2-Zn^{2+} molecule under DFT/B3LYP/631g+LANL2DZ

Bond	DMSO	Acetone	CCl$_4$	Toluene
R(1,9)	1.3842	1.3847	1.3901	1.3898
R(1,10)	1.4035	1.4028	1.3958	1.3961
R(2,12)	1.352	1.3548	1.3782	1.3771
R(2,32)	1.9791	1.9747	1.9172	1.9191
R(3,14)	1.3828	1.3824	1.3783	1.3786
R(3,28)	1.0022	1.0017	0.9953	0.9956
R(4,15)	1.3982	1.398	1.3961	1.3962
R(4,29)	0.9791	0.979	0.9787	0.9787
R(5,11)	1.3296	1.3319	1.3524	1.3512
R(5,32)	2.0722	2.0568	1.9705	1.9745
R(6,16)	1.3839	1.383	1.3743	1.3748
R(6,30)	0.9841	0.9842	0.9843	0.9843
R(7,22)	1.3931	1.3923	1.3844	1.3849
R(7,31)	0.9803	0.9802	0.98	0.98
R(8,9)	1.419	1.4192	1.4227	1.4224
R(8,11)	1.4271	1.4262	1.4196	1.4199
R(8,14)	1.4324	1.4327	1.4346	1.4345
R(9,15)	1.3962	1.3958	1.3905	1.3908
R(10,12)	1.4015	1.4018	1.404	1.4038
R(10,13)	1.4592	1.4589	1.4534	1.4537
R(11,12)	1.452	1.4513	1.443	1.4434
R(13,18)	1.4233	1.4233	1.4231	1.423
R(13,19)	1.4242	1.4243	1.426	1.4259
R(14,17)	1.395	1.3948	1.3943	1.3944
R(15,16)	1.4096	1.4101	1.4154	1.4151
R(16,17)	1.4107	1.4105	1.4093	1.4094
R(17,23)	1.0837	1.0837	1.0832	1.0832
R(18,20)	1.4007	1.4006	1.3986	1.3988
R(18,24)	1.0823	1.0823	1.0821	1.0821
R(19,21)	1.3972	1.3967	1.3928	1.393
R(19,25)	1.0834	1.0833	1.0833	1.0833
R(20,22)	1.4099	1.4101	1.4122	1.4121
R(20,26)	1.0879	1.088	1.088	1.088
R(21,22)	1.4113	1.4114	1.4131	1.413
R(21,27)	1.0855	1.0854	1.0848	1.0849

Table 4.6. Optimized bond angles of HER2-Zn^{2+} molecule under DFT/B3LYP/631g+LANL2DZ

Angle	DMSO	Acetone	CCl$_4$	Toluene
A(9,1,10)	122.2836	122.3829	123.0368	123.0045
A(12,2,32)	112.1496	111.5198	107.891	108.0723
A(14,3,28)	109.3075	109.347	110.119	110.0659
A(15,4,29)	113.0661	113.1459	113.5592	113.5204
A(11,5,32)	109.2436	109.039	106.8482	106.9516
A(16,6,30)	111.074	111.1055	111.5865	111.5548
A(22,7,31)	112.7666	112.8106	113.5311	113.4954
A(9,8,11)	118.0528	117.9998	117.4423	117.467
A(9,8,14)	118.6692	118.6766	118.5431	118.5487
A(11,8,14)	123.2779	123.3236	124.0142	123.984
A(1,9,8)	120.851	120.7732	120.4163	120.4317
A(1,9,15)	117.5723	117.6411	117.7202	117.7111
A(8,9,15)	121.5767	121.5857	121.8631	121.8565
A(1,10,12)	119.0382	118.9884	118.2728	118.3143
A(1,10,13)	113.3913	113.3664	113.406	113.3835
A(12,10,13)	127.5705	127.6452	128.3109	128.2898
A(5,11,8)	121.5001	121.3261	120.5111	120.5571
A(5,11,12)	118.3555	118.3908	118.4424	118.4295
A(8,11,12)	120.1444	120.2831	121.0416	121.0084
A(2,12,10)	123.4876	123.433	122.6491	122.7198
A(2,12,11)	116.8824	116.9944	117.5945	117.5472
A(10,12,11)	119.63	119.5726	119.7356	119.7098
A(10,13,18)	121.1	121.1424	121.5274	121.5179
A(10,13,19)	120.8054	120.7467	120.1894	120.195
A(18,13,19)	118.0946	118.1109	118.2792	118.2821
A(3,14,8)	120.1088	120.1755	120.8005	120.7612
A(3,14,17)	119.7031	119.6596	119.2014	119.2344
A(8,14,17)	120.1881	120.1648	119.9976	120.0038
A(4,15,9)	125.3537	125.4567	125.914	125.8714

A(4,15,16)	116.2687	116.1827	115.8591	115.8991
A(9,15,16)	118.3776	118.3606	118.2241	118.2268
A(6,16,15)	119.5367	119.533	119.6296	119.6278
A(6,16,17)	118.7474	118.7463	118.7579	118.7553
A(15,16,17)	121.7159	121.7207	121.6124	121.6168
A(14,17,16)	119.4725	119.4915	119.7589	119.7467
A(14,17,23)	120.7712	120.7498	120.5339	120.5457
A(16,17,23)	119.7563	119.7587	119.7071	119.7075
A(13,18,20)	120.9287	120.9123	120.7559	120.7564
A(13,18,24)	118.7184	118.7323	119.0097	119
A(20,18,24)	120.3529	120.3554	120.2344	120.2436
A(13,19,21)	121.1305	121.1358	121.1473	121.1429
A(13,19,25)	119.8964	119.902	119.7204	119.7171
A(21,19,25)	118.9731	118.9622	119.13	119.1376
A(18,20,22)	119.868	119.8605	119.8697	119.8683
A(18,20,26)	119.8037	119.8175	119.8292	119.8289
A(22,20,26)	120.3283	120.322	120.3011	120.3027
A(19,21,22)	119.7753	119.7629	119.661	119.6633
A(19,21,27)	120.9968	121.0387	121.4491	121.4299
A(22,21,27)	119.2279	119.1983	118.8894	118.9062
A(7,22,20)	122.8158	122.8509	123.1804	123.1662
A(7,22,21)	116.9813	116.9316	116.535	116.5494
A(20,22,21)	120.2028	120.2175	120.2846	120.2844
A(2,32,5)	83.3689	84.0559	89.0324	88.7831

Table 4.7. Optimized bond lengths of HER3-Zn^{2+} molecule under DFT/B3LYP/631g+LANL2DZ

Bond	DMSO	Acetone	CCl_4	Toluene
R(1,9)	1.3948	1.3947	1.393	1.3931
R(1,10)	1.3974	1.3969	1.3914	1.3917
R(2,12)	1.3888	1.3887	1.3872	1.3873
R(2,28)	0.9913	0.991	0.988	0.9881
R(3,14)	1.3443	1.3462	1.3662	1.3652
R(3,32)	1.9458	1.9411	1.8823	1.8849
R(4,15)	1.4009	1.4004	1.3957	1.396
R(4,29)	0.9793	0.9793	0.979	0.979
R(5,11)	1.3178	1.3198	1.3439	1.3424
R(5,32)	2.0014	1.9925	1.9286	1.9311
R(6,16)	1.3846	1.3837	1.3744	1.3749
R(6,30)	0.9842	0.9842	0.9843	0.9843
R(7,22)	1.3917	1.3912	1.384	1.3844
R(7,31)	0.9803	0.9802	0.9801	0.9801
R(8,9)	1.431	1.4312	1.4322	1.4322
R(8,11)	1.4289	1.4288	1.4319	1.4316
R(8,14)	1.4545	1.4545	1.4524	1.4525
R(9,15)	1.3881	1.388	1.3884	1.3883
R(10,12)	1.3818	1.3826	1.393	1.3924
R(10,13)	1.4616	1.461	1.4537	1.4541
R(11,12)	1.451	1.4496	1.4358	1.4364
R(13,18)	1.4215	1.4216	1.4232	1.4231
R(13,19)	1.4228	1.423	1.4261	1.4259
R(14,17)	1.4145	1.4135	1.4031	1.4035
R(15,16)	1.4137	1.4137	1.4133	1.4134
R(16,17)	1.4003	1.4007	1.4041	1.404
R(17,23)	1.0841	1.0841	1.0833	1.0834
R(18,20)	1.4006	1.4004	1.3984	1.3984
R(18,24)	1.0815	1.0815	1.0814	1.0814
R(19,21)	1.397	1.3967	1.3928	1.393

R(19,25)	1.0834	1.0835	1.0838	1.0838
R(20,22)	1.4105	1.4105	1.412	1.4119
R(20,26)	1.0875	1.0876	1.0877	1.0877
R(21,22)	1.411	1.4112	1.4132	1.4131
R(21,27)	1.0854	1.0853	1.0849	1.0849

Table 4.8. Optimized bond angles of HER3-Zn^{2+} molecule under DFT/B3LYP/631g+LANL2DZ

Angle	DMSO	Acetone	CCl_4	Toluene
A(9,1,10)	122.4093	122.4603	123.0321	122.9984
A(12,2,28)	107.1562	107.2111	108.0992	108.0412
A(14,3,32)	126.9668	126.5204	121.6404	121.8619
A(15,4,29)	112.7395	112.7355	113.1075	113.0798
A(11,5,32)	124.0282	123.7492	119.7858	119.9987
A(16,6,30)	110.9673	111.0191	111.5936	111.5623
A(22,7,31)	112.9439	112.9842	113.576	113.5351
A(9,8,11)	116.4961	116.4194	115.9464	115.9682
A(9,8,14)	118.4893	118.429	117.4566	117.524
A(11,8,14)	125.0144	125.1514	126.5955	126.5065
A(1,9,8)	121.7589	121.7483	121.5252	121.5366
A(1,9,15)	115.7515	115.7393	115.6478	115.6625
A(8,9,15)	122.4894	122.5121	122.8257	122.7996
A(1,10,12)	117.3794	117.3362	116.9757	116.9951
A(1,10,13)	113.6571	113.7096	113.831	113.8376
A(12,10,13)	128.9624	128.9528	129.1895	129.1634
A(5,11,8)	126.3799	126.3243	125.8681	125.8796
A(5,11,12)	114.1682	114.1168	113.8395	113.8604
A(8,11,12)	119.4517	119.5587	120.2899	120.2575
A(2,12,10)	122.134	122.0804	121.1754	121.2308
A(2,12,11)	115.363	115.4453	116.6327	116.5632
A(10,12,11)	122.5003	122.4711	122.1837	122.1975
A(10,13,18)	121.6024	121.5898	121.7735	121.7483

A(10,13,19)	120.1588	120.1647	119.933	119.9579
A(18,13,19)	118.2384	118.2448	118.2935	118.2938
A(3,14,8)	123.0227	123.0414	123.0088	122.9955
A(3,14,17)	118.9448	118.8674	117.8086	117.891
A(8,14,17)	118.0323	118.0911	119.1764	119.108
A(4,15,9)	125.4176	125.3925	125.4254	125.4208
A(4,15,16)	116.3285	116.348	116.1681	116.1827
A(9,15,16)	118.2538	118.2595	118.4065	118.3965
A(6,16,15)	119.1901	119.2358	119.8157	119.7815
A(6,16,17)	119.3473	119.3312	119.1766	119.1826
A(15,16,17)	121.4625	121.4328	121.0076	121.0359
A(14,17,16)	121.2719	121.274	121.115	121.1242
A(14,17,23)	119.152	119.1702	119.3315	119.3291
A(16,17,23)	119.5758	119.5556	119.5534	119.5466
A(13,18,20)	120.8545	120.8484	120.7197	120.7275
A(13,18,24)	119.7089	119.7072	119.7136	119.7116
A(20,18,24)	119.4366	119.4444	119.5667	119.5609
A(13,19,21)	121.1141	121.1093	121.1499	121.1432
A(13,19,25)	119.8389	119.848	119.8366	119.8428
A(21,19,25)	119.0468	119.0425	119.0134	119.0139
A(18,20,22)	119.855	119.8554	119.917	119.9119
A(18,20,26)	119.7461	119.7375	119.6715	119.6756
A(22,20,26)	120.3989	120.4071	120.4115	120.4125
A(19,21,22)	119.7192	119.7189	119.6515	119.6569
A(19,21,27)	121.0129	121.049	121.4407	121.4201
A(22,21,27)	119.2678	119.232	118.9078	118.9229
A(7,22,20)	122.8754	122.8961	123.2144	123.1905
A(7,22,21)	116.9064	116.8814	116.5176	116.5433
A(20,22,21)	120.2182	120.2225	120.268	120.2662
A(3,32,5)	94.1835	94.7973	101.1392	100.776

It's worth mentioning that the solvent impact resulted in small structural alterations. In the case of HER1-Zn^{2+} complex, the O4-Zn^{2+} and O6-Zn^{2+} distances are found to be 1.9703 and 1.9831Å in DMSO and 1.9656 and 1.97687Å in acetone media respectively. The O4-Zn^{2+} and O6-M Zn^{2+} distances found to be shortened in non-polar solvents and the corresponding values are 1.9166 and 1.9269 Å in CCl_4 and 1.9190 and 1.9290 Å in toluene respectively. It is also observed that in HER1-Zn^{2+} complex, O4-Zn^{2+} shows minimum distance than O6-Zn^{2+} irrespective of nature of solvent. According to the findings, the stability of the coordination bonds in HER1-Zn^{2+} is observed to be weakened due to the action of the polar solvents.

The coordination distances of O5-Zn^{2+}, and O2-Zn^{2+} interactions in HER2-Zn^{2+} are found to be 2.0722 and 1.9791Å in DMSO. The coordination distances of HER2-Zn^{2+} complexes in DMSO medium are found to be shortened by 0.015, 0.102, 0.098Å for O5-Zn^{2+} and 0.004, 0.062, 0.060Å for O3-Zn^{2+} in acetone, CCl_4 and toluene respectively. On comparing O5-Zn^{2+} and O3-Zn^{2+} interaction distances, metal ions possess weaker affinity towards O5 atom because, the stronger interaction of Zn^{2+} with O2 atom slightly destabilizes the O5-Zn^{2+} interactions in HER2-Zn^{2+} system. The interaction distance between Zn^{2+} and the O3 atom was found to be shorter in all solvents than with the O5 atom.

Furthermore, the HER3-Zn^{2+} complex, exhibited an interaction distance larger than HER1-M^{2+}, but shorter HER2-Zn^{2+} complex. In all the HER3-M^{2+} complexes, metal ions possessed shorter coordination distance with O2 than O5 atom. DMSO effect were studied for HER3-

Zn^{2+} complex indicate that the solvent had a minimal impact on structural features. A large coordination distances were found in non-polar media compared to polar media. The O5- Zn^{2+} distance found to be 2.0014, 1.9925, 1.9286, and 1.9311Å and O5- Zn^{2+} distance is found to be 1.9458, 1.9411, 1.8823, 1.8849Å in DMSO, acetone, CCl_4 and toluene solvents respectively.
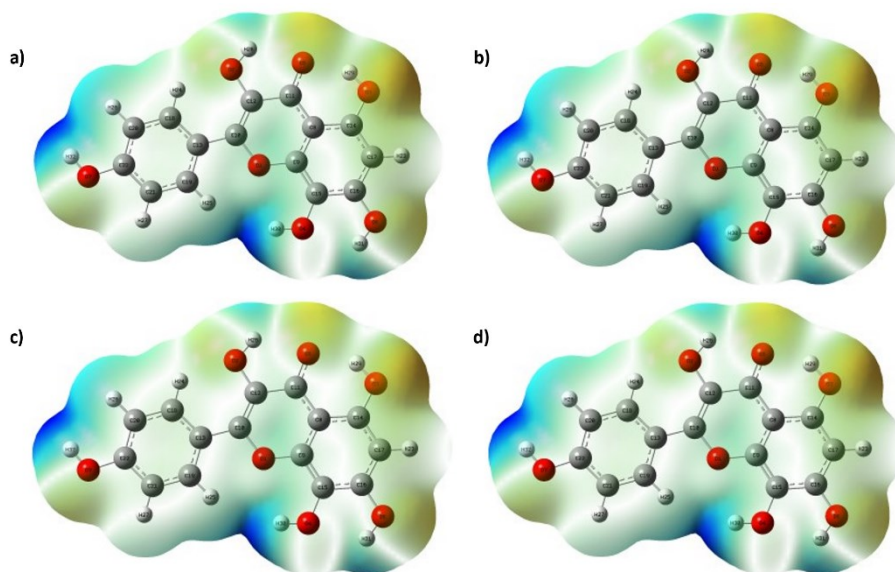
4.5 Molecular electrostatic potential map (MEP)

Fig. 4.3. Molecular electrostatic potential map of herbacetin in **a)** DMSO, **b)** acetone, **c)** CCl4, **d)** toluene

The molecular electrostatic potential (MEP) maps are extremely effective for identifying and predicting a molecule's reactive locations [40]. At a particular position r (x, y, z), the electrostatic potential V(r) is defined as a function of the interaction energy between the electrical charge generated by the electrons, nuclei, and protons put at r. The ESP

maps of herbacetin in DMSO, acetone, CCl$_4$, and toluene phase are shown in **Fig. 4.3**. The blue areas reflect nucleophilic sites, while the red areas show relative electron abundance electrophilic site [41]. The potential lowers as red<green< blue, with blue showing the most preferred location for attraction and red showing the largest site for repulsion. Electronegative molecules are covered by regions with a negative potential, whereas hydrogen atoms are covered by regions with a positive potential. According to MEP the reactive nucleophilic centres for coordination with metal ions are oxygen atoms.

4.6 Interaction energies

Interaction energy has been computed at B3LYP/631g +LANL2DZ and level of theory to acquire a better understanding of the stability of the interaction of HERN- Zn $^{2+}$ chelates. The fact that all complexes have negative interaction energy values in all the selected solvents indicates that there is considerable interaction between herbacetin and metal ion. The calculated interaction energy showed that the chemical stability of herbacetin with Zn^{2+} is as follows: HER1- Zn $^{2+}$>HER3- Zn $^{2+}$>HER2- Zn $^{2+}$ in all the solvent (**Fig. 4.4**). The interaction energies of HER1-Zn^{2+} complexes are found to be -211.159, -224.881, -432.546, and -417.798kcal/mol in DMSO, acetone, CCl4 and toluene media respectively. Compared to HER1- Zn^{2+} complexes, HER2- Zn^{2+} is destabilised by a factor 33.28, 38.084, 103.943, 99.482kcal/mol in DMSO, acetone, CCl$_4$ and toluene media respectively. Similarly, while comparing with HER1- Zn^{2+}, the HER3- Zn^{2+} complex is found to be destabilised by 29.749, 34.067, 95.119, 90.966kcal/mol in DMSO, acetone, CCl$_4$ and toluene media

respectively. It is also important to note that, non-polar solvents stabilize all the complexes compared to polar solvents. Among the possible chelation sites, HER1- Zn^{2+} is found to be more favourable site thermodynamically. Naturally, the electrostatic interaction between the dication and dianion (HER1- Zn^{2+}) is significantly stronger compared to the interaction between the dication and anion (HER1-Zn^{2+} and, HER1- Zn^{2+}) which is clearly evident from the interaction energy values. Moreover, the considerable value of interaction energy shows that the most affinity of herbacetin for Zn^{2+} is found in CCl4 solvent.
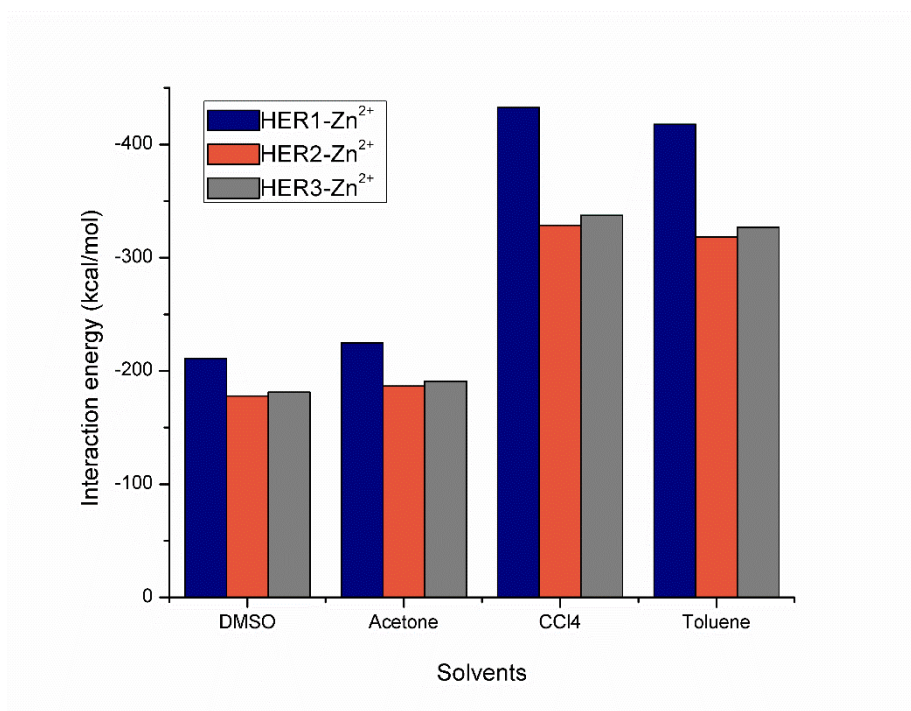

Fig. 4.4. The interaction energies of HERN-Zn^{2+} complexes

4.7 Molecular orbital analysis

One of the most useful molecular orbital models for assessing and analysing a molecule's chemical reactivity is the frontier molecular orbital approach [42]. This method is based on the idea that the creation of bonds between atoms is caused by the movement of electrons from the highest occupied molecular orbital (HOMO) to the lowest unoccupied molecular orbital (LUMO). Thus, the HOMO orbital defines electron donating capacity, while the LUMO orbital characterises electron receiving ability [43]. The energy gap between these two orbitals causes the molecule to be more polarizable, which is often linked with high chemical reactivity and, as a result, low kinetic stability [44]. **Figs. 4.5. a) and b)** lists the HOMO-LUMO orbital energies of herbacetin and HER1-Zn^{2+} in DMSO, acetone, CCl_4, toluene respectively. The band gap of herbacetin in is found to be 3.437, 3.438, 3.4493.448eV in DMSO, acetone, CCl_4 and toluene respectively. The HOMO-LUMO orbital energies of HER2-Zn^{2+}, and HER3-Zn^{2+} shown in **Figs. 4.5. c) and d)** From the results, it is clear that the band gap of herbacetin is higher than that of all the studied herbacetin metal chelates in all the solvent medium. The interaction of metal ions with herbacetin, on the other hand, reduces the HOMO-LUMO energy gap, resulting in increased chemical reactivity and, as a result, a destabilisation of the kinetic stability in comparison to the isolated herbacetin. Among the chelated complexes, HER1-Zn^{2+} in CCl_4 medium showed the lowest band gap of 1.746eV infer its high reactivity whereas HER3-Zn^{2+} in DMSO showed highest band gap of 3.052eV. The narrower energy gap for HER1-Zn^{2+} in CCl_4 medium

suggests that charge transfer interactions dominate over electrostatic interactions between ligand atoms and metal ions. Additionally, including the polar solvent effect results in a wide separation of the HOMO-LUMO orbitals compared to non-polar solvents, resulting in a reduced charge transfer between them for all the HERN-M^{2+} chelates, which agrees with the charge transfer study.
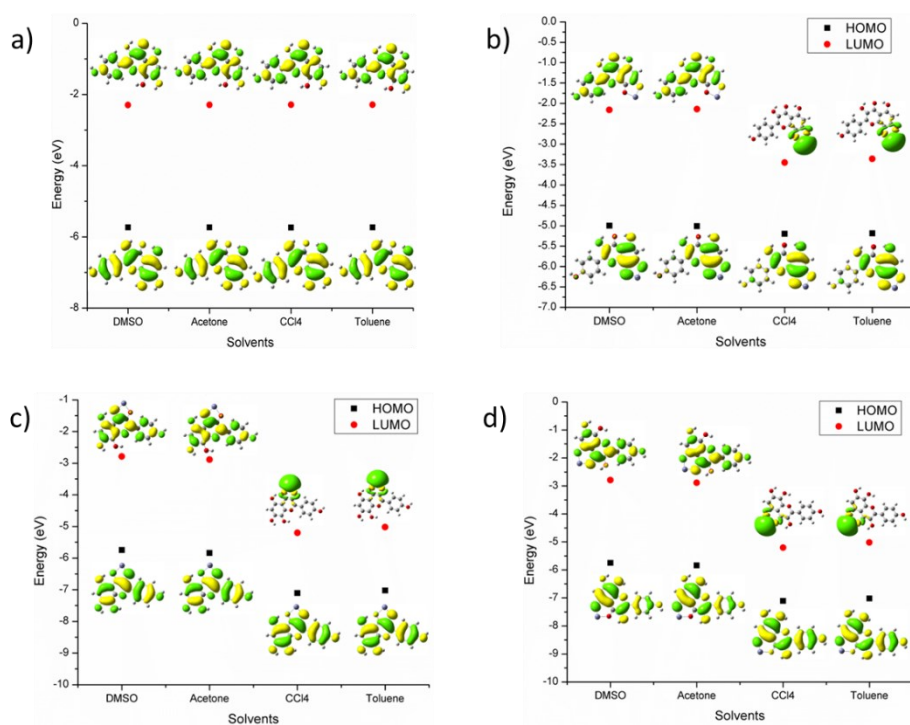

Fig. 4.5. HOMO and LUMO energies of **a)** herbacetin and **b)** HER1-Zn^{2+}, **c)** HER2-Zn^{2+}, **d)** HER3-Zn^{2+} in DMSO, acetone, CCl$_4$, and toluene

4.8 Natural population analysis

The net atomic charge of metal ions in complexes provides useful information concerning charge transfer between metal ions and donor ligand atoms (oxygen atoms in herbacetin). The difference

between the charges of the metal ions in the complex and the isolated state can be used to calculate how much charge the metal ions gain from the donor ligand atoms during complexation. Natural population analysis (NPA) has been performed in both gas and DMSO solvent phases at the B3LYP/631g+(LANL2DZ) level of theory to determine the individual atomic charges of the donor ligand atoms and metal ions in the complexes. The amount of charge on donor ligand atoms, O2, O3, O4, O5, and O6 of herbacetin before complexation were determined to be -0.70987, -0.71372, -0.72642, -0.67779, and -0.69379e in DMSO, -0.70951, -0.71255, -0.72634, -0.67971, and -0.69297e in acetone, -0.70571, -0.69974, -0.72512, -0.66516 and -0.68374e in CCl$_4$ and -0.70591, -0.70044, -0.72520, -0.66576, and -0.68425e in toluene respectively.
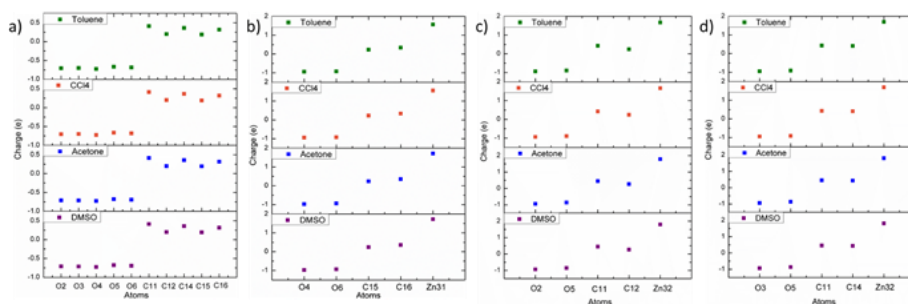

Fig. 4.6. Natural population analysis of **a)** herbacetin and **b)** HER1-M^{2+} **b)** HER2-M^{2+} **b)** HER3-M^{2+} complexes in DMSO, acetone, CCl$_4$, and toluene

Natural population analysis of herbacetin and HER1-Zn^{2+} complexes is shown in **Figs. 4.6 a)** and **b)** and that of HER2- Zn^{2+} and HER3- Zn^{2+} complexes in various solvents is shown in **Figs. 4.6. c)** and **d)** respectively. After complexation, it was noted that the net charge on O4 and O6 atom of HER1- Zn^{2+} complex was found to be increased by

0.2467 and 0.23899, 0.2455 and 0.24088, 0.21486 and 0.23819, and, 0.21735 and 0.23949e in DMSO, acetone, CCl_4 and toluene respectively. Similarly, the calculated net charges on metal ions for HER1-Zn^{2+} complexes are found to be 1.7242 in DMSO, 1.7127 in acetone, 1.55705 in CCl_4, and 1.56672 in toluene. The quantity of positive charges neutralised in CCl_4 solvent is found to be higher than other solvents. The order in which Zn^{2+} gain charge; CCl_4 > toluene > acetone > DMSO, is perfectly correlates with the interaction energy order.

Similarly, the calculated net charges on metal ions for HER2-Zn^{2+} complex are found to be 1.79938, 1.78935, 1.66453, and 1.67254e in DMSO, acetone, CCl_4 and toluene respectively. In contrast to other solvents, Zn^{2+} gained a significant amount of negative charge from donor oxygen atoms of herbacetin in CCl_4 medium. For HER3-M^{2+} complexes, 0.1874e amount of positive charge in DMSO, 0.19558e in acetone, 0.30708 in CCl_4, and 0.29995e in toluene has been neutralised. The order in which metal ions gain charge in all the solvent is perfectly correlated with the interaction energy order. Generally, it is hypothesised that polar solvents reduce the quantity of charge transfer between metal ions and donor ligand atoms. All the complexes showed considerable ligand-to-metal charge transfer interactions.

4.9 Natural bond orbital (NBO) analysis

NBO analysis was performed to explain the charge transfer [45] between herbacetin and metal ions in HER1-Zn^{2+} complex and the related data is given in **Table 4.9**. The stability scale for donor-accepter

interaction in complex is denoted by E(2) value. Higher the E(2) more stable will be the complex. The study revealed that the most favourable donor-acceptor interaction is due to the charge from lone pair of oxygen atoms of herbacetin to the anti-bonding orbital of metal ion, Zn^{2+}. The higher E(2) value of HER1- Zn^{2+} indicate the strong interaction of herbacetin molecule with Zn^{2+} ion among all other complexes. In each HERN-Zn^{2+} complexes, interaction of donor atoms with Zn^{2+} ion is found be in CCl4>toluene >acetone>DMSO media, which is in good agreement with the interaction energy.

Table 4.9. The computed E(2) value (in kcal/mol) of HER1-M^{2+} complexes from NBO analysis

Complex	Charge transfer	E(2) (kcal/mol)			
		DMSO	Acetone	CCl$_4$	Toluene
HER1- Zn^{2+}	LP(O4) → LP*Zn31	35.88	37.28	54.21	53.27
	LP(O6) → LP*Zn31	32.63	34.07	50.15	49.30
HER2- Zn^{2+}	LP(O2) → LP*Zn31	30.33	31.79	32.09	27.04
	LP(O5) → LP*Zn31	15.13	17.30	37.02	35.98
HER3- Zn^{2+}	LP(O3) → LP*Zn31	33.47	34.89	44.81	44.85
	LP(O5) → LP*Zn31	22.98	24.75	41.79	40.93

4.10 Quantum theory of atoms in molecules (QTAIM)

QTAIM analysis at the bond critical points (BCPs) in gas and DMSO medium was done to characterize the nature of interactions between herbacetin and metal ions [46]. The AIM results of HER1-Zn^{2+}, HER2-Zn^{2+}, and HER3-Zn^{2+} are provided in **Tables 4.10** , **4.11**

and **4.12** respectively. A stronger interaction corresponds to an increase in electron density ($\rho(r)$) at the BCP. The value of M-O electron density in the HERN-Zn^{2+} complexes indicate that Zn^{2+} and herbacetin interact more in CCl_4 solvent and less interacted in DMSO medium which perfectly correlate with the interaction energy values. The estimated $\rho(r)$ values of the complexes also suggest that herbacetin-metal interaction in HER1-Zn^{2+} through the O4 is greater than O6 in all the selected media. The electron density values show that Zn^{2+} interacts more with O2 in the HER2-Zn^{2+}complex where as with O3 in the HER3-Zn^{2+}complex, which is in good agreement with the previously mentioned interaction distances. The Laplacian electron density $\nabla^2 \rho(\mathbf{r}) > 0$ and the hypothesized ratio of kinetic energy density (G(r)) to potential energy density (V(r)) at the BCP $0.5 < -G(\mathbf{r})/V(\mathbf{r}) < 1$, the interactions are partially or partly covalent [47]. From the table, the positive $\nabla^2 \rho(r)$ of M-O bonds in all the complexes indicate their non-covalent nature. Furthermore, the hypothesised ratio of kinetic energy density (G(r)) to potential energy density (V(r)) at the BCP is employed to characterise the type of interaction. The ratio of -G(r)/V(r) for M-O bond is close to one in all complexes indicate the electrostatic interaction [30]. Covalent interaction is characterised by higher ELF and LOL values, while electrostatic interaction is characterised by lower ELF and LOL values [34]. The small values of ELF and LOL again confirm the electrostatic interaction of M-O bonds in all the complexes. The topological view of ELF plot of HER1-Zn^{2+}, HER2-Zn^{2+}, HER3-Zn^{2+} is shown in **Figs. 4.7, 4.8** and **4.9** respectively. **Figs. 4.10, 4.11** and **4.12** shows the topological view of LOL of HER1-Zn^{2+}, HER2-Zn^{2+}, and HER3-Zn^{2+} respectively.

Table 4.10. Calculated topological parameters (in a.u) at the BCPs of M-O bonds HER1-Zn^{2+}

Complex	Bond	Solvent	$\rho(r)$	$\nabla^2\rho(r)$	-G(r)/$V(r)$	ELF	LOL
HER1-Zn^{2+} HER1-Zn^{2+}	Zn-O4	DMSO	0.078	0.441	0.873	0.130	0.277
		Acetone	0.079	0.448	0.872	0.132	0.279
		CCl$_4$	0.090	0.516	0.862	0.146	0.291
		Toluene	0.089	0.513	0.862	0.145	0.290
	Zn-O6 Zn-O6	DMSO	0.076	0.424	0.874	0.127	0.275
		Acetone	0.077	0.433	0.873	0.129	0.276
		CCl4	0.088	0.501	0.862	0.144	0.289
		Toluene	0.087	0.498	0.863	0.143	0.289

Table 4.11. Calculated topological parameters (in a.u) at the BCPs of M-O bonds of HER2-Zn^{2+}

Complex	Bond	Solvent	$\rho(r)$	$\nabla^2\rho(r)$	-G(r)/$V(r)$	ELF	LOL
HER2-Zn^{2+}	Zn-O2	DMSO	0.076	0.433	0.879	0.125	0.273
		Acetone	0.077	0.438	0.878	0.127	0.274
		CCl$_4$	0.089	0.523	0.867	0.143	0.288
		Toluene	0.089	0.520	0.868	0.142	0.287
	Zn-O5	DMSO	0.060	0.315	0.875	0.108	0.257
		Acetone	0.063	0.333	0.876	0.111	0.260
		CCl4	0.078	0.444	0.872	0.130	0.277
		Toluene	0.078	0.439	0.872	0.129	0.276

Table 4.12. Calculated topological parameters (in a.u) at the BCPs of M-O bonds of HER3-Zn^{2+}

Complex	Bond	Solvent	$\rho(r)$	$\nabla^2 \rho(r)$	-G(r)/V(r)	ELF	LOL
HER3-Zn^{2+}	Zn-O3	DMSO	0.080	0.490	0.891	0.120	0268
		Acetone	0.081	0.497	0.890	0.122	0.270
		CCl$_4$	0.095	0.597	0.876	0.140	0.285
		Toluene	0.095	0.592	0.877	0.139	0.285
	Zn-O5	DMSO	0.069	0.410	0.895	0.108	0.256
		Acetone	0.071	0.422	0.894	0.110	0.258
		CCl4	0.085	0.521	0.885	0.127	0.274
		Toluene	0.084	0.517	0.885	0.126	0.274
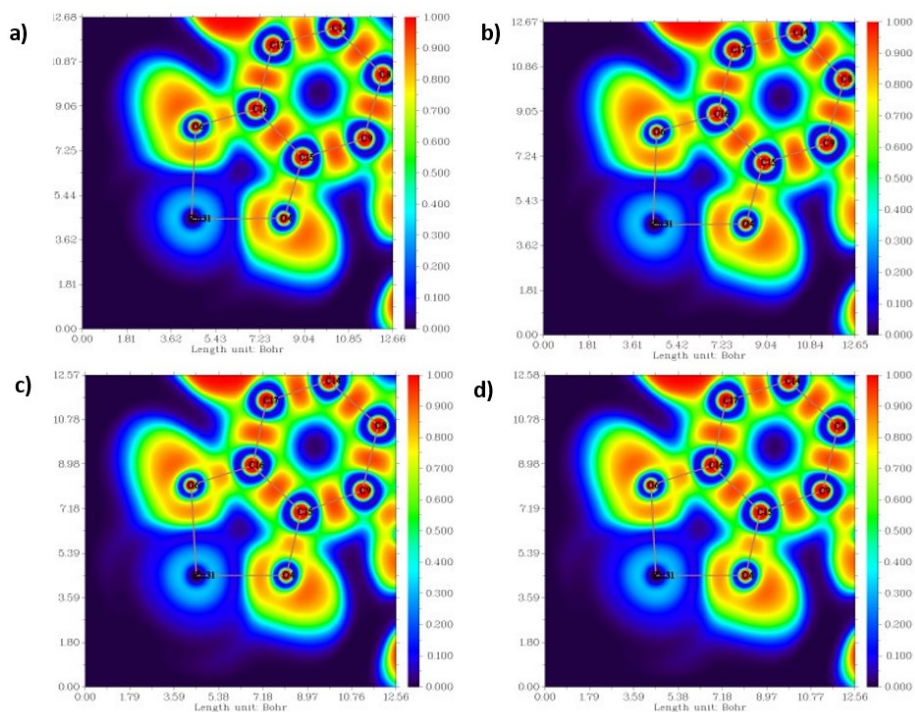
Fig. 4.7. ELF plots of the metal-oxygen interactions of HER1-Zn^{2+} in **a)** DMSO, **b)** acetone, **c)** CCl4, **d)** toluene
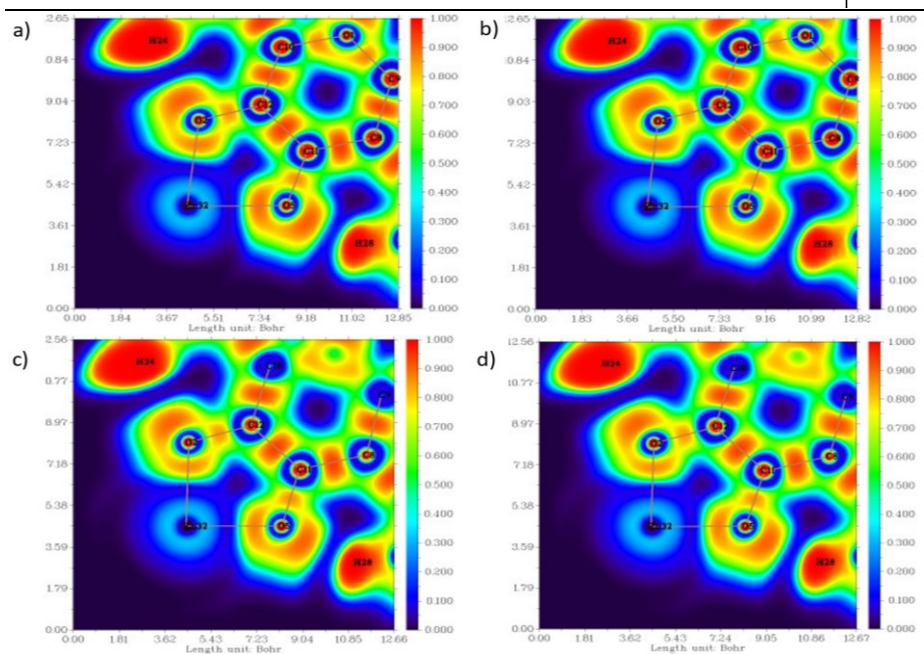
Fig. 4.8. ELF plots of the metal-oxygen interactions of HER2-Zn^{2+} in **a)** DMSO, **b)** acetone, **c)** CCl4, **d)** toluene
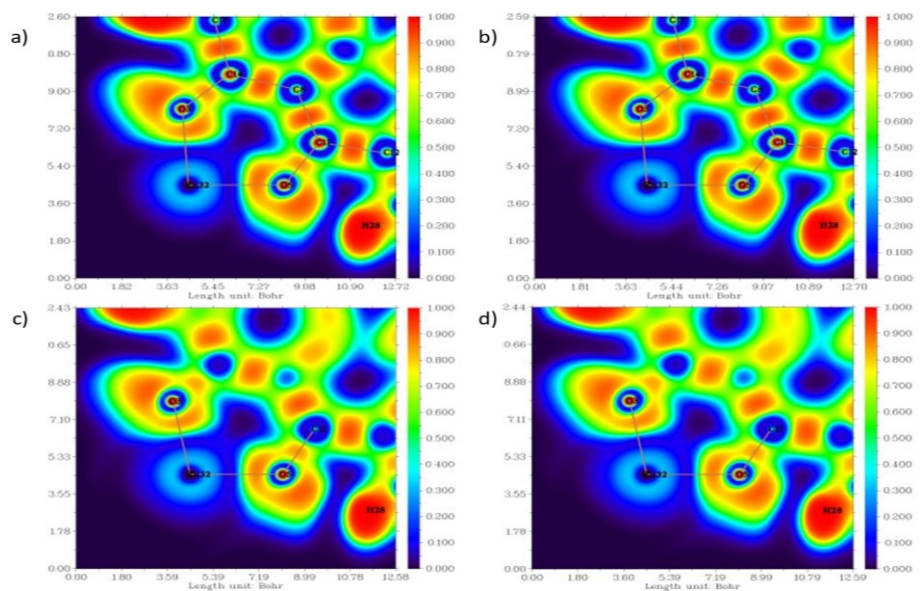
Fig. 4.9. ELF plots of the metal-oxygen interactions of HER3-Zn^{2+} in **a)** DMSO, **b)** acetone, **c)** CCl4, **d)** toluene
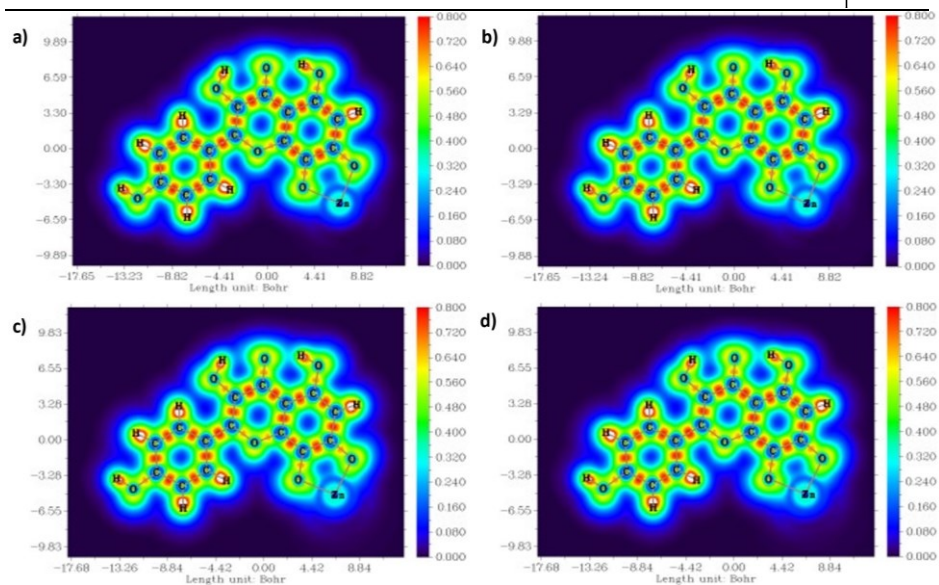
Fig. 4.10. LOL plots of the metal-oxygen interactions of HER1-Zn^{2+} in **a)** DMSO, **b)** acetone, **c)** CCl4, **d)** toluene
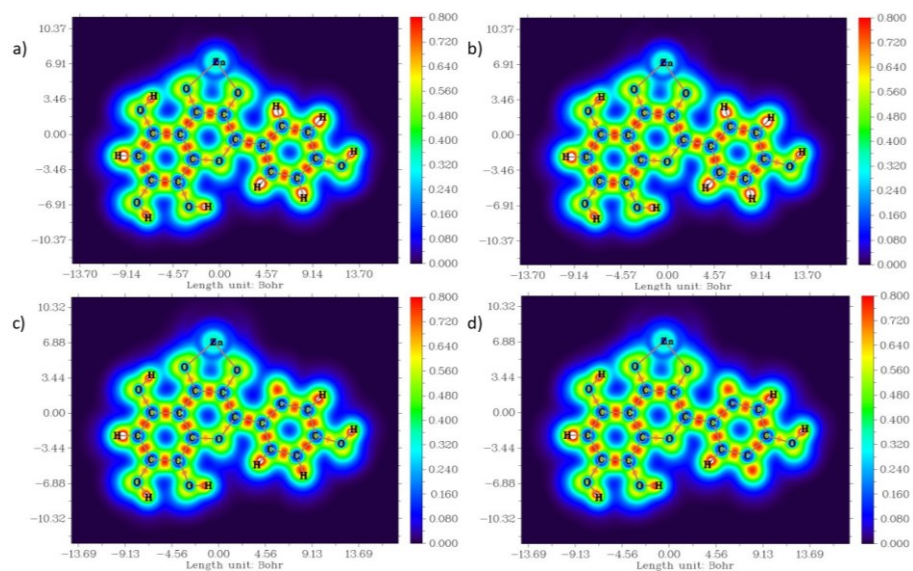
Fig. 4.11. LOL plots of the metal-oxygen interactions of HER2-Zn^{2+} in **a)** DMSO, **b)** acetone, **c)** CCl4, **d)** toluene
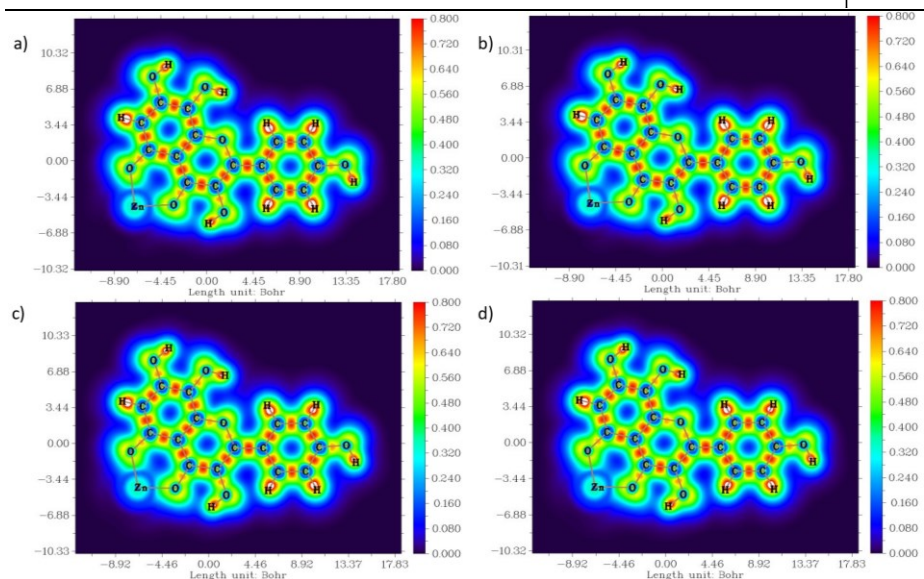
Fig. 4.12. LOL plots of the metal-oxygen interactions of HER3-Zn^{2+} in **a)** DMSO, **b)** acetone, **c)** CCl4, **d)** toluene

4.11 Effect on metal ions on the anti-oxidant activity of herbacetin

Herbacetin is an effective free radical scavenger, and this free radical scavenging ability is thought to be responsible for its antioxidant activity. Even though, the metal ions are complexed at the hydroxyl groups of herbacetin and the other phenolic OH groups remain intact, it is claimed that the complex, in addition to parent herbacetin, can participate in free-radical scavenging activities. In order to understand the effect of metal ion on the anti-oxidant activity of herbacetin molecule, we have calculated all the numerical parameters (bond dissociation enthalpy (BDE), ionisation potential (IP), proton dissociation enthalpy (PDE), proton affinity (PA), electron transfer enthalpy (ETE)) associated with the possible anti-oxidant mechanisms, hydrogen atom transfer (HAT), single-electron transfer followed by

proton transfer (SET-PT) and sequential proton loss electron transfer (SPLET) [48, 49].

Table 4.13. Numerical parameters associated with anti-oxidant mechanism of herbacetin

Radical	Solvent	Hydroxyl group	BDE	AIP	PDE	PA	ETE
•OH	DMSO	12-OH	-31.91	48.36	-80.27	-45.80	13.89
		14-OH	-22.22	48.36	-70.58	-39.94	17.73
		15-OH	-37.64	48.36	-86.00	-49.71	12.07
		16-OH	-27.12	48.36	-75.48	-49.08	21.96
		22-OH	-28.25	48.36	-76.62	-47.20	18.95
	Toluene	12-OH	-28.53	95.70	-124.2	-60.52	31.99
		14-OH	-17.83	95.70	-113.5	-52.14	34.31
		15-OH	-37.51	95.70	-133.2	-65.66	28.15
		16-OH	-24.31	95.70	-120.01	-63.70	39.39
		22-OH	-27.09	95.70	-122.80	-66.17	39.07
	CCl4	12-OH	-28.35	98.98	-127.33	-61.60	33.25
		14-OH	-17.61	98.98	-116.60	-53.10	35.49
		15-OH	-37.47	98.98	-136.44	-66.78	29.31
		16-OH	-24.13	98.98	-123.1	-64.75	40.63
		22-OH	-27.03	98.98	-126.00	-67.42	39.39
	Acetone	12-OH	-31.6	51.71	-83.31	-46.63	15.03
		14-OH	-21.82	51.71	-73.53	-40.62	18.80
		15-OH	-37.58	51.71	-89.29	-50.69	13.11
		16-OH	-26.83	51.71	-78.54	-49.35	22.52
		22-OH	-27.56	51.71	-79.27	-48.38	20.82
•OOH	DMSO	12-OH	1.017	50.64	-49.63	-15.15	16.17
		14-OH	10.71	50.64	-39.93	-9.296	20.00
		15-OH	-4.713	50.64	-55.35	-19.06	14.35
		16-OH	5.805	50.64	-44.84	-18.44	24.24
		22-OH	4.672	50.64	-45.97	-16.56	21.23
	Toluene	12-OH	6.013	94.93	-88.92	-25.21	31.22
		14-OH	16.71	94.93	-78.22	-16.82	33.53
		15-OH	-2.971	94.93	-97.90	-30.35	27.38
		16-OH	10.23	94.93	-84.70	-28.39	38.62
		22-OH	7.446	94.93	-87.49	-30.86	38.30

	CCl4	12-OH	6.264	97.97	-91.71	-25.98	32.24
		14-OH	17.01	97.97	-80.97	-17.48	34.49
		15-OH	-2.85	97.97	-100.8	-31.15	28.31
		16-OH	10.49	97.97	-87.48	-29.13	39.62
		22-OH	7.59	97.97	-90.38	-31.80	39.39
	Acetone	12-OH	1.47	53.81	-52.33	-15.65	17.13
		14-OH	11.25	53.81	-42.55	-9.642	20.92
		15-OH	-4.50	53.81	-58.31	-19.71	15.21
		16-OH	6.25	53.81	-47.56	-18.37	24.62
		22-OH	5.51	53.81	-48.29	-17.40	22.92

The numerical values of herbacetin associated with all the possible anti-oxidant mechanisms are given in **Table 4.13**. The findings demonstrate that the parameters governing the three mechanisms are of vastly different magnitudes, and this evidence can be used to determine which anti-oxidant mechanism is preferred over the others. For describing the HAT mechanism, the BDE is the most trustworthy thermodynamic parameter and this approach includes the transfer of a H atom from an antioxidant's hydroxyl group to a free radical [50]. The lowest BDE is associated with higher radical scavenging activity[51]. Although BDE values are negative for the scavenging of •OH and •OOH, the more negative value of •OH than other radical values, indicating that herbacetin is a more effective radical scavenger for •OH than for •OOH. Herbacetin is a better radical scavenger through the HAT mechanism in polar media than in non-polar medium, according to the BDE values, which indicate a small preference for the scavenging of radical species in DMSO and acetone medium compared to CCl4 and toluene medium. The lowest BDE value of 15-OH of

herbacetin (in all the solvents) indicates its strong anti-oxidant effect compared to the other phenolic OH groups.

In SET-PT, one electron is transferred from the antioxidant to the free radical, resulting in the creation of a radical cation, which is then deprotonated. The most essential parameters in determining this mechanism's feasibility are IP and PDE. The higher electron donating capacity is associated with low IP value [52]. Since the single electron transfer step in the SET-PT mechanism is much slower than the proton transfer step, the SET step is regarded as the rate-determining step for the entire mechanism. Since the AIP values are all positive in every media, the electron transfer step in the process must be endothermic. Since the AIP values in DMSO and acetone are lower than those in CCl_4 and toluene, the SET-PT mechanism is more efficient in a medium with high polarity than one with low polarity. Furthermore, AIP values also suggest that herbacetin prefers to scavenge •OH in DMSO and acetone media were as •OOH in CCl_4 and toluene through the SET-PT mechanism.

PA and ETE are the numerical parameters associated with SPLET mechanism [50]. **Table 4.13** makes it evident that the energy needed for the first step (PA) is significantly lower for scavenging •OH and •OOH in all solvents, which supports the choice of the SPLET mechanism over the HAT and SET-PT mechanisms for these radicals. The PA value indicates that herbacetin is more efficient in scavenging •OH than •OOH through the SPLET mechanism. It is also important to note that, the PA value is low for 15-OH in polar solvents were as 22-

OH in non-polar solvents. Additionally, compared to polar medium, the SPLET mechanism is favoured by non-polar medium.

In the current study we have also investigated the anti-oxidant activity of more stable herbacetin-Zn^{2+}complex (HER1-Zn^{2+}) in DMSO, acetone, CCl_4 and toluene solvents and the corresponding numerical parameters are given in **Table 4.14**. The HER1-Zn^{2+} contain three free OH groups (12-OH, 14-OH and 22-OH) in its structure. These OH groups have improved anti-oxidant activity as a result of metal chelation, as evidenced by the fact that their BDE values are lower than those of the corresponding OH groups of un-complexed herbacetin molecule. Among the hydroxyl groups, 12-OH showed lowest BDE value hence high radical scavenging capacity in all the solvents irrespective of their nature. It's worth to mention that low BDE value for •OH than •OOH is related to the potential scavenging of •OH over •OOH radical. Additionally, it has been revealed that the HAT mechanism prefers polar environments over non-polar environments. As in the case of SET-PT mechanism, the positive value of AIP appears to rule out the possibility of the described process occurring in all the selected media. However, it is evident from AIP values that the SET-PT mechanism is more effective in polar solvents like DMSO and acetone than in non-polar solvents like CCl4 and toluene. Much like the herbacetin molecule, HER1-Zn2+ also favours to scavenge •OH in DMSO and acetone media and •OOH in CCl4 and toluene scavenge by means of the SET-PT mechanism. The AIP values of HER1-Zn^{2+} in both the medium were found to be lower than

herbacetin molecule indicating that the chelated complexes are more active in radical scavenging activity than the isolated one.

The energy required to complete the first step of SPLET reaction (PA) is significantly lower than those required by the HAT and SET-PT mechanisms, implying that this is the most preferable anti-oxidant mechanism. In this mechanism, 22-OH demonstrated the lowest PA value in all solvents, indicating a higher antioxidative capability. The enhancement in anti-oxidant activity brought on by metal chelation was readily explained by the PA values. The SPLET mechanism is more favourable in non-polar media than polar medium, same like in the herbacetin molecule.

Table 4.14. Nnumerical parameters associated with anti-oxidant mechanism of HER1-Zn^{2+} complex

Radical	Solvents	Hydroxyl group	BDE	AIP	PDE	PA	ETE
•OH	DMSO	12-OH	-35.53	27.27	-62.79	-46.86	11.33
		14-OH	-30.82	27.27	-58.09	-35.94	5.12
		22-OH	-30.31	27.27	-57.58	-50.18	19.87
	Acetone	12-OH	-34.71	30.98	-65.69	-47.22	12.51
		14-OH	-30.44	30.98	-61.42	-36.81	6.37
		22-OH	-29.76	30.98	-60.74	-50.96	21.21
	CCl4	12-OH	-28.90	83.88	-112.78	-59.85	30.95
		14-OH	-20.76	83.88	-104.64	-47.57	26.81
		22-OH	-27.18	83.88	-111.06	-65.49	38.32
	Toluene	12-OH	-29.18	80.30	-109.49	-55.57	26.38
		14-OH	-21.81	80.30	-102.11	-46.47	24.67
		22-OH	-27.29	80.30	-107.59	-64.42	37.13
•OOH	DMSO	12-OH	-2.60	29.54	-32.15	-16.21	13.61
		14-OH	2.11	29.54	-27.44	-5.295	7.40
		22-OH	2.62	29.54	-26.93	-19.54	22.15
	Acetone	12-OH	-1.63	33.08	-34.71	-16.24	14.61
		14-OH	2.70	33.08	-30.44	-5.828	8.47
		22-OH	3.32	33.08	-29.76	-19.98	23.3

	CCl4	12-OH	5.72	82.88	-77.16	-24.23	29.95
		14-OH	13.86	82.88	-69.02	-11.95	25.81
		22-OH	7.44	82.88	-75.44	-29.87	37.32
	Toluene	12-OH	5.36	79.53	-74.17	-20.26	25.61
		14-OH	12.73	79.53	-66.80	-11.16	23.9
		22-OH	7.26	79.53	-72.28	-29.11	36.36

4.12 Molecular docking

Docking studies were conducted with the herbacetin molecule to assess its qualified binding poses within the selected target proteins, AChE2, and BChE. For AChE2, and BChE, tacrine [53] was chosen as a control ligand. Herbacetin presented good binding interaction with all the selected target proteins which were comparable with the well-known standard drug tacrine. Molecular docking studies showed that herbacetin possessed a negative binding energy value -9.0 kcal/mol and -9.6 kcal/mol with AChE2 and BChE respectively which indicate the stability of the complex. Interestingly these binding affinity values were higher than that of tacrine with AChE2 (-8.6 kcal/mol) and BChE (-8.2 kcal/mol). **Figs. 4.13. a), b), c) and d)** shows the 3D image of herbacetin-AChE2 complex, interaction analysis of herbacetin-AChE2 complex, 3D images of herbacetin-BChE complex, and the interaction analysis of herbacetin-BChE complex respectively.
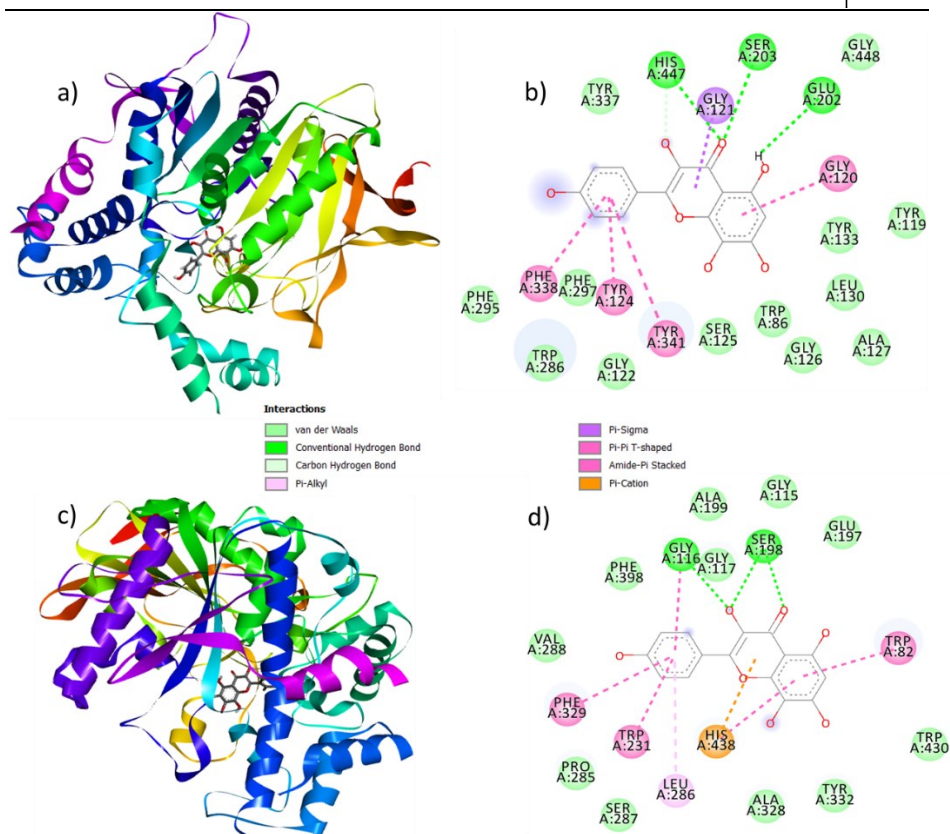
Fig. 4.13. a) 3D Structure of herbacetin-AChE2 complex, **b)** interaction diagram of herbacetin-AChE2 complex, **c)** 3D structure of herbacetin-BChE complex, **d)** interaction diagram of herbacetin-BChE complex obtained using Discovery Studio Visualizer

The interaction analysis revealed that, herbacetin shows conventional hydrogen bonds, pi-sigma, pi-pi T shaped, amide pi stacked and van der Waals interactions with neighbouring amino acid residues of AChE2 protein. In particular, residues GLU202, SER203, and HIS447 were formed three hydrogen bonds with herbacetin molecule. A pi-sigma was observed between the GLY121 and pi electron cloud of the molecule. Apart from that, two types of molecular interactions were formed *via* pi-pi T shaped interaction with residues

TYR124, PHE338, and TYR341 and amide pi stacked interaction with GLY120. The molecule is well interacted with amino acid residues, TYR337, GLY448, TYR133, ALA127, LEU130, GLY126, TRP86, SER125, PHE297, and PHE295, through van der Waals interactions. Herbacetin was found to be involved in hydrogen bonding interaction with the residues, SER198, and GLY116 of BChE. A significant number of van der Waals interactions were observed between herbacetin and BChE. Precisely, amino acid residues, ALA328, TYR332, TRP430, GLU197, GLY115, ALA199, GLY117, PHE398, and VAL288. The amino acid residue, HIS438 possessed a pi-cation interaction with the molecule. Few other residues, TRP82, PHE329, and TRP231 participated in pi-pi T shaped interaction. A pi- alkyl interaction was found between LEU82 with herbacetin molecule. It was also noted that the molecule formed van der Waals interactions with the aminoacid residues, ALA328, TYR332, TRP430, GLU197, GLY115, ALA199, GLY117, PHE398, and VAL288 within the active site.

4.13 *In-silico* ADME and drug-likeness prediction

The ADME analysis is a crucial step in weeding out a few interesting chemical entities from a vast chemical dataset. The ADME profile of the herbacetin molecule was thus be predicted using SwissADME, which is publically available at http://www.swissadme.ch [54]. Molecular weight, lipophilicity, water solubility, as well as Lipinski's rule of five [55] of herbacetin molecule are given in **Table 4.15**. Orally active drugs must follow the Lipinski five rule, which states that molecular weight (MW) should not exceed 500 g/mol, hydrogen bond acceptors (HBA) should not exceed 10, hydrogen bond

donors (HBD) should not exceed 5, LogP value should not exceed 5, and the number of rotatable bonds should not be less than 10, with a violation of two or more rules indicating that the molecule is not orally active. The molecular weight of herbacetin was 302.24 g/mol and it comes within the limit 500 g/mol according to Lipinski rule. The logP value of the herbacetin was less than 5, ranging from -0.56 to 2.17. The HBA number was 7 and less than 10; the number of HBD atoms was 5. Hence herbacetin follow Lipinski five rule with no violation. According to aqueous solubility methods, log S (ESOL), log S (ALI), and log S (SILICOS-IT), herbacetin is soluble in water.

Table 4.15. Molecular weight, lipophilicity, water solubility, as well as Lipinski's rule of five of herbacetin molecule

Molecule	Molecular weight (g/mol)	Number of hydrogen bond acceptors	Number of hydrogen bond donors	Log P	Log S (ESOL)	Log S (ALI)	Log S (SILICOS-IT)
Herbacetin	302.24	7	5	1.5	-3.55	-4.56	-3.24

Conclusion

The chelating ability of herbacetin molecule with Zn^{2+} in both polar (DMSO and acetone) and non-polar solvents(CCl_4 and toluene) were analyzed. FMO analysis shows that the HOMO-LUMO gap of all the complexes are less than that of herbacetin, indicating the increased chemical reactivity due to complexation. Among the three possible chelation sites, HER1-Zn^{2+} identified as the best site for Zn^{2+} ion in all the solvents. The interaction energy analysis showed that, HER1-Zn^{2+} is more stable in non-polar solvents than in polar solvents. Natural

population analysis explained the charge transfer between the oxygen atoms of herbacetin and metal ions. QTAIM, ELF, and LOL supported the partially covalent electrostatic interaction between herbacetin and metal ions. The SPLET mechanism is thought to be the most effective way for herbacetin to scavenge •OH and •OOH, according to an analysis of the many thermodynamic energy factors connected to various potential antioxidant mechanisms. Herbacetin's ability to scavenge •OH is stronger than its ability to scavenge •OOH, and the antiradical mechanism is strengthened in nonpolar media as compared to polar medium. The investigation of the antioxidant properties of herbacetin-Zn^{2+} complexes showed the enhanced anti-oxidant activity of phenolic groups due to metal chelation. HERN-Zn^{2+}complexes are found to follow the SPLET mechanism, which was found to be more effective in non-polar media than polar ones, just as the herbacetin molecule. Molecular docking studies showed that herbacetin could act as an anti-cholinesterase agent. Both the metal chelation as well as molecular docking studies theoretically explains the anti-Alzheimer's property of the phytochemical herbacetin. More interestingly, an outstanding bioactivity score of 0.55 was obtained for the herbacetin molecule using the Swiss ADME online programme. This study thus proves the potential of phytochemicals in the pharmaceutical field. Similar studies are anticipated to improve the understanding of bio-activity of existing phytochemicals and bring up novel potential molecules for similar applications.

References

1. Lincoln KM, Richardson TE, Rutter L, Gonzalez P, Simpkins JW, Green KN: **An N-heterocyclic amine chelate capable of antioxidant capacity and amyloid disaggregation**. *ACS Chem Neurosci* 2012, **3**(11):919-927.

2. Hong H, Kim BS, Im H-I: **Pathophysiological role of neuroinflammation in neurodegenerative diseases and psychiatric disorders**. *Int Neurourol J* 2016, **20**(Suppl 1):S2.

3. Crous-Bou M, Minguillón C, Gramunt N, Molinuevo JL: **Alzheimer's disease prevention: from risk factors to early intervention**. *Alzheimers Res Ther* 2017, **9**(1):1-9.

4. Bachurin SO, Bovina EV, Ustyugov AA: **Drugs in clinical trials for Alzheimer's disease: the major trends**. *Med Res Rev* 2017, **37**(5):1186-1225.

5. Girek M, Szymański P: **Tacrine hybrids as multi-target-directed ligands in Alzheimer's disease: Influence of chemical structures on biological activities**. *Chemical Papers* 2019, **73**(2):269-289.

6. Loveman E, Green C, Kirby J, Takeda A, Picot J, Payne E, Clegg A: **The clinical and cost-effectiveness of donepezil, rivastigmine, galantamine and memantine for Alzheimer's disease**. *Health Technology Assessment (Winchester, England)* 2006, **10**(1):iii-iv, ix.

7. Soto C: **Unfolding the role of protein misfolding in neurodegenerative diseases**. *Nature Reviews Neuroscience* 2003, **4**(1):49-60.

8. Drago D, Bolognin S, Zatta P: **Role of metal ions in the Aβ oligomerization in Alzheimer's disease and in other neurological disorders**. *Current Alzheimer Research* 2008, **5**(6):500-507.

9. Molina-Holgado F, Hider RC, Gaeta A, Williams R, Francis P: **Metals ions and neurodegeneration**. *BioMetals* 2007, **20**(3):639-654.

10. Rivera-Mancía S, Pérez-Neri I, Ríos C, Tristán-López L, Rivera-Espinosa L, Montes S: **The transition metals copper and iron in**

neurodegenerative diseases. *Chem Biol Interact* 2010, **186**(2):184-199.

11. Marino T, Pavelka M, Toscano M, Russo N: **Structural and binding properties of metal ion chelators relevant to Alzheimer's disease. A theoretical investigation**. *Int J Quantum Chem* 2012, **112**(9):2109-2114.

12. Mladěnka P, Macáková K, Filipský T, Zatloukalová L, Jahodář L, Bovicelli P, Silvestri IP, Hrdina R, Saso L: **In vitro analysis of iron chelating activity of flavonoids**. *J Inorg Biochem* 2011, **105**(5):693-701.

13. Perron NR, Brumaghim JL: **A review of the antioxidant mechanisms of polyphenol compounds related to iron binding**. *Cell Biochem Biophys* 2009, **53**(2):75-100.

14. Fouegue Tamafo AD, Ghogomu JN, Nkungli NK, Bikélé Mama D, Younang E: **Quantum chemical investigation on the antioxidant activity of neutral and anionic forms of Juglone: metal chelation and its effect on radical scavenging activity**. *Journal of Chemistry* 2017, **2017**.

15. Hussein SA, Barakat HH, Nawar MA, Willuhn G: **Flavonoids from Ephedra aphylla**. *Phytochemistry* 1997, **45**(7):1529-1532.

16. Péter Zomborszki Z, Kúsz N, Csupor D, Peschel W: **Rhodiosin and herbacetin in Rhodiola rosea preparations: additional markers for quality control?** *Pharm Biol* 2019, **57**(1):295-305.

17. Fliniaux O, Corbin C, Ramsay A, Renouard S, Beejmohun V, Doussot J, Falguières A, Ferroud C, Lamblin F, Lainé E: **Microwave-assisted extraction of herbacetin diglucoside from flax (Linum usitatissimum L.) seed cakes and its quantification using an RP-HPLC-UV system**. *Molecules* 2014, **19**(3):3025-3037.

18. Biao Y, Jiannan H, Yaolan C, Shujie C, Dechun H, Mcclements DJ, Chongjiang C: **Identification and characterization of antioxidant and immune-stimulatory polysaccharides in flaxseed hull**. *Food Chem* 2020, **315**:126266.

19. Deshpande R, Raina P, Shinde K, Mansara P, Karandikar M, Kaul-Ghanekar R: **Flax seed oil reduced tumor growth, modulated immune responses and decreased HPV E6 and E7 oncoprotein expression in a murine model of ectopic cervical cancer**. *Prostaglandins & other lipid mediators* 2019, **143**:106332.

20. Liang S, Li X, Ma X, Li A, Wang Y, Reaney MJ, Shim YY: **A flaxseed heteropolysaccharide stimulates immune responses and inhibits hepatitis B virus**. *International journal of biological macromolecules* 2019, **136**:230-240.

21. Limanaqi F, Biagioni F, Busceti CL, Polzella M, Fabrizi C, Fornai F: **Potential antidepressant effects of Scutellaria baicalensis, Hericium erinaceus and Rhodiola rosea**. *Antioxidants* 2020, **9**(3):234.

22. LIU SH, HSIAO YW, Chong E, Singhal R, FONG MC, TSAI YN, HSU CP, CHEN YC, CHEN YJ, CHIOU CW: **Rhodiola inhibits atrial arrhythmogenesis in a heart failure model**. *J Cardiovasc Electrophysiol* 2016, **27**(9):1093-1101.

23. Zhang X, Zhu J, Yan J, Xiao Y, Yang R, Huang R, Zhou J, Wang Z, Xiao W, Zheng C: **Systems pharmacology unravels the synergic target space and therapeutic potential of Rhodiola rosea L. for non-small cell lung cancer**. *Phytomedicine* 2020, **79**:153326.

24. Bifulco G, Dambruoso P, Gomez-Paloma L, Riccio R: **Determination of relative configuration in organic compounds by NMR spectroscopy and computational methods**. *Chem Rev* 2007, **107**(9):3744-3779.

25. Wyrzykowski D, Hebanowska E, Nowak-Wiczk G, Makowski M, Chmurzyński L: **Thermal behaviour of citric acid and isomeric aconitic acids**. *J Therm Anal Calorim* 2011, **104**(2):731-735.

26. Hu W-P, Huang C-H: **The intrinsic stability of the noble gas-coordinated transition-metal complex ions**. *Journal of the American Chemical Society* 2001, **123**(10):2340-2343.

27. Alexander BD, Dines TJ: ***Ab initio* calculations of the structures and vibrational spectra of ethene complexes**. *The Journal of Physical Chemistry A* 2004, **108**(1):146-156.

28. Tomasi J, Mennucci B, Cammi R: **Quantum mechanical continuum solvation models**. *Chem Rev* 2005, **105**(8):2999-3094.

29. Kaviani S, Izadyar M: **The possibility of iron chelation therapy in the presence of different HPOs; a molecular approach to the non-covalent interactions and binding energies**. *J Mol Struct* 2018, **1166**:448-455.

30. Reed AE, Curtiss LA, Weinhold F: **Intermolecular interactions from a natural bond orbital, donor-acceptor viewpoint**. *Chem Rev* 1988, **88**(6):899-926.

31. Mary CPV, Vijayakumar S, Shankar R: **Metal chelating ability and antioxidant properties of Curcumin-metal complexes–A DFT approach**. *J Mol Graphics Modell* 2018, **79**:1-14.

32. Ahamed TS, Rajan VK, Sabira K, Muraleedharan K: **DFT and QTAIM based investigation on the structure and antioxidant behavior of lichen substances Atranorin, Evernic acid and Diffractaic acid**. *Comput Biol Chem* 2019, **80**:66-78.

33. Hou X-J, Gopakumar G, Lievens P, Nguyen MT: **Chromium-doped germanium clusters CrGe n (n= 1− 5): geometry, electronic structure, and topology of chemical bonding**. *The Journal of Physical Chemistry A* 2007, **111**(51):13544-13553.

34. Kaviani S, Shahab S, Sheikhi M, Ahmadianarog M: **DFT study on the selective complexation of meso-2, 3-dimercaptosuccinic acid with toxic metal ions (Cd2+, Hg2+ and Pb2+) for pharmaceutical and biological applications**. *J Mol Struct* 2019, **1176**:901-907.

35. Janani S, Rajagopal H, Muthu S, Aayisha S, Raja M: **Molecular structure, spectroscopic (FT-IR, FT-Raman, NMR), HOMO-LUMO, chemical reactivity, AIM, ELF, LOL and Molecular docking studies on 1-Benzyl-4-(N-Boc-amino) piperidine**. *J Mol Struct* 2021, **1230**:129657.

36. SangeethaMargreat S, Ramalingam S, Al-Maqtari HM, Jamalis J, Sebastian S, Periandy S, Xavier S: **Synthesis, spectroscopic, quantum computation, electronic, AIM, Wavefunction (ELF, LOL) and Molecular Docking investigation on (E)-1-(2, 5-**

dichlorothiophen-3-yl)-3-(thiophen-2-yl)-2-propen-1-one. *Chemical Data Collections* 2021, **33**:100701.

37.   Madala NE, Kabanda MM: **LC-MS based validation and DFT investigation on the antioxidant properties of clovamide:• OH and• OOH scavenging and Cu (II) chelation mechanisms**. *J Mol Struct* 2021, **1236**:130349.

38.   Puthanveedu V, Muraleedharan K: **Phytochemicals as Potential Inhibitors for COVID-19 Revealed by Molecular Docking, Molecular Dynamic Simulation and DFT Studies**. Structural Chemistry 2022 33:1423–1443.

39.   Nogara PA, Saraiva RdA, Caeran Bueno D, Lissner LJ, Lenz Dalla Corte C, Braga MM, Rosemberg DB, Rocha JBT: **Virtual screening of acetylcholinesterase inhibitors using the Lipinski's rule of five and ZINC databank**. *BioMed research international* 2015, **2015**.

40.   Saral A, Sudha P, Muthu S, Sevvanthi S, Irfan A: **Molecular structure spectroscopic Elucidation, IEFPCM solvation (UV–Vis, MEP, FMO, NBO, NLO), molecular docking and biological assessment studies of lepidine (4-Methylquinoline)**. *J Mol Liq* 2022, **345**:118249.

41.   Prasana JC, Muthu S, Abraham CS: **Molecular docking studies, charge transfer excitation and wave function analyses (ESP, ELF, LOL) on valacyclovir: a potential antiviral drug**. *Comput Biol Chem* 2019, **78**:9-17.

42.   Wazzan NA, Al-Qurashi OS, Faidallah HM: **DFT/and TD-DFT/PCM calculations of molecular structure, spectroscopic characterization, NLO and NBO analyses of 4-(4-chlorophenyl) and 4-[4-(dimethylamino) phenyl]-2-oxo-1, 2, 5, 6-tetrahydrobenzo [h] quinoline-3-carbonitrile dyes**. *J Mol Liq* 2016, **223**:29-47.

43.   Demircioğlu Z, Kaştaş ÇA, Büyükgüngör O: **Theoretical analysis (NBO, NPA, Mulliken Population Method) and molecular orbital studies (hardness, chemical potential, electrophilicity and Fukui function analysis) of (E)-2-((4-hydroxy-2-methylphenylimino) methyl)-3-methoxyphenol**. *J Mol Struct* 2015, **1091**:183-195.

44.   Kosar B, Albayrak C: **Spectroscopic investigations and quantum chemical computational study of (E)-4-methoxy-2-[(p-tolylimino) methyl] phenol**. *Spectrochimica Acta Part A: Molecular and Biomolecular Spectroscopy* 2011, **78**(1):160-167.

45.   Chaudhary AP, Shukla AK, Kant P: **Design, synthesis, antibacterial evaluation, molecular docking and computational study of 4-alkoxy/aryloxyphenyl cyclopropyl methane oxime derivatives**. *Comput Biol Chem* 2021, **91**:107434.

46.   Hossain MR, Hasan MM, Nishat M, Ahmed F, Ferdous T, Hossain MA: **DFT and QTAIM investigations of the adsorption of chlormethine anticancer drug on the exterior surface of pristine and transition metal functionalized boron nitride fullerene**. *J Mol Liq* 2021, **323**:114627.

47.   Kumar PSV, Raghavendra V, Subramanian V: **Bader's theory of atoms in molecules (AIM) and its applications to chemical bonding**. *Journal of Chemical Sciences* 2016, **128**(10):1527-1536.

48.   Farrokhnia M: **Density functional theory studies on the antioxidant mechanism and electronic properties of some bioactive marine meroterpenoids: Sargahydroquionic acid and sargachromanol**. *ACS omega* 2020, **5**(32):20382-20390.

49.   Reza Nazifi SM, Asgharshamsi MH, Dehkordi MM, Zborowski KK: **Antioxidant properties of Aloe vera components: a DFT theoretical evaluation**. *Free Radical Res* 2019, **53**(8):922-931.

50.   Puthanveedu V, Pulikkool C, Poonkottil N, Muraleedharan K: **Theoretical Probing to the Reactivity and Biological Effects of the Phytochemical, Coumestrol and its Derivatives**. *Chemical Physics Impact* 2022:100080.

51.   Ma Y, Feng Y, Diao T, Zeng W, Zuo Y: **Experimental and theoretical study on antioxidant activity of the four anthocyanins**. *J Mol Struct* 2020, **1204**:127509.

52.   Bendary E, Francis R, Ali H, Sarwat M, El Hady S: **Antioxidant and structure–activity relationships (SARs) of some phenolic and anilines compounds**. *Annals of Agricultural Sciences* 2013, **58**(2):173-181.

53.   Pohanka M, Kuca K, Kassa J: **New performance of biosensor technology for Alzheimer's disease drugs: in vitro comparison of tacrine and 7-methoxytacrine**. *Neuroendocrinology Letters* 2008, **29**(5):755.

54.   Daina A, Michielin O, Zoete V: **SwissADME: a free web tool to evaluate pharmacokinetics, drug-likeness and medicinal chemistry friendliness of small molecules**. *Sci Rep* 2017, **7**(1):1-13.

55.   Lipinski CA, Lombardo F, Dominy BW, Feeney PJ: **Experimental and computational approaches to estimate solubility and permeability in drug discovery and development settings**. *Adv Drug Del Rev* 1997, **23**(1-3):3-25.

Chapter 5

Study on structural detailing of gossypetin and its medicinal application in UV filtering, radical scavenging, and metal chelation open up through NCI, TD-DFT, QTAIM, ELF, and LOL analysis

Abstract

Density functional theory (DFT) computations were used to investigate gossypetin's antioxidant effects via $\cdot OH$, $\cdot OOH$, and $\cdot NO_2$ scavenging and Zn^{2+} chelation mechanisms in solvent phases. Intramolecular hydrogen bonding, which accounts for the stability of generated radicals, was explained using non-covalent interaction (NCI) analysis. Investigations have been done on three primary operating mechanisms, sequential proton loss electron transfer (SPLET), single electron transfer-proton transfer (SET-PT), and H-atom transfer (HAT). SPLET mechanism was found to be the most advantageous for the radical-scavenging activity for $\cdot OH$ and $\cdot OOH$ and HAT for $\cdot NO_2$ radicals. UV absorption in the region 200-400nm suggests that gossypetin can act as a UV filter and the nature of excitation was described by hole-electron analysis. The interaction energy analysis predicted the best chelation site in gossypetin. The bond critical point (BCP) analysis explained the electrostatic nature of donor-acceptor interaction. The influence of explicit solvent effects is also taken into account.

5.1 Introduction

Flavonoids are important classes of natural compounds belonging to a group of plant secondary metabolites with a polyphenolic structure that can be extensively found in various fruits and vegetables [1]. They are essential components in several nutraceuticals, pharmacological, medical, and cosmetic uses because they have a wide range of health-promoting benefits. This is due to their ability to control important cellular enzyme functions as well as their antioxidative, anti-inflammatory, anti-mutagenic, and anti-carcinogenic capabilities [2]. The majority of flavonoids' known effects are associated with their antioxidant characteristics, which can directly neutralize free radicals, block oxygen-reduction pathway enzymes, and sequester transitory metal cations. Hydroxyl functional groups in flavonoids are vital for their ability to scavenge free radicals or chelate redox active metal ions [3]. Chelation of metal ions by flavonoids is a natural technique to diminish or eliminate their undesired catalytic behaviour in ROS generation *via* Fenton-like chemistry; indeed, metal-flavonoid complexes are a viable alternative to manufactured chelators that can cause toxicity issues [4]. These characteristics inspired researchers to study the structure, biochemical functions, and evolution of polyphenols in the realm of pharmacology [5-8].

Over the past few decades, oxidation processes and the function of free radicals in living systems have drawn more attention [9-12]. Reactive oxygen species like superoxide and hydroxyl radicals are produced during the oxygen intake necessary for cell metabolism. Peroxyl radicals are produced when this species reacts with lipid

molecules, and they interact with nucleic acids and proteins to cause a variety of changes that ultimately alter their functional properties [13]. Similar to reactive oxygen species (ROS), reactive nitrogen species (RNS) result from interactions between free radicals produced by living things to build more durable species that have a variety of biological consequences [14]. These processes are known to contribute to the formation of several major ailments, including cancer, atherosclerosis, inflammatory, coronary heart diseases, and aging. Oxidative stress is caused by an imbalance between the generation of oxidant species and antioxidant defenses. In its more extreme form, oxidative stress may lead to widespread macromolecule oxidation and cell death [15]. Natural polyphenols are capable of delaying, inhibiting, or even stopping oxidative reactions through a variety of mechanisms, including chain breaking through the donation of hydrogen atoms or electrons that transform free radicals into more stable species, chelating metal ions involved in the production of reactive oxygen species, converting lipid peroxides into stable end products, and blocking the harmful effects of prooxidant enzymes [16].

Gossypetin (3,5,7,8,3',4'-hexahydroxy flavone) is one of the important components found in the blooms and calyx of Hibiscus sabdariff (roselle) [17]. Anti-mutagenic [18], anti-microbial [19], anti-atherosclerotic[20], and antioxidant properties[21] have all been documented for gossypetin. As we continue to investigate the value of theoretical predictions in the evaluation of pharmacological action, the current study concentrates on the structural and electronic exploration of the gossypetin molecule. The NBO analysis will shed light on how

stable the molecule is. The NCI analysis shows that the presence of an intramolecular hydrogen bond improves the molecule's stability. A detailed TD-DFT electronic transitions analysis explains the UV-filtering ability of the molecule under study. The antioxidant potential of gossypetin from the thermodynamic point of view was explored towards reactive oxygen species like •OH, •OOH, and reactive nitrogen species like •NO_2 by calculating the bond dissociation enthalpy (BDE) values of the aromatic –OH group adiabatic ionization potential (IP), proton dissociation enthalpies (PDE), proton affinities (PA) and electron transfer enthalpies (ETE) and comparing to phenolic compounds using M06/6–311G. DFT study determines the most likely chelation site for the Zn^{2+} metal ion in the gossypetin molecule and therefore the most stable complex. QTAIM analysis predicts the nature of donor-acceptor interaction in the Zn chelated complex in both polar and non-polar solvents.

5.2 Materials and methods

The Gaussian 16 program package was used to perform all geometry optimizations at the M06/6–311G level of theory. For ensuring the optimal geometries corresponding to energy minima (i.e., no imaginary vibrations), vibration analysis was used in this work. The Polarizable Continuum Solvent Model using the integral equation formalism variant (IEFPCM) as developed in Gaussian 16 software was used to treat solvent effects in dimethyl sulfoxide (DMSO), water, CCl_4, and toluene. Electronic transitions were estimated using time-dependent density functional theory (TD-DFT) for the molecule in gas and water medium using CAM-B3LYP. Information of tremendous

importance to the study of electronic structure and transition behaviour can be found in abundance in the wave functions produced by quantum chemical computations. The phrase "an electron leaves a hole and goes to an electron" can be used to describe the electron excitation process, where hole and electron are actual space functions. Here, certain hole-electron interaction features, including Sm, Sr, D, and indices, excitation energy, and Coulomb attractive energy (details about these parameters are provided in chapter 2) are computed in the same level of theory to simply evaluate and explain the characteristics of electron excitation using some quantitative numerical methods.

Calculations are performed using the Multiwfn 3.7 tool for several different parameters, including the NCI, orbital overlap distance function, QTAIM, delocalization index, ELF, LOL, and hole-electron interaction analyses utilizing Gaussian09 formatted checkpoint files.

The difference between the sums of the enthalpies of the reactant and product species is taken into account for calculating the numerical parameters (equation for calculating these parameters are given in chapter 5) associated with various mechanisms [22].

The binding energies between Zn^{2+} and gossypetin molecule ($E_{Binding\ energy}$) were computed using the following equation [23]:

$$E_{Binding\ energy} = E_{Complex} - E_{Gossypetin} + E_{Zn}^{2+} \qquad (12)$$

$E_{Complex}$, $E_{Gossypetin}$, and E_{Zn}^{2+} denote the energy of complex, gossypetin, and Zn^{2+} respectively.

Using features in the bond critical points (BCP) and delocalization indices, QTAIM analysis was used to analyze the charge and spin populations at specific atoms, as well as to estimate the character of interatomic interactions.

5.3 Optimization
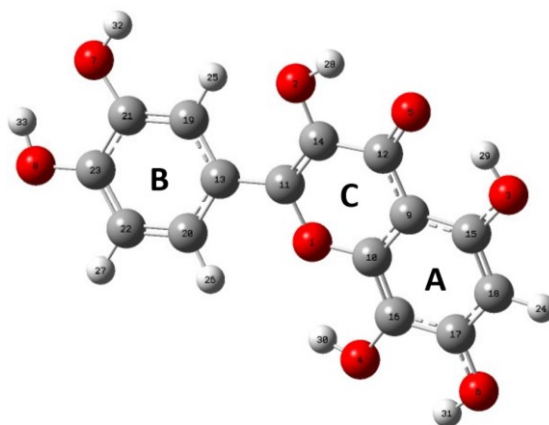
Fig. 5.1. Optimized geometry of gossypetin under M06/6311G

We compared the experimental ^{13}C NMR data of gossypetin with computed NMR at several levels of theory, which are presented in **Tables 5.1** and **5.2**, to choose the optimal basis set for gossypetin. M06/6311G with a higher Pearson correlation coefficient of 0.8734 (**Table 5.3**) was chosen for further studies.

Table 5.1 Comparison of experimental ^{13}C NMR with computed NMR values of gossypetin under B3LYP functional

Carbon atom	Experimental	631G	631G+DP	631G++DP	631G'	631G'+DP	631G'++DP	6311G	6311G+DP	6311G++DP
C12	175.9	172.2	169.5	169.2	172.2	169.0	168.4	181.4	180.1	180.3
C15	152.1	151.3	152.3	152.0	151.3	151.4	151.0	163.6	162.3	162.5
C17	152.5	147.8	148.8	148.5	147.8	148.2	147.8	159.4	159.0	159.3
C11	146.5	146.5	145.6	145.5	146.5	145.2	145.1	156.5	155.5	155.6
C23	147.5	144.4	145.1	144.9	144.4	144.7	144.2	155.8	152.7	152.9
C10	144.76	141.1	140.8	140.5	141.1	140.4	139.9	151.3	150.4	150.5
C21	115.3	140.1	140.7	140.4	140.3	140.2	139.8	150.0	149.5	149.7
C14	135.3	135.2	134.7	134.5	135.2	134.3	133.8	144.4	143.5	143.7
C16	124.6	123.3	122.7	122.7	123.3	122.2	122.1	133.2	131.4	131.6
C13	122.2	120.4	122.6	122.5	120.4	122.2	121.9	130.4	130.2	130.4
C20	115.2	118.0	118.3	118.0	118.0	118.1	117.7	128.5	126.9	127.0
C19	120.1	112.9	113.4	113.3	112.9	113.1	112.8	122.3	121.7	121.8
C22	144.85	112.9	112.7	112.4	112.9	112.4	112.0	121.7	120.9	121.1
C9	102.6	104.1	102.5	102.6	104.1	101.9	101.8	110.1	107.8	108.0
C18	97.8	98.6	96.5	96.2	98.6	96.19	95.74	107.0	103.4	103.6

Table 5.2 Comparison of experimental ^{13}C NMR with computed NMR values of gossypetin under M06 functional

Carbon atom	Experimental	631G	631G+DP	631G++DP	631G'	631G'+DP	631G'++DP	6311G	6311G+DP	6311G++DP
C12	175.9	176.1	169.0	169.0	169.8	168.7	169.0	182.3	179.9	180.0
C15	152.1	158.4	151.4	151.5	156.3	156.1	155.9	162.8	161.3	161.8
C17	152.5	154.6	147.6	147.5	154.5	154.1	154.1	158.8	157.9	158.3
C11	146.5	150.2	143.2	143.5	149.9	149.3	149.7	154.9	153.6	154.1
C23	147.5	149.6	142.5	142.4	147.4	146.3	146.4	153.1	149.3	149.6
C10	144.76	146.7	139.7	139.7	146.7	145.9	145.6	148.9	148.2	148.5
C21	115.3	144.9	137.9	138.2	141.8	140.8	140.3	148.1	147.1	147.4
C14	135.3	138.5	131.5	131.5	136.1	133.1	133.0	142.2	140.8	141.1
C16	124.6	127.2	120.2	120.1	124.9	121.8	122.2	130.3	128.2	128.4
C13	122.2	125.8	118.7	119.6	122.4	121.7	121.7	129.8	126.7	127.1
C20	115.2	125	118.0	117.9	121.8	119.3	119.9	127.9	126.6	126.7
C19	120.1	120.4	113.4	113.9	118.1	115.7	115.9	123.1	121.2	121.7
C22	144.85	119.1	112.1	112.1	116.8	114.7	114.9	122.5	120.3	120.6
C9	102.6	105.7	98.7	98.91	104.1	99.86	99.87	107.1	102.4	103.0
C18	97.8	103.5	96.44	96.42	101.9	97.89	97.86	106.5	101.8	102.1

Table 5.3 Pearson correlation coefficient between experimental ^{13}C NMR and computed NMR values of gossypetin under different levels of theory

Functional	Basis set	Pearson correlation coefficient
B3LYP	631G	0.8601
	631G+DP	0.8575
	631G++DP	0.8573
	631G'	0.8601
	631G'+DP	0.8580
	631G'++DP	0.8581
	6311G	0.8602
	6311G+DP	0.8620
	6311G++DP	0.8622
M06	631G	0.8691
	631G+DP	0.8691
	631G++DP	0.8676
	631G'	0.8678
	631G'+DP	0.8673
	631G'++DP	0.8702
	6311G	0.8734
	6311G+DP	0.8706
	6311G++DP	0.8704

Gossypetin molecule contains six hydroxyl groups in their structure so it is important to carry out potential energy scanning to get the lowest energy conformer. The stable conformer of the gossypetin molecule was then optimized under M06/6311G (**Fig. 5.1.**) and the corresponding geometrical parameters are given in **Tables 5.4-5.6**.

Table 5.4 The optimized bond length of gossypetin under M06/6311G

Bond	Bond length (Angstrom)
R(1,10)	1.3789
R(1,11)	1.3943
R(2,14)	1.3717
R(2,28)	0.9831
R(3,15)	1.3579
R(3,29)	0.9882
R(4,16)	1.3851
R(4,30)	0.9691
R(5,12)	1.2763
R(6,17)	1.3627
R(6,31)	0.9746
R(7,21)	1.3877
R(7,32)	0.9674
R(8,23)	1.3666
R(8,33)	0.9742
R(9,10)	1.4037
R(9,12)	1.4249
R(9,15)	1.4155
R(10,16)	1.3767
R(11,13)	1.4501
R(11,14)	1.3622
R(12,14)	1.4449
R(13,19)	1.409
R(13,20)	1.4045
R(15,18)	1.3853
R(16,17)	1.3959
R(17,18)	1.391
R(18,24)	1.0804
R(19,21)	1.3772
R(19,25)	1.0822
R(20,22)	1.3867
R(20,26)	1.0805
R(21,23)	1.3972
R(22,23)	1.3859
R(22,27)	1.082

Table 5.5 The optimized bond angle of gossypetin under M06/6311G

Bond angle	Angle (degree)
A(10,1,11)	121.6787
A(14,2,28)	107.1211
A(15,3,29)	110.8187
A(16,4,30)	112.36
A(17,6,31)	111.0068
A(21,7,32)	113.4682
A(23,8,33)	110.5609
A(10,9,12)	118.4536
A(10,9,15)	118.5925
A(12,9,15)	122.9538
A(1,10,9)	121.4443
A(1,10,16)	116.9219
A(9,10,16)	121.6335
A(1,11,13)	112.7918
A(1,11,14)	118.1083
A(13,11,14)	129.0998
A(5,12,9)	124.3012
A(5,12,14)	118.2385
A(9,12,14)	117.4602
A(11,13,19)	120.9327
A(11,13,20)	120.4267
A(19,13,20)	118.6406
A(2,14,11)	122.6409
A(2,14,12)	114.5043
A(11,14,12)	122.8547
A(3,15,9)	120.8357
A(3,15,18)	119.1313
A(9,15,18)	120.033
A(4,16,10)	124.8221

A(4,16,17)	116.5106
A(10,16,17)	118.667
A(6,17,16)	119.2631
A(6,17,18)	119.3526
A(16,17,18)	121.3843
A(15,18,17)	119.6892
A(15,18,24)	120.3742
A(17,18,24)	119.9366
A(13,19,21)	119.6725
A(13,19,25)	119.7696
A(21,19,25)	120.5578
A(13,20,22)	120.9698
A(13,20,26)	119.5241
A(22,20,26)	119.5057
A(7,21,19)	124.7553
A(7,21,23)	113.8798
A(19,21,23)	121.3649
A(20,22,23)	119.9878
A(20,22,27)	121.7464
A(23,22,27)	118.2658
A(8,23,21)	120.4202
A(8,23,22)	120.2154
A(21,23,22)	119.3644

Table 5.6 Optimized dihedral of gossypetin under M06/6311G

Dihedral	Angle (degree)
D(11,1,10,9)	-0.079
D(11,1,10,16)	-179.884
D(10,1,11,13)	-179.71
D(10,1,11,14)	0.1747
D(28,2,14,11)	179.6019
D(28,2,14,12)	-0.2539
D(29,3,15,9)	0.0302
D(29,3,15,18)	179.982
D(30,4,16,10)	2.4164
D(30,4,16,17)	-177.786
D(31,6,17,16)	-0.0072
D(31,6,17,18)	-179.958
D(32,7,21,19)	-0.3868
D(32,7,21,23)	179.643
D(33,8,23,21)	0.0471
D(33,8,23,22)	179.9762
D(12,9,10,1)	-0.0098
D(12,9,10,16)	179.7862
D(15,9,10,1)	179.953
D(15,9,10,16)	-0.251
D(10,9,12,5)	179.9149
D(10,9,12,14)	0.0007
D(15,9,12,5)	-0.0461
D(15,9,12,14)	-179.96
D(10,9,15,3)	-179.953
D(10,9,15,18)	0.0958
D(12,9,15,3)	0.0081
D(12,9,15,18)	-179.943
D(1,10,16,4)	-0.1337
D(1,10,16,17)	-179.927
D(9,10,16,4)	-179.939

D(9,10,16,17)	0.268
D(1,11,13,19)	-177.971
D(1,11,13,20)	1.9954
D(14,11,13,19)	2.16
D(14,11,13,20)	-177.874
D(1,11,14,2)	179.9699
D(1,11,14,12)	-0.1864
D(13,11,14,2)	-0.1666
D(13,11,14,12)	179.6771
D(5,12,14,2)	0.037
D(5,12,14,11)	-179.818
D(9,12,14,2)	179.9566
D(9,12,14,11)	0.1011
D(11,13,19,21)	179.9181
D(11,13,19,25)	-0.1685
D(20,13,19,21)	-0.0484
D(20,13,19,25)	179.865
D(11,13,20,22)	-179.93
D(11,13,20,26)	0.2943
D(19,13,20,22)	0.0372
D(19,13,20,26)	-179.739
D(3,15,18,17)	-179.919
D(3,15,18,24)	0.041
D(9,15,18,17)	0.0334
D(9,15,18,24)	179.9932
D(4,16,17,6)	0.1072
D(4,16,17,18)	-179.943
D(10,16,17,6)	179.9177
D(10,16,17,18)	-0.1325
D(6,17,18,15)	179.9334
D(6,17,18,24)	-0.0266
D(16,17,18,15)	-0.0163
D(16,17,18,24)	-179.976

D(13,19,21,7)	-179.966
D(13,19,21,23)	0.0017
D(25,19,21,7)	0.1209
D(25,19,21,23)	-179.911
D(13,20,22,23)	0.0214
D(13,20,22,27)	-179.908
D(26,20,22,23)	179.7976
D(26,20,22,27)	-0.1313
D(7,21,23,8)	-0.0417
D(7,21,23,22)	-179.971
D(19,21,23,8)	179.9869
D(19,21,23,22)	0.0573
D(20,22,23,8)	-179.998
D(20,22,23,21)	-0.0682
D(27,22,23,8)	-0.0667
D(27,22,23,21)	179.8631

5.4 Noncovalent interaction (NCI) /reduced density gradient (RDG) plot

The newly created NCI (noncovalent interactions) index allows for the real-space depiction of both attractive (van der Waals and hydrogen-bonding) and repulsive (steric) interactions depending on the characteristics of the electron density. As a result, it is the best index to represent how stabilizing and destabilizing contributions interact to form stable minima on hydrogen-bonding potential-energy surfaces (PESs) [24]. The NCI plot is created by graphing the Reduced Density Gradient (s) vs the sign of λ_2 (Eigenvalues for the electron density of the Hessian matrix). In the low-density gradient zone, the plot shows spikes. It is a typical NCI interaction trace, and as it advances away

from zero, it gets stronger and stronger. **Fig. 5.2a**, shows the NCI plot of gossypetin. The presence of a hydrogen bond is the cause of the spike that occurs at about -0.040 a.u. The weak Van der Waals attraction is what causes the spikes in the region between -0.010 and +0.010 a.u. The presence of the steric effect is indicated by the spikes near + 0.020 a.u.
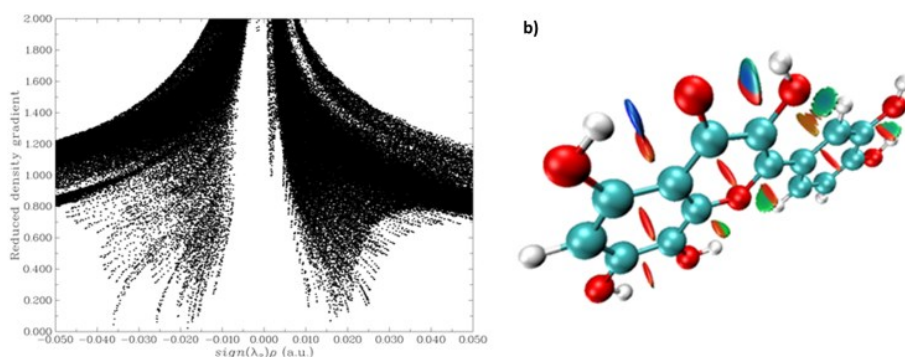
Fig. 5.2. a) NCI plot and **b)** RDG plot of gossypetin molecule

The isosurface of the gossypetin molecule is shown in **Fig. 5.2b**. The presence of a hydrogen bond is indicated by the development of a blue color isosurface next to the carbonyl oxygen, O5 and H28 as well as between O5 and H29 in the molecule, which causes the spikes near 0.040 a.u. in the NCI plot. The presence of a steric effect is shown by the red isosurface that can be observed amid the rings are responsible for the spikes above 0.020 a.u. Low electron densities (greenish-red isosurface) have appeared between OH groups.

5.5 Electronic properties

Six radicals were produced from an absolute minimum of gossypetin after the hydrogen was removed from the hydroxyl groups.

According to the optimization process, the 16-OH radical is the most stable among the others in all the selected solvent systems. The energy values of gossypetin and all the possible radicals in the selected solvents are given in **Table 5.7**. The hydrogen bond between the hydroxyl group at position 15 and the C12-O carbonyl must be broken for this group to radicalize. Thus, a repulsive effect that results in the radical's destabilization is created by the quinoid-like structure that is generated on ring A and the C12-O carbonyl ring of C. Radical produced at 21-OH is more stable than that of 23-OH because the presence of hydrogen bonding interaction between O7 and H33. Having hydroxyl groups in the para position of 16-OH may provide added stability, explaining why 16-OH is more stable than 21-OH.

Table 5.7 Electronic energies for neutral molecule and radicals in different solvents at M06/6311G level of theory

Molecule/Radical	Energy (kcal/mol)			
	DMSO	Water	Toluene	CCl$_4$
Gossypetin	-739629.64	-739629.83	-739220.00	-739622.45
14-OH	-739231.42	-739231.67	-739222.53	-739222.06
15-OH	-739222.19	-739222.50	-739211.72	-739211.19
16-OH	-739237.53	-739237.71	-739230.97	-739230.62
17-OH	-739226.52	-739226.79	-739217.05	-739216.56
21-OH	-739231.08	-739231.27	-739224.34	-739223.99
23-OH	-739229.04	-739229.30	-739220.0002	-739219.53

To gain a deeper understanding of the chemical reactivity of the compound, the actual density functional theory-based descriptors were

defined, including electronegativity, chemical hardness, chemical softness, electrical trophilicity index, and chemical potential.

According to Koopman's theorem the ionisation potential (I) and electron affinity (A) is given by;

$$I = -E_{HOMO} \tag{13}$$

$$A = -E_{LUMO} \tag{14}$$

where E_{HOMO} and E_{LUMO} denote the energies of the highest occupied molecular orbital (HOMO) and the energy of the lowest unoccupied molecular orbital (LUMO). The other global properties were computed by using the equations given below [25];

$$\text{Hardness } (\eta) = (I-A)1/2 \tag{15}$$

$$\text{Electronegativity } (\chi) = (I+A)1/2 \tag{16}$$

$$\text{Softness } (s) = 1/(2\eta) \tag{17}$$

$$\text{Chemical potential } (\mu) = -\chi \tag{18}$$

$$\text{Electrophilicity index } (\omega) = \mu^2/2\eta \tag{19}$$

As is widely known, an atom or molecule with a higher electronic affinity tends to absorb electrons more readily, while a system with a low ionization potential suggests that electrons are lost more readily [26]. In contrast to hardness, which evaluates the resistance to charge transfer, electronegativity assesses a chemical species' propensity to attract electrons. Gossypetin is discovered to be more stable by the maximal hardness concept [15]. As can be observed from **Table 5.8**, gossypetin has a high electron affinity (2.41 eV) and

ionization potential (6.29 eV) (which is comparable to quercetin), which explains its biological antioxidant effect. A further indication of the molecule's antioxidant capacity is its low chemical potential, which shows a propensity to give electrons rather than capture them.

Table 5.8 Chemical properties of gossypetin at M06/6311G level of theory

Properties	Gossypetin
Electron affinity (eV)	2.41
Ionization potential (eV)	6.29
Hardness (eV)	1.94
Electronegativity (eV)	4.35
Chemical potential (eV)	-4.35
Softness (eV)	0.26
Electrophilic index (eV)	4.88

5.6 TD-DFT electronic transitions vs. UV–Vis spectroscopy
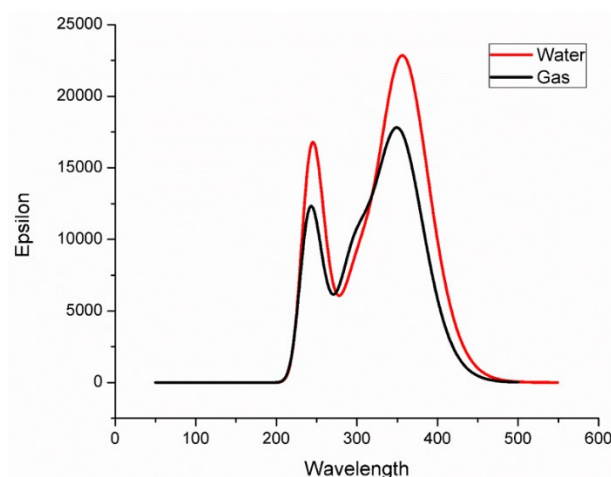
Fig. 5.3. Computed UV spectrum of gossypetin in gaseous and aqueous phase under CAMB3LYP/6311G

Among the techniques used to compute electronic transitions, TD-DFT is the most widely used and economically advantageous one for the analysis of excited states and the prediction of UV-Visible spectra [27]. According to earlier studies, CAM-B3LYP is very helpful for accurately describing excited states, particularly for charge transfer states, and for producing more trustworthy results [27, 28]. A Time-dependent DFT approach was carried out on an optimized gossypetin molecule with CAM-B3LYP/6311G basis set. To explore the aqueous phase, the IEFPCM (Integral Equation Formalism Polarizable Continuum Model) solvent model was used. UVA, UVB, and UVC are three regions of UV radiations, with UVA having a long wavelength (320–400 nm), UVB having a medium wavelength (290–320 nm), and UVC having a short wavelength (200–290 nm). When both UV A and UV B rays are exposed to the skin, it can occasionally result in sunburn, long-term skin damage like wrinkles, skin cancer like melanoma, aging of the skin, *etc*. The UV spectrum of gossypetin in gas and the aqueous phase is given in **Fig. 5.3**. **Fig. 5.4** shows the molecular orbitals that are a part of the major transition and have the strongest oscillatory strength. The calculated oscillator strength (f), and λ_{max} along with the orbitals involved are given in **Table 5.9**.

Table 5.9 Wavelength (λ_{max}), oscillator strength (f), orbitals involved for the absorbance peak of gossypetin calculated by TD-DFT/CAM-B3LYP/6311G

Solvent	Wavelength (nm)	Oscillatory strength (f)	Orbitals involved
Gas	352.99	0.4181	HOMO→LUMO
	299.49	0.2233	HOMO-1→LUMO
	267.74	0.0000	HOMO-5→LUMO
	263.39	0.0295	HOMO-2→LUMO
	260.40	0.0174	HOMO-3→LUMO
	241.87	0.2852	HOMO-2→LUMO
Water	358.53	0.5464	HOMO→LUMO
	303.45	0.1936	HOMO-1→LUMO
	265.05	0.0059	HOMO-3→LUMO
	263.48	0.0002	HOMO-5→LUMO
	262.19	0.0416	HOMO-2→LUMO
	244.38	0.3912	HOMO→LUMO+1

The gas phase absorption spectra show two distinct peaks with λ_{max} at 352.99 nm and 241.87 nm, respectively. The peak at 241.87 nm with oscillatory strength 0.2852 corresponds to the transition from HOMO-2 to LUMO in the gas phase, where maximal absorption (352.99 nm) with oscillatory strength 0.4181 is resulted by the HOMO to LUMO transition.
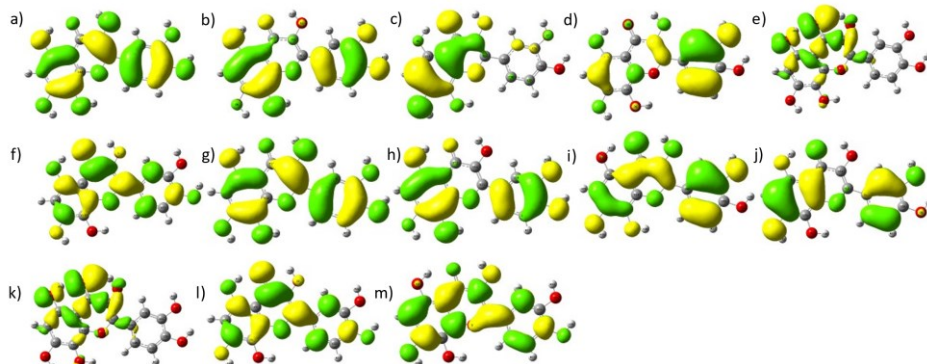
Fig. 5.4. Topology of orbitals having maximum contribution towards the absorption bands a) HOMO, b) HOMO-1, c) HOMO-2, d) HOMO-3, e) HOMO-5, f) LUMO in the gas phase, g) HOMO, h) HOMO-1, i) HOMO-2, j) HOMO-3, k) HOMO-5, l) LUMO and m) LUMO +1 in water

Gossypetin's UV spectra in water displayed two distinct peaks at 358.53 and 244.38 nm. The strongest peak occurs at 338.57 nm as a result of the transition from HOMO to LUMO. The HOMO to LUMO+1 transition is responsible for the second dominant peak at 244.38 nm. In this case, HOMO - LUMO is responsible for the intense transition while HOMO - LUMO+ 1 is responsible for the second dominant transition. When the solution becomes more polar, it is seen that both the bands' absorption maxima are redshifted. Gossypetin's bathochromic shift in polar media was caused by greater stability of π^* orbitals (excited state) than π orbitals (ground state). The oscillator strengths are shown to increase when the solvent becomes polar, which may be the result of improved orbital overlap. This increase in overlap is discovered to be noticeable in the absorption of both peaks. UV absorbance in the range of 200-400nm indicates that the gossypetin molecule can act as a perfect UV filter.

5.7 Hole-electron analysis

The electron-hole analysis is a very potent and useful set of techniques for investigating the properties of electron excitation. It refers to the electron excitation as occurring from "hole to electron" and analyses the distribution of "holes" to determine where the electron originates and the distribution of "electrons" to determine where the electron is excited to go. The electron is excited either locally (LE), charge-transfer (CT), or *via* a Rydberg excitation (R). In a CT excitation, the hole and electron will be separated by a greater distance, whereas in an LE excitation, the hole and electron will share the same spatial range. This difference allows the charge density to travel from one location to another [29]. Additionally, it offers a thorough understanding of all the different electron transfer characters. It is a highly useful method for determining the type of electron excitations [30]. Multiwfn 3.8 is a very powerful and substantial tool for doing electron excitation analysis.
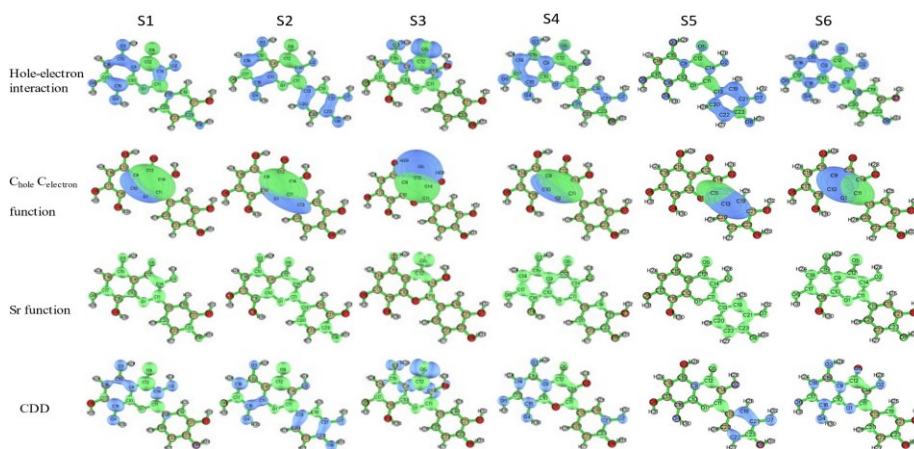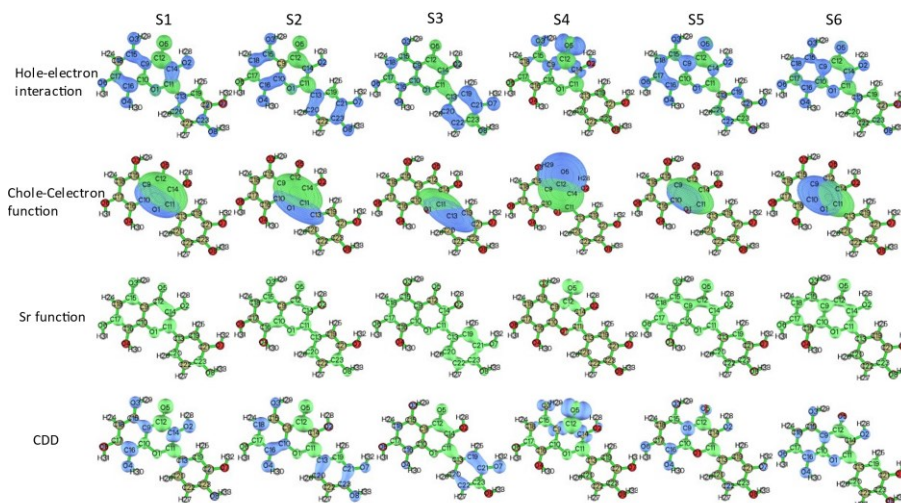

Fig. 5.5. The hole-electron distribution, Chole – Celec function, Sr function, and charge density difference (CDD) of gossypetin for the lowest six excitation states in the gas phase

The hole–electron interaction properties including, Sm, Sr, D, H, and t indices, excitation energy, and Columb attractive energy are examined at the same theoretical level and presented in **Table 5.10**. **Fig. 5.5** displays the hole-electron distribution, Chole-Celec function, Sr function, and charge density difference (CDD) of gossypetin in the gas phase. The large D index value associated with the S0 → S3 excitation (1.550 Å), which is a charge transfer (CT) excitation. As the predicted top limit is 1.0 and all of the excited states' Sr index values are significantly higher (apart from S0 → S3), we may infer that nearly half of the hole and electron are completely matched and these transitions are solely local excitations. The Sr values should be in the range of 0.8 a.u. for $\pi \to \pi *$ transition. So, it is clear that S0 → S4, S0 → S5, and S0 → S6 are associated with $\pi \to \pi *$ transitions. S0 → S1, S0 → S2 may follow n → π* transition on the rings A or B (or) keto group.

The H index represents the width of the typical dispersion of holes and electrons. The distribution of the hole and electron from S0 → S3 in the local area can be seen on the hole and electron map. So, their H index values are smaller than those of other excitations which again supports the charge transfer excitation. The values of their H indices are higher for the excitations from S0 to S1, S2, S4, S5, and S6 because the distributions of holes and electrons are wider.

Table 5.10 Hole–electron interaction properties for gossypetin in the gas phase

Excitation	Sm(a.u.)	Sr(a.u.)	D index (Å)	H index (Å)	t index (Å)	Excitation energy (eV)	Columb attractive energy (eV)
S1	0.382	0.655	0.885	3.067	-1.049	3.512	5.006
S2	0.3742	0.680	1.243	3.434	-0.990	4.140	4.616
S3	0.1982	0.435	1.550	2.045	0.232	4.631	6.369
S4	0.619	0.868	0.590	3.392	-1.559	4.707	4.768
S5	0.622	0.872	0.991	3.267	-1.732	4.761	4.830
S6	0.562	0.832	0.951	3.147	-1.583	5.126	4.932

The excitations from S0 to S2, S3, and S4 have t indices with discernible negative values, suggesting that there is very little separation between the hole and the electron. They consequently adhere to the local excitation type (LE). It is more logical to think of S0 → S1 as a CT excitation because the index is quite positive (0.232 Å), showing that the separation of the hole and electron is evident

The hole-electron coulomb attractive energy is connected to the features of electron excitation. The major distribution of holes and electrons are separated from one another at greater distances the Coulomb energy decreases. It is evident from the data that S0 → S1 have substantial Coulomb attraction energy since their hole and electron has a relatively small spatial range. The hole-electron analysis of gossypetin in the water phase is not discussed in the main text. The

hole-electron distribution, Chole-Celec function, Sr function, and charge density difference (CDD) of gossypetin in water solvent are shown in **Fig. 5.6,** and the corresponding Hole – electron interaction properties are given in **Table 5.11**.

Table 5.11 Hole–electron interaction properties for gossypetin in water

Excitation	Sm(a.u.)	Sr(a.u.)	D index (Å)	H index (Å)	τ Index (Å)	Excitation energy (eV)	Columb attractive energy (eV)
S1	0.398	0.672	0.716	3.114	-0.977	3.458	4.979
S2	0.370	0.668	1.215	3.418	-0.829	4.086	4.618
S3	0.549	0.825	1.152	3.471	-1.789	4.678	4.697
S4	0.199	0.442	1.539	2.059	0.205	4.706	6.359
S5	0.620	0.867	0.407	3.334	-1.826	4.729	4.782
S6	0.570	0.837	0.829	3.162	-1.690	5.074	4.934

Fig. 5.6. The hole-electron distribution, cole – celec function, Sr function, and charge density difference (CDD) of gossypetin for the lowest six excitation states in water

5.8 Antioxidant activity

Three significant radicals, including •OOH, •NO$_2$, and •OH, are taken into account in physiological media to demonstrate the impact of free radical nature on the gossypetin scavenging reactions. BDE values determine the single-step HAT process. Both SET-PT and SPLPT are two-step mechanisms that are independently controlled by IPs and PAs, which are connected to the first step's reaction enthalpies. Therefore, for all the investigated compounds in various media, the computed BDEs, IPs, and PAs were used to identify the thermodynamically preferable mechanism of radical scavenging behaviour.

Table 5.12 BDE values (kcal/mol) of gossypetin at various solvents

Radical	Hydroxyl group	BDE			
•OH		DMSO	Water	Toluene	CCl$_4$
	14-OH	-30.97	-31.07	-27.79	-27.62
	15-OH	-22.01	-22.15	-17.34	-17.11
	16-OH	-36.86	-36.88	-35.95	-35.90
	17-OH	-26.20	-26.31	-22.54	-22.35
	21-OH	-30.66	-30.69	-29.59	-29.53
	23-OH	-28.69	-28.80	-25.36	-25.20
•OOH	14-OH	2.59	2.44	7.56	7.82
	15-OH	11.56	11.36	18.01	18.33
	16-OH	-3.29	-3.37	-0.60	-0.46
	17-OH	7.36	7.20	12.82	13.09
	21-OH	2.90	2.82	5.76	5.91
	23-OH	4.87	4.72	14.07	10.24
•NO$_2$	14-OH	1.18	1.06	4.63	4.81
	15-OH	10.14	9.99	15.08	15.32
	16-OH	-4.71	-4.74	-3.53	-3.46
	17-OH	5.95	5.83	9.88	10.08
	21-OH	1.49	1.45	2.83	2.90
	23-OH	3.46	3.34	7.06	7.24

The HAT mechanism normally refers to a process in which antioxidants lose hydrogen atoms to free radicals through homolytic cleavage of phenolic hydroxyl groups, and in which the BDE values are frequently used to assess the radical scavenging activity. The ability to scavenge free radicals is stronger the lower the BDE values [31]. The computed thermodynamic parameter, BDE for the HAT mechanism in polar solvents like DMSO and water as well as non-polar solvents like CCl_4 and toluene are given in **Table 5.12**. With the lowest BDE, the most active system can function through the H-atom transfer mechanism both in the gas phase and in the solution. The capacity for H atom abstraction and the scavenging of free radicals may both be enhanced by an increase in the amount of OH groups [32]. Hydrogen bonds serve to stabilize the phenoxyl radicals produced by the abstraction of the H atom in flavonoids. The presence of OH groups at particular positions on the flavonoid core is also a major factor in the effectiveness of flavonoids to scavenge free radicals. The OH group of the flavonoid core with the most abstractable hydrogen is the one that is targeted for radical attack, according to the minimal value of the BDE of OH bonds [15]. Table 5 lists the BDE values of the HAT mechanism in each of the chosen solvents between gossypetin and the aforementioned radicals. All HAT reactions involving the •OH radical are exergonic and have largely negative BDE values. It is important to note that, except 16-OH, the HAT reactions involving •OOH, and •NO_2 radicals are primarily endergonic due to the positive BDE value. Additionally, of all the hydroxyl groups found in gossypetin, 16-OH

was discovered to be the most favorable radical site, which is evident from the radical energy previously discussed. Gossypetin is a more effective radical scavenger for •OH than for •OOH and •NO$_2$, as evidenced by the lowest BDE value of •OH compared to other radical values. According to the BDE values, which show a slight preference for the scavenging of radical species in DMSO and water medium compared to CCl$_4$ and toluene medium, gossypetin is a better radical scavenger through the HAT mechanism in polar media than in non-polar medium. Water medium is discovered to be more preferred for HAT mechanisms among the solvents.

Table 5.13 AIP and PDE values (kcal/mol) of gossypetin at various solvents

Radical	Hydroxyl group	DMSO		Water		Toluene		CCl$_4$	
		AIP	PDE	AIP	PDE	AIP	PDE	AIP	PDE
•OH	14-OH	45.86	-76.83	44.81	-75.88	93.74	-121.53	97.03	-124.65
	15-OH	45.86	-67.87	44.81	-66.96	93.74	-111.09	97.03	-114.14
	16-OH	45.86	-82.72	44.81	-81.70	93.74	-129.70	97.03	-132.93
	17-OH	45.86	-72.06	44.81	-71.12	93.74	-116.28	97.03	-119.38
	21-OH	45.86	-76.53	44.81	-75.51	93.74	-123.33	97.03	-126.56
	23-OH	45.86	-74.56	44.81	-73.61	93.74	-119.11	97.03	-122.23
•OOH	14-OH	47.96	-45.37	46.98	-44.53	92.56	-85.00	95.60	-87.78
	15-OH	47.96	-36.41	46.98	-35.62	92.56	-74.55	95.60	-77.28
	16-OH	47.96	-51.26	46.98	-50.35	92.56	-93.16	95.60	-96.06
	17-OH	47.96	-40.60	46.98	-39.78	92.56	-79.74	95.60	-82.51
	21-OH	47.96	-45.06	46.98	-44.16	92.56	-86.80	95.60	-89.69
	23-OH	47.96	-43.10	46.98	-42.26	92.56	-50.36	95.60	-85.36
•NO$_2$	14-OH	22.42	-21.24	21.54	-20.46	62.95	-58.32	65.75	-60.94
	15-OH	22.42	-12.28	21.54	-11.55	62.95	-47.87	65.75	-50.43
	16-OH	22.42	-27.13	21.54	-26.28	62.95	-66.48	65.75	-69.21
	17-OH	22.42	-16.47	21.54	-15.71	62.95	-53.06	65.75	-55.66
	21-OH	22.42	-20.94	21.54	-20.09	62.95	-60.12	65.75	-62.85
	23-OH	22.42	-18.97	21.54	-18.19	62.95	-55.89	65.75	-58.51

Another important mechanism for the antioxidant process is called SET-PT, which involves a proton transfer step after an electron donation from the antioxidants. IP and PDE values were calculated and are shown in **Table 5.13** to assess the thermodynamic potential of the SET-PT mechanism for the molecule under investigation. Comparing the trends of computed AIPs and BDEs, a small difference can be seen. In polar solvents, •NO$_2$ is found to have the lowest value, followed by •OH and then •OOH, but in nonpolar solvents, •NO$_2$ is found to have the lowest value, followed by •OOH and then •OH. The solvent effect has considerably impacted AIPs and it is vital to remember that polar solvents favor the SET-PT mechanism more than non-polar solvents.

Table 5.14 PA and ETE values (kcal/mol) of gossypetin at various solvents

Radical	Hydroxyl group	DMSO		Water		Toluene		CCl$_4$	
		PA	ETE	PA	ETE	PA	ETE	PA	ETE
•OH	14-OH	-45.30	14.33	-45.03	13.96	-60.31	32.52	-61.44	33.81
	15-OH	-39.25	17.24	-39.05	16.90	-51.58	34.24	-52.56	35.45
	16-OH	-48.26	11.40	-47.95	11.07	-63.81	27.86	-64.94	29.04
	17-OH	-47.88	21.8	-47.61	21.30	-62.13	39.59	-63.20	40.85
	21-OH	-45.96	15.29	-45.64	14.94	-62.24	32.65	-63.42	33.88
	23-OH	-44.27	15.57	-43.97	15.18	-59.85	34.49	-61.01	35.82
•OOH	14-OH	-13.84	16.43	-13.68	16.12	-23.78	31.34	-24.57	32.38
	15-OH	-7.78	19.34	-7.70	19.06	-15.05	33.06	-15.69	34.02
	16-OH	-16.79	13.50	-16.60	13.23	-27.28	26.68	-28.07	27.61
	17-OH	-16.41	23.78	-16.26	23.46	-25.60	38.41	-26.33	39.42
	21-OH	-14.49	17.40	-14.29	17.11	-25.70	31.47	-26.55	32.45
	23-OH	-12.80	17.67	-12.63	17.34	15.94	1.39	-24.14	34.39
•NO$_2$	14-OH	10.29	-9.11	10.39	-9.31	2.90	1.73	2.28	2.53
	15-OH	16.34	-6.20	16.37	-6.38	11.63	3.44	11.15	4.16
	16-OH	7.33	-12.04	7.46	-12.20	-0.60	-2.94	-1.22	-2.24
	17-OH	7.71	-1.76	7.81	-1.98	1.08	8.80	0.51	9.57
	21-OH	9.63	-8.14	9.78	-8.33	0.98	1.86	0.30	2.60
	23-OH	11.32	-7.86	11.44	-8.10	3.36	3.69	2.70	4.53

Similar to the SET-PT, SPLET is a two-step mechanism in which phenolic hydroxyl is deprotonated and then an electron transfer procedure takes place. The calculated PAs and ETEs for gossypetin in various solvents are given in **Table 5.14**. The SPLET mechanism was chosen over the HAT and SET-PT mechanisms for scavenging •OH and •OOH because the PA value is much lower in all solvents. The lower BDE than PA suggests that the HAT mechanism is prioritized over the SPLET mechanism in the case of the •NO2 radical case. Additionally, it is noteworthy that among all the solvents, 16-OH has the lowest PA value. Furthermore, polar solvents are more favorable to the SPLET mechanism than non-polar solvents for •OH and •OOH whereas a reverse trend is observed for •NO2.

5.9 Metal chelation
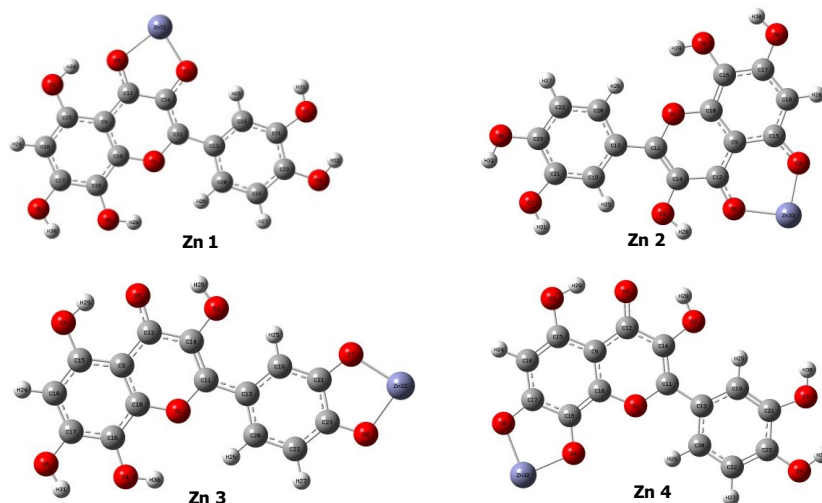
Fig. 5.7. Possible chelation sites for Zn^{2+} in gossypetin molecule in water

The possible metal chelation sites in the gossypetin molecule are shown in **Fig. 5.7**. Using the DFT method B3LYP and a mixed basis set 631g+LANL2DZ (631g for non-metal atoms and LANL2DZ for metal), the equilibrium geometries of Zn^{2+} chelated gossypetin complexes were optimized in DMSO, water, CCl_4 and toluene media. Zn 3 and Zn 4 complexes showed negative binding energy values in all the media, which suggests that the reactions are spontaneous. According to the positive and negative binding energies of Zn 1 and Zn 2 in polar and non-polar media, respectively, gossypetin interacts more with the Zn^{2+} ion in non-polar solvents than in polar media. Generally speaking, CCl_4 was the solvent where gossypetin and Zn^{2+} ion interacted best. Taking into account the calculated energetics, Zn 4 is the exclusive preferred position in gossypetin. The interaction energy values of Zn 4 was found to be -13.292, -8.999, -234.359, and -219.659 kcal/mol in DMSO, water, CCl_4, and toluene respectively (**Fig. 5.8**). The binding energy values of Zn 1, Zn 2, and Zn 3 are given in **Figs 5.9, 5.10** and **5.11** respectively.
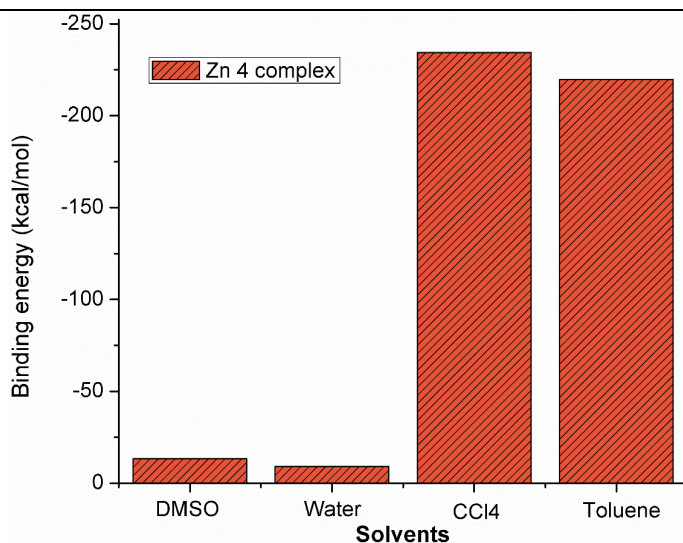
Fig. 5.8. Interaction energy of Zn 4 in various solvents
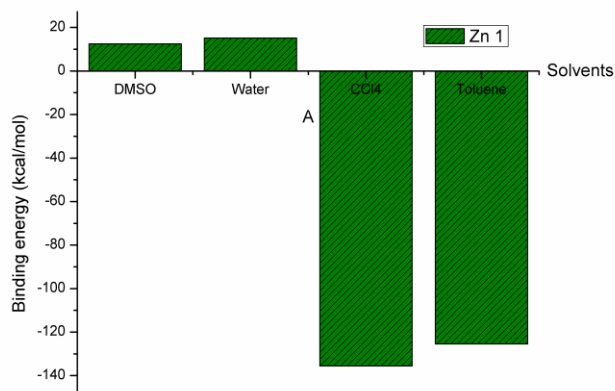
Fig. 5.9. Interaction energy of Zn 1 in various solvents
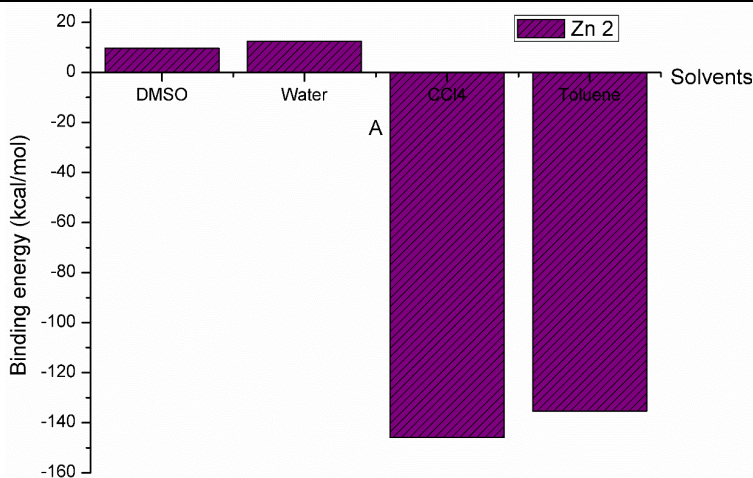
Fig. 5.10. Interaction energy of Zn 2 in various solvents
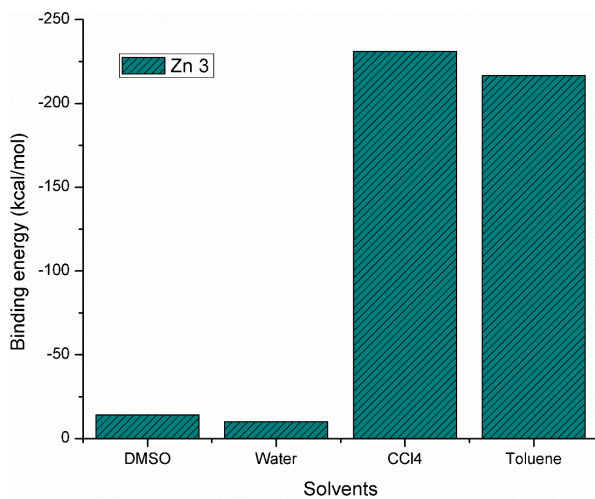
Fig. 5.11. Interaction energy of Zn3 in various solvents

5.10 QTAIM charge and delocalisation index

Bader's quantum theory of atoms in molecules (QTAIM) can be used to investigate the topology of charge (or spin) density [33]. An important approach for obtaining further information on the nature and character of chemical bonds is the analysis of bond critical points (BCPs) and delocalization indices. BCPs are saddle points of electron density between two atoms forming a chemical bond [34]. Bader's QT-AIM is a helpful tool for researching and examining the nature of chemical interactions between ligands and metal ions in complexes based on electron density topology. **Table 5.15** shows the topological properties of all electrons $\rho(r)$, Laplacian of electron densities $\nabla\rho(r)$, Langragrain kinetic energy $(G(r))$ to potential energy density $(V(r))$ ratio, and delocalization indices DI of Zn-O bonds in the Zn 4 complex in selected solvent phases. An increase in electron density (r)) at the BCP reflects a stronger contact. Higher electron densities at Zn-O4 bonds than Zn-O6 in the Zn 4 complex indicate stronger interactions between Zn^{2+} and O4 atoms than O6 atoms in all the solvents.

Additionally, stronger interactions in non-polar media than polar media are indicated by higher electron densities at BCP in non-polar solvents compared to polar solvents. The higher electron density on M-O bonds in CCl_4 can be used to explain the lower interaction energy value for Zn 4 in CCl_4 discussed before. Negative values of the Laplacian electron density ($\nabla^2 \rho(r)$) are used to depict covalent bonds, whereas positive values are used to show non-covalent bonds [35]. The positive $\nabla^2 \rho(r)$ value obtained at each BCP of the complex is a clear indication of non-covalent interaction. The calculated -G(r)/V(r) value

close to one, points to the electrostatic interaction. Additionally, the low values of ELF and LOL support the electrostatic interaction of M-O bonds once more [23]. The delocalization indices (DIs) are a measure of the number of electrons shared (or exchanged) between the two atoms, and they fundamentally constitute a formal bond arrangement [36]. It is observed that the trend of the DI value and the electron density are comparable. Zn-O4 exhibits greater delocalization than Zn-O6 during the whole solvent phase. The DI readings are significantly influenced by the solvent's polarity. In comparison to non-polar media, polar media have a higher DI value. ELF and LOL plots of Zn 4 in different solvents are given in **Fig. 5.12**.
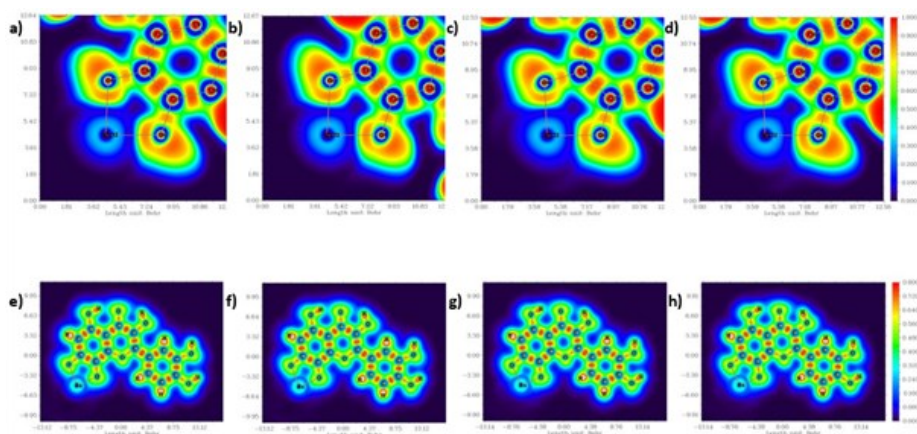
Fig. 5.12. ELF plots of the metal-oxygen interactions of Zn 4 in a) DMSO, b) water, c) CCl₄, d) toluene and LOL plots of the metal-oxygen interactions of Zn 4 e) DMSO, f) water, g) CCl₄, h) toluene

Table 5.15 Calculated topological parameters (in a.u) at the BCPs and delocalization index of M-O bonds in Zn 4 complex

solvent	Bond	$\rho(r)$	$\nabla^2 \rho(r)$	$-G(r)/V(r)$	ELF	LOL	DI
DMSO	Zn-O6	0.0774	0.4346	0.8691	0.1281	0.2756	0.9723
	Zn-O4	0.0809	0.4619	0.8690	0.1314	0.2784	1.0178
Water	Zn-O6	0.0770	0.4314	0.8693	0.1275	0.2751	0.9683
	Zn-O4	0.0806	0.4604	0.8693	0.1310	0.2781	1.0148
CCl$_4$	Zn-O6	0.0909	0.5250	0.8585	0.1458	0.2906	1.1055
	Zn-O4	0.0933	0.5438	0.8578	0.1479	0.2923	1.1415
Toluene	Zn-O6	0.0904	0.5216	0.8591	0.1450	0.2899	1.0994
	Zn-O4	0.0926	0.5389	0.8584	0.1471	0.2916	1.1347

Conclusion

Quantum chemical investigation based on density functional theory was used to explore the structure, electronic properties, and multiple pharmacological activities like UV-filtering effect, anti-oxidant activity, and metal chelating ability. According to RDG plot the molecule possesses a strong intramolecular hydrogen bond between O5 with nearby H28 and H29 atoms. According to the orbital overlap integral function, H24 has the highest, and C22 has the lowest isosurface energy. The capacity of the molecule to filter out UV light was explained by UV absorption in the 200–400 nm range, and a bathochromic shift was observed in the presence of polar solvent. Hole-electron analysis explained the nature of excitation for the lowest six excitation states of gossypetin in the gas phase. Gossypetin's bond dissociation enthalpy (BDE), ionization potential (IP), proton

dissociation enthalpy (PDE), proton affinity (PA), and electron transfer enthalpy (ETE) for •OH, •OOH, and NO2 radicals in polar and non-polar media are the subjects of the study. In preference to SPLET or SET-PT process for •NO$_2$ radical, the one-step hydrogen atom transfer (HAT) mechanism is the most preferred explanation for the antioxidant mechanism. Additionally, gossypetin is a better radical scavenger through the HAT mechanism in polar media than in non-polar medium. The results indicated that the most advantageous mechanism for elucidating the radical-scavenging activity for •OH and •OOH radicals would be the SPLET mechanism. Additionally, polar solvents are preferable to non-polar solvents for the SPLET mechanism in the case of •OH and •OOH, but the trend is the opposite for •NO$_2$. Lower BDE and PA values demonstrated that among the six hydroxyl groups, 16-OH was the most effective location for scavenging all free radicals. Binding energy values suggest that Zn 4 is the most stable complex in all the media. According to the QTAIM study, gossypetin and Zn^{2+} interact in a way that is electrostatic in nature.

References

1.   Russo M, Moccia S, Spagnuolo C, Tedesco I, Russo GL: **Roles of flavonoids against coronavirus infection**. *Chem Biol Interact* 2020:109211.

2.   Owona BA, Abia WA, Moundipa PF: **Natural compounds flavonoids as modulators of inflammasomes in chronic diseases**. *International immunopharmacology* 2020, **84**:106498.

3.   Trouillas P, Marsal P, Siri D, Lazzaroni R, Duroux J-L: **A DFT study of the reactivity of OH groups in quercetin and taxifolin antioxidants: The specificity of the 3-OH site**. *Food Chem* 2006, **97**(4):679-688.

4.   Lekka CE, Ren J, Meng S, Kaxiras E: **Structural, electronic, and optical properties of representative Cu− flavonoid complexes**. *The Journal of Physical Chemistry B* 2009, **113**(18):6478-6483.

5.   Catanzaro M, Corsini E, Rosini M, Racchi M, Lanni C: **Immunomodulators inspired by nature: a review on curcumin and echinacea**. *Molecules* 2018, **23**(11):2778.

6.   Nones J, de Sampaio Spohr TCL, Gomes FCA: **Effects of the flavonoid hesperidin in cerebral cortical progenitors in vitro: indirect action through astrocytes**. *Int J Dev Neurosci* 2012, **30**(4):303-313.

7.   Uysal S, Ugurlu A, Zengin G, Baloglu MC, Altunoglu YC, Mollica A, Custodio L, Neng NR, Nogueira JM, Mahomoodally MF: **Novel in vitro and in silico insights of the multi-biological activities and chemical composition of Bidens tripartita L**. *Food Chem Toxicol* 2018, **111**:525-536.

8.   Yan Z, Li P, Xiao Y, Cao L, Yao L: **Phytotoxic Effects of Allelochemical Acacetin on Seed Germination and Seedling Growth of Selected Vegetables and Its Potential Physiological Mechanism**. *Agronomy* 2022, **12**(5):1038.

9.   Kiselova Y, Ivanova D, Chervenkov T, Gerova D, Galunska B, Yankova T: **Correlation between the in vitro antioxidant activity and polyphenol content of aqueous extracts from Bulgarian herbs**. *Phytotherapy Research: An International Journal Devoted to Pharmacological and Toxicological Evaluation of Natural Product Derivatives* 2006, **20**(11):961-965.

10. Piga A, Del Caro A, Corda G: **From plums to prunes: influence of drying parameters on polyphenols and antioxidant activity**. *J Agric Food Chem* 2003, **51**(12):3675-3681.

11. Tagliazucchi D, Verzelloni E, Bertolini D, Conte A: **In vitro bio-accessibility and antioxidant activity of grape polyphenols**. *Food Chem* 2010, **120**(2):599-606.

12. Volf I, Ignat I, Neamtu M, Popa VI: **Thermal stability, antioxidant activity, and photo-oxidation of natural polyphenols**. *Chemical Papers* 2014, **68**(1):121-129.

13. Riley P: **Free radicals in biology: oxidative stress and the effects of ionizing radiation**. *Int J Radiat Biol* 1994, **65**(1):27-33.

14. Patel RP, McAndrew J, Sellak H, White CR, Jo H, Freeman BA, Darley-Usmar VM: **Biological aspects of reactive nitrogen species**. *Biochimica et Biophysica Acta (BBA)-Bioenergetics* 1999, **1411**(2-3):385-400.

15. Kumaresan R: **A DFT study on the structural, electronic properties and radical scavenging mechanisms of calycosin, glycitein, pratensein and prunetin**. *Computational and Theoretical Chemistry* 2012, **985**:14-22.

16. Chaillou LL, Nazareno MA: **New method to determine antioxidant activity of polyphenols**. *J Agric Food Chem* 2006, **54**(22):8397-8402.

17. Xie X, Liu K, Liu F, Chen H, Wang X, Zu X, Ma X, Wang T, Wu Q, Zheng Y: **Gossypetin is a novel MKK3 and MKK6 inhibitor that suppresses esophageal cancer growth in vitro and in vivo**. *Cancer letters* 2019, **442**:126-136.

18. Francis A, Shetty T, Bhattacharya R: **Modulating effect of plant flavonoids on the mutagenicity of N-methyl-N′-nitro-N-nitrosoguanidine**. *Carcinogenesis* 1989, **10**(10):1953-1955.

19. Jeong HJ, Ryu YB, Park S-J, Kim JH, Kwon H-J, Kim JH, Park KH, Rho M-C, Lee WS: **Neuraminidase inhibitory activities of flavonols isolated from Rhodiola rosea roots and their in vitro anti-influenza viral activities**. *Biorg Med Chem* 2009, **17**(19):6816-6823.

20. Wedworth SM, Lynch S: **Dietary flavonoids in atherosclerosis prevention**. *The Annals of pharmacotherapy* 1995, **29**(6):627-628.

21. de Whalley CV, Rankin SM, Hoult JRS, Jessup W, Leake DS: **Flavonoids inhibit the oxidative modification of low density lipoproteins by macrophages**. *Biochem Pharmacol* 1990, **39**(11):1743-1750.

22. Madala NE, Kabanda MM: **LC-MS based validation and DFT investigation on the antioxidant properties of clovamide:• OH and• OOH scavenging and Cu (II) chelation mechanisms**. *J Mol Struct* 2021, **1236**:130349.

23. Kaviani S, Shahab S, Sheikhi M, Ahmadianarog M: **DFT study on the selective complexation of meso-2, 3-dimercaptosuccinic acid with toxic metal ions (Cd2+, Hg2+ and Pb2+) for pharmaceutical and biological applications**. *J Mol Struct* 2019, **1176**:901-907.

24. Contreras-García J, Yang W, Johnson ER: **Analysis of hydrogen-bond interaction potentials from the electron density: integration of noncovalent interaction regions**. *The Journal of Physical Chemistry A* 2011, **115**(45):12983-12990.

25. Puthanveedu V, Muraleedharan K: **Phytochemicals as Potential Inhibitors for COVID-19 Revealed by Molecular Docking, Molecular Dynamic Simulation and DFT Studies**. Structural Chemistry 2022 33:1423–1443.

26. Puthanveedu V, Pulikkool C, Poonkottil N, Muraleedharan K: **Theoretical Probing to the Reactivity and Biological Effects of the Phytochemical, Coumestrol and its Derivatives**. *Chemical Physics Impact* 2022:100080.

27. Komjáti B, Urai Á, Hosztafi S, Kökösi J, Kováts B, Nagy J, Horváth P: **Systematic study on the TD-DFT calculated electronic circular dichroism spectra of chiral aromatic nitro compounds: A comparison of B3LYP and CAM-B3LYP**. *Spectrochimica Acta Part A: Molecular and Biomolecular Spectroscopy* 2016, **155**:95-102.

28. Kupfer S, Guthmuller J, Gonzalez L: **An assessment of RASSCF and TDDFT energies and gradients on an organic donor–acceptor dye assisted by resonance raman spectroscopy**. *J Chem Theory Comput* 2013, **9**(1):543-554.

29.   Isravel AD, Jeyaraj JK, Thangasamy S, John WJ: **DFT, NBO, HOMO-LUMO, NCI, stability, Fukui function and hole–Electron analyses of tolcapone**. *Computational and Theoretical Chemistry* 2021, **1202**:113296.

30.   Prasana JC, Muthu S, Abraham CS: **Molecular docking studies, charge transfer excitation and wave function analyses (ESP, ELF, LOL) on valacyclovir: a potential antiviral drug**. *Comput Biol Chem* 2019, **78**:9-17.

31.   Shang C, Zhang Y, Sun C, Wang L: **Tactfully improve the antioxidant activity of 2′-hydroxychalcone with the strategy of substituent, solvent and intramolecular hydrogen bond effects**. *J Mol Liq* 2022, **362**:119748.

32.   Priyadarsini KI, Maity DK, Naik G, Kumar MS, Unnikrishnan M, Satav J, Mohan H: **Role of phenolic OH and methylene hydrogen on the free radical reactions and antioxidant activity of curcumin**. *Free Radical Biol Med* 2003, **35**(5):475-484.

33.   Eno EA, Patrick-Inezi FA, Louis H, Gber TE, Unimuke TO, Agwamba EC, Ikenyirimba OJ, Akpanke JA, Oyoita E, Ejiofor EU: **Theoretical investigation and antineoplastic potential of Zn (II) and Pd (II) Complexes of 6-Methylpyridine-2-carbaldehyde-N (4)-ethylthiosemicarbazone**. *Chemical Physics Impact* 2022, **5**:100094.

34.   Bader RF: **Atoms in molecules**. *Acc Chem Res* 1985, **18**(1):9-15.

35.   Karaush NN, Baryshnikov GV, Minaeva VA, Minaev BF: **A DFT and QTAIM study of the novel d-block metal complexes with tetraoxa [8] circulene-based ligands**. *New J Chem* 2015, **39**(10):7815-7821.

36.   Bader RF, Stephens ME: **Spatial localization of the electronic pair and number distributions in molecules**. *Journal of the American Chemical Society* 1975, **97**(26):7391-7399.

Chapter 6

Phytochemicals as Potential Inhibitors for COVID-19 Revealed by Molecular Docking, Molecular Dynamic Simulation and DFT Studies

Abstract

The COVID-19 pandemic outbreak demands the designing of potential drugs as there is no specific treatment available. Thanks to their safety and effectiveness, phytochemicals have been used to treat various diseases, including antiviral therapeutics. Molecular docking is a simple, quick, and effective way to screen a variety of molecules for structure-based drug design. Here, we investigate molecular docking experiments on compounds present in plant species, C.hirsutus and R.rosea and show their potential for the treatment of COVID-19. Almost all the components showed higher binding energies than the built-in ligand, and those with significantly higher binding energies were explored further. Molecular mechanics-based generalized born surface area calculations were used to re-rank the top candidates, rhodionidin and cocsoline, and their stability in association with viral protease was confirmed. Density functional theory was used for detailed investigations of the geometries, electrical properties, and molecule electrostatic potential of rhodionidin and cocsoline. Using the frontier molecular orbitals method, the charge transfer within the molecule was calculated. Chemical reactivity and intermolecular interactions were studied using molecular electrostatic potential maps. These in silico discoveries will simulate the identification of powerful COVID-19 inhibitors, and similar research is likely to make a significant contribution to antiviral drug discovery.

6.1. Introduction

Infectious diseases are a major threat to public health and social well-being. The coronavirus family gained immense attention, when a new human coronavirus called COVID-19 first appeared in the city of Wuhan, China in December 2019 [1]. The global epidemic of severe acute respiratory syndrome (SARS-CoV-2) has impacted the whole world economy as well [2]. Coronavirus comes under the Coronaviridae [3] family in the order *nidovirale[4]*. Coronavirus contains crown-like spikes on the virus'outer surface [5]. The viruses are subdivided into four genera, alpha, beta, gamma, and delta coronavirus depending upon their genotypic and serological features [6]. The nucleotide sequence present in SARS-CoV-2 indicates that it belongs to the *betacoronavirus* category [7, 8]. Symptoms of COVID-19 include dry cough, fever, malaise, shortness of breath and breathing difficullty [9, 10].Drugs such as hydroxychloroquine [11], choloroquine phosphate [12], lopinavir [13], andremdesivir [14] are the antiviral therapies available for the coronavirus as of now. However, their effectiveness remains uncertain and needs further evaluation. In short, until now, there is no Food and Drug Administration (FDA) approved or specific drug for Covid-19 infection.

Plant species are an immense source of biologically important secondary metabolites such as flavonoids, alkaloids, glycosides, tannins, terpenoids, polyphenols, saponins [15, 16] *etc*. Drug development with phytochemicals is well-known among the numerous therapeutic approaches that have been developed for the treatment of various infections, including SARS-CoV-2. However, detection of

potential inhibitors using traditional methods is expensive as well as time-consuming. Therefore, in recent years, the use of *in silico* identification of druggable molecules is gaining tremendous attention as they offer fast and easy detection of potent drugs against various diseases [17, 18]. The discovery and isolation of medicinally important therapeutic compounds from higher plants for various diseases has been well established [19-23].

The screening of herbs that may contain anti-coronavirus compounds from a huge library of species is a big challenge. *Cocculus hirsutus L.*(*C.hirsutus),*a climbing shrub abundant with alkaloids, flavanoids, and phenolic compounds, comes under *Menispermaceae* family [24]. The plant has historically been disparaged for its peculiar property of healing many kinds of cuts and wounds and is common in tropical and subtropical environment [25]. It has been shown that this plant is one of the best candidates for treating various diseases such as gonorrhoea, spermatorrhoea, urinary disorders, diarrhoea and hyperglycemia, [26] *etc*. The phytochemicals present in this plant are involved in antimalarial [27], antibacterial [26], hyperglycaemic [28], anti-inflammatory, analgesic [28] diuretic and laxative [29] activities. The genus *Rhodiola,* belonging to the family Crassulaceae, is composed of almost 200 species. The well-known species among them is *Rhodiola rosea L.(R. rosea).* This plant is also called golden root or arctic root [30], is mainstream among herbal medicines and is commonly seen at higher altitudes in the arctic and in mountain ranges throughout Europe and Asia [31]. The medicinal application of *R.rosea* includes its ability to control psychological stress and mental strength,

change the neurotransmitter levels and central nervous system (CNS) activity, resistance to high altitude sickness, treat fatigue [32-36], and also act as an anti-depressant and anti-inflammatory drug [37]. Phytochemical analysis on *R.rosea* showed that the plant is well-equipped with bioactive components like organic acids, flavonoids, monoterpenes, triterpene, tannins, large amounts of phenolic compounds and some specific phenylpropane derivatives like rosavins [38].

The key druggable target of SARS-CoV-2 involves 3-chymotrypsin-like protease (3CL[pro]), papain-like protease (PL[pro]), RNA-dependent RNA polymerase, and spike (S) proteins [39, 40]. In this work, 6LU7, main protease (M[pro]) of COVID-19, crystallised by Liu et al. (2020), is used as a potential protein target for the phytochemicals selected. The *in silico* docking model is the main protease, which regulates the major functions of the virus and has a strongly preserved catalytic domain from the SARS virus [41]. Some of its roles involve the virus' replication, making it an attractive target for drug development [42]. Usable bioinformatics techniques such as molecular docking can be implemented using comprehensive 3D-structures of related biomolecule and phytochemicals to rapidly classify promising and potential drug candidates. In order to completely unravel the fundamental interactions responsible for drug-receptor binding and subsequent structural modifications, this can be accompanied with atomistic molecular dynamics, leading to changes in biological system function. The current work focuses on the identification of bioactive components present in the herbs *C.hirsutus*

and R.rosea and their antiviral activity towards COVID 19 main protease 6LU7 with the aid of molecular docking and molecular dynamic simulation studies. Towards the end we use density functional theory (DFT) at the B3LYP/6-31++G(d,p) level of theory to find the optimal structures of the molecules from each plant that have the maximum binding affinity with the specified target. Following that, their reactivities were predicted at the same level of theory using frontier orbital investigations. Furthermore, molecular electrostatic potential surfaces were investigated to determine which parts of a molecule are the most reactive nucleophilic and electrophilic against reactive biological potentials.

6.2. Materials and methods

6.2.1 Molecular docking

Preparation of Protein/Receptor

The crystal structure of COVID-19 main protease in complex with an inhibitor N3 (PDB ID- 6LU7) with resolution 2.16 Å was downloaded from RCSB protein data bank database (www.rcsb.org) as .pdb format. The 6LU7 protein contains two chains, A and C, in which A represents the protein and C corresponds to the inbuilt ligand. Prior to the detailed docking analysis, chain A was chosen as the target for this study and then the preparation of the protein was performed using AutoDock tool. The selected protein complex contains an inbuilt ligand N-[(5-METHYLISOXAZOL-3-YL) CARBONYL]ALANYL-L-VALYL-N~1~-((1R,2Z)-4-(BENZYLOXY)-4-OXO-1-{[(3R)-2-

OXOPYRROLIDIN-3-YL]METHYL}BUT-2-ENYL)-L-
LEUCINAMIDE.

Both the water molecules and non-interacting ions, along with the native ligand, were eliminated from the crystal structure. The missing hydrogens were added in order to alleviate the stress of the crystal structure and make the protein accessible for use in the AutoDock docking simulation program. After the structural minimization, the protein was prepared using AutoDock Tools (version1.5.6) (ADT), graphical user interface, which involves the addition of hydrogen atoms, Gasteiger charges calculation and merging of non-polar hydrogens to carbon atoms. The generated macromolecular structure was then saved as pdbqt file.

Ligand Preparation

Most of the ligands were downloaded from the PubChem database (https://pubchem.ncbi.nlm.nih.gov/). The downloaded ligands in .sdf format were converted into .pdb file using OpenBabel software (version 2.4.1). The ligands structures that were unavailable in the PubChem database were created using Maestro and the structures were downloaded in pdb format. Ligand input files for docking was prepared using AutoDock Tools and saved as pdbqt files.

Docking

For the detailed analysis of intermolecular interactions and binding modes between the protein and specific phytochemicals present in *C. hirsutus* and *R. rosea*, the molecular docking studies were

executed for selected ligands using AutoDock Vina software. A grid box with dimension X:15, Y:22, Z:20Å with a grid spacing of 1.0 Å centered at X: -9.491, Y:11.784, Z: 65.363A^0 was identified as protein target docking site. The interactions between active sites in the target and ligand conformation, including the type of interaction and bond distances, were identified using Discovery Studio Visualiser.

6.2.2 Binding energy calculations using Prime/MMGBSA studies

The calculation of free energy provides a quantitative estimate of protein-ligand interactions that can predict the stability of protein-ligand complexes. Molecular mechanics-generalized born surface area (MM-GB/SA) was conducted with Prime module of Schrodinger 2018 to calculate binding energy of protein-ligand complexes.MM-GBSA method in Prime was used for rescoring the docked pose of ligands together with calculation of coulomb energy, covalent binding energy, hydrogen-bonding correction, pi-pi packing correction, lipophilic energy, generalized born electrostatic solvation energy, van der Waals energy.

6.2.3 Molecular Dynamics Simulation

To forecast the stability of protein-ligand complexes, molecular dynamic simulations were performed in Desmond package of the Schrodinger suit. The chosen protein-ligand complexes were first immersed in the TIP4P water box, extending 10 Å beyond any atoms of the complex. The orthorhombic boundary condition box selected, and buffer method is used for box size calculation. To neutralise charges, counter ions (3 Na$^+$) were added. The MD was conducted at a

temperature of 310K and 1.63 bar pressure over 100 ns in the NPT ensemble with recording intervals of 12ps for trajectory. Simulations were performed with the force field of OPLS-3e. The Desmond simulation interaction diagram method from Maestro was used to sketch plots and figures.

6.2.4 Quantum chemical analysis

Density Functional Theory (DFT) is an intriguing method for probing many biological features of interest. The current study employs DFT analysis to highlight the electronic features of the phytochemicals. The geometry optimizations of the selected compounds cocsoline (from *C.hirsutus*) and rhodionidin (from *R.rosea*) were carried out using Gaussian16 at the B3LYP/6-31++G(d,p) level. Based on the optimised structure in the gas phase, electronic characteristics such as HOMO-LUMO energies and molecular electrostatic potential (MEP) were computed. The natural population analysis, as well as global reactivity descriptors, were further investigated for the selected compounds.

6.3 Molecular docking analysis of phtochemicals present in *C.hirsutus* and *R.rosea*

The essential parts of the structure-based drug designing phase involve the docking of small molecules into the receptor's active site and evaluating the binding affinity of ligand towards target protein. In the current study, the selected protein, 6LU7 contains a peptide like inbuilt ligand N3 **(Fig. 6.1.)** that exhibits very potent inhibition against COVID-19 virus M^{pro} [43]. In order to compare the binding affinity as

well as the inhibition potency of selected phytochemicals, the docking process was also performed on the native ligand.
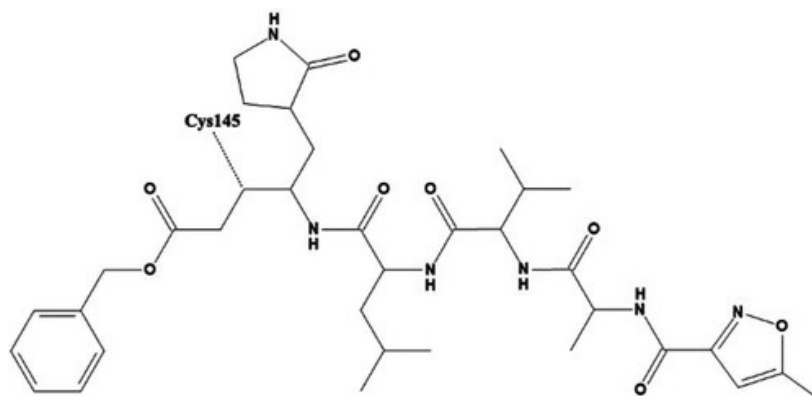
Fig. 6.1 Two-dimensional image of inbuilt ligand N3, figure taken from reference [44]

The plant *C.hirsutus* as a rich source of potential anti-coronavirus drugs could be evaluated by analysing molecular docking results and comparing these with the values of in-built ligand. The structures of the phytochemicals with highest binding affinity values are presented in **Fig. 6.2.** The binding affinity values of the phytochemicals present in *C.hirsutus* as calculated from the software AutoDock Vina is shown in **Table 6.1** and the binding affinity values of the components in *C.hirsutus* with high inhibition efficiency than that of in-built ligand N3 is shown in **Fig. 6.3a**. The binding affinity of N3 with the target protein obtained from the docking study was -7.0 kcal/mol. Highest binding energy value of -9.1 kcal/mol was observed for the phytoconstituent, cocsoline. The flavonoids rutin, liquiritin and quercetin with binding energy values -8.8, -7.5 and -7.5 kcal/mol

respectively prove that they could also act as possible inhibitors against 6LU7 protein target. Isotrilobine, coclaurine, cohirsine, and lupeol, exhibiting binding affinity values like -8.6, -7.6, -7.4, -7.3 and -7.1 kcal/mol respectively are still higher than that of binding affinity of native ligand N3.

Table 6.1 The binding affinity values of the phytochemicals present in *C.hirsutus* as calculated from the software AutoDock Vina

Inhibitors	Binding affinity (kcal/mol)
Cocsoline	-9.1
Rutin	-8.8
Isotrilobine	-8.6
Coclaurine	-7.6
Liquiritin	-7.5
Quercetin	-7.5
Cohirsinine	-7.5
Cohirsitinine	-7.5
Jamtinine	-7.5
Shaheenine	-7.5
Cohirsine	-7.4
Lupeol	-7.3
Betulin	-7.1
N3[a]	-7.0
Campestrol	-6.9
Jamtine	-6.8
Haiderine	-6.9
Hirsutine	-6.7
Lirioresinol	-6.5
Squalene	-6.0

*Native ligand N3

Cocsoline   Rutin   Isotrilobine   Coclaurine

Liquiritin   Quercetin   Cohirsinine   Cohirsitinine

jamtinine   shaheenine
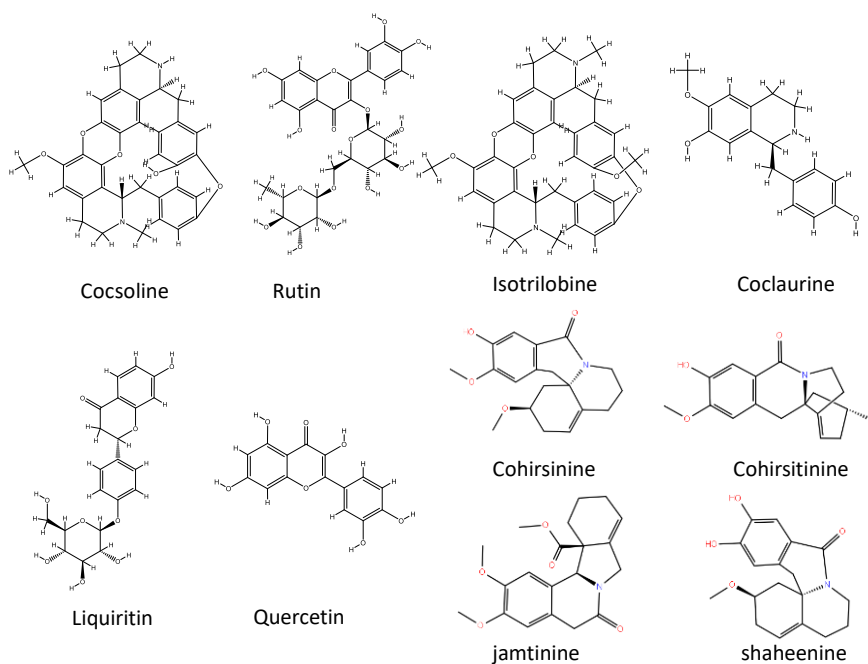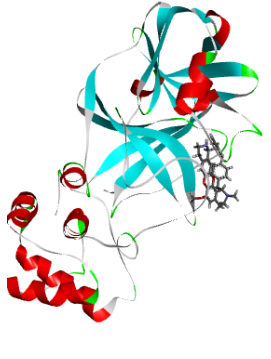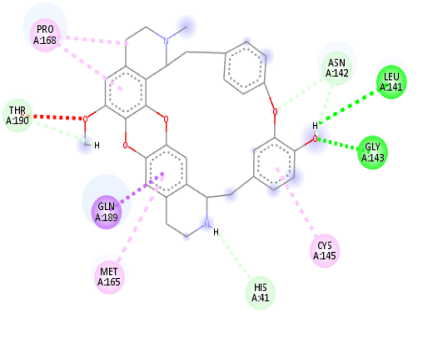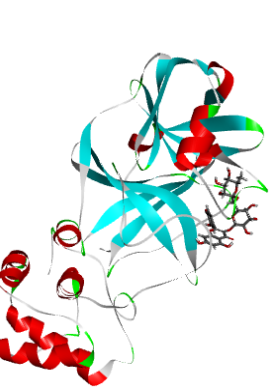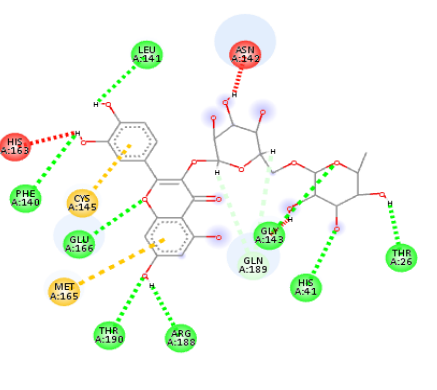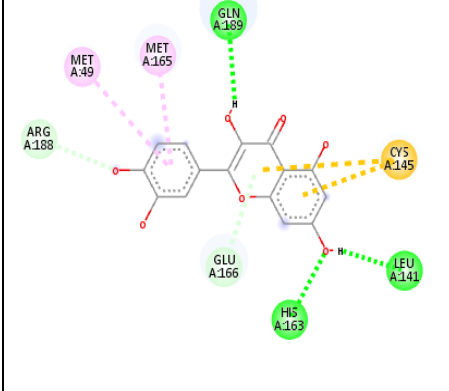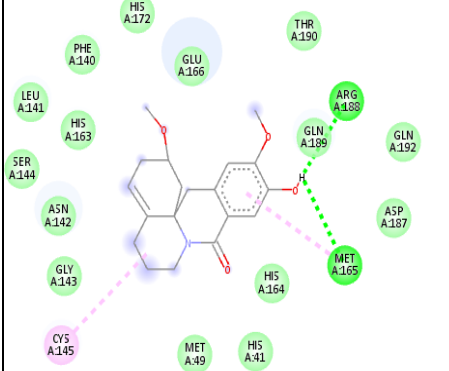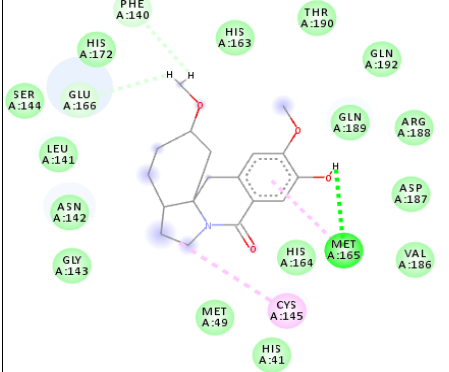
Fig. 6.2 The Phytochemicals present in *C.hirsutus,* showing a strong binding affinity (less than or equal to -7.5 kcal/mol) for SARS-CoV-2

Table 6.2 The 3D images of phytochemicals of the plant, *C.hirsutus* having low binding energy values<-7.4 kcal/mol within the active site of 6LU7 and their interactions with the target protein

Phytochemical	3D image of inhibitors within the active site of 6LU7	2D interaction between inhibitor and target
Cocsoline		
Rutin		

Isotrilobine		
Coclaurine		
Liquiritin		

Quercetin		
Cohirsinine		
Cohirsitinine		
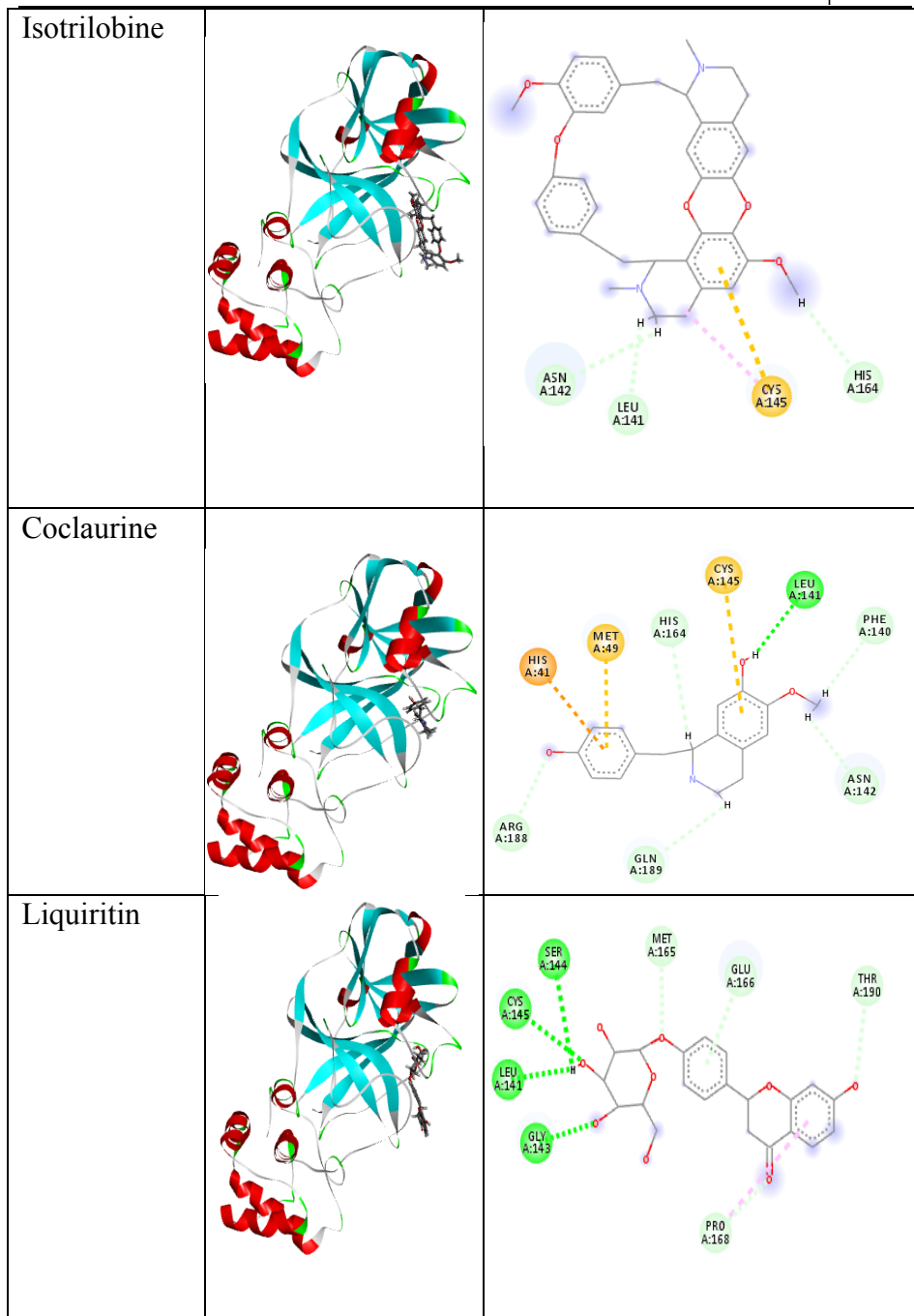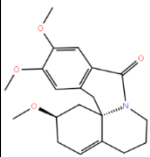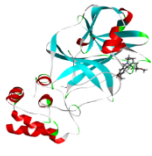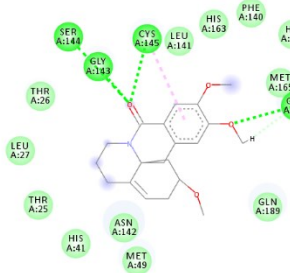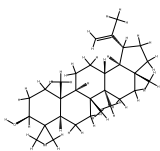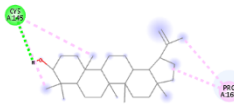
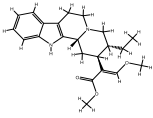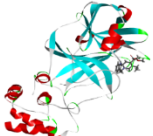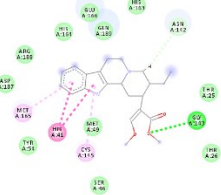| Jamtinine		
Shaheenine		
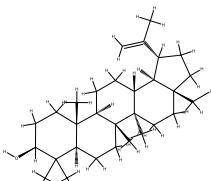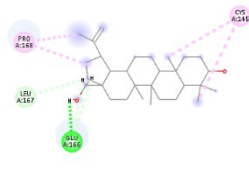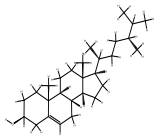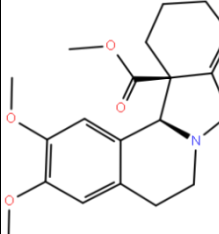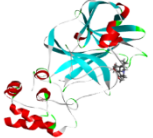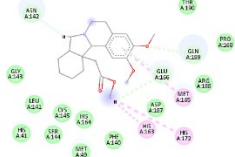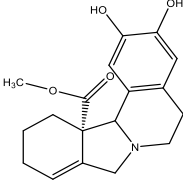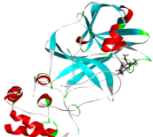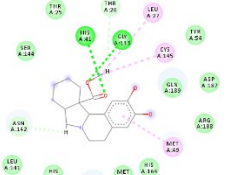
Docking analysis of phytochemicals of the plant *C.hirsutus* shows that all of them show strong interactions with the surrounding amino acid residues. The two-dimensional, as well as the three-dimensional interactions of components of C.*hirsutus* having low binding energy values<-7.4 kcal/mol with 6LU7, are represented in **Table 6.2**. Cocsoline, having the highest binding affinity possess hydrogen bond interaction between its hydroxyl group and amino acid residues LEU141 and GLY143 near to it. This molecule, within the protein active site, shows hydrophobic interactions such as alkyl and

pi-alkyl interactions with CYS145, MET165, and PRO168. The molecule has interacted well with a number of aminoacid residues like ASN142, HIS41, THR190 and GLN189 near to it. The structure, 3D images of the phytochemicals within the active site of 6LU7, and 2D interaction of the phytochemicals present in the plant C.*hirsutus,* with binding energy values greater than -7.4 kcal/mol with the target is given in **Table 6.3**.

Table 6.3 The structure (2ndcoloumn), 3D images (3rd) of the phytochemicals within the active site of 6LU7, and 2D interaction of the phytochemicals (4th) present in the plant *C.hirsutus,* with binding energy values greater than -7.4kcal/mol with the target

Inhibitor	Structure	3D image of inhibitor within the active site	2D interaction between inhibitor and target
Cohirsine			
Lupeol			

Betulin			
Campestr ol			
Jamtine			
Haiderin e			
Hirsutine			

| Lirioresinol | | | |
| Squalene | | | |

Fig. 6.3 a) The binding affinity values of the components in *C.hirsutus* with high inhibition efficiency than that of in-built ligand N3 as calculated from the software AutoDock Vina **b)** The binding affinity values of the components in *R.rosea* with high inhibition efficiency than that of in-built ligand N3 as calculated from the software AutoDock Vina

*Native ligand N3 shown in red colour

357

The majority of the chemicals found in *R.rosea* had good binding affinity values with the specified protein target, 6LU7, according to data from molecular docking. The most of the binding affinity values were found to be greater, with some even being comparable to the native ligand N3. The molecular docking results of bioactive components present in *R.rosea* with SARS-CoV-2 are shown in the **Table 6.4** and the binding affinity values of the components with high inhibition efficiency than that of in-built ligand N3 is shown in **Fig. 6.3b.**

Table 6.4 The binding affinity values for the phytochemicals present in *R.rosea* as calculated from the software AutoDock Vina

Inhibitors	Binding affinity (kcal/mol)
Rhodionidin	-9.6
Rhodiolgidin	-8.9
Rhodalin	-8.6
Rhodalidin	-8.5
Rhodionin	-8.0
Rhodiolgin	-8.0
Rosavin	-7.9
Rosarin	-7.8
Kaempferol	-7.7
Rhodiosin	-7.6
Gossypetin	-7.4
Herbacetin	-7.3
Sachaliside	-7.3
Rhodioloside	-7.0
Rosin	-7.0
Vimalin	-7.0

N3[*]	-7.0
Picein	-6.9
Rosiridin	-6.9
Gallic acid	-5.5
Rosiridol	-5.1
Geraniol	-4.9
Cinnamylalchohol	-4.7
limonene	-4.5
Alpha-pinene	-4.3
decanol	-4.0

*Native ligand N3

The binding affinity of phytochemicals present in *R.rosea* ranges from -9.6 to -4.0 kcal/mol and most of the components show higher inhibition tendency towards SARS-CoV-2 compared to the native ligand. Among the bioactive components selected, rhodionidin, rhodiolgidin, rhodalin, rhodalidin, rhodionin, and rhodiolgin, coming under the flavonoid category exhibited lowest binding energy values such as -9.8, -8.9, -8.6, -8.5, -8.0, -8.0 kcal/mol respectively. The structures of phytochemicals of *R.rosea* having low binding energy values less than or equal to -8.0kcal/mol is shown in **Fig. 6.4**. The flavonoids such as kaempferol, rhodiosin, gossypetin, and herbacetin also show high binding affinity values which are still higher than the binding affinity of inbuilt ligand (-7.0 kcal/mol). Rosavin, rosarin and sachaliside, belonging to the phenyl proponoid group, also showed a high affinity towards the target protein. Docking studies revealed that rosin and vimalin (belonging to phenylproponoids) and rhodioloside (belonging to phenylethanoids) show a binding energy value with the

SARS-CoV-2 which is equal to the binding energy of inbuilt ligand with the same target. Other components like picein, rosiridin, gallic acid, rosiridol, geraniol, cinnamyl alcohol, limonene, alpha-pinene, and decanol exhibit low inhibition for the target More interestingly, these values are still comparable with the native ligand.
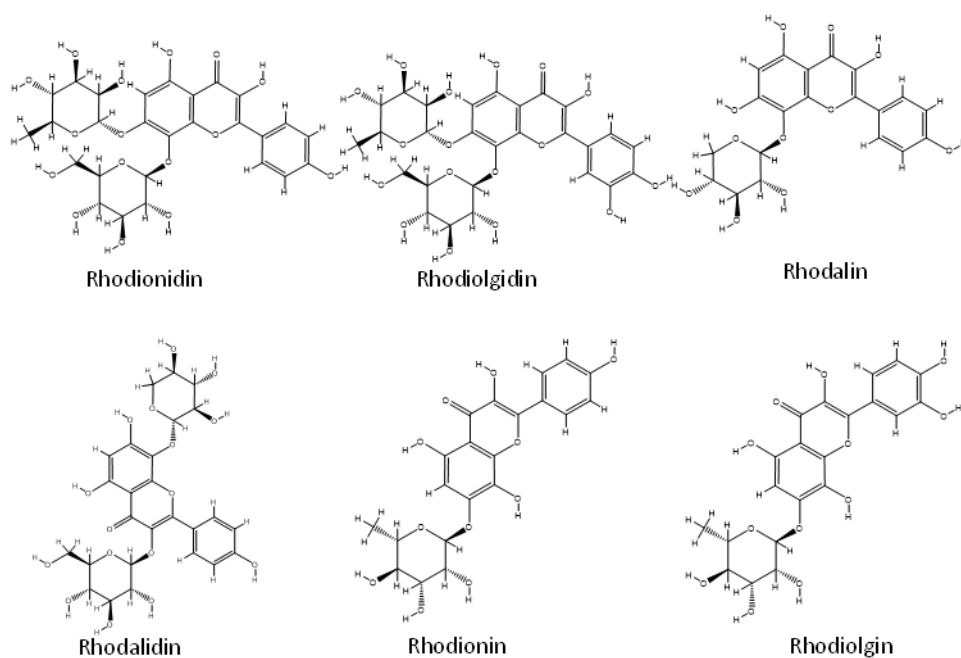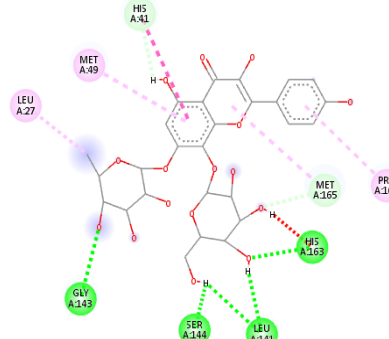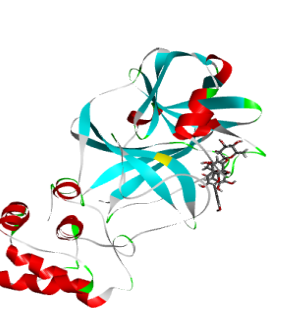

Rhodionidin   Rhodiolgidin   Rhodalin

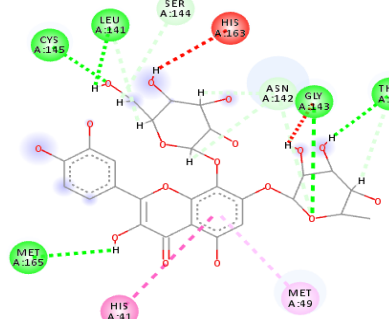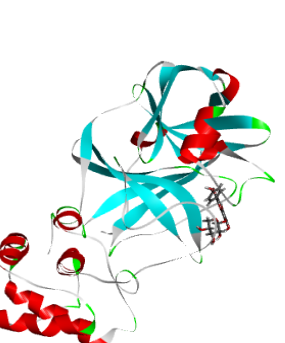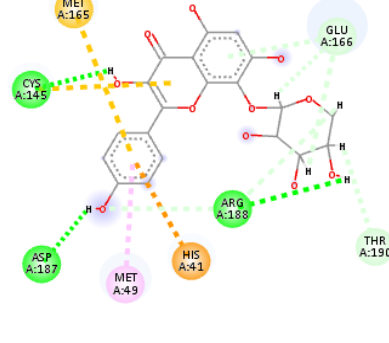Rhodalidin   Rhodionin   Rhodiolgin

Fig. 6.4. Selection of structures of phytochemicals present in *R. rosea* that show strong binding affinity (binding energy values less than or equal to -8 kcal/mol) towards the SARS-CoV-2

Table 6.5 The 3D images of the phytochemicals present in the plant *R. Rosea* having low binding energy values<-7.9 kcal/mol within the active site of 6LU7 and their interactions with 6LU7

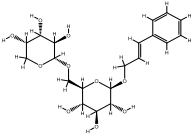| Phytochemical	3D image of inhibitors within the active site of 6LU7	2D interaction between inhibitor and target
Rhodionidin		
Rhodiolgidin		
Rhodalin		

Rhodalidin		
Rhodionin		
Rhodiolgin		
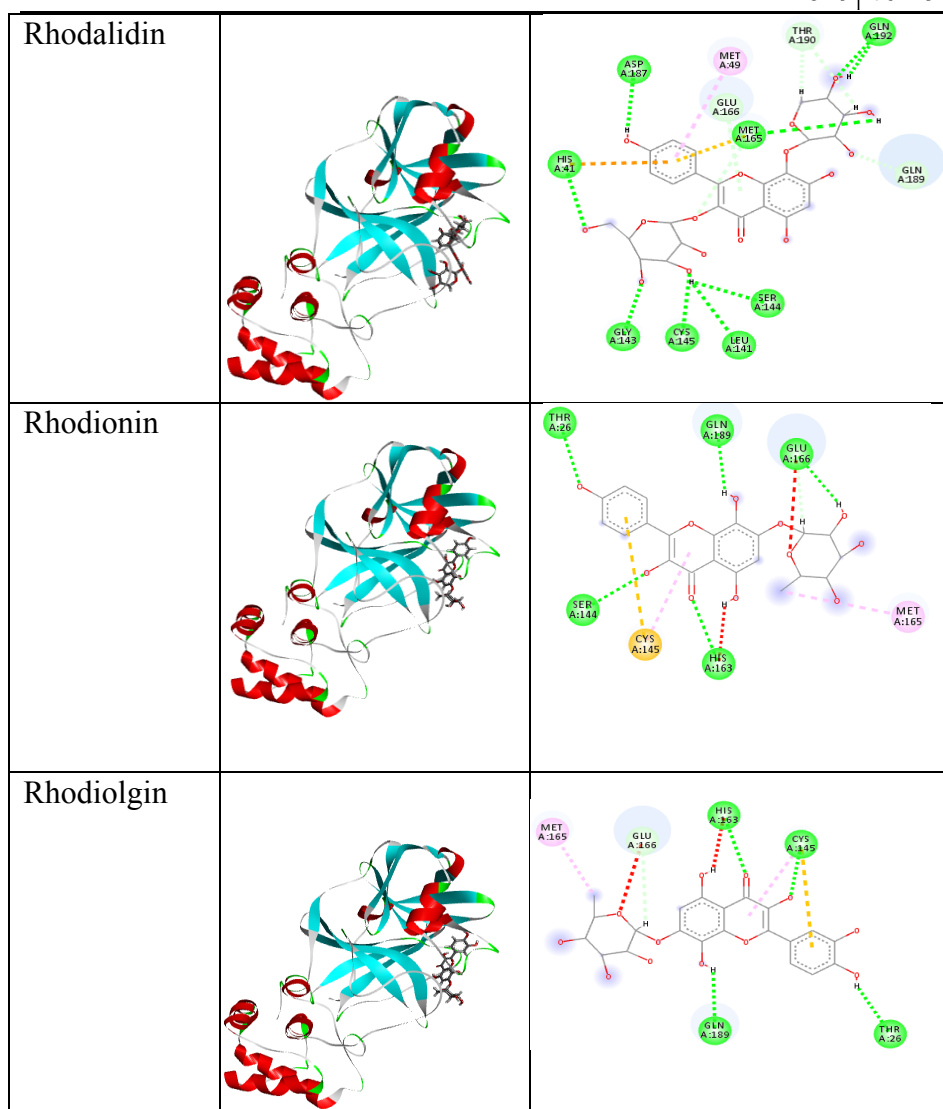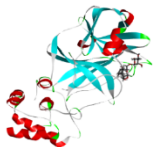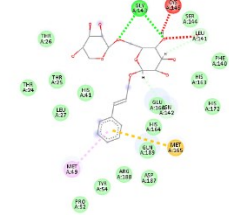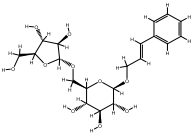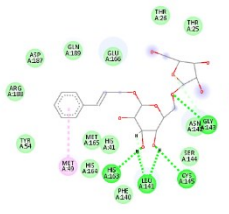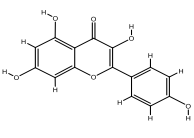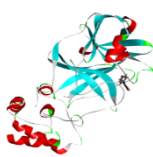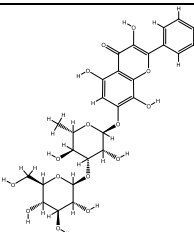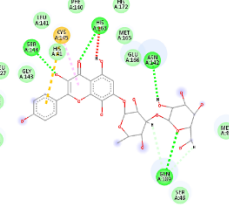
The three- and two-dimensional binding interactions of best scoring components present in R.rosea having low binding energy values<-7.9 kcal/mol with 6LU7 are provided in **Table 6.5**. The major interactions involved are conventional hydrogen bonding, alky, pi-alkyl, pi-pi, pi-S, pi-cation, carbon-hydrogen bond, and pi donor
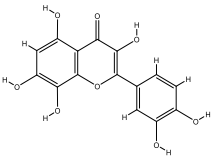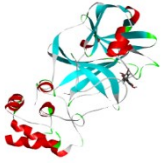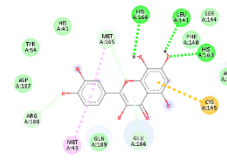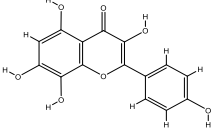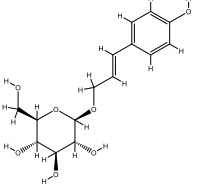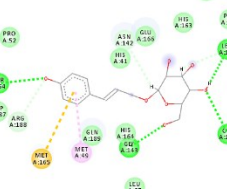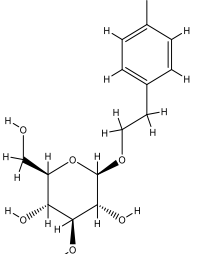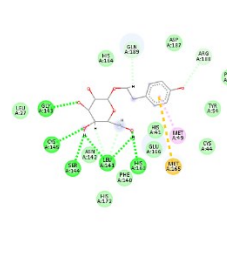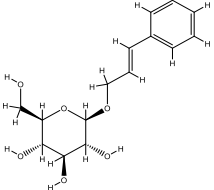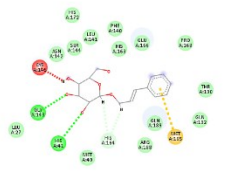
hydrogen bond and all of the chemical components shows very strong interaction with the protein studied.
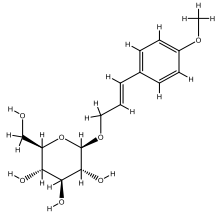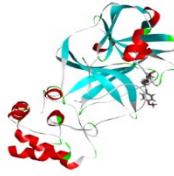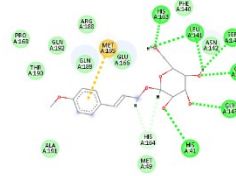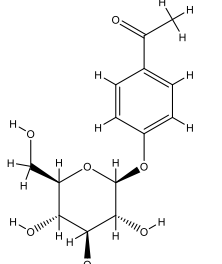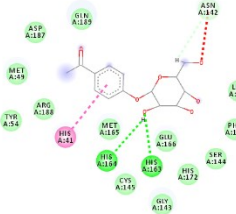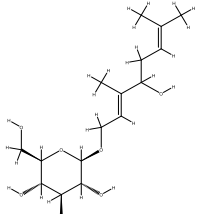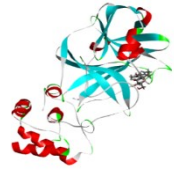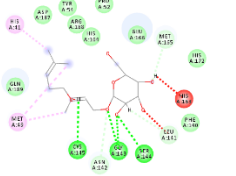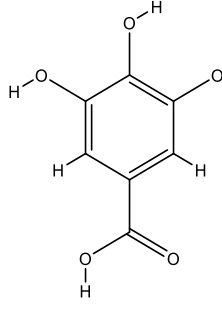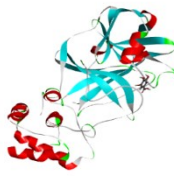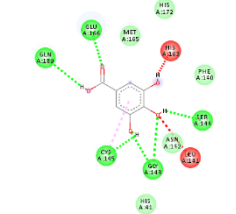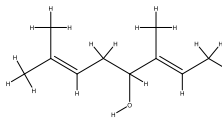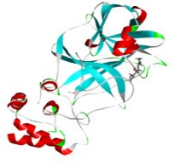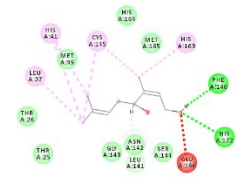
The detailed visualisation of stable conformer of rhodionidin, the top-ranked (binding energy value of -9.6 kcal/mol) SARS-CoV-2 inhibitor at the binding site of 6LU7 reveals the existence of a strong hydrogen bond interaction between hydroxyl groups present in the ligand and GLY143, SER144, LEU141, and HIS163 amino acid residues of the target protein. A π-π interaction exists between the inhibitor and HIS41 residue present in the active site of 6LU7. Alkyl and aromatic fragments present in the inhibitor form hydrophobic interactions such as alkyl and pi alkyl interaction with LEU27, MET49, PRO168 and MET165 residues. Furthermore, the molecule is well fixed within the cavity of the active site.

From the detailed interaction studies of phytochemicals present in the herb *R. rosea* showing high binding energy with selected protein proved that all components are potential inhibitors and possess strong interactions with the target. The structure, 3D images of the phytochemicals within the active site of 6LU7, and 2D interaction of the phytochemicals present in the plant *R. rosea,* with binding energy values greater than -8.0kcal/mol with the target is given in **Table 6.6**.

Table 6.6 The structure (2ndcoloumn), 3D images (3rd) of the phytochemicals within the active site of 6LU7, and 2D interaction of the phytochemicals (4th) present in the plant *R. rosea,* with binding energy values greater than -8.0kcal/mol with the target

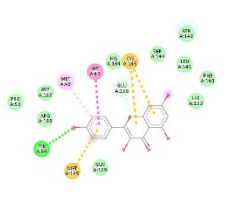| Inhibitor	Structure	3D image of inhibitor within the active site	2D interaction between inhibitor and target
Rhosavin			
Rhosarin			
Kaempferol			
Rhodiosin			

Gossypetin			
Herbacetin			
Sachaliside			
Rhodioloside			
Rosin			

Vimalin			
Picein			
Rosiridin			
Gallic acid			
Rosiridol			

Geraniol			
Cinnamyl alchohol			
Limonene			
Alpha-pinene			
Decanol			

6.4 Molecular dynamic simulation using Desmond package

Since docking is a static view of the molecule's binding position in the protein's active site, Molecular dynamics (MD) simulation attempts to quantify atomic motions over time by integrating the classical motion equation of Newton. The dynamic behaviour of the molecular system is simulated in MD, in order to assess the stability of the protein-ligand complex. For the MD analysis with the OPLS3e force field, the docked conformers of cocsoline and rhodionidin with the highest predictive binding energy of −9.1 and -9.6 kcal/mol were therefore used. The dynamic features of these two selected systems were calculated during the period of 100 ns simulation. We evaluated the stability of the docked compounds in the active pocket of 6LU7 by using root mean square deviation (RMSD) and its effects on the stability of the entire system.
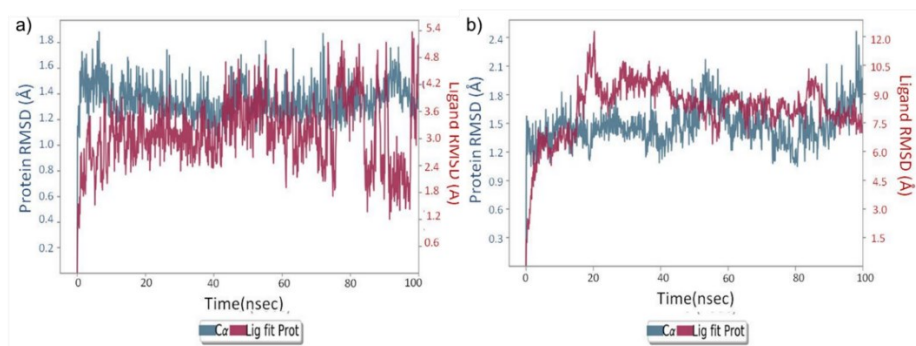
Fig. 6.5 RMSD analysis for MD simulation trajectories for **a)** rhodionidin:6lu7 complex **b)** cocsoline:6lu7 complex

RMSD plot in **Fig. 6.5a.** indicates the rhodionidin:6lu7 complex MD trajectory for 100 ns. The complex appears to be stabilised within a short time with respect to the reference frame at

time 0 ns, during the simulation phase. The RMSD variation of 6lu7 was only around 1.6 Å which can be considered insignificant. This in turn means that the protein RMSD appears to be stable during the simulation, indicating that the protein has not undergone major conformation changes. Fluctuation within 20-40 ns of the trajectory was observed in the case of ligand RMSD which indicate major conformational changes of the ligand. After 40 ns, the ligand RMSD stabilised again and remained constant until the end of the simulation period of 100ns. The ligand has undergone conformational changes with an overall RMSD of 6 Å, possibly because of a large number of rotatable bonds that contribute to its flexibility. The protein RMSD appears to be constant with negligible variation which means that the protein is undergoing minimum conformational change during the simulation. The rhodionidin:6lu7 complex's overall RMSD plot shows that the ligand is less stably connected to the protease binding site.

The RMSD plot in **Fig. 6.5b.** shows that the cocsoline:6lu7 complex stabilised immediately after the simulation started, relative to the reference frame at 0 ns. During the simulation, the complex appears to be stabilised with regard to the reference frame at time 0 ns. It is possible to see a small divergence at the end of the simulation, i.e. 80 ns. The fluctuation, however, lies within the acceptable range of 1-3 Å, and can therefore be considered non-significant. In this complex, since the ligand and protein backbone RMSD plots were lying over each other, it is possible to conclude a stable complex formation. RMSD value analysis reveals that the complex cocsoline:6lu7 was more stable compared to the rhodionidin:6lu7 complex.
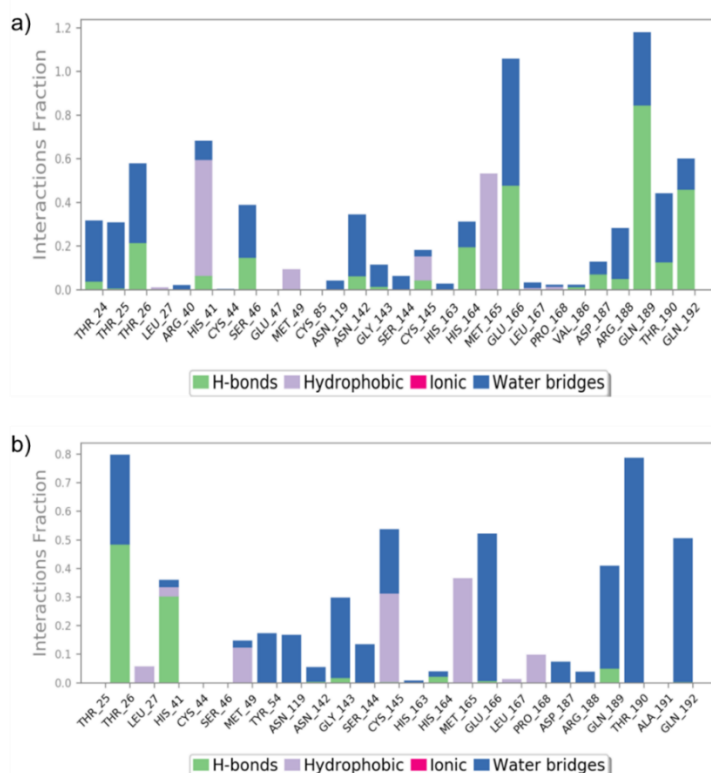
Fig. 6.6 a) Rhodionidin: 6LU7, **b)** Cocsoline : 6LU7 contact throughout the trajectory
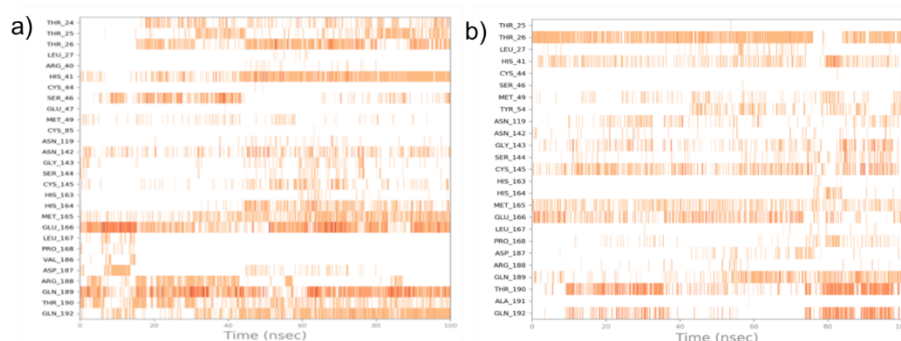
Fig. 6.7 a) Rhodionidin: 6LU7 and **b)** Cocsoline: 6LU7 interactions shown in each trajectory frame by the active site amino acids, no interactions are represented by white while stronger interactions by the dark colour

The position of the binding modes of compounds rhodionidin and cocsoline has also been verified by the MD modelling counterpart. During the simulation, protein interactions with the ligand were regulated. Such interactions can be arranged and analysed as depicted in **Fig. 6.6.** Protein-ligand interactions have been classified as hydrogen bonds, hydrophobic, ionic and water bridges. In order to keep the protein-ligand complex stable, the form of amino acid residues present in the active site of the target protein plays a crucial role. **Fig. 6.6a.** indicate the type of contacts maintained in the entire trajectory of rhodionidin:6LU7 complex. In the case of rhodionidin, GLN189, GLU166, GLN192 were able to hold down the hydrogen bonding interactions during 85%, 48% and 47% of the time, respectively. It also showed a greater number of hydrogen bonding contacts with THR26, SER46, HIS164, and THR190 around 10-20% of the time. Hydrophobic interactions were found with HIS41, MET165, CYS145, and MET49, during 60, 55, 15 and 10% respectively. Water bridge hydrogen bonding where one water molecule used as a bridge between ligand and protein was also formed with GLU166, GLN189, THR24, THR25, THR26, SER46, ASN142, ARG188, THR190 and GLN192.

The various types of interaction between cocsoline and 6LU7 at the active site during the entire simulation period is represented in **Fig. 6.6b.** Cocsoline showed hydrogen bonding interaction with THR26 and HIS41 which were 49% and 30% of the time, respectively. It also exhibits weak hydrogen bonding contacts with GLN189, GLY143, HIS164, and GLU166 less than 10% of the time. Cocsoline possess

multiple water bridge hydrogen bonding with THR190, GLN192, GLN189, GLU166, CYS145, GLY143, SER144, TYR54, ASN119, THR25, HIS41, MET49, ASN142, HIS163, HIS164, ASP189, and ARG188 residues.

Relevant timeline contacts of the compounds rhodionidin and cocsoline with the amino acid residues that were present in the targets are also studied and briefly provided in **Fig. 6.7.** The darker colour reflects the high number of ties to the amino acid.

6.5 MMGBSA analysis

MMGBSA is a popular analysis method to calculate the average binding energy of equilibrated MD trajectory of the systems. MMGBSA calculations were conducted in order to provide a better ranking of the ligands, and determination of predictive binding energies. The binding free energies of the two selected systems indicate the binding affinity of ligands with 6LU7.The values obtained after measurement were estimated free binding energies with a more negative value, suggesting a stronger binding energy. **Table 6.7** depicts the average binding energy, coulomb energy, covalent binding energy, Hydrogen-bonding correction, Pi-pi packing correction, Lipophilic energy, Generalized Born electrostatic solvation energy, van der Waals energy of rhodionidin and cocsoline with 6LU7. Rhodionidin exhibited highest negative binding energy of -80.40 kcal/mol. MMGBSA calculation revealed that cocsoline showed an approximate binding energy value of -75.07 kcal/mol.

Table 6.7 MMGBSA analysis of Rhodionidin and Cocsoline with 6lu7

Molecule	ΔG Binding (kcal/mol)	Coulomb (kcal/mol)	Covalent (kcal/mol)	H-bonding (kcal/mol)	Bind packing (kcal/mol)	Lipo (kcal/mol)	Solv_GB (kcal/mol)	vdW (kcal/mol)
Rhodionidin	-80.40	-41.28	7.53	-3.91	-3.05	-16.78	39.04	-61.95
Cocsoline	-75.07	-18.38	3.82	-1.49	-1.92	-24.17	29.18	-62.10

6.6 DFT studies

6.6.1 Geometry optimization

The optimized structures of cocsoline and rhodionidin obtained at B3LYP/6-31++G(d,p) level are given in **Fig. 6.8** and the corresponding geometrical parameters are given in **Tables 6.8-6.13**. The total energy of cocsoline and rhodionidin computed at the same basis set are -1800.92 and -2251.14hartree respectively. A molecule's dipole moment is a three-dimensional vector that depicts the molecular charge distribution. As a result, it can be used as a descriptor to characterise the charge flow within a molecule. The DFT/ B3LYP/6-31++G(d,p) computations showed that, the rhodionidin and cocsoline processed a dipole moment value of 8.88 Debye, and 2.54 Debye respectively. Rhodionidin has a greater dipole moment than cocsoline, indicating that it is softer. The large number of hydroxyl groups in the structure of rhodionidin may facilitates a greater number of hydrogen bond formation.
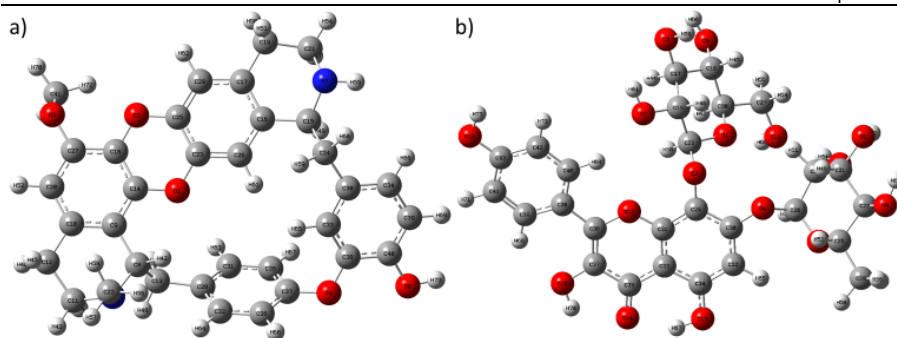
Fig. 6.8 Optimized geometry of **a)** cocsoline and **b)** rhodionidin obtained from DFT/ B3LYP/6-31++G(d,p) calculation

Table 6.8 Optimized bond length of cocsoline under DFT/ B3LYP/6-31++G(d,p)

Bond	Bond length (A^0)	Bond	Bond length (A^0)	Bond	Bond length (A^0)	Bond	Bond length (A^0)
R(1,14)	1.3834	R(9,14)	1.3988	R(19,21)	1.5252	R(30,33)	1.3982
R(1,23)	1.3823	R(10,12)	1.516	R(19,50)	1.0947	R(30,34)	1.3965
R(2,18)	1.3823	R(10,20)	1.3974	R(19,51)	1.0961	R(31,35)	1.3915
R(2,25)	1.381	R(11,12)	1.5368	R(20,27)	1.3907	R(31,63)	1.0849
R(3,27)	1.3714	R(11,43)	1.0936	R(20,52)	1.0845	R(32,36)	1.3944
R(3,41)	1.4333	R(11,44)	1.0945	R(21,53)	1.105	R(32,64)	1.0851
R(4,37)	1.3907	R(12,45)	1.0968	R(21,54)	1.0929	R(33,38)	1.392
R(4,38)	1.3767	R(12,46)	1.095	R(22,56)	1.0929	R(33,65)	1.0818
R(5,40)	1.3669	R(13,28)	1.5133	R(22,57)	1.0933	R(34,39)	1.3954
R(5,73)	0.9628	R(13,47)	1.0919	R(22,58)	1.1021	R(34,66)	1.085
R(6,8)	1.471	R(13,48)	1.0935	R(23,25)	1.3923	R(35,37)	1.3919
R(6,11)	1.4651	R(14,18)	1.3925	R(23,26)	1.3842	R(35,67)	1.0836
R(6,22)	1.4616	R(15,16)	1.5301	R(24,30)	1.516	R(36,37)	1.3905
R(7,15)	1.469	R(15,24)	1.5668	R(24,59)	1.0917	R(36,68)	1.0836
R(7,21)	1.4608	R(15,49)	1.1052	R(24,60)	1.0931	R(38,40)	1.4031
R(7,55)	1.0142	R(16,17)	1.4043	R(25,29)	1.3843	R(39,40)	1.3928
R(8,9)	1.5299	R(16,26)	1.4004	R(26,61)	1.081	R(39,69)	1.0866
R(8,13)	1.5698	R(17,19)	1.5141	R(28,31)	1.3984	R(41,70)	1.0895
R(8,42)	1.0914	R(17,29)	1.4004	R(28,32)	1.4002	R(41,71)	1.0955
R(9,10)	1.4017	R(18,27)	1.4	R(29,62)	1.0847	R(41,72)	1.092

Table 6.9 Optimized bond angles of cocsoline under DFT/ B3LYP/6-31++G(d,p)

Bond angles	Angle(^{0})	Bond angles	Angle(^{0})	Bond angles	Angle(^{0})
A(4,1,23)	116.7754	A(17,19,50)	109.9005	A(31,35,67)	120.8444
A(18,2,25)	116.2075	A(17,19,51)	109.5105	A(37,35,67)	119.7245
A(27,3,41)	116.192	A(21,19,50)	110.3639	A(32,36,37)	119.4132
A(37,4,38)	117.04	A(21,19,51)	108.7873	A(32,36,68)	121.2737
A(40,5,73)	109.2511	A(50,19,51)	107.1956	A(37,36,68)	119.3011
A(8,6,11)	111.1967	A(10,20,27)	121.5947	A(4,37,35)	120.4924
A(8,6,22)	113.1512	A(10,20,52)	120.6581	A(4,37,36)	119.0747
A(11,6,22)	113.1637	A(27,20,52)	117.7361	A(35,37,36)	120.4285
A(15,7,21)	113.2416	A(7,21,19)	108.1426	A(4,38,33)	122.9291
A(15,7,55)	109.0114	A(7,21,53)	112.4284	A(4,38,40)	117.4395
A(21,7,55)	110.4693	A(7,21,54)	108.6942	A(33,38,40)	119.6112
A(6,8,9)	112.6361	A(19,21,53)	109.6458	A(34,39,40)	121.1022
A(6,8,13)	110.5046	A(19,21,54)	110.4186	A(34,39,69)	119.8771
A(6,8,42)	106.5451	A(53,21,54)	107.5136	A(40,39,69)	119.0197
A(9,8,13)	112.6386	A(6,22,56)	109.2853	A(5,40,38)	117.8792
A(9,8,42)	107.1361	A(6,22,57)	109.0875	A(5,40,39)	123.4247
A(13,8,42)	106.9677	A(6,22,58)	114.5633	A(38,40,39)	118.696
A(8,9,10)	121.9844	A(56,22,57)	107.8345	A(3,41,70)	105.9698
A(8,9,14)	119.6388	A(56,22,58)	107.7411	A(3,41,71)	110.4039
A(10,9,14)	118.3649	A(57,22,58)	108.123	A(3,41,72)	111.3964
A(9,10,12)	120.3583	A(1,23,25)	121.5571	A(70,41,71)	109.4429
A(9,10,20)	119.6325	A(1,23,26)	118.5197	A(70,41,72)	109.6505
A(12,10,20)	119.9577	A(25,23,26)	119.9203	A(71,41,72)	109.8928
A(6,11,12)	113.5683	A(15,24,30)	114.7211	(23,1,14,9)	-170.9649
A(6,11,43)	108.6637	A(15,24,59)	109.6707	D(23,1,14,18)	8.2334
A(6,11,44)	107.8746	A(15,24,60)	106.8378	D(14,1,23,25)	-7.1053
A(12,11,43)	110.3874	A(30,24,59)	110.0153	D(14,1,23,26)	173.5165
A(12,11,44)	109.4114	A(30,24,60)	109.3784	D(25,2,18,14)	-6.2721
A(43,11,44)	106.6774	A(59,24,60)	105.7958	D(25,2,18,27)	172.9226
A(10,12,11)	112.3627	A(2,25,23)	121.5678	D(18,2,25,23)	7.4246
A(10,12,45)	108.615	A(2,25,29)	118.9824	D(18,2,25,29)	-173.5955
A(10,12,46)	110.0889	A(23,25,29)	119.442	D(41,3,27,18)	68.8262
A(11,12,45)	109.9146	A(16,26,23)	121.3847	D(41,3,27,20)	-115.05

A(11,12,46)	109.6915	A(16,26,61)	121.3515	D(27,3,41,70)	177.9704
A(45,12,46)	105.9622	A(23,26,61)	117.2566	D(27,3,41,71)	59.5553
A(8,13,28)	113.6355	A(3,27,18)	121.4924	D(27,3,41,72)	-62.8333
A(8,13,47)	110.2398	A(3,27,20)	119.3207	D(38,4,37,35)	62.7579
A(8,13,48)	107.3741	A(18,27,20)	119.0754	D(38,4,37,36)	-118.0046
A(28,13,47)	108.9368	A(13,28,31)	120.6826	D(37,4,38,33)	26.0314
A(28,13,48)	109.5018	A(13,28,32)	121.3187	D(37,4,38,40)	-155.6152
A(47,13,48)	106.9312	A(31,28,32)	117.9625	D(73,5,40,38)	-179.541
A(1,14,9)	117.1629	A(17,29,25)	121.2005	D(73,5,40,39)	0.5995
A(1,14,18)	120.8206	A(17,29,62)	120.4758	D(11,6,8,9)	48.7755
A(9,14,18)	122.0115	A(25,29,62)	118.3224	D(11,6,8,13)	-78.1803
A(7,15,16)	109.8688	A(24,30,33)	120.7906	D(11,6,8,42)	165.9627
A(7,15,24)	108.5524	A(24,30,34)	121.5149	D(22,6,8,9)	-79.883
A(7,15,49)	110.2327	A(33,30,34)	117.6736	D(22,6,8,13)	153.1611
A(16,15,24)	115.0075	A(28,31,35)	121.4023	D(22,6,8,42)	37.3042
A(16,15,49)	105.9619	A(28,31,63)	119.4308	D(8,6,11,12)	-62.0422
A(24,15,49)	107.1235	A(35,31,63)	119.1507	D(8,6,11,43)	174.6927
A(15,16,17)	121.3894	A(28,32,36)	121.2299	D(8,6,11,44)	59.4021
A(15,16,26)	119.8996	A(28,32,64)	119.4437	D(22,6,11,12)	66.6096
A(17,16,26)	118.6072	A(36,32,64)	119.3056	D(22,6,11,43)	-56.6555
A(16,17,19)	121.0873	A(30,33,38)	122.106	D(22,6,11,44)	-171.946
A(16,17,29)	119.4399	A(30,33,65)	119.9301	D(8,6,22,56)	-59.9137
A(19,17,29)	119.4728	A(38,33,65)	117.9637	D(8,6,22,57)	-177.5873
A(2,18,14)	122.229	A(30,34,39)	120.7615	D(8,6,22,58)	61.076
A(2,18,27)	118.4741	A(30,34,66)	120.204	D(11,6,22,56)	172.4488
A(14,18,27)	119.292	A(39,34,66)	119.0318	D(11,6,22,57)	54.7752
A(17,19,21)	110.995	A(31,35,37)	119.3929	D(11,6,22,58)	-66.5615

Table 6.10 Optimized dihedral angles of cocsoline under DFT/ B3LYP/6-31++G(d,p)

Dihedral angles	Angle(^{0})	Dihedral angles	Angle(^{0})	Angle(^{0})	Dihedral angles
D(21,7,15,16)	-50.773	D(1,14,18,2)	-1.5973	D(25,23,26,16)	0.6488
D(21,7,15,24)	-177.3153	D(1,14,18,27)	179.2144	D(25,23,26,61)	-178.3893
D(21,7,15,49)	65.6394	D(9,14,18,2)	177.5615	D(15,24,30,33)	-94.3506
D(55,7,15,16)	-174.1756	D(9,14,18,27)	-1.6268	D(15,24,30,34)	83.9437
D(55,7,15,24)	59.2821	D(7,15,16,17)	16.7514	D(59,24,30,33)	29.8509
D(55,7,15,49)	-57.7632	D(7,15,16,26)	-167.0038	D(59,24,30,34)	-151.8548
D(15,7,21,19)	69.8636	D(24,15,16,17)	139.563	D(60,24,30,33)	145.6511
D(15,7,21,53)	-51.3342	D(24,15,16,26)	-44.1922	D(60,24,30,34)	-36.0547
D(15,7,21,54)	-170.2388	D(49,15,16,17)	-102.3156	D(2,25,29,17)	-178.6661
D(55,7,21,19)	-167.5394	D(49,15,16,26)	73.9291	D(2,25,29,62)	0.9162
D(55,7,21,53)	71.2628	D(7,15,24,30)	-123.2313	D(23,25,29,17)	0.3359
D(55,7,21,54)	-47.6418	D(7,15,24,59)	112.3849	D(23,25,29,62)	179.9182
D(6,8,9,10)	-20.1183	D(7,15,24,60)	-1.8335	D(13,28,31,35)	175.0451
D(6,8,9,14)	158.6046	D(16,15,24,30)	113.2551	D(13,28,31,63)	-3.4772
D(13,8,9,10)	105.6924	D(16,15,24,59)	-11.1287	D(32,28,31,35)	-2.7931
D(13,8,9,14)	-75.5847	D(16,15,24,60)	-125.3471	D(32,28,31,63)	178.6846
D(42,8,9,10)	-136.9546	D(49,15,24,30)	-4.2116	D(13,28,32,36)	-174.2266
D(42,8,9,14)	41.7683	D(49,15,24,59)	-128.5955	D(13,28,32,64)	4.1036
D(6,8,13,28)	-110.2586	D(49,15,24,60)	117.1862	D(31,28,32,36)	3.5972
D(6,8,13,47)	127.1316	D(15,16,17,19)	-2.8831	D(31,28,32,64)	-178.0726
D(6,8,13,48)	10.99	D(15,16,17,29)	177.0003	D(24,30,33,38)	176.0059
D(9,8,13,28)	122.787	D(26,16,17,19)	-179.1751	D(24,30,33,65)	-3.8104
D(9,8,13,47)	0.1772	D(26,16,17,29)	0.7084	D(34,30,33,38)	-2.3521
D(9,8,13,48)	-115.9645	D(15,16,26,23)	-177.1462	D(34,30,33,65)	177.8315
D(42,8,13,28)	5.3343	D(15,16,26,61)	1.8525	D(24,30,34,39)	-177.7156
D(42,8,13,47)	-117.2755	D(17,16,26,23)	-0.7975	D(24,30,34,66)	2.8861
D(42,8,13,48)	126.5828	D(17,16,26,61)	178.2012	D(33,30,34,39)	0.6299
D(8,9,10,12)	2.4553	D(16,17,19,21)	19.7958	D(33,30,34,66)	-178.7684
D(8,9,10,20)	179.8439	D(16,17,19,50)	142.1615	D(28,31,35,37)	-0.8194
D(14,9,10,12)	-176.2832	D(16,17,19,51)	-100.3332	D(28,31,35,67)	-178.5645
D(14,9,10,20)	1.1054	D(29,17,19,21)	-160.0876	D(63,31,35,37)	177.7069
D(8,9,14,1)	0.7068	D(29,17,19,50)	-37.7219	D(63,31,35,67)	-0.0381
D(8,9,14,18)	-178.4813	D(29,17,19,51)	79.7834	D(28,32,36,37)	-0.7796
D(10,9,14,1)	179.4757	D(16,17,29,25)	-0.4942	D(28,32,36,68)	177.9498
D(10,9,14,18)	0.2876	D(16,17,29,62)	179.9324	D(64,32,36,37)	-179.1121
D(9,10,12,11)	-12.9435	D(19,17,29,25)	179.3911	D(64,32,36,68)	-0.3827
D(9,10,12,45)	108.8747	D(19,17,29,62)	-0.1822	D(30,33,38,4)	-179.0917
D(9,10,12,46)	-135.5199	D(2,18,27,3)	-1.5436	D(30,33,38,40)	2.5891
D(20,10,12,11)	169.6764	D(2,18,27,20)	-177.6767	D(65,33,38,4)	0.7281
D(20,10,12,45)	-68.5054	D(14,18,27,3)	177.6753	D(65,33,38,40)	-177.5911
D(20,10,12,46)	47.1	D(14,18,27,20)	1.5422	D(30,34,39,40)	0.8328
D(9,10,20,27)	-1.1793	D(17,19,21,7)	-50.5732	D(30,34,39,69)	-179.5495

D(9,10,20,52)	-179.9382	D(17,19,21,53)	72.334	D(66,34,39,40)	-179.7619
D(12,10,20,27)	176.2199	D(17,19,21,54)	-169.3816	D(66,34,39,69)	-0.1442
D(12,10,20,52)	-2.539	D(50,19,21,7)	-172.6695	D(31,35,37,4)	-177.0249
D(6,11,12,10)	42.5725	D(50,19,21,53)	-49.7623	D(31,35,37,36)	3.7479
D(6,11,12,45)	-78.503	D(50,19,21,54)	68.5222	D(67,35,37,4)	0.7457
D(6,11,12,46)	165.373	D(51,19,21,7)	69.9848	D(67,35,37,36)	-178.4814
D(43,11,12,10)	164.8887	D(51,19,21,53)	-167.108	D(32,36,37,4)	177.8021
D(43,11,12,45)	43.8132	D(51,19,21,54)	-48.8235	D(32,36,37,35)	-2.9598
D(43,11,12,46)	-72.3108	D(10,20,27,3)	-176.3832	D(68,36,37,4)	-0.9525
D(44,11,12,10)	-78.0094	D(10,20,27,18)	-0.165	D(68,36,37,35)	178.2855
D(44,11,12,45)	160.9151	D(52,20,27,3)	2.4105	D(4,38,40,5)	0.6783
D(44,11,12,46)	44.7911	D(52,20,27,18)	178.6287	D(4,38,40,39)	-179.4554
D(8,13,28,31)	-121.5951	D(1,23,25,2)	-0.7998	D(33,38,40,5)	179.0886
D(8,13,28,32)	56.1698	D(1,23,25,29)	-179.7752	D(33,38,40,39)	-1.045
D(47,13,28,31)	1.7296	D(26,23,25,2)	178.5698	D(34,39,40,5)	179.2346
D(47,13,28,32)	179.4945	D(26,23,25,29)	-0.4055	D(34,39,40,38)	-0.6238
D(48,13,28,31)	118.3535	D(1,23,26,16)	-179.9625	D(69,39,40,5)	-0.3863
D(48,13,28,32)	-63.8816	D(1,23,26,61)	0.9994	D(69,39,40,38)	179.7552

Table 6.11 Optimized bond lengths of rhodionidin under DFT/ B3LYP/6-31++G(d,p)

Bond	Bond length(A^0)	Bond	Bond length(A^0)	Bond	Bond length(A^0)
R(1,20)	1.4241	R(14,35)	1.256	R(27,55)	1.0933
R(1,23)	1.4281	R(15,37)	1.3562	R(28,56)	1.0909
R(2,25)	1.4472	R(15,70)	0.9768	R(28,57)	1.0931
R(2,26)	1.3933	R(16,43)	1.3645	R(28,58)	1.092
R(3,23)	1.3958	R(16,73)	0.9632	R(29,30)	1.4049
R(3,29)	1.3838	R(17,18)	1.5261	R(29,31)	1.3984
R(4,26)	1.4431	R(17,19)	1.5312	R(30,32)	1.4015
R(4,30)	1.3579	R(17,44)	1.0946	R(31,33)	1.406
R(5,17)	1.4347	R(18,20)	1.5386	R(32,34)	1.3863
R(5,59)	0.9661	R(18,45)	1.1025	R(32,65)	1.0811
R(6,18)	1.4202	R(19,23)	1.5299	R(33,34)	1.4193
R(6,60)	0.9649	R(19,46)	1.1004	R(33,35)	1.4357
R(7,19)	1.4166	R(20,27)	1.5269	R(35,37)	1.447
R(7,61)	0.9653	R(20,47)	1.1016	R(36,37)	1.3681
R(8,21)	1.4268	R(21,22)	1.5288	R(36,38)	1.4624
R(8,62)	0.9678	R(21,24)	1.5287	R(38,39)	1.4105
R(9,22)	1.423	R(21,48)	1.0937	R(38,40)	1.4067
R(9,63)	0.9652	R(22,25)	1.531	R(39,41)	1.3858
R(10,24)	1.4269	R(22,49)	1.099	R(39,68)	1.079
R(10,64)	0.9697	R(23,50)	1.1	R(40,42)	1.3878
R(11,27)	1.4285	R(24,26)	1.5391	R(40,69)	1.0811
R(11,66)	0.9625	R(24,51)	1.0909	R(41,43)	1.3958
R(12,31)	1.3576	R(25,28)	1.5167	R(41,71)	1.0831
R(12,36)	1.3757	R(25,52)	1.097	R(42,43)	1.3965
R(13,34)	1.3427	R(26,53)	1.0914	R(42,72)	1.0863
R(13,67)	0.9857	R(27,54)	1.092		

Table 6.12 Optimized bond angles of rhodionidin under DFT/ B3LYP/6-31++G(d,p)

Bond angles	Angle(^{0})	Bond angles	Angle(^{0})	Bond angles	Angle(^{0})
A(20,1,23)	114.1693	A(24,21,48)	108.9957	A(3,29,31)	121.1047
A(25,2,26)	116.5415	A(9,22,21)	110.4155	A(30,29,31)	118.0616
A(23,3,29)	116.7876	A(9,22,25)	108.4885	A(4,30,29)	116.726
A(26,4,30)	117.5987	A(9,22,49)	110.4108	A(4,30,32)	121.791
A(17,5,59)	108.838	A(21,22,25)	109.5485	A(29,30,32)	121.4754
A(18,6,60)	108.1804	A(21,22,49)	109.418	A(12,31,29)	117.8215
A(19,7,61)	107.2252	A(25,22,49)	108.5249	A(12,31,33)	120.7987
A(21,8,62)	106.0293	A(1,23,3)	108.8845	A(29,31,33)	121.3689
A(22,9,63)	106.8075	A(1,23,19)	108.3447	A(30,32,34)	120.02
A(24,10,64)	107.4508	A(1,23,50)	109.4567	A(30,32,65)	120.1431
A(27,11,66)	110.2467	A(3,23,19)	108.7089	A(34,32,65)	119.8238
A(31,12,36)	122.6063	A(3,23,50)	110.6783	A(31,33,34)	119.2835
A(34,13,67)	107.7847	A(19,23,50)	110.7133	A(31,33,35)	118.8366
A(37,15,70)	104.5453	A(10,24,21)	107.3501	A(34,33,35)	121.8775
A(43,16,73)	109.9252	A(10,24,26)	110.595	A(13,34,32)	119.5516
A(5,17,18)	111.348	A(10,24,51)	110.5621	A(13,34,33)	120.6957
A(5,17,19)	111.2422	A(21,24,26)	111.5965	A(32,34,33)	119.7481
A(5,17,44)	104.1191	A(21,24,51)	109.6063	A(14,35,33)	124.1888
A(18,17,19)	112.6416	A(26,24,51)	107.1557	A(14,35,37)	118.744
A(18,17,44)	108.6017	A(2,25,22)	108.6059	A(33,35,37)	117.0659
A(19,17,44)	108.4608	A(2,25,28)	106.9624	A(12,36,37)	119.0825
A(6,18,17)	111.5047	A(2,25,52)	108.9071	A(12,36,38)	112.6423
A(6,18,20)	108.3268	A(22,25,28)	113.6009	A(37,36,38)	128.271
A(6,18,45)	110.1789	A(22,25,52)	108.6913	A(15,37,35)	114.856
A(17,18,20)	110.2421	A(28,25,52)	109.9692	A(15,37,36)	123.5418
A(17,18,45)	108.6481	A(2,26,4)	112.8318	A(35,37,36)	121.5982
A(20,18,45)	107.8748	A(2,26,24)	114.7005	A(36,38,39)	122.0154
A(7,19,17)	110.3397	A(2,26,53)	105.6123	A(36,38,40)	119.8847
A(7,19,23)	110.2644	A(4,26,24)	105.4523	A(39,38,40)	118.0996
A(7,19,46)	110.5042	A(4,26,53)	108.5432	A(38,39,41)	121.0095
A(17,19,23)	108.6095	A(24,26,53)	109.6021	A(38,39,68)	119.9434
A(17,19,46)	110.2842	A(11,27,20)	114.1333	A(41,39,68)	119.0471
A(23,19,46)	106.7585	A(11,27,54)	105.4565	A(38,40,42)	120.8101
A(1,20,18)	109.5631	A(11,27,55)	111.2649	A(38,40,69)	120.2854
A(1,20,27)	108.5316	A(20,27,54)	108.9949	A(42,40,69)	118.9037

A(1,20,47)	110.1502	A(20,27,55)	108.6526	A(39,41,43)	120.1155
A(18,20,27)	110.0124	A(54,27,55)	108.1313	A(39,41,71)	120.7912
A(18,20,47)	108.5666	A(25,28,56)	109.7345	A(43,41,71)	119.093
A(27,20,47)	110.0106	A(25,28,57)	110.3831	A(40,42,43)	120.291
A(8,21,22)	110.95	A(25,28,58)	110.3493	A(40,42,72)	119.6947
A(8,21,24)	111.0919	A(56,28,57)	108.7956	A(43,42,72)	120.0139
A(8,21,48)	106.1945	A(56,28,58)	108.9889	A(16,43,41)	117.5652
A(22,21,24)	111.3997	A(57,28,58)	108.5509	A(16,43,42)	122.7615
A(22,21,48)	108.0049	A(3,29,30)	120.7207	A(41,43,42)	119.6733

Table 6.13 Optimized dihedral angles of rhodionidin under DFT/ B3LYP/6-31++G(d,p)

Dihedral angles	Angle(^{0})	Dihedral angles	Angle(^{0})	Dihedral angles	Angle(^{0})
D(23,1,20,18)	62.3779	D(44,17,19,23)	67.348	D(22,25,28,57)	-60.4524
D(23,1,20,27)	-177.4784	D(44,17,19,46)	-175.9845	D(22,25,28,58)	179.5609
D(23,1,20,47)	-56.985	D(6,18,20,1)	-174.2205	D(52,25,28,56)	-62.6176
D(20,1,23,3)	176.1053	D(6,18,20,27)	66.544	D(52,25,28,57)	177.4848
D(20,1,23,19)	-65.8224	D(6,18,20,47)	-53.8879	D(52,25,28,58)	57.4981
D(20,1,23,50)	54.997	D(17,18,20,1)	-51.9625	D(3,29,30,4)	-0.9206
D(26,2,25,22)	-58.493	D(17,18,20,27)	-171.198	D(3,29,30,32)	178.0971
D(26,2,25,28)	178.5275	D(17,18,20,47)	68.3701	D(31,29,30,4)	-177.0981
D(26,2,25,52)	59.719	D(45,18,20,1)	66.5283	D(31,29,30,32)	1.9197
D(25,2,26,4)	-69.8364	D(45,18,20,27)	-52.7072	D(3,29,31,12)	2.6272
D(25,2,26,24)	50.9507	D(45,18,20,47)	-173.1391	D(3,29,31,33)	-178.5638
D(25,2,26,53)	171.7444	D(7,19,23,1)	179.0548	D(30,29,31,12)	178.7892
D(29,3,23,1)	-76.3706	D(7,19,23,3)	-62.7611	D(30,29,31,33)	-2.4017
D(29,3,23,19)	165.787	D(7,19,23,50)	59.0176	D(4,30,32,34)	178.7182
D(29,3,23,50)	43.9871	D(17,19,23,1)	58.0386	D(4,30,32,65)	0.0385
D(23,3,29,30)	101.1033	D(17,19,23,3)	176.2228	D(29,30,32,34)	-0.2497
D(23,3,29,31)	-82.8365	D(17,19,23,50)	-61.9986	D(29,30,32,65)	-178.9294
D(30,4,26,2)	-86.39	D(46,19,23,1)	-60.8706	D(12,31,33,34)	-179.9975
D(30,4,26,24)	147.681	D(46,19,23,3)	57.3135	D(12,31,33,35)	-0.5578
D(30,4,26,53)	30.3035	D(46,19,23,50)	179.0922	D(29,31,33,34)	1.2288
D(26,4,30,29)	-138.6341	D(1,20,27,11)	57.3644	D(29,31,33,35)	-179.3315
D(26,4,30,32)	42.3514	D(1,20,27,54)	-60.2209	D(30,32,34,13)	179.8074
D(59,5,17,18)	-63.0522	D(1,20,27,55)	-177.8379	D(30,32,34,33)	-0.9774
D(59,5,17,19)	63.4881	D(18,20,27,11)	177.2282	D(65,32,34,13)	-1.5087
D(59,5,17,44)	-179.8901	D(18,20,27,54)	59.6428	D(65,32,34,33)	177.7066
D(60,6,18,17)	45.3831	D(18,20,27,55)	-57.9741	D(31,33,34,13)	179.707
D(60,6,18,20)	166.8667	D(47,20,27,11)	-63.2154	D(31,33,34,32)	0.5009
D(60,6,18,45)	-75.3443	D(47,20,27,54)	179.1992	D(35,33,34,13)	0.285
D(61,7,19,17)	-43.1176	D(47,20,27,55)	61.5822	D(35,33,34,32)	-178.9211

D(61,7,19,23)	-163.0948	D(8,21,22,9)	60.5142	D(31,33,35,14)	-179.6117
D(61,7,19,46)	79.1157	D(8,21,22,25)	179.9353	D(31,33,35,37)	-0.0326
D(62,8,21,22)	83.6148	D(8,21,22,49)	-61.206	D(34,33,35,14)	-0.1872
D(62,8,21,24)	-40.8867	D(24,21,22,9)	-175.159	D(34,33,35,37)	179.3919
D(62,8,21,48)	-159.2658	D(24,21,22,25)	-55.7378	D(14,35,37,15)	0.2794
D(63,9,22,21)	-46.1788	D(24,21,22,49)	63.1208	D(14,35,37,36)	179.5736
D(63,9,22,25)	-166.2394	D(48,21,22,9)	-55.4912	D(33,35,37,15)	-179.3235
D(63,9,22,49)	74.9528	D(48,21,22,25)	63.93	D(33,35,37,36)	-0.0293
D(64,10,24,21)	-160.9555	D(48,21,22,49)	-177.2114	D(12,36,37,15)	179.8954
D(64,10,24,26)	77.0836	D(8,21,24,10)	49.5108	D(12,36,37,35)	0.6638
D(64,10,24,51)	-41.4394	D(8,21,24,26)	170.845	D(38,36,37,15)	0.7031
D(66,11,27,20)	73.8635	D(8,21,24,51)	-70.6149	D(38,36,37,35)	-178.5286
D(66,11,27,54)	-166.5379	D(22,21,24,10)	-74.736	D(12,36,38,39)	172.6385
D(66,11,27,55)	-49.5327	D(22,21,24,26)	46.5981	D(12,36,38,40)	-7.5561
D(36,12,31,29)	-179.9318	D(22,21,24,51)	165.1382	D(37,36,38,39)	-8.1262
D(36,12,31,33)	1.252	D(48,21,24,10)	166.1852	D(37,36,38,40)	171.6791
D(31,12,36,37)	-1.294	D(48,21,24,26)	-72.4807	D(36,38,39,41)	179.7051
D(31,12,36,38)	178.019	D(48,21,24,51)	46.0594	D(36,38,39,68)	-0.2348
D(67,13,34,32)	178.7243	D(9,22,25,2)	179.9155	D(40,38,39,41)	-0.1036
D(67,13,34,33)	-0.4834	D(9,22,25,28)	-61.2019	D(40,38,39,68)	179.9565
D(70,15,37,35)	0.3819	D(9,22,25,52)	61.5669	D(36,38,40,42)	-179.5341
D(70,15,37,36)	-178.8968	D(21,22,25,2)	59.3161	D(36,38,40,69)	0.795
D(73,16,43,41)	179.0237	D(21,22,25,28)	178.1987	D(39,38,40,42)	0.2788
D(73,16,43,42)	-1.0598	D(21,22,25,52)	-59.0325	D(39,38,40,69)	-179.3921
D(5,17,18,6)	-63.9581	D(49,22,25,2)	-60.0935	D(38,39,41,43)	-0.1975
D(5,17,18,20)	175.677	D(49,22,25,28)	58.7891	D(38,39,41,71)	179.9671
D(5,17,18,45)	57.6611	D(49,22,25,52)	-178.4421	D(68,39,41,43)	179.743
D(19,17,18,6)	170.2732	D(10,24,26,2)	76.0381	D(68,39,41,71)	-0.0924
D(19,17,18,20)	49.9083	D(10,24,26,4)	-159.193	D(38,40,42,43)	-0.1535
D(19,17,18,45)	-68.1076	D(10,24,26,53)	-42.5335	D(38,40,42,72)	179.6141
D(44,17,18,6)	50.1145	D(21,24,26,2)	-43.3929	D(69,40,42,43)	179.5218
D(44,17,18,20)	-70.2504	D(21,24,26,4)	81.376	D(69,40,42,72)	-0.7106
D(44,17,18,45)	171.7337	D(21,24,26,53)	-161.9645	D(39,41,43,16)	-179.7544
D(5,17,19,7)	60.3124	D(51,24,26,2)	-163.3862	D(39,41,43,42)	0.3264
D(5,17,19,23)	-178.7178	D(51,24,26,4)	-38.6173	D(71,41,43,16)	0.0838
D(5,17,19,46)	-62.0503	D(51,24,26,53)	78.0422	D(71,41,43,42)	-179.8354
D(18,17,19,7)	-173.8617	D(2,25,28,56)	179.2653	D(40,42,43,16)	179.9328
D(18,17,19,23)	-52.8919	D(2,25,28,57)	59.3677	D(40,42,43,41)	-0.1524
D(18,17,19,46)	63.7756	D(2,25,28,58)	-60.619	D(72,42,43,16)	0.1659
D(44,17,19,7)	-53.6218	D(22,25,28,56)	59.4452	D(72,42,43,41)	-179.9192

6.6.2 Natural population analysis (NPA) and molecular electrostatic potential (MEP) calculations

Molecular polarizability, dipole moment, electronic structure, molecular reactivity, and many other aspects of molecular systems are influenced by atomic charges. The creation of donor and acceptor pairs involving the charge transferring molecule is suggested by the charge distributions over the atoms. The distribution of electrons in various sub shells of atomic orbitals is revealed by a natural population analysis (NPA) of an organic molecule [45]. The natural charges on atoms of cocsoline and rhodionidin are given in **Table 6.14** and **Table 6.15** respectively. The value of natural charges informs that the atom O10 and O5 were showed more electronegativity in cocsoline and rhodionidin respectively than all other oxygen atoms. Among the two nitrogen atoms present in rhodionidin, N7 was more electronegative than N6 atom. On other hand H67 of cocsoline and H73 of rhodionidin were possessed high electropositive value.

Table 6.14 The natural charges on atoms of cocsoline calculated under DFT/ B3LYP/6-31++G(d,p)

Atom with number	Natural charge	Atom with number	Natural charge	Atom with number	Natural charge
O1	-0.61608	C25	0.11209	H49	0.17917
O2	-0.60443	C26	0.42277	H50	0.16055
O3	-0.56579	C27	-0.04182	H51	0.20232
O4	-0.56832	C28	-0.58562	H52	0.18214
O5	-0.74962	C29	0.31144	H53	0.18942
O6	-0.74207	C30	0.30742	H54	0.18801
O7	-0.73267	C31	0.31173	H55	0.19396

O8	-0.75343	C32	-0.33928	H56	0.22399
O9	-0.74592	C33	-0.26458	H57	0.20485
O10	-0.77376	C34	0.40427	H58	0.20846
O11	-0.75721	C35	0.45172	H59	0.46319
O12	-0.48107	C36	0.32245	H60	0.47688
O13	-0.66685	C37	0.19105	H61	0.47221
O14	-0.68832	C38	-0.13628	H62	0.47816
O15	-0.68158	C39	-0.13762	H63	0.47442
O16	-0.66728	C40	-0.14611	H64	0.49738
C17	0.07465	C41	-0.26048	H65	0.24829
C18	0.08538	C42	-0.28936	H66	0.4742
C19	0.07487	C43	0.33181	H67	0.50614
C20	0.09108	H44	0.20341	H68	0.23775
C21	0.08571	H45	0.16869	H69	0.24768
C22	0.0825	H46	0.179	H70	0.50011
C23	0.43941	H47	0.18083	H71	0.22267
C24	0.06096	H48	0.20121	H72	0.20166
				H73	0.47060

Table 6.15 The natural charges on atoms of rhodionidin calculated under DFT/ B3LYP/6-31++G(d,p)

Atom with number	Natural charge	Atom with number	Natural charge	Atom with number	Natural charge
O1	-0.52301	C 25	0.25684	H49	0.18135
O2	-0.51843	C 26	-0.12553	H50	0.20602
O3	-0.59358	C 27	0.43116	H51	0.21479
O4	-0.52784	C28	-0.0429	H52	0.21451
O5	-0.66359	C29	-0.21052	H53	0.16073
N6	-0.58127	C30	-0.04229	H54	0.19579
N7	-0.67442	C31	-0.18599	H55	0.35232
C8	0.10144	C32	-0.1904	H56	0.19146
C9	-0.12319	C33	-0.25236	H57	0.19031

C10	-0.0301	C34	-0.21128	H58	0.16462
C11	-0.18439	C35	-0.23911	H59	0.21806
C12	-0.38164	C36	-0.23511	H60	0.21934
C13	-0.41174	C37	0.28812	H61	0.21029
C14	0.27304	C38	0.2822	H62	0.2174
C15	-0.0229	C39	-0.26334	H63	0.2063
C16	-0.0585	C40	0.27411	H64	0.21103
C17	-0.03401	C41	-0.20129	H65	0.2162
C18	0.1735	H42	0.21273	H66	0.20104
C19	-0.40005	H43	0.19657	H67	0.22018
C20	-0.27856	H44	0.18965	H68	0.22056
C21	-0.17441	H45	0.20447	H69	0.20191
C22	-0.35356	H46	0.20965	H70	0.18408
C23	0.22297	H47	0.20441	H71	0.16365
C24	-0.40195	H48	0.22366	H72	0.17909
				H73	0.46795

The three-dimensional charge distributions of molecules will be depicted by the molecular electrostatic potential surface. The MEP surface can also be viewed as a map of electron excess and deficient areas [46, 47]. The MEP must be determined to validate the evidence of the drug's reactivity as inhibitors. Despite the fact that the MEP, that indicates the molecule size and shape of the positive, negative, and neutral electrostatic potentials and these could be used to anticipate physicochemical property relationships based on the molecular structure of medications in development. Furthermore, the molecular electrostatic potential can be used to evaluate a drug's responsiveness to electrophilic and nucleophilic assaults. The MEP diagram of both cocsoline and rhodionidin calculated at DFT/ B3LYP/6-31++G(d,p) are given in **Fig. 6.9.** In the MEP, the largest negative region, which is

shown red, is the favoured site for electrophilic attack. As a result, an attacking electrophile will be drawn to the negatively charged sites, whereas the blue regions will attract the reverse. The change in the drug's binding affinity with the active site receptor could be due to differences in the mapping of the electrostatic potential around it.
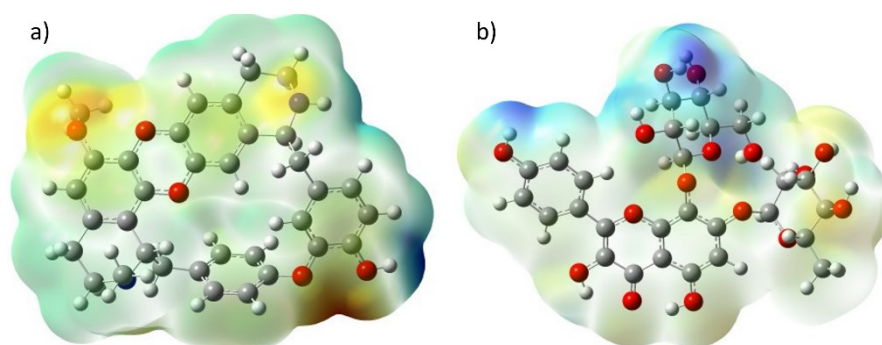
Fig. 6.9 MEP of **a)** cocsoline and **b)** rhodionidin under DFT/B3LYP/6-31++G(d,p)

6.6.3 Frontier molecular orbital (FMO) analysis

The value of highest occupied molecular orbital (HOMO) and lowest unoccupied molecular orbital (LUMO) energy can be used to determine a molecule's ability to donate and receive electrons. The fundamental idea of FMO theory can be summarised in the form of a simple rule that states that the maximum positive overlap between LUMO (empty state) and HOMO (filled state) orbitals is required for a simple reaction course. HOMO (highest occupied molecular orbital) is related to ionisation potential, while LUMO (lowest unoccupied molecular orbital) is related to electron affinity[48]. These molecular orbitals are important in electrical and optical characteristics, and pharmacological investigations, as well as providing biological

mechanism information[49]. The energy gap of the frontier molecular orbital (i.e., FMO) supports the stability of structure. FMOs also provide information on a molecule's kinetic stability and chemical reactivity. The FMOs theory demonstrated that the HOMO and LUMO energy levels had the greatest impact on the bioactivities of small structural medicines. The HOMOs are the ones who provide electrons, whereas the LUMOs are the ones who accept them. Furthermore, the FMOs aid in the prediction of a molecule's most reactive site[50]. The FMOs in the electronic transitions and their energies difference (**Fig. 6.10**) are determined in order to anticipate the energetic behaviours and reactivity of chloroquine and chloroquine phosphate against COVID-19 virus. In fig the negative phase is represented by the colour green, whereas the positive phase is represented by the colour red.

Rhodionidin showed the most lying HOMO than cocsoline and consequently it could be a better electron donor drug. The energy gap of rhodionidin and cocsoline are 3.6662 and 4.7775eV respectively. Rhodionidin's small energy gap allows electrons to move more freely, making the molecule soft and reactive and this result is in strong agrrement with the high dipolemoment of rhodionidin. The HOMO of a certain drug and the LUMO with the adjacent residues could share the orbital interactions during the binding process.

a) E_{LUMO} : -0.7614eV

Band gap: 4.7775eV

E_{HOMO} : -5.5389eV

b) E_{LUMO} : -2.2558eV

Band gap: 3.6662eV

E_{HOMO} : -5.9220eV
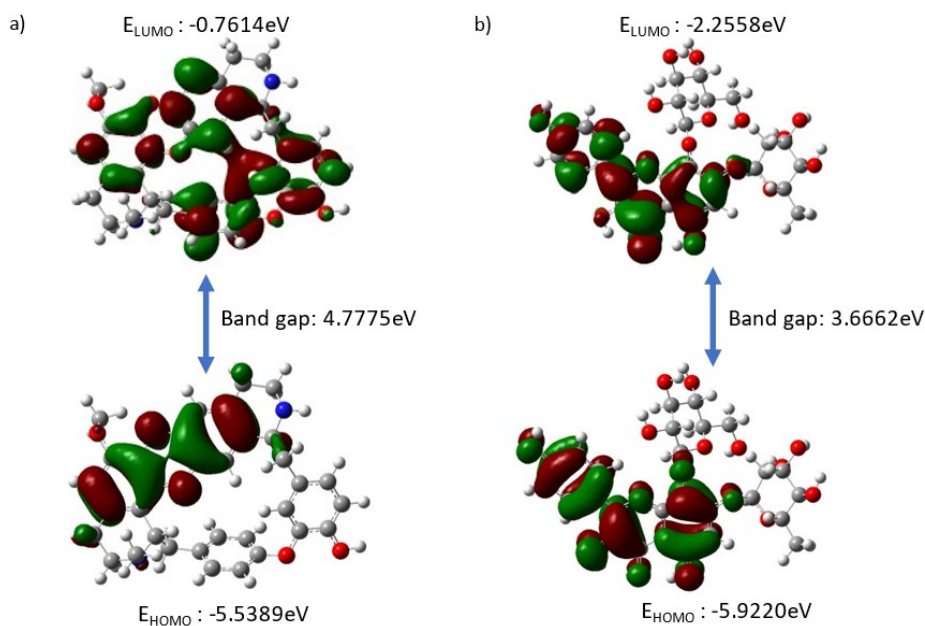
Fig. 6.10 Frontier molecular orbitals of a) cocsoline and b) rhodionidin obtained from DFT/ B3LYP/6-31++G(d,p) calculations

6.6.4 Chemical reactivity descriptors

The E_{HOMO} and E_{LUMO} are markers that can be used to forecast a molecule's ionisation potential (I= -E_{HOMO}) and electron affinity (A= -E_{LUMO}). Other chemical reactivity descriptors such as hardness(η), softness(S), electronegativity(χ), chemical potential(μ) and electrophilicity index(ω) are estimated using the frontier molecular orbitals and are shown in **Fig. 6.11**.
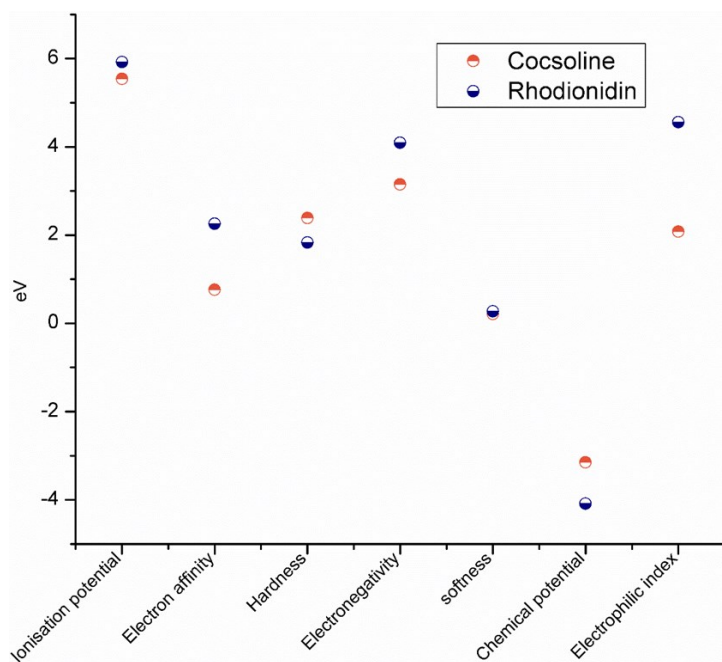
Fig. 6.11 Global descriptive parameters of **a)** cocsoline and **b)** rhodionidin obtained from DFT/ B3LYP/6-31++G(d,p) calculations

The electronegativity ($\chi = (I+A)1/2$) value predicts the molecule's ability to attract electrons, i.e., lewis acid, whereas lower values of χ indicate a suitable base. The χ value is found to be 3.15 and 4.09 for cocsoline and rhodionidin respectively. The global hardness ($\eta=(I-A)1/2$) is a measure of their charge transfer prohibition, while the global softness (S= 1/2η) characterises a molecule's ability to take electrons. Because they may easily transmit electrons to acceptors, soft molecules have a smaller energy gap between frontier molecular orbitals and are more reactive than harder molecules. The hardness of cocsoline (2.39eV) was higher than that of rhodionidin (1.83eV) whereas the softness of cocsoline (0.21eV) is lower than that of

rhodionidin (0.27eV). The electrophilicity index (ω) $=\mu^2/2\eta$ determined for cocsoline and rhodionidine is 2.07 and 4.56eV respectively. The chemical potential ($\mu = -\chi$) for is found to be -3.15eV for cocsoline and -4.09eV for rhodionidin.

Conclusion

Components present in the two medicinal herbs R.*rosea* and C.*hirsutus* were subjected to molecular docking studies in order to identify possible COVID-19 M^{pro} inhibitors. Using AutoDock Vina software, the binding energy values of all the components present in both plants were determined. The findings of *in silico* molecular docking studies of *R.rosea* and *C.hirsutus* indicate that most of the phytochemicals have moderate to potent antiviral activity against SARS-CoV-2 M^{pro}. The components' high affinity is also found to be dependent on the nature and strength of bonding within the protein's active site. The flavonoid rhodionidin, which is found in the *R.rosea* plant and has the lowest binding energy of -9.6 kcal/mol, and the alkaloid cocsoline, which is found in the species *C.hirsutus* and has a binding energy of -9.1 kcal/mol, have been described as the best potential drug against the novel coronaviruses. MMGBSA analysis was used to help rank the ligands with the highest binding affinity for 6LU7. MD simulations of rhodionidin and cocsoline with target indicate that the complex cocsoline:6lu7 was more stable compared to the rhodionidin:6lu7 complex. The DFT/ B3LYP/6-31++G(d,p) approach was used to optimise the molecular structures of cocsoline and rhodionidin (having highest binding affinity with the target protein), as well as to identify their geometrical characteristics.

Frontier orbitals, gap energies, natural population analysis and reactivity descriptors are some of the molecular features that have been discussed. According to the findings, the minimal energy gap is associated with a high binding affinity for rhodionidin. The molecule gets softer and more reactive as the gap energy decreases, making electron flow easier. Following that, the estimated MEP maps reveal that positive potential sites are more advantageous for nucleophilic attack, while negative potential sites are more favorable for electrophilic attack. These findings further motivate *in vitro* and *in vivo* studies of the identified components for the cure of COVID-19. These findings are also expected to stimulate further research into the production of safe and successful anti-coronavirus or other antiviral drugs derived from naturally occurring compounds.

References

1.   Sohrabi C, Alsafi Z, O'Neill N, Khan M, Kerwan A, Al-Jabir A, Iosifidis C, Agha R: **World Health Organization declares global emergency: A review of the 2019 novel coronavirus (COVID-19)**. *International Journal of Surgery* 2020.

2.   Prem K, Liu Y, Russell TW, Kucharski AJ, Eggo RM, Davies N, Flasche S, Clifford S, Pearson CA, Munday JD: **The effect of control strategies to reduce social mixing on outcomes of the COVID-19 epidemic in Wuhan, China: a modelling study**. *The Lancet Public Health* 2020.

3.   Mani JS, Johnson JB, Steel JC, Broszczak DA, Neilsen PM, Walsh KB, Naiker M: **Natural product-derived phytochemicals as potential agents against coronaviruses: a review**. *Virus Research* 2020:197989.

4.   Fehr AR, Perlman S: **Coronaviruses: an overview of their replication and pathogenesis**. In: *Coronaviruses.* Springer; 2015: 1-23.

5.   Yang Y, Peng F, Wang R, Guan K, Jiang T, Xu G, Sun J, Chang C: **The deadly coronaviruses: The 2003 SARS pandemic and the 2020 novel coronavirus epidemic in China**. *J Autoimmun* 2020:102434.

6.   Chu DK, Pan Y, Cheng SM, Hui KP, Krishnan P, Liu Y, Ng DY, Wan CK, Yang P, Wang Q: **Molecular diagnosis of a novel coronavirus (2019-nCoV) causing an outbreak of pneumonia**. *Clinical chemistry* 2020, **66**(4):549-555.

7.   Elfiky AA, Mahdy SM, Elshemey WM: **Quantitative structure-activity relationship and molecular docking revealed a potency of anti-hepatitis C virus drugs against human corona viruses**. *J Med Virol* 2017, **89**(6):1040-1047.

8.   Ibrahim IM, Abdelmalek DH, Elshahat ME, Elfiky AA: **COVID-19 spike-host cell receptor GRP78 binding site prediction**. *Journal of Infection* 2020.

9.   Hui DS, Azhar EI, Madani TA, Ntoumi F, Kock R, Dar O, Ippolito G, Mchugh TD, Memish ZA, Drosten C: **The continuing 2019-nCoV epidemic threat of novel coronaviruses to global health—The latest 2019 novel coronavirus outbreak in Wuhan, China**. *International Journal of Infectious Diseases* 2020, **91**:264.

10. Nie Q-H, Luo X-D, Zhang J-Z, Su Q: **Current status of severe acute respiratory syndrome in China**. *World journal of gastroenterology: WJG* 2003, **9**(8):1635.

11. Cortegiani A, Ingoglia G, Ippolito M, Giarratano A, Einav S: **A systematic review on the efficacy and safety of chloroquine for the treatment of COVID-19**. *Journal of critical care* 2020.

12. Wang M, Cao R, Zhang L, Yang X, Liu J, Xu M, Shi Z, Hu Z, Zhong W, Xiao G: **Remdesivir and chloroquine effectively inhibit the recently emerged novel coronavirus (2019-nCoV) in vitro**. *Cell research* 2020, **30**(3):269-271.

13. Yao TT, Qian JD, Zhu WY, Wang Y, Wang GQ: **A systematic review of lopinavir therapy for SARS coronavirus and MERS coronavirus—A possible reference for coronavirus disease-19 treatment option**. *J Med Virol* 2020.

14. Holshue ML, DeBolt C, Lindquist S, Lofy KH, Wiesman J, Bruce H, Spitters C, Ericson K, Wilkerson S, Tural A: **First case of 2019 novel coronavirus in the United States**. *New England Journal of Medicine* 2020.

15. Shahidi F: **Antioxidant factors in plant foods and selected oilseeds**. *Biofactors* 2000, **13**(1-4):179-185.

16. Shahidi F, McDonald J, Chandrasekara A, Zhong Y: **Phytochemicals of foods, beverages and fruit vinegars: chemistry and health effects**. *Asia Pacific Journal of Clinical Nutrition* 2008, **17**.

17. ul Qamar MT, Alqahtani SM, Alamri MA, Chen L-L: **Structural basis of SARS-CoV-2 3CLpro and anti-COVID-19 drug discovery from medicinal plants**. *Journal of pharmaceutical analysis* 2020.

18. ul Qamar MT, Maryam A, Muneer I, Xing F, Ashfaq UA, Khan FA, Anwar F, Geesi MH, Khalid RR, Rauf SA: **Computational screening of medicinal plant phytochemicals to discover potent pan-serotype inhibitors against dengue virus**. *Scientific reports* 2019, **9**(1):1-16.

19. Balunas MJ, Kinghorn AD: **Drug discovery from medicinal plants**. *Life sciences* 2005, **78**(5):431-441.

20. Chen H, Liu RH: **Potential mechanisms of action of dietary phytochemicals for cancer prevention by targeting cellular**

signaling transduction pathways. *J Agric Food Chem* 2018, **66**(13):3260-3276.

21.   R Vasanthi H, ShriShriMal N, K Das D: **Phytochemicals from plants to combat cardiovascular disease**. *Curr Med Chem* 2012, **19**(14):2242-2251.

22.   Rath SN, Jena L, Patri M: **Understanding ligands driven mechanism of wild and mutant aryl hydrocarbon receptor in presence of phytochemicals combating Parkinson's disease: an in silico and in vivo study**. *J Biomol Struct Dyn* 2020, **38**(3):807-826.

23.   Uddin MS, Kabir MT, Tewari D, Mathew B, Aleya L: **Emerging signal regulating potential of small molecule biflavonoids to combat neuropathological insults of Alzheimer's disease**. *Science of The Total Environment* 2020, **700**:134836.

24.   Brahmam P, Sunita K: **Phytochemical Investigation and In vitro Antimalarial Activity of Acalypha indica (L.) and Cocculus hirsutus (L.) From Prakasam District, Andhra Pradesh, India**. *Biomedical and Pharmacology Journal* 2018, **11**(4):2123-2134.

25.   Thavamani BS, Mathew M, Dhanabal S: **Cocculus hirsutus: Molecular docking to identify suitable targets for hepatocellular carcinoma by in silico technique**. *Pharmacognosy magazine* 2016, **12**(Suppl 3):S350.

26.   Meena MK, Singh N, Patni V: **In vitro multiple shoot induction through axillary bud of Cocculus hirsutus (L.) Diels: A threatened medicinal plant**. *African Journal of Biotechnology* 2012, **11**(12):2952-2956.

27.   Meena MK, Singh N, Patni V: **Determination of bioactive components of the leaves of Cocculus hirsutus (L.) Diels using GC-MS analysis**. *Int J Pharm Pharm Sci* 2014, **6**:327-329.

28.   Badole S, Patel N, Bodhankar S, Jain B, Bhardwaj S: **Antihyperglycemic activity of aqueous extract of leaves of Cocculus hirsutus (L.) Diels in alloxan-induced diabetic mice**. *Indian journal of pharmacology* 2006, **38**(1):49.

29.   Ganapaty S, Dash G, Subburaju T, Suresh P: **Diuretic, laxative and toxicity studies of Cocculus hirsutus aerial parts**. *Fitoterapia* 2002, **73**(1):28-31.

30.   Sharma S, Agarwal N: **A review on herbs with antidepressant properties**. *International Journal* 2011, **2**(1):2229.

31. Van Diermen D, Marston A, Bravo J, Reist M, Carrupt P-A, Hostettmann K: **Monoamine oxidase inhibition by Rhodiola rosea L. roots**. *Journal of ethnopharmacology* 2009, **122**(2):397-401.

32. Brown RP, Gerbarg PL, Ramazanov Z: **Rhodiola rosea**. *A phytomedicinal overview HerbalGram* 2002, **56**:40-52.

33. Mattioli L, Perfumi M: **Rhodiola rosea L. extract reduces stress- and CRF-induced anorexia in rats**. *J Psychopharm* 2007, **21**(7):742-750.

34. Saura J, Luque J, Cesura A, Da Prada M, Chan-Palay V, Huber G, Löffler J, Richards J: **Increased monoamine oxidase B activity in plaque-associated astrocytes of Alzheimer brains revealed by quantitative enzyme radioautography**. *Neuroscience* 1994, **62**(1):15-30.

35. Shevtsov V, Zholus B, Shervarly V, Vol'Skij V, Korovin Y, Khristich M, Roslyakova N, Wikman G: **A randomized trial of two different doses of a SHR-5 Rhodiola rosea extract versus placebo and control of capacity for mental work**. *Phytomedicine* 2003, **10**(2-3):95-105.

36. Shih J, Thompson R: **Monoamine oxidase in neuropsychiatry and behavior**. *Am J Hum Genet* 1999, **65**(3):593.

37. Zhu B-W, Sun Y-M, Yun X, Han S, PIAO M-L, Murata Y, Tada M: **Reduction of noise-stress-induced physiological damage by radices of Astragali and Rhodiolae: glycogen, lactic acid and cholesterol contents in liver of the rat**. *Bioscience, biotechnology, and biochemistry* 2003, **67**(9):1930-1936.

38. Panossian A, Wikman G, Sarris J: **Rosenroot (Rhodiola rosea): traditional use, chemical composition, pharmacology and clinical efficacy**. *Phytomedicine* 2010, **17**(7):481-493.

39. Ganzera M, Yayla Y, Khan IA: **Analysis of the marker compounds of Rhodiola rosea L.(golden root) by reversed phase high performance liquid chromatography**. *Chemical and pharmaceutical bulletin* 2001, **49**(4):465-467.

40. Mhatre S, Naik S, Patravale V: **A molecular docking study of EGCG and theaflavin digallate with the druggable targets of SARS-CoV-2**. *Comput Biol Med* 2021, **129**:104137.

41. Wu C, Liu Y, Yang Y, Zhang P, Zhong W, Wang Y, Wang Q, Xu Y, Li M, Li X: **Analysis of therapeutic targets for SARS-CoV-2 and discovery of potential drugs by computational methods**. *Acta Pharmaceutica Sinica B* 2020.

42. Anand K, Ziebuhr J, Wadhwani P, Mesters JR, Hilgenfeld R: **Coronavirus main proteinase (3CLpro) structure: basis for design of anti-SARS drugs**. *Science* 2003, **300**(5626):1763-1767.

43. Bacha U, Barrila J, Velazquez-Campoy A, Leavitt SA, Freire E: **Identification of novel inhibitors of the SARS coronavirus main protease 3CLpro**. *Biochemistry* 2004, **43**(17):4906-4912.

44. Peele KA, Durthi CP, Srihansa T, Krupanidhi S, Ayyagari VS, Babu DJ, Indira M, Reddy AR, Venkateswarulu T: **Molecular docking and dynamic simulations for antiviral compounds against SARS-CoV-2: A computational study**. *Informatics in medicine unlocked* 2020, **19**:100345.

45. Hatada R, Okuwaki K, Mochizuki Y, Handa Y, Fukuzawa K, Komeiji Y, Okiyama Y, Tanaka S: **Fragment Molecular Orbital Based Interaction Analyses on COVID-19 Main Protease−Inhibitor N3 Complex (PDB ID: 6LU7)**. *Journal of chemical information and modeling* 2020, **60**(7):3593-3602.

46. Mumit MA, Pal TK, Alam MA, Islam MA-A-A-A, Paul S, Sheikh MC: **DFT studies on vibrational and electronic spectra, HOMO–LUMO, MEP, HOMA, NBO and molecular docking analysis of benzyl-3-N-(2, 4, 5-trimethoxyphenylmethylene) hydrazinecarbodithioate**. *J Mol Struct* 2020, **1220**:128715.

47. Lakshminarayanan S, Jeyasingh V, Murugesan K, Selvapalam N, Dass G: **Molecular electrostatic potential (MEP) surface analysis of chemo sensors: An extra supporting hand for strength, selectivity & non-traditional interactions**. *Journal of Photochemistry and Photobiology* 2021, **6**:100022.

48. Sharma D, Tiwari S: **Comparative computational analysis of electronic structure, MEP surface and vibrational assignments of a nematic liquid crystal: 4-n-methyl-4-cyanobiphenyl**. *J Mol Liq* 2016, **214**:128-135.

49. Abraham CS, Prasana JC, Muthu S: **Quantum mechanical, spectroscopic and docking studies of 2-amino-3-bromo-5-nitropyridine by density functional method**. *Spectrochimica Acta Part A: Molecular and Biomolecular Spectroscopy* 2017, **181**:153-163.

50. Fleming I: **Frontier orbitals and organic chemical reactions**: Wiley; 1977.

Chapter 7

Electronic-scale DFT and atomic-scale MC explorations to the corrosion inhibition activity of herbacetin and gossypetin

Abstract

We propose a comparison of the anti-corrosive properties of the molecules herbacetin and gossypetin with the well-researched green corrosion inhibitor quercetin using the computational funnel method, Monte Carlo (MC) simulation. Herbacetin and gossypetin may protonate more frequently, according to the quantum chemical calculation, and the O3 atom was determined to be the most conducive to protonation. The interaction of inhibitors with the Fe (110)/100 H_2O interface was studied using MC simulations to determine the most stable configuration and adsorption energy. It was discovered that the adsorption of inhibitor molecules on mild steel surfaces occurred spontaneously. Herbacetin and gossypetin were suggested as possible green anti-corrosive compounds by both DFT and MC analyses.

7.1 Introduction

Corrosion of metals is an unpleasant process that causes significant economic losses around the world owing to the deterioration of metal surfaces [1]. Iron is one of these metals, and it is regarded to be the backbone of contemporary industry. Corrosion inhibitors, which are routinely employed in acid solutions, are commonly utilized to protect iron surfaces against corrosion. In the recent few decades, there has been significant progress in corrosion research, particularly in the fields of the synthesis and design of new corrosion inhibitors in material and industrial chemicals that act by adsorbing on the metal surface [2, 3].

The most frequent method for eliminating unwanted scales, oxides, and other impurities and contaminations from metal surfaces is the acid pickling procedure [4, 5]. Due to its widespread use in chemical cleaning and pickling procedures, hydrochloric acid's importance in numerous industries is undeniable. One of the troublesome issues for companies is severe corrosion produced by the presence of such an aggressive ion [6]. As a result, establishing preventative methods to control the rate of corrosion in this medium is a major concern. Corrosion inhibitors are frequently added to aggressive acids in order to prevent extensive metal dissolution during acid treatment which includes organic compounds, having heteroatoms like O, N, S, and pairstoms having lone pairs of electrons and π bonds [7]. Despite their great inhibition efficacy, the majority of synthetic inhibitors are unsafe and produce hazardous waste waters that are damaging to the ecosystem and human health [8]. As a result,

researchers have placed a high value on the usage of cost-effective and environmentally beneficial corrosion inhibitors. Plant extracts are one of the most important kinds of environmentally beneficial corrosion inhibitors [9-12]. Natural-source extracts contain a considerable quantity of aromatic rings, carbonyl (-C=O), carboxylic (-COOH), hydroxyl (-OH), and amine (-NH, -NH2) groups, among other chemical components. As a result, these compounds could be used as inhibitors to slow the corrosion of mild steel in acidic environments. Adsorption of inhibitor molecules on metal surfaces is mediated by a strong coordination connection between iron and the lone pair of electrons of heteroatoms (e.g., N, O) [13-15]. There are numerous publications on the use of green corrosion inhibitors derived from plant extracts.

Quantum chemical approaches have recently become very effective tools in determining the molecular structures, electronic structure, and reactivity of compounds, thanks to significant advances in supercomputers. Because experimental methods for determining corrosion inhibition efficiencies and understanding the inhibition mechanisms of chemical compounds are generally expensive and time consuming, it has become common practise to perform quantum chemical calculations to predict the corrosion inhibition performances of molecules [16-19]. The conceptual density functional theory (DFT) has been successfully used to characterise the structural nature of the inhibitor on the corrosion process, as well as to comprehend the chemical reactivity and site selectivity of molecular systems [20-22].

Herbacetin (HTIN) and Gossypetin (GTIN) have previously been found to have various biological activities, however its corrosion inhibition effectiveness has yet to be investigated. According to current researches, heteroatoms can aid in the electron donation activity of organic compounds with vacant orbitals (anticorrosion effect). The reason for picking these molecules is that its structure is full of oxygen, making it capable of chemical interaction with metal cations, and it is structurally linked to quercetin (8-hydroxy analogue), which is a powerful corrosion inhibitor. The primary purpose of the current effort is to study the fundamental insights into the surface adsorption characteristics and interfacial adhesion mechanism of green corrosion inhibitors, HTIN and GTIN using Monte Carlo (MC) method. Additionally, we have studied the basic electronic-level understanding regarding the electronic-structure characteristics of these molecules with high inhibition potential by theoretical methods based on quantum chemical calculation. In order to relate the electrical and molecular structure to the inhibitory effect and strength, this technique can be greatly anticipated and facilitated through the use of quantum calculations. We have also compared thed the anti-corrosive potential of these molecules with quercetin. To our knowledge, there is no information on the inhibitory effect of HTIN and GTIN on its anticorrosive properties.

7.2 Materials and Methodology

7.2.1 DFT modelling

To gain a basic electronic-level understanding of the electronic-structure properties of inhibitor molecules electronic-scale modelling

based on DFT was applied. The corrosion inhibiting compounds of green inhibitor are likely to coexist in neutral and protonated forms under acidic pH circumstances, thus it's important to look at the protonated molecules as well [23]. Apart from the neutral form of molecules, the protonated form was also taken into account for DFT modelling in order to assess acidic situations. One of the oxygen heteroatoms of the compound was protonated by covalent bonding of a proton to investigate the impact of protonation on the electrical structure and adhesion properties. DFT modelling is done to optimise the geometry of both neutral and protonated form of herbacetin under B3LYP/6-31G and gossypetin under M06/6-311G which is all implemented in Gaussian 16 package. Using protonation affinity (PA) and basicity (B), the best protonation site in the inhibitor molecule can be chosen.

An inhibitor molecule's protonation reaction was explained as:

$$Inhibitor + H^+ \; \square \quad Inhibitor - H^+ \tag{1}$$
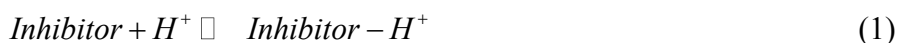
Wherein the Inhibitor, H^+, and Inhibitor-H^+, refer to the neutral inhibitor, proton, and protonated inhibitor respectively. The following formulas were used to determine the amount of PA and B were needed for this reaction.

$$PA = -\Delta H = H\left(Inhibitor - H^+\right) - \left(H\left(Inhibitor\right) + H\left(H^+\right)\right) \tag{2}$$

$$B = -\Delta G = G\left(Inhibitor - H^+\right) - \left(G\left(Inhibitor\right) + G\left(H^+\right)\right) \tag{3}$$

The H and G terms, which are calculated from frequency calculations of optimised neutral and protonated species, are the sums of electronic and thermal enthalpy and electronic and thermal Gibbs free energy, respectively. For monoatomic proton,

$$H\left(H^+\right) = \frac{3}{2}RT \tag{4}$$

$$G\left(H+\right) = \frac{3}{2}RT + TS\left(H^+\right) \tag{5}$$

where T is the absolute temperature (298 K), S is the proton entropy, and R is the universal gas constant. For proton, the entropy value was 108.95 J/(mol.K).

Non-equilibrium version of the IEF-PCM model with water as the solvent was used to replicate the aqueous media in which the inhibitor compounds are frequently used. The global reactivity descriptors were calculated using DFT Koopman's theorem, which relates the energy of the molecules' highest occupied molecular orbital (E_{HOMO}) to the energy of their lowest unoccupied molecular orbital (E_{LUMO}).

The fraction of electrons transported between inhibitor molecules and Fe atoms (ΔN) was determined using theoretical values of 0 and 7.0 eV for global hardness and electronegativity of Fe, respectively.

$$\Delta N = \frac{\chi_{Fe} - \chi_{inh}}{2\left(\eta_{Fe} + \eta_{inh}\right)} \tag{6}$$

7.2.2 Molecular simulation

The adsorption of compounds under evaluation on the stainless-steel surface was assessed using molecular simulations such as Monte Carlo (MC) and molecular dynamics (MD). Earlier studies indicated that an iron (110) surface was used to mimic stainless steel [24-26]. The iron unit cell was cleaved along the (110) facet and its thickness was fixed to $6A^0$ using the surface builder module of Materials Studio software. By introducing a $30A^0$ vacuum space in the direction normal to the substrate, the split iron surface was transformed into a three-dimensional cell (i.e., z direction). The surface was then periodically replicated along the x and y axes to create a (15x15) supercell. MC simulations were used to find the most favourable adsorption mode of the considered molecules over the Fe (110) substrate. The adsorption of all molecules (neutral and protonated) over this surface of iron was investigated using MC simulation, which is accessible in the Adsorption Locator module (Materials Studio package) [27]. The Forcite module in the Materials Studio simulation [27] programme was used to do the optimization and MD simulation. Molecular simulations were performed using the COMPASS force field [23, 28], which is a widely utilised force field.

7.3 quantum chemical calculations

The link between an organic inhibitor's ability to inhibit and its molecular/electronic structure has been demonstrated to be describable by quantum chemical calculations.

Neutral species

In accordance with the molecular orbital theory the efficiency of an interaction between two reacting molecules is based on how their frontier orbitals (HOMO/LUMO) interact. Therefore, the distribution of the highest occupied molecular orbital (HOMO) and the lowest unoccupied molecular orbital (LUMO), as well as the energy gap between them, were examined in order to understand the adsorption and subsequent corrosion inhibitive efficiency of the explored molecules. Donor-acceptor relationships between the atoms of the inhibitor and the metal are frequently used to describe how an inhibitor will bind to a metal surface. While an inhibitor's E_{LUMO} is frequently linked to its propensity to take electrons from the metal's d-orbitals, the inhibitor's E_{HOMO} refers to its tendency to donate electron(s) to the metal atom's vacant d-orbitals. The trends in electronic properties of HTIN, GTIN and quercetin are given in **Table 7.1**.

Table 7.1 Gas phase quantum chemical parameters of HTIN, GTIN and quercetin in gas phase

Parameters	HTIN (B3LYP/6-31G)	GTIN (M06/6-311G)	Quercetin (B3LYP/6-31G)	Quercetin (M06/6-311G)
E_{HOMO} (eV)	-5.75	-6.29	-5.78	-7.20
E_{LUMO} (eV)	-2.29	-2.41	-2.27	-1.40
Band gap (eV)	3.45	3.88	3.51	5.8
Dipole moment (Debye)	5.28	3.82	0.28	0.23
ΔN	0.86	0.68	0.85	0.47
Electron affinity (eV)	2.30	2.41	5.78	7.2
Ionisation potential (eV)	5.75	6.29	2.27	1.4
Hardness (eV)	1.72	1.94	4.02	4.30
Electronegativity (eV)	4.02	4.35	1.76	2.90

The band gap (ΔE) is another crucial factor that governs the adsorption of molecules on metallic surfaces. Molecules become more reactive toward inhibiting corrosion as ΔE decreases. From table 7.1 its clear that both HTIN and GTIN possess small band gap than that of quercetin which is a clear indication of its high inhibition effect.

In order to associate an inhibitor's inhibition efficiency with its ability to donate electrons to the metal surface, the number of electrons transferred (ΔN) is utilised. A value of ΔN< 3.6 indicates that the inhibitor's inhibition efficiency rises as the metal surface's electron-donating capacity rises. The ΔN values suggest that, are in good agreement with Lukovits's study.

According to some authors, a decrease in inhibition efficiency results from an increase in dipole moment, with the justification that low values of dipole moment will encourage the accumulation of the inhibitor in the surface layer. According to a different theory, greater dipole moments will improve inhibition effectiveness because more dipole-dipole interactions will occur between the inhibitor molecules and the metal surface. Higher dipolemoment values of both HTIN and GTIN imply their higher inhibition potential.

Protonated species

Both HTIN and GTIN are monoprotonated at its all possible oxygen atoms and gas phase geometry optimizations and frequency calculations were performed on each mono-protonated species. **Tables 7.2** lists the PA and B of HTIN protonated from their different oxygen atoms in gaseous state and those of GTIN is given in **Table 7.3**. Based

on the data, it is evident that all oxygen atoms in all compounds have positive PA and B values, indicating a tendency for protonation. Furthermore, according to the greatest values of these electronic characteristics, the oxygen atom 3 of both HTIN and GTIN had the largest protonation chance.

Tables 7.2. The PA and B of HTIN protonated from their different oxygen atoms in gaseous state

Protonation sites	PA (kJ/mol)	B (kJ/mol)
1H+	723.99	694.20
2H+	900.84	868.75
3H+	930.75	899.62
4H+	769.98	741.05
5H+	861.32	824.02
6H+	766.89	742.40
7H+	750.18	720.52

Tables 7.3. The PA and B of GTIN protonated from their different oxygen atoms in gaseous state

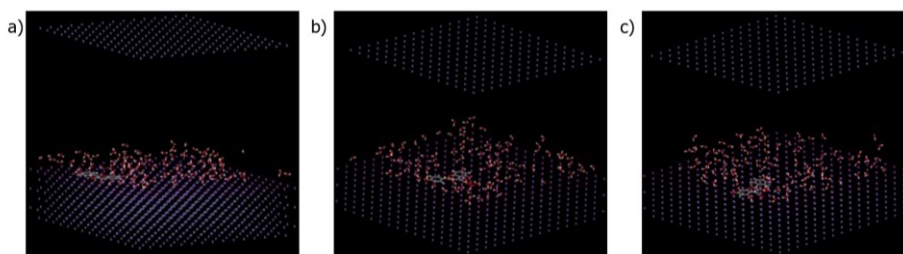| Protonation sites	PA (kJ/mol)	B (kJ/mol)
1H+	707.33	675.29
2H+	879.17	845.66
3H+	910.48	879.82
4H+	714.84	683.72
5H+	879.17	845.64
6H+	752.94	721.92
7H+	764.28	732.46
8H+	760.45	729.06

7.4 Monte Carlo simulation results

Fig. 7.1 The most stable **a)** quercetin, **b)** HTIN and **c)** protonated HTIN adsorption patterns respectively on the surface of Fe(110) in the presence of 100 water molecules

To get molecular-level knowledge on the adsorption of green inhibitor chemicals over the mild steel adsorbent, which was represented by the surface of iron (110), computational methods based on Monte Carlo (MC) was used. **Figs. 7.1a**, **7.1b**, and **7.1c** depicts the most stable quercetin, HTIN and protonated HTIN adsorption patterns respectively on the surface of Fe(110) in the presence of 100 water molecules. The corresponding values for the outputs and descriptors are provided in **Table 7.4**. The parameters include the total energy of the substrate-adsorbate configuration, which is calculated as the product of the energies of the adsorbate components, the rigid adsorption energy, and the deformation energy. The Fe (110) surface is used as the substrate, and its energy is assumed to be zero. Additionally, adsorption energy details the amount of energy released (or needed) during the relaxed adsorbate component's adsorptive process on the substrate. The total of the rigid adsorption energy and the deformation energy for the adsorbate component is known as the adsorption energy. When the rigid adsorbate component was adsorbed on the substrate (prior to the geometry optimization stage), energy was

released (or required) during that process. The deformation energy records the power expended during the relaxation of the deposited adsorbate component on the substrate surface. (dEad/dNi) measures the energy of substrate-adsorbate configurations in which one of the adsorbate components has been eliminated.

Table 7.4 Outputs and descriptors calculated by Monte Carlo simulation for the lowest adsorption configurations of quercetin, neutral HTIN, protonated HTIN

Molecule	Total energy	Adsorption energy	Rigid adsorption energy	Deformation energy	MOL. dEad/dNi	Water. dEad/dNi
	Kcal/mol					
Quercetin ((B3LYP/6-31G)	-1551.02	-2858.23	-1608.05	-1250.18	-1487.26	-12.01
HTIN	-1612.28	-2957.96	-1682.42	-1275.54	-1531.63	-10.73
Protonated HTIN	-1558.52	-2905.55	-1620.33	-1285.23	-1541.88	-7.88

The system with the most stable and powerful adsorption is indicated by the highest negative adsorption energy. From table 7.4 it is clear that, HTIN showed most stable adsorption system than quercetin. In every instance, the inhibitors' adsorption energies are far higher than those of water molecules. This suggests the prospect of water molecules gradually being replaced on the surface of iron, leading to the creation of a permanent layer that can shield the iron from aqueous corrosion. **Fig. 7.2** depicts the images of quercetin, neutrally charged GTIN and protonated equilibrated cells of GTIN obtained from atomistic MC simulations. These images show that the molecules are concentrated close to the iron substrate and that their

skeletons are parallel to the metallic surface. Based on the tabulated energetic results (**Table 7.5**), it can be shown that the computed adsorption energies for GTIN is higher than that of quercetin.
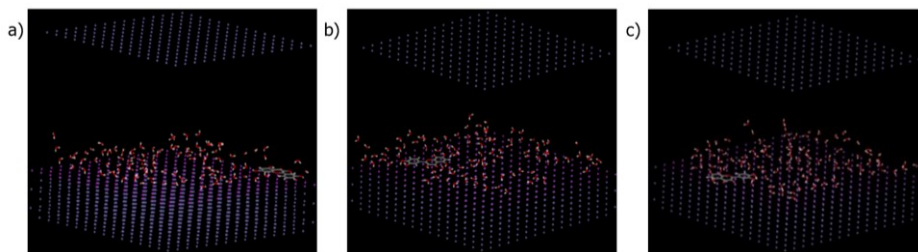

Fig. 7.2. The most stable a) quercetin, b) HTIN and c) protonated HTIN adsorption patterns respectively on the surface of Fe(110) in the presence of 100 water molecules

Table 7.5 Outputs and descriptors calculated by Monte Carlo simulation for the lowest adsorption configurations of quercetin, neutral GTIN, protonated GTIN

Molecule	Total energy	Adsorption energy	Rigid adsorption energy	Deformation energy	MOL. dEad/dNi	Water. dEad/dNi
	Kcal/mol					
Quercetin (M06/6-311G)	-1612.31	-1577.86	-1616.89	39.03	-209.42	-7.91
GTIN	-1610.91	-1592.35	-1630.61	38.26	-221.76	-0.55
Protonated GTIN	-1579.30	-1569.34	-1590.92	21.58	-252.96	-8.16

Conclusion

Three structurally similar plant derived compounds, quercetin, herbacetin, and gossypetin were computationally evaluated for their inhibitory effect on mid steel (Fe (110) plane). According to the proton affinity and basicity studies, the oxygen atom 3 of both HTIN and GTIN had the largest protonation probability. The negative adsorption

energy obtained for both neutral and protonated forms of molecules suggested that adsorption is spontaneous. Monte Carlo simulation parameters supported the higher corrosion inhibition potential of HTIN and GTIN than that of quercetin molecule.

References

1.   Schmitt G: **Global needs for knowledge dissemination, research, and development in materials deterioration and corrosion control**. *World Corrosion Organization* 2009, **38**:14.

2.   Hackerman N: **The theory and practice of corrosion and its control in industry**. *Langmuir* 1987, **3**(6):922-924.

3.   Hamani H, Douadi T, Daoud D, Al-Noaimi M, Chafaa S: **Corrosion inhibition efficiency and adsorption behavior of azomethine compounds at mild steel/hydrochloric acid interface**. *Measurement* 2016, **94**:837-846.

4.   Hassannejad H, Nouri A: **Sunflower seed hull extract as a novel green corrosion inhibitor for mild steel in HCl solution**. *J Mol Liq* 2018, **254**:377-382.

5.   Prabakaran M, Kim S-H, Mugila N, Hemapriya V, Parameswari K, Chitra S, Chung I-M: **Aster koraiensis as nontoxic corrosion inhibitor for mild steel in sulfuric acid**. *Journal of industrial and engineering chemistry* 2017, **52**:235-242.

6.   Alibakhshi E, Ramezanzadeh M, Bahlakeh G, Ramezanzadeh B, Mahdavian M, Motamedi M: **Glycyrrhiza glabra leaves extract as a green corrosion inhibitor for mild steel in 1 M hydrochloric acid solution: experimental, molecular dynamics, Monte Carlo and quantum mechanics study**. *J Mol Liq* 2018, **255**:185-198.

7.   Erdoğan Ş, Safi ZS, Kaya S, Işın DÖ, Guo L, Kaya C: **A computational study on corrosion inhibition performances of novel quinoline derivatives against the corrosion of iron**. *J Mol Struct* 2017, **1134**:751-761.

8.   Paul S, Koley I: **Corrosion inhibition of carbon steel in acidic environment by papaya seed as green inhibitor**. *Journal of Bio- and Tribo-Corrosion* 2016, **2**(2):6.

9.   Fang Y, Suganthan B, Ramasamy RP: **Electrochemical characterization of aromatic corrosion inhibitors from plant extracts**. *Journal of Electroanalytical Chemistry* 2019, **840**:74-83.

10.   Popoola LT: **Organic green corrosion inhibitors (OGCIs): a critical review**. *Corrosion Reviews* 2019, **37**(2):71-102.

11.   Saxena A, Prasad D, Haldhar R, Singh G, Kumar A: **Use of Saraca ashoka extract as green corrosion inhibitor for mild steel in 0.5 M H2SO4**. *J Mol Liq* 2018, **258**:89-97.

12.   Verma C, Ebenso EE, Bahadur I, Quraishi M: **An overview on plant extracts as environmental sustainable and green corrosion inhibitors for metals and alloys in aggressive corrosive media**. *J Mol Liq* 2018, **266**:577-590.

13.   Benabdellah M, Benkaddour M, Hammouti B, Bendahhou M, Aouniti A: **Inhibition of steel corrosion in 2 M H3PO4 by artemisia oil**. *Appl Surf Sci* 2006, **252**(18):6212-6217.

14.   El-Etre A: **Inhibition of acid corrosion of carbon steel using aqueous extract of olive leaves**. *Journal of Colloid and Interface Science* 2007, **314**(2):578-583.

15.   Satapathy A, Gunasekaran G, Sahoo S, Amit K, Rodrigues P: **Corrosion inhibition by Justicia gendarussa plant extract in hydrochloric acid solution**. *Corrosion science* 2009, **51**(12):2848-2856.

16.   Hajiahmadi Z, Tavangar Z: **Extensive theoretical study of corrosion inhibition efficiency of some pyrimidine derivatives on iron and the proposal of new inhibitor**. *J Mol Liq* 2019, **284**:225-231.

17.   Li X, Deng S, Xie X: **Experimental and theoretical study on corrosion inhibition of oxime compounds for aluminium in HCl solution**. *Corrosion Science* 2014, **81**:162-175.

18.   Yu F, Chen S, Chen Y, Li H, Yang L, Chen Y, Yin Y: **Experimental and theoretical analysis of polymerization reaction process on the polydopamine membranes and its corrosion protection properties for 304 Stainless Steel**. *J Mol Struct* 2010, **982**(1-3):152-161.

19.   Zhang F, Tang Y, Cao Z, Jing W, Wu Z, Chen Y: **Performance and theoretical study on corrosion inhibition of 2-(4-pyridyl)-benzimidazole for mild steel in hydrochloric acid**. *Corrosion Science* 2012, **61**:1-9.

20.   Behzadi H, Roonasi P, Momeni MJ, Manzetti S, Esrafili MD, Obot I, Yousefvand M, Mousavi-Khoshdel SM: **A DFT study of pyrazine derivatives and their Fe complexes in corrosion inhibition process**. *J Mol Struct* 2015, **1086**:64-72.

21. Hsissou R, Abbout S, Seghiri R, Rehioui M, Berisha A, Erramli H, Assouag M, Elharfi A: **Evaluation of corrosion inhibition performance of phosphorus polymer for carbon steel in [1 M] HCl: Computational studies (DFT, MC and MD simulations)**. *Journal of Materials Research and Technology* 2020, **9**(3):2691-2703.

22. Yadav M, Gope L, Kumari N, Yadav P: **Corrosion inhibition performance of pyranopyrazole derivatives for mild steel in HCl solution: Gravimetric, electrochemical and DFT studies**. *J Mol Liq* 2016, **216**:78-86.

23. Olasunkanmi LO, Obot IB, Kabanda MM, Ebenso EE: **Some quinoxalin-6-yl derivatives as corrosion inhibitors for mild steel in hydrochloric acid: experimental and theoretical studies**. *The Journal of Physical Chemistry C* 2015, **119**(28):16004-16019.

24. Dutta A, Saha SK, Banerjee P, Sukul D: **Correlating electronic structure with corrosion inhibition potentiality of some bis-benzimidazole derivatives for mild steel in hydrochloric acid: combined experimental and theoretical studies**. *Corrosion Science* 2015, **98**:541-550.

25. Fu J, Zang H, Wang Y, Li S, Chen T, Liu X: **Experimental and theoretical study on the inhibition performances of quinoxaline and its derivatives for the corrosion of mild steel in hydrochloric acid**. *Industrial & engineering chemistry research* 2012, **51**(18):6377-6386.

26. Saha SK, Ghosh P, Hens A, Murmu NC, Banerjee P: **Density functional theory and molecular dynamics simulation study on corrosion inhibition performance of mild steel by mercapto-quinoline Schiff base corrosion inhibitor**. *Physica E: Low-dimensional systems and nanostructures* 2015, **66**:332-341.

27. Asfia MP, Rezaei M, Bahlakeh G: **Corrosion prevention of AISI 304 stainless steel in hydrochloric acid medium using garlic extract as a green corrosion inhibitor: electrochemical and theoretical studies**. *J Mol Liq* 2020, **315**:113679.

28. Bahlakeh G, Ramezanzadeh B, Ramezanzadeh M: **Cerium oxide nanoparticles influences on the binding and corrosion protection characteristics of a melamine-cured polyester resin on mild steel: an experimental, density functional theory and molecular dynamics simulation study**. *Corrosion Science* 2017, **118**:69-83.

Chapter 8
Conclusion and Future Outlook

'Biodiversity' is a buzzword these days, but 'chemodiversity' is just as important to life on Earth as biodiversity. Thousands of distinct configurations of low-molecular-weight organic molecules are produced by living organisms like bacteria, fungi, animals, or plants. Many of these are classified as natural products or secondary metabolites since they appear to have no role in basic growth and development processes but plays a key role in diverse survival functions in nature. Natural products' relevance in medicine, agriculture, and industry has prompted extensive investigations into their production, biosynthesis, and biological activity. Despite this, we still know very little about their true functions in nature. Clearly, scientific interest in the components and mechanisms involved in the beneficial properties of fruits and vegetables has fuelled this research. A computational study has been performed on polyphenols like coumestrol, herbacetin and gossypetin. We have also focussed on the polyphenols present in two medicinally important plants, C. hirsutus and R. rosea.

We started by carefully assessing the reactivity and bioactivity of coumestrol and its derivatives. DAM and FEDAM plots of coumestrol substituted at C-15th position in gas phase showed that 15-NH_2 coumestrol showed better anti-oxidant character. 15-NH_2 coumestrol processed a lower BDE value than its parent molecule, coumestrol. The evaluation of numerical parameters associated with various anti-oxidant mechanisms suggested, HAT as the most preferred mechanism. According to a molecular docking analysis, most of the derivatives under study were effective inhibitors for cancer-

causing kinases. With BRAF, Aurora A, VEGFR2, JAK3, and LCK, respectively, 17-Ph C processed the greatest binding affinity value of -11.1, -10.4, -11.1, and -11.1kcal/mol, which was significantly greater than that of coumestrol. The strong binding affinity of 19-Ph C for MCL-1, LCK, and MMP3 suggested that it could be an effective anticancer medication.

In the investigation that follows, the metal-chelating ability of herbacetin, with Zn^{2+} metal ion in various solvents was explored with the aid of density functional theory. FMO analysis showed the increased chemical reactivity of herbacetin due to complexation. The charge transfer between the oxygen atoms of herbacetin and metal ions was well explained by natural population analysis. QTAIM, ELF, and LOF supported the non-covalent interaction, specifically the electrostatic interaction between herbacetin and metal ions. Herbacetin's ability to combat free radicals like •OH and •OOH was improved by the metal chelation and the SPLET mechanism was found to be the preferred mechanism. Molecular docking studies showed that herbacetin possessed a negative binding energy value of -9.0 kcal/mol and -9.6 kcal/mol with AChE2 and BChE respectively which were comparable with the well-known standard drug tacrine. The interaction analysis revealed that herbacetin showed conventional hydrogen bonds, pi-sigma, pi-pi T shaped, amide pi stacked, and van der Waals interactions with neighboring amino acid residues of both proteins.

Next, we focused on the gossypetin's structural details and its medical uses, particularly for metal chelation, radical scavenging, and

UV filtering. A bathochromic shift was noticed in the presence of polar solvent, and UV absorption in the 200–400 nm region was used to explain the molecule's ability to block UV radiation. For NO2, the HAT mechanism was determined to be the most advantageous, and for OH and OOH, the SPLET mechanism. The optimal metal chelation location within the gossypetin molecule was suggested by the interaction energy study. According to the QTAIM investigation, the interaction between gossypetin and Zn is electrostatic in nature. It was intriguing to note that metal chelation made gossypetin's anti-oxidant activity stronger.

In the work that follows, we attempted to create brand-new anti-COVID-19 medications using phytochemicals found in two crucial plants for medicine, *R.rosea* and *C.hirsutus*. The majority of them exhibit moderate to powerful antiviral activity against SARS-CoV-2 Mpro, according to *In silico* molecular docking studies. The best candidate for a treatment for the novel coronaviruses has been reported as rhodionidin, which comes from the *R.rosea* plant (-9.6 kcal/mol), and cocsoline, an alkaloid from *C.hirsutus* (-9.1 kcal/mol). According to MD simulations of rhodionidin and cocsoline with a target, the cocsoline:6lu7 complex was more stable than the rhodionidin:6lu7 complex. Some of the molecular characteristics that have been discussed include reactivity descriptors, band gaps, natural population analysis, and frontier orbitals.

We have also interested in identifying the industrial application of polyphenols other than in pharmaceutical field. So in the final

chapter, we have conducted a comparative study on anti-corrosive nature of three structurally similar molecules herbacetin, gossypetin, and quercetin using DFT modelling and MC simulation analysis. The oxygen atom 3 of both HTIN and GTIN had the highest chance of protonation, as shown by the studies on proton affinities and basicity. The results for both neutral and protonated forms of molecules showed a negative adsorption energy, which suggested that adsorption occurs spontaneously. When compared to quercetin molecules, HTIN and GTIN have a stronger capacity to suppress corrosion, according to Monte Carlo simulation parameters.

So the entire work gives a clear idea of the bioactivity and industrial applications of some selected polyphenols *via* theoretical calculations. Several extention of these works are possible in near future and some of the are,

- *In vitro* analysis on top hits obtained by molecular docking studies.

- Investigation on multi-drugability of polyphenols

- Metal sensing application of polyphenols and studying the influence of pH, temperature, *etc*.

- Quantum chemical calculations on ion sensing by polyphenols.

- Expansion of radical scavenging effect of poly phenols towards more reactive radical species and deep understanding on reaction mechanisms.

- Studying corrosion inhibition of polyphenols for the metals, Cu, Al, *etc*.

Details of Publication

Journal publications

- Puthanveedu, Vinduja, Chandana Pulikkool, Nithin Poonkottil, and K. Muraleedharan. "Theoretical probing to the reactivity and biological effects of the phytochemical, coumestrol and its derivatives." *Chemical Physics Impact* 4 (2022): 100080.

- Puthanveedu, Vinduja, and Karuvanthodi Muraleedharan. "Phytochemicals as potential inhibitors for COVID-19 revealed by molecular docking, molecular dynamic simulation and DFT studies." *Structural Chemistry* 33, no. 5 (2022): 1423-1443.

- Puthanveedu, Vinduja, TK Shameera Ahamed, and K. Muraleedharan. "Theoretical insights into Zn2+ chelated complexes of herbacetin for the application in Alzheimer's disease." *Chemical Physics Impact* 6 (2023): 100163.

- Puthanveedu, Vinduja, and K. Muraleedharan. "Study on structural detailing of gossypetin and its medicinal application in UV filtering, radical scavenging, and metal chelation open up through NCI, TD-DFT, QTAIM, ELF, and LOL analysis." *Computational and Theoretical Chemistry* 1225 (2023): 114126.

- Puthanveedu, Vinduja, and Karuvanthodi Muraleedharan. "Electronic-scale DFT and atomic-scale MC explorations to the corrosion inhibition activity of herbacetin and gossypetin." *Journal of Molecular Graphics and Modelling* (Submitted)

Book chapters

- A Computational modelling of the structure, Frontier Molecular Orbital (FMO) analysis and Global & Local descriptive parameters of a photochemical 'Coumestrol' "Mathematics Applied to Engineering in Action-Advanced Theories, Methods, and Models;**CRC Press, 2020**.

- Theoretical Studies on Anti-Oxidant Activity of the Phytochemical, Coumestrol and Its Derivatives, **IntechOpen, 2021**

Seminar presentations

- A paper presented on the topic "A Computational approach to the Structure, Frontier Molecular Orbital (FMO) and global & local descriptors of a phytochemical, Medicagol" at National Seminar on Recent Trends in Materials Science (NSRTMS-2019), Government College, Chittur, Kerala. ISBN:9789353915612

- **Best oral presentation**: "*Insilico* anti-cancer studies on phytochemical, Coumestrol", 1st International Conference on Recent Advances in Physics & Material Science-2020.

- Oral presentation: Coumestrol as chemotherapeutic drug: A molecular docking investigation to its interaction with protein kinases, Two Day International Virtual Conference On Energy, Environment And Health, **Sree ayyappa college chengannur, KERALA**, 2020

- Oral presentation: **"**Phytochemicals as anti-corona virus drugs: A Molecular Docking Approach", virtual international conference on Surface chemistry, Annamalai University, SUCH 2020

- **Oral presentation 3rd prize**, "In silico identification of potent COVID-19 papain-like

  protease inhibitors from plant-derived compounds" University of Calicut, Kerala,2021.

- Oral presentation: "Molecular docking guided study on herbacetin as anti-cholinesterase agent for Alzheimer's disease1", international virtual conference on recent trends in material science, Bannari Amman Institute of Technology, Sathyamangalam, Tamilnadu, 2021, ISBN:9789355786333

- Oral presentation: Photoprotective and anti-cancer potential of Coumestrol: theoretical study, virtual international conference on Surface chemistry, Annamalai University, SUCH 2022